uOttawa

L'Université canadienne
Canada's university

FACULTÉ DES ÉTUDES SUPÉRIEURES ET POSTOCTORALES

uOttawa

L'Université canadienne
Canada's university

FACULTY OF GRADUATE AND POSDOCTORAL STUDIES

Siamak Lashkari
AUTEUR DE LA THÈSE / AUTHOR OF THESIS

Ph.D. (Chemical Engineering)
GRADE / DEGREE

Department of Chemical Engineering
FACULTÉ, ÉCOLE, DÉPARTEMENT / FACULTY, SCHOOL, DEPARTMENT

Fundamental Aspects of Membrane Characterization by Constant Volume and Constant Pressure Techniques

TITRE DE LA THÈSE / TITLE OF THESIS

Boguslaw Kruczek
DIRECTEUR (DIRECTRICE) DE LA THÈSE / THESIS SUPERVISOR

CO-DIRECTEUR (CO-DIRECTRICE) DE LA THÈSE / THESIS CO-SUPERVISOR

EXAMINATEURS (EXAMINATRICES) DE LA THÈSE / THESIS EXAMINERS

David Taylor

Johannes Wijmans

Jules Thibault

Jason Zhang

Gary W. Slater
Le Doyen de la Faculté des études supérieures et postdoctorales / Dean of the Faculty of Graduate and Postdoctoral Studies

Fundamental Aspects of Membrane Characterization by Constant Volume and Constant Pressure Techniques

by

Siamak Lashkari

Thesis submitted to the Faculty of Graduate and Postdoctoral Studies in partial fulfillment of the requirements for the degree of

Doctorate in Philosophy

in the Department of Chemical and Biochemical Engineering
Faculty of Engineering
University of Ottawa
September, 2008

Your file Votre référence
ISBN: 978-0-494-51816-8
Our file Notre référence
ISBN: 978-0-494-51816-8

Statement of Contribution of Collaborators

I hereby declare that I am the sole author of this thesis. The analytical and numerical methods as well as C# and LabView codes were all carried out by me. I designed and assembled the fully automated bubble flowmeter and carried out the experiments with this system. Qiang Wang helped me with the experiments of sweep gas system. Sweep gas system and one of constant volume systems were designed by Dr. B. Kruczek, my supervisor. The other constant volume system was designed by Dr. Tabe-Mohamadi and belongs to Dr. T. Matsuura. I used it for my thesis with his permission.

My supervisor, Dr. Boguslaw Kruczek, of the Department of Chemical and Biochemical Engineering, University of Ottawa supervised my work during the last five years of research and provided editorial corrections to this thesis report.

Signature: _____ Date: 16 December, 2008

Abstract

Membrane characterization in laboratory-scale systems is an important step in the membrane development process. However, transport properties of polymeric gas separation membranes reported in the literature, such as permeability, diffusion, and solubility coefficients, are typically not reproducible. This variation is often explained on basis of differences in molecular weight, purity, crystallinity and membrane casting conditions. It is also acknowledged that different laboratories use different testing systems and different testing protocols. This thesis investigates fundamental aspects of the two basic membrane characterization methods – constant volume (CV) and constant pressure (CP) techniques.

Considering CV technique, the effect of non-negligible resistance to gas accumulation was extended into the actual configurations of CV systems by studying the effect of the presence of a single and multiple resistance-free tanks downstream from the membrane. Using the concept of an asymptotic solution, the resistance to gas accumulation in the receiving volumes of gradually increasing complexity was characterized by means of a position-dependent time lag. The derived analytical solutions provide a convenient tool for assessing the resistance in existing CV systems and for the design of new CV systems. In addition, recognizing that in a slip flow regime the diffusion coefficient varies with pressure, the set of governing partial differential equations was solved numerically. Analytical and numerical solutions showed good agreement with the experimental results collected from two different configurations of the receiving volume. Moreover, using an optimization procedure in combination with the numerical method, the permeability and diffusion coefficients in membrane were estimated from the data obtained under high resistance to gas accumulation.

With respect to CP technique, the phenomena of back diffusion and back permeation and their combined effect on the experimentally determined permeability coefficients were investigated. A mathematical model that allows estimation of an error arising from back diffusion and back permeation was derived from the first principles. The theoretical predictions were then compared with experimental results obtained in a specially designed, fully-automated CP system, in single gas permeation tests involving nitrogen and oxygen. The experimental results confirmed theoretically predicted trends

resulting from the phenomena of back diffusion and back permeation. However, the influence of these phenomena on the experimentally determined permeability coefficients was greater than that predicted by the model.

Using a CP system with sweep gas designed and built in our laboratory, a novel procedure for the evaluation of the diffusion coefficient of a single gas in membranes exposed to gas mixtures of known composition was developed. For O_2/N_2 and CH_4/N_2 systems the results indicate that the diffusion coefficients of nitrogen and oxygen in poly(phenylene oxide) membrane are enhanced in the presence of another gas, but the diffusion coefficient of methane decreases in the presence of nitrogen. This novel method is expected to become an important tool in fundamental studies on the mechanisms of gas transport in polymeric membranes.

Résumé

La caractérisation des membranes à l'échelle de laboratoire est une étape importante dans le développement des membranes. Cependant, les propriétés de transport des membranes en polymère pour la séparation des gaz rapportées dans la littérature, telles que la perméabilité, la diffusion, et les coefficients de solubilité, sont peu reproductibles. Cette variation est souvent justifiée par les différences de poids moléculaire, de la pureté, de la cristallinité et des conditions de fabrication des membranes. Il est important de noter que les différents laboratoires emploient différents systèmes et différents protocoles expérimentaux. Cette thèse s'intéresse aux aspects fondamentaux des deux méthodes de base de caractérisation des membranes – les méthodes à volume constant et à pression constante.

Pour la méthode à volume constant, l'effet de la résistance non-négligeable à l'accumulation de gaz a été étudié pour des configurations réelles de systèmes à volume constant en considérant l'influence d'un ou plusieurs réservoirs placés en aval de la membrane et ayant une résistance négligeable. Basé sur la solution asymptotique de l'équation décrivant le système, la résistance à l'accumulation de gaz dans des volumes de réception de complexité croissante a été caractérisée au moyen d'un délai qui est fonction de la position. Les solutions analytiques développées dans cette thèse fournissent un outil précieux pour évaluer la résistance des systèmes à volume constant existants et pour la conception de nouveaux systèmes. De plus, étant donné que dans un régime d'écoulement non adhérant le coefficient de diffusion varie avec la pression, l'ensemble des équations différentielles partielles a été résolu numériquement. Les solutions analytiques et numériques représentent adéquatement les résultats expérimentaux obtenus pour deux configurations différentes des volumes de réception. Finalement, une méthode d'optimisation couplée à la solution numérique a permis d'estimer la perméabilité et les coefficients de diffusion dans la membrane à partir des données obtenues pour un système dont la résistance à l'accumulation du gaz est élevée.

Pour la méthode à pression constante, les phénomènes de la rétrodiffusion et rétroperméation et leur effet combiné sur les coefficients de perméabilité déterminés

expérimentalement ont été étudiés. Un modèle mathématique permettant l'estimation de l'erreur causée par la rétrodiffusion et la rétroperméation a été dérivé à partir des principes de base. Les prédictions théoriques ont été comparées aux résultats expérimentaux de perméation d'un mélange binaire azote/oxygène obtenus dans un système à pression constante complètement automatisé et conçu spécialement pour cette étude. Les résultats expérimentaux ont confirmé les tendances théoriques et résultantes des phénomènes de la rétrodiffusion et de la rétroperméation. L'influence de ces deux phénomènes sur les coefficients de perméabilité déterminés expérimentalement était plus grande que celle prévue par le modèle.

L'utilisation d'un un gaz de purge dans un système à pression constante conçu et construit dans notre laboratoire a permis de développer une méthode originale pour estimer le coefficient de diffusion d'un gaz simple dans des membranes exposées à des mélanges de gaz de compositions connues. Pour les systèmes O_2/N_2 et CH_4/N_2, les résultats indiquent que les coefficients de diffusion d'azote et d'oxygène dans la membrane de polyphényle augmentent en présence d'un autre gaz. D'autre part, le coefficient de diffusion du méthane diminue en présence de l'azote. On s'attend à ce que cette méthode originale devienne un outil important pour des études fondamentales sur les mécanismes de transport des gaz dans les membranes polymériques.

Acknowledgements

I would like to take this opportunity to thank the people who helped me throughout my Ph.D. studies at the University of Ottawa.

Foremost, I would like to acknowledge my supervisor, Dr. Boguslaw Kruczek for giving me the opportunity to pursue this interesting research project. His dedicated supervision and constant support were great inspiration for me to continue and complete this work.

I would like to thank Qiang Wang who helped me on performing part of experimental tasks and also other graduate students, faculty and staff in University of Ottawa for sharing their knowledge with me.

I would like to thank Dr. Takeshi Matsuura and Dr. Arturo Macchi for their care and support during the last four years. They also generously allowed me to use their experimental equipment.

I would like to express my gratitude to examiners of the thesis, Dr. H. Wijmans from Membrane Technology & Research, Inc., Dr. Tibault, Dr. Taylor, and Dr. Zhang from Chemical & Biochemical Engineering Department, University of Ottawa who provide great suggestions for improving the quality of the thesis. Special thanks to Dr. Tibault for providing the French translation of the abstract.

I would like to admire the support and love from my father, my mother, and my brothers, Babak and Bahman who have been my inspiration during difficult times.

Special thanks to my dear wife, Roza Tizvar, for her admirable love, thoughtful guidance and being always there for me.

Table of Contents

List of Tables

List of Figures

Appendices:

Chapter 1

Introduction

This thesis deals with problems encountered in measurement of transport properties in gas separation membrane characterization.

1.1 Overview

The number of researches and studies in gas separation membranes has been increased in the past few decades due to their more cost-effective and environmentally friendly processes compared to other gas separation processes (e.g. adsorption and cryogenic distillation). The possibility to formulate membranes with high mechanical, thermal, and chemical stability makes membranes ideal choice for harsh environments such as sour gas and corrosive vapors. Industrial membrane systems make lower foot print and consume lower energy compare to their competitors. Separation of nitrogen and oxygen from air is a highlight in gas separation membrane applications. There is a great prospect for gas separation membrane industry due to infinite combination for hybrid membranes and several surface modification methods. Baker presented perspective future of gas and vapor membrane industry in various publications [1-3].

Membrane characterization using bench-scale experiments has been a fundamental step in the development of membrane processes. However, the major drawback of these experiments so far is that the transport properties of gas separation membranes are often not reproducible. Generally, characterization of gas separation membranes involves evaluation of three fundamental transport parameters of the gas in membrane: permeability (P), diffusion (D), and solubility (S) coefficients. Permeability is the measure of the membrane productivity. Solubility indicates the condensability of gas molecules on membrane surface when diffusion coefficient represents the speed of

molecules passing through the membrane matrix. Based on the solution diffusion model these parameters are related together as [4]:

$$P = D \times S \tag{1.1}$$

There are two methods for membrane characterization: constant pressure (CP) and constant volume (CV) techniques. In a CP system, the permeate side of the membrane is either open to atmosphere or is swept with a gas usually at atmospheric pressure. This way, the gas permeation tests are performed at a constant trans-membrane pressure. On the other hand, in a CV system, the permeate side of the membrane is initially at vacuum, and as the gas permeates through the membrane, the pressure at the permeate side increases. Consequently, the gas permeation tests in a CV system are carried out at a variable trans-membrane pressure. Even though most membrane laboratories use CV systems, a quick look at the most recent publications in gas separation membranes shows that besides the popular CV systems, CP systems are also being employed for membrane characterization. It is noticed that the data provided by these two systems are not consistent. The difference is usually blamed on the lower absolute pressure of CV systems, compared to that of CP systems for the same driving force across the membrane. Although such variations have been accepted in the literature, there is no rigorous explanation behind it [5]. To compare the data of these systems, one should obtain repeatable, accurate, and consistent results from each of them.

1.2 Constant volume system

Constant volume (CV) systems have been used for the measurement of gas permeation through semi-permeable membranes since the mid nineteenth century [6,7]. The permeation rate is determined from the rate of pressure rise in a known receiving volume using the following equation, which is derived from the ideal gas law:

$$Q = \frac{V}{RT}\frac{dp}{dt} \tag{1.2}$$

where V is the volume of the receiver, R is the universal gas constant, T is the absolute temperature, t is the time, and p is the pressure. The constant volume technique allows measurements of flow rates in the order of 10^{-8} mol/s and less, where other measurement techniques fail or require sophisticated built up. Since the introduction of a tim

e lag method by Daynes [8] in 1920, CV systems are also widely used for the evaluation of membrane diffusivity. Knowing membrane permeability and diffusivity, the third fundamental intrinsic membrane property, solubility, may also be determined from Equation (1.1).

Although not explicitly stated, the measurements in CV systems rely on the assumption that there is no resistance to gas accumulation in the receiver. In other words, as a gas molecule enters the receiver at a specific point, it can be found anywhere within the receiver with the same probability. However, as shown in previous publications from our laboratory [9-11], this "unwritten" assumption is not valid. Assuming the receiver to be a straight cylinder, in which gas accumulation is a diffusive process characterized by a constant diffusion coefficient (D), the resistance to gas transport downstream from the tested medium, may be quantified by the time lag, $\theta(x)$, using the following expression [9]:

$$\theta(x) = \frac{l^2}{6D} - \frac{(l-x)^2}{2D} \tag{1.3}$$

where l is the length of the cylinder, and x is the distance of the pressure sensor from the flow source. Depending on x, i.e., the position where the pressure rise is monitored, $\theta(x)$ may be a positive or negative number. At the limit of $x = l$, Equation (1.3) simplifies to $\theta(l) = l^2/6D$, which corresponds to the maximum positive value, while at other limit of $x = 0$, Equation (1.3) simplifies to $\theta(0) = -l^2/3D$, which corresponds to the maximum negative value.

For a diffusion coefficient in the outflow receiver to be constant, gas molecules must collide more frequently with the receiver's wall than with themselves. Thus the diffusion coefficient in Equation (1.3) must refer to the Knudsen diffusion coefficient, which is evaluated from [12]:

$$D = \frac{2}{3} r \sqrt{\frac{8RT}{\pi M}} \tag{1.4}$$

where, r is the radius of the receiver, and M is the molar mass of the gas.

The difference between $\theta(l)$ and $\theta(0)$ from Equation (1.3) implies the existence of a constant pressure gradient within the receiver during a "pseudo steady state"

accumulation. Since before the gas starts to flow into the receiver the pressure within the receiver is constant, there must be a transient period, during which the pressure gradient develops and consequently the pressure response is a function of position within the receiver. In such a transient period, using Equation (1.2) for the evaluation of the flow into the receiver could lead to a very significant error. The existence of a transient period, during which application of Equation (1.2) leads to large errors, was verified experimentally [11]. Moreover, since typically during the accumulation there is a transition from Knudsen diffusion to slip flow regime, in which the diffusion coefficient increases with pressure, the pressure gradient within the receiver gradually decreases as the pressure increases. This implies that after the initial transient period, the pressure response within the receiver remains to be a function of the position, which was also verified experimentally [11].

In real systems, the outflow receiver is never just a straight cylindrical tube; it consists of a series of interconnected tanks to vary the volume of the receiver in order to accommodate a wide range of flow rates into the receiver. Since the Knudsen diffusion coefficient is proportional to the internal radius, the resistance to gas accumulation in tanks practically does not exist. In another paper from our laboratory, assuming constant diffusion coefficient and the outflow receiver composed of a straight cylindrical tube connecting a flow source at $x = 0$ with a resistance-free tank at $x = l$, the following expression for the position-dependent time lag in the connecting tube was derived [10]:

$$\theta(x) = \frac{\frac{l^2}{D}\left(\frac{l}{6} + \frac{V}{2A}\right)}{l + \frac{V}{A}} - \frac{(l-x)^2}{2D} - \frac{V(l-x)}{AD} \tag{1.5}$$

where V is the volume of the tank, and A is the cross sectional area of the tube. With $V = 0$, Equation (1.5) simplifies to Equation (1.3). On the other hand, with $V > 0$, because of the third term, $\theta(x)$ tends to be a large negative number, leading to an underestimation of the time lag of the tested medium. The error is magnified as the distance between the pressure sensor and the tank, $l - x$, increases. The radius of the connecting tube has a major effect on the error, since A is proportional to r^2, while D is proportional to r. The existence of a large negative time lag in the configuration in which a flow source

(membrane) is connected with a resistance free tank via a standard 1/4" tube was confirmed experimentally [11]. The actual negative error in the time lag was even greater than that predicted from Equation (1.5), because in reality D is not constant, but due to transition from Knudsen diffusion to slip flow regime increases during the course of time lag experiment.

The ultimate objective of the part of this thesis related to constant volume system was to complete the investigation of the effect of resistance to gas accumulation on membrane characterization initiated in our laboratory. More specifically, to generalize the mathematical analysis, in order to model the actual configurations of the outflow receivers. While fulfilling this objective could provide an indispensible tool for the design of new constant volume systems, another objective was to demonstrate the possibility of Reconciliation of the membrane properties from the data collected in high resistance conditions. The latter objective requires setting up of another objective related to verification of the reconciled membrane properties experimentally, which requires a design and construction of a constant volume system in which the resistance to gas accumulation is eliminated or at least minimized.

1.3 Constant pressure system

Constant pressure – variable volume technique is an alternative method for the characterization of gas separation membranes. In short, this technique is referred to as a constant pressure (CP) method and testing systems utilizing this method are referred to as CP systems.

In a CP system, the permeate side of the membrane is open to atmosphere, or is swept with a gas at atmospheric pressure. In case of a CP system open to atmosphere, there is a driving force for the diffusion of the air components, which are not present in the permeating gas, towards the membrane (back diffusion). If there is a nonzero partial pressure of the back diffusion gases at the permeate side of the membrane, they may permeate to the feed side of the membrane (back permeation). Tran studied gas permeation properties of modified polyphenylene oxide (PPO) membranes in a CP system equipped with a bubble flowmeter [13]. She observed unusually high permeability ratios of CO_2/CH_4 and O_2/N_2 at low feed pressures. She speculated that these

values resulted from underestimation of the permeability coefficients of the slower gases (i.e., N_2 and CH_4) and overestimation of faster gases (CO_2 and O_2) due to back diffusion and back permeation phenomena. Although these phenomena are inherent to CP systems, they were not adequately addressed in the literature.

Therefore, the major objective related to CP systems was to systematically study the phenomena of back diffusion and back permeation. More specifically, to develop from first principles a mathematical model that would allow estimating an error arising from these phenomena on the apparent gas permeability, and to verify the developed model in appropriately designed series of experiments.

To examine the effect of back diffusion and back permeation of gases in membrane characterization, very low flow rate of gases need to be measured accurately. The measurement of very low gas flow rates using a bubble flow meter is both extremely time consuming and susceptible to human errors. There are on the market automated bubble flow meters, the application of which could save time of the researcher and eliminate or at least minimize human-related errors. However, these automated bubble flow meters still require a manual formation of the bubble. Therefore, another objective of this thesis was to develop an appropriate tool for the systematic study of the phenomena of back diffusion and back permeation. More specifically, the aim of this part was to improve the existing soap flowmeters to make the measurements of low flow rates of gases both fully automated and more accurate.

1.4 Constant pressure system with sweep gas

Even the best fully automated bubble flow meters will not allow monitoring the changes in flow rate with a frequency sufficient for dynamic gas permeation experiments used for the determination of the diffusion coefficient. On the other hand, electronic mass flow meters or equivalent instruments that would allow for a continuous monitoring of time-dependent changes of gas permeation across the membrane are not designed to operate for very low gas permeation rates typical in characterization of gas separation membranes. Consequently, constant pressure systems are generally limited for the measurement of the permeability and selectivity of membranes. To use a CP system in a

dynamic gas permeation experiments generally requires sweeping of the permeate side of the membrane with a gas.

The theoretical basis for the application of CP systems in dynamic gas permeation experiments were provided by Ziegel et al. [14] in 1969. However, the method proposed by Ziegel et al. has gained a very limited interest, and only few researchers, mostly in the field of pervaporation, have used it [15-20]. The reason for the lack of popularity of this methods is related to the required accuracy of the permeate flow measurement. Zeigel et al. [14] employed a hydrogen detector to accurately measure the permeate rate of hydrogen over its isotope deuterium through a poly(vinyl fluoride) membrane. The carrier gas was nitrogen. Pye et al. [15] employed a gas chromatography to study the permeabilities of CH_4/H_2 mixture passing through the polyimide membranes. Watson et al. [16-18] employed this method along with a mass spectrometer and a vacuum permeation cell to study the pervaporation. On the other hand, Yeom et al. [19] commented the apparatus design used by Watson et al., and presented an improved equipment for the measurement of the diffusion coefficient in pervaporation of water vapour through a hydrophilic poly(vinyl alcohol) membrane and a hydrophobic poly(dimethylsiloxane) membrane. Kim and Lee [20] used the apparatus of Yeom et al. [19] to study the gas transport properties of organic–inorganic hybrids of poly(amide-6-b-ethylene oxide) and silica prepared via in situ polymerization.

In all of above-mentioned studies the only considerations in the selection of a sweep gas were: (1) its non-interaction with the membrane material, and (2) no overlapping peaks with the forward permeating gases in gas chromatography analysis. The major problem with the first criterion is the actual absence of interactions with the membrane material. On the other hand, even if the sweep gas does not interact with the membrane, it will back permeate through the membrane, and this may affect the characterized transport coefficients of the forward permeating gases.

Consequently, another objective of this thesis was to develop a procedure for the determination of the diffusion coefficient in a constant pressure with a sweep gas, in which both the feed and the sweep streams were composed of the same gas. At the same time, another motivation for the implementation of a CP system with sweep, was to control the partial pressure of a back permeating gas at the permeate side of membrane in

order to study directly the effect of back permeation on the membrane characterization using a forward permeating gas.

1.5 Thesis objectives

The ultimate objective of this thesis is to provide accurate measurement of transport properties in gas separation membranes. This objective cannot be accomplished without a thorough understanding of fundamentals related with a specific testing technique, and having reliable and accurate testing systems. Therefore, this thesis aims to resolve inconsistencies of data produced by different systems and to pinpoint some inherited errors associated with the currently available systems. Constant volume systems and constant pressure systems are investigated during this study. The following sections summarize the main objectives of the current work under the headings corresponding to sections 1.2-1.4.

Constant volume system

1. Application of concept of the position-dependent time lag to a single accumulation tank receiver, in which the tank can be placed anywhere along the main line of the receiver.
2. Application of concept of the position-dependent time lag to any configuration of the receiver, in particular to multiple-tank systems.
3. Evaluation of the resistance to gas accumulation in any configuration of the receiver without assuming a constant diffusion coefficient. This objective requires a numerical solution of a set of partial differential equations.
4. Reconciliation of the membrane properties from the data collected at high-resistance conditions. This objective, apart from the numerical solution, requires utilization of an optimization procedure.
5. Design of a resistance-free receiver for the verification of the reconciled membrane properties.

Constant pressure system

6. Design and construction of a fully automated bubble flow meter for a continuous and hands-free monitoring of low gas flow rates.
7. Experimental demonstration of the effect of back diffusion and back permeation on the apparent permeability coefficient of the forward permeating gas in a traditional constant pressure system.
8. Development of a model to assess the effects of the combined phenomena of back diffusion and back permeation.

Constant pressure system with sweep

9. Measurement of the diffusion coefficient in CP system with sweep, without any influence of back permeation.
10. Measurement of the diffusion coefficient of single gases in the presence of controlled back permeation.

1.6 Thesis outline

This thesis is prepared in a paper format and is divided in three parts each of which representing a separate measurement technique. Part I is devoted to constant volume system. Part II is related to membrane characterization in a traditional constant pressure systems, with a special focus on the phenomena of back permeation and back diffusion. Part III deals with a constant pressure system with sweep gas.

Part I consist of three papers (Chapters 2-4). The first paper (Chapter 2) provides details of an analytical solution for the calculation of time lag in the main tube to which one resistance-free tank can be attached at any position. The second paper (Chapter 3) demonstrates the Reconciliation of the membrane properties from the data collected at high resistance condition. The reconciled membrane properties are compared with the experimentally determined properties from a specially designed CV system, in which the resistance to gas accumulation is minimized. The third paper (Chapter 4) generalizes the analytical approach for any configuration of the receiver, which allows the optimization

of the position of pressure sensor in the receivers associated with resistance to gas, and provides guidance for the design of resistance-free receivers.

Part II, which deals with a constant pressure system equipped with a bubble flow meter, contains two papers. In the first paper (Chapter 5), the design and application of a fully automated soap bubble flowmeter is explained. The second paper (Chapter 6) demonstrates the actual application of the constructed fully automated bubble flow meter in a systematic study of the phenomena of back diffusion and back permeation in a traditional constant pressure system.

Part III contains only one paper (Chapter 7), which is an explicit application of Part II. In Chapter 7, the possibility of the direct measurement of the diffusion coefficient of single gases with and without the presence of back permeation is demonstrated. Parts II and III are in the same category, but they are split because of the measurement techniques they utilize.

Chapter 8 summarizes the most important conclusions and recommendations arising from this work. In addition, there are three appendices. Appendix A is a paper, which I coauthored, and which is continued in Part I of the thesis. Appendix B provides details of the derivation of the analytical solution presented in Chapter 4. Appendix C provides additional information related to Part II, which has not been published, but would be helpful to anyone intending to continue this work.

References

1. R.W. Baker, Future directions of membrane gas separation technology, Industrial & engineering chemistry research 41 (6) (2002) 1393-1411.
2. R.W. Baker, Membrane technology in the chemical industry: Future directions, Chapter in Membrane Technology, 2nd edition, Editors: Dr. Suzana Pereira Nunes, Dr. Klaus-Viktor Peinemann, Wiley-VCH Verlag GmbH & Co. KGaA, Weinheim, 2006.
3. R.W. Baker, Membranes for vapour/gas separation, Membrane Technology and Research, Inc. Publication, Menlo Park, CA, 2006.
4. R.E. Kesting, Synthetic polymeric membranes: A structural prospective, 2nd edition, Joh Wiely & Sons, New York, 1985.
5. Guillain Mauviel, Julien Berthiaud, C´ecile Vallieres, Denis Roizard, Eric Favre, Dense membrane permeation: From the limitations of the permeability concept back to the solution-diffusion model, J. Membr. Sci. 266 (2005) 62–67.
6. K. Ghosal and B.D. Freeman, Gas separation using polymer membranes: an overview, Polymers for Advanced Technologies, 5 (1994) 673-697.
7. V.T. Sannett, The transport of gases in synthetic polymeric membranes –– a historic perspective, J. Membrane Sci. 3(2) (1978) 97-115.
8. H. A. Daynes, The process of diffusion through a rubber membrane, Proceedings of the Royal Society of London, Series A, 97 (685) (Jun. 1, 1920) 286-307.
9. B. Kruczek, H.L. Frisch, R. Chapanian, Analytical solution for the effective time lag of a membrane in a permeate tube collector in which Knudsen flow regime exists, J. Membr. Sci. 256 (2005) 57-63.
10. B. Kruczek, F. Shemshaki, S. Lashkari, R. Chapanian, H.L. Frisch, Effect of a resistance-free tank on the resistance to gas transport in high vacuum tube, J. Membr. Sci. 280 (2006) 29-36.
11. R. Chapanian, F. Shemshaki, B. Kruczek, Error in Measurement of Gas Flow Rate by the Pressure Rise Technique Arising from the Resistance to Accumulation of Gases in Vacuum Tubes, Can. J. Chem. Eng., 86(4) (2008) 712-719.
12. Leonard B. Loab, "The Kinetic Theory of Gases" 3rd ed., Dover Publication, Inc., New York (1961) 278-300.

13. A. Tran, Development of and Gas Permeation Study of Homo and Copolymers from the Family of Polyphenylene Oxides, MASc Thesis, University of Ottawa, Ottawa, ON, 2003.
14. K.D. Ziegel, H.K. Frensdorff, D.E. Blair, Measurement of hydrogen transport in poly-(vinyl Fluoride) films by the permeation-rate method, Journal of polymer Science: Part A-2, 7 (1969) 809-819.
15. D.G. Pye, H.H. Hoehn, M. Panar, Measurement of gas permeability of polymers. II. Apparatus for determination of permeabilities of mixed gases and vapors, Journal of Applied Polymer Science 20 (1976) 287-301.
16. J.M. Watson, P.A. Payne, A study of organic compound pervaporation through silicon rubber, J. Membr, Sci. 49 (1990) 171-205.
17. J.M. Watson, G.S. Zhang, P.A. Payne, The diffusion mechanism in silicon rubber, J. Membr. Sci. 73 (1992) 55-71.
18. J.M. Watson, M.G. Baron, Precise static and dynamic permeation measurements using a continous-flow vacuum cell, J. Membr. Sci. 106 (1995) 259-268.
19. C.K. Yeom, B.S. Kim, J.M. Lee, Precise on-line measurements of permeation transients through dense polymeric membranes using a new permeation apparatus, J. Membr. Sci. 161 (1999) 55-66.
20. J.H. Kim, Y.M. Lee, Gas permeation properties of poly(amid-6-b-ethylene oxide)-silica hybrid membranes, J. Membr. Sci. 193 (2001) 209-225.

Part I

Constant Volume System

This part focuses on the resistance to gas accumulation in receivers of constant volume systems. It contains four papers one of which can be found in Appendix A of this thesis. Three other papers are presented in Chapters 2 to 4.

Chapter 2

General Solution for the Time Lag of a Single-Tank Receiver in the Knudsen Flow Regime and its Implications for the Receiver's Configuration

S. Lashkari[1], B. Kruczek[1]*, H.L. Frisch[2]

Journal of Membrane Science, 283 (2006) 88-101

[1] Department of Chemical Engineering
University of Ottawa
161 Louis Pasteur Street
Ottawa, ON K1N 6N5, Canada
Fax: (613) 562-5172
Phone: (613) 562-5800 ext. 6302
E-mail: kruczek@eng.uottawa.ca

[2] Department of Chemistry
University at Albany
1400 Washington Avenue
Albany, NY 12222
USA

* **To whom correspondence should be addressed.**

Abstract

Constant volume systems are commonly used for the determination of the diffusion, permeability and solubility coefficients of gases in porous and nonporous media. In this paper we present important considerations for the design of an outflow receiver of a constant volume system to minimize the possible resistance to gas transport downstream from the tested medium. The receiver considered in this paper consists of the main tube, a tank, and a tube connecting the main tube with the tank. The resistance of the receiver is quantified using the concepts of the asymptotic solution and the time lag by assuming that gas accumulation in the receiver occurs in the Knudsen flow regime. The effects of the volume of the tank, the position at which the tank is connected to the main tube, the length of the connecting tube, as well as, the position of the pressure sensor in the receiver are discussed.

Keywords: Constant Volume Systems, Time Lag, Asymptotic Solution, Diffusion Coefficient, Fick's 2nd Law of Diffusion

2.1 Introduction

The time lag permeation technique is an effective characterization method, which originates from the time lag concept introduced nearly a century ago [1]. Essentially, a typical time lag experiment involves monitoring of the pressure response downstream from the tested medium, which results from a step change in the upstream pressure; and the time lag is the intercept of the asymptote to the pressure response curve with the time axis [2]. The time lag is a measure of the resistance to gas transport in the tested medium, which in turn is inversely related with the diffusion coefficient in the tested medium. The time lag analyses rely on the assumption that there is no resistance to gas transport upstream and downstream from the tested medium.

Assuming the outflow volume to be a straight cylinder, in which gas accumulation is a diffusive process characterized by a constant diffusion coefficient (D), the resistance to gas transport downstream from the tested medium, may be quantified by the time lag, $\theta(x)$, using the following expression [3]:

$$\theta(x) = \frac{l^2}{6D} - \frac{(l-x)^2}{2D} \tag{2.1}$$

where l is the length of the cylinder, and x is the distance of the pressure sensor from the flow source. At the limit of $x = l$, Equation (2.1) simplifies to $\theta(l) = l^2/6D$, which represents the actual resistance of a cylindrical receiver. The expression for $\theta(l)$ is identical to the expression for the time lag of a slab membrane, initially at zero concentration, in which the diffusion coefficient is constant [4]. This is not surprising, because in the analysis leading to Equation (2.1) the receiver is effectively treated as a slab membrane [3]. The pressure response may be monitored anywhere along the receiver, and the actual time lag of the receiver strongly depends, as indicated by Equation (2.1), on the distance of the pressure sensor from the flow source. At the other limit of $x = 0$, Equation (2.1) simplifies to $\theta(0) = -l^2/3D$, which is identical to the expression for an inlet time lag of a slab membrane [5]. Therefore, the resistance to gas transport downstream for the tested medium may lead, depending on the position of the pressure sensor, to over or underestimation of the time lag of the medium. On the other hand, the resistance to gas transport in the inflow volume would prevent a perfect step

change in the upstream pressure, which would always lead to an overestimation of the time lag of the medium [6].

For a diffusion coefficient in the outflow receiver to be constant, gas molecules must collide more frequently with the receiver's wall than with themselves. Thus the diffusion coefficient in Equation (2.1) must refer to the Knudsen diffusion coefficient, which is evaluated from [7,8]:

$$D = \frac{2}{3} r \sqrt{\frac{8RT}{\pi M}} \tag{2.2}$$

where, r is the radius of the receiver, R is the gas constant, T is the absolute temperature, and M is the molar mass of the gas. As pointed out in Ref. [3], some research groups evacuate the outflow receiver to 10^{-6} – 10^{-7} Pa absolute pressures [9,10], while the conditions for Knudsen diffusion in standard 6.35 mm (1/4") and 12.7 mm (1/2") tubes already exist at pressures less than 0.5 Pa and 0.2 Pa, respectively [3]. Moreover, the diffusion coefficient at the beginning of a slip flow regime does not vary considerably from the respective value in the Knudsen flow regime. For example, in case of a standard 6.35 mm (1/4") tube the diffusion coefficient up to 10 Pa does not exceed the corresponding Knudsen diffusion coefficient by more than 10% [11].

In real systems, the outflow receiver is never a straight cylindrical tube; it consists of a series of interconnected tanks to vary the volume of the receiver in order to accommodate a wide range of flow rates into the receiver [12-14]. Since the Knudsen diffusion coefficient is proportional to the internal radius, the resistance to gas accumulation in tanks practically does not exist. On the other hand, the presence of a resistance-free tank in the outflow receiver may greatly amplify the resistance to gas transport in a tube connecting the flow source with the tank [11].

In our recent paper [11], we considered the configuration in which the outflow receiver consists of a straight cylindrical tube connecting a flow source at $x = 0$ with a resistance-free tank at $x = l$. Assuming a constant diffusion coefficient in the connecting tube, the time lag within the tube is given by:

$$\theta(x) = \frac{\frac{l^2}{D}\left(\frac{l}{6} + \frac{V}{2A}\right)}{l + \frac{V}{A}} - \frac{(l-x)^2}{2D} - \frac{V(l-x)}{AD} \tag{2.3}$$

where V is the volume of the tank, A is the cross sectional area of the tube and x is the distance of the pressure sensor from the flow source. With $V = 0$, Equation (2.3) simplifies to Equation (2.1). On the other hand, with $V > 0$, because of the third term, $\theta(x)$ tends to be a large negative number, leading to an underestimation of the time lag of the tested medium. The error is magnified as the distance between the pressure sensor and the tank, $l - x$, increases. The radius of the connecting tube has a great effect on the error, since A is proportional to r^2, while D is proportional to r. The existence of a large negative time lag in the configuration in which a flow source (membrane) is connected with a resistance-free tank via a standard 6.35 mm (1/4") tube was confirmed experimentally [11]. The actual negative error in the time lag was even greater than that predicted from Equation (2.3), because in reality D is not constant, but rather increases during the course of time lag experiment, i.e. as the pressure in the receiver increases.

The fact that D increases during the course of a time lag experiment is responsible for a dependence of the slope of the asymptote to the pressure response curve on the position of the pressure sensor within the outflow volume [11]. In turn, this slope is directly proportional to the permeability coefficient (P_m) of the gas in the membrane. Moreover, since for solution-diffusion membranes the solubility coefficient (S_m) may be evaluated from the ratio of the permeability coefficient and the diffusion coefficient (D_m), the resistance to accumulation of the gas in the outflow volume may affect the all three transport coefficients determined in a single time lag permeation experiment.

In this paper, we present the mathematical solution of a more general problem, in which the resistance-free tank may be placed anywhere along the tube. In real systems, in which the receiver consists of a series of interconnected tanks, the tanks are located at different distances from the flow source. Therefore, the solution presented here will be applicable for the case in which only one of the tanks is available for gas accumulation while the other tanks are closed. Similarly to Ref. 9, solving the governing partial differential equation required a constant diffusion coefficient of the gas in the tube, which is the case in the Knudsen flow regime.

2.2 Mathematical formulation of the problem

Figure 2.1 presents a simplified configuration of a constant volume receiver consisting of a main cylindrical tube of length $l = l_1 + l_2$, a cylindrical tank of volume V, and a cylindrical tube L3 of length l_3, which connects the tank with the main tube. The volume of the tank may be added to or removed from the volume of the receiver by means of a valve (not shown in Figure 2.1), which is installed on L3.

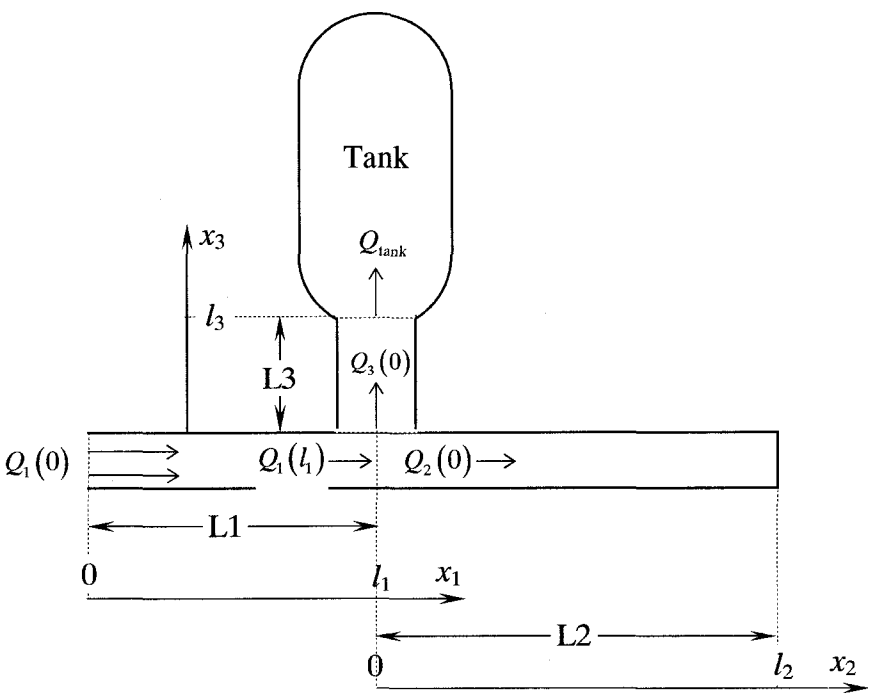

Figure 2.1. Simplified configuration of an outflow receiver for the modeling purposes.

In the foregoing derivation it is assumed that the volume of the tank is a part of the total volume of the receiver. The radius of the tank is much greater than the radius of the tubes. The tube L3 is attached to the main tube at the distance l_1 from the flow source, so that L3 divides the main tube into two parts, L1 and L2, with the respective lengths $l_1$and l_2. In a special case in which $l_2 = 0$ and L1 and L3 have the same radii the analysis simplifies to that described in Ref. [11].

To generalize the analysis, we will allow for the two parts of the main tube L1 and L2 to have different cross sectional areas of A_1 and A_2, respectively, which are different from the cross sectional area A_3 of L3 Consequently, the corresponding diffusion

coefficients in L1, L2 and L3 are D_1, D_2, and D_3, respectively. A pressure sensor to monitor the pressure rise can be placed anywhere along L1, L2 and L3, as well as, anywhere in the tank. Initially, there is no flow of the gas, and the tubes and the tank are at a uniform pressure. At time $t > 0$, the gas starts to flow into L1, and is accumulated in the receiver. The gas flow entering L1 may originate from any source, including membrane permeation. However, to simplify the mathematical analysis, it will be assumed the flow rate entering L1 at $t > 0$ is constant.

If the receiver is initially at very high vacuum, and thus the conditions for Knudsen diffusion exist, the gas transport in each tube is governed by Fick's second law:

$$\frac{\partial p_i(x_i,t)}{\partial t} = D_i \frac{\partial^2 p_i(x_i,t)}{\partial x_i^2} \tag{2.4}$$

where subscript i = 1, 2, 3 indicates L1, L2, L3, respectively.

Since the Knudsen diffusion coefficient is directly proportional to the radius of the tube, the diffusion coefficient in the tank is much greater than the diffusion coefficients in the tubes. Consequently, at a given time the pressure in the tank is expected to be uniform and equal to the pressure at the tank entrance, $x_3 = L_3$. In other words, since the diffusion coefficient in the tank is large, the tank is said to be resistance-free. Starting from the ideal gas law it can be shown that the rate of pressure change in the tank is given by the following expression:

$$\frac{dp_{\text{tank}}(t)}{dt} = Q_{\text{tank}}(t)\frac{RT}{V} \tag{2.5}$$

where, $Q_{\text{tank}}(t)$ is the gas flow rate entering the tank. It is important to emphasize that $Q_{\text{tank}}(t) < Q_1(0,t)$, because some gas flows into L2 at the rate of $Q_2(0,t)$. Moreover, because of the resistance to gas transport in L3, for some time after initiation of the flow into the receiver, $Q_{\text{tank}}(t) \neq Q_3(0,t)$.

The determination of $Q_{\text{tank}}(t)$, $Q_2(0,t)$ and $Q_3(0,t)$ requires solving Equation (2.4) in L1, L2, and L3 and thus obtaining the pressure

responses $p_1(x_1,t)$, $p_2(x_2,t)$, and $p_3(x_3,t)$, respectively. This, in turn requires an initial and six boundary conditions. For all tubes the initial condition is given by:

$$p_1(x_1,0) = p_2(x_2,0) = p_3(x_3,0) = p_o = constant \tag{2.6}$$

At the entrance to the main tube (x_1 = 0), the boundary condition is expressed in terms of the gas flow rate entering the tube and Fick's first law:

$$\left(\frac{\partial p_1(x_1,t)}{\partial x_1}\right)_0 = -\frac{RT}{D_1}\frac{Q_1(0,t)}{A_1} \tag{2.7}$$

At l_1, which is a junction of L1, L2, and L3 one can write three boundary conditions. First, the continuity equation at l_1 leads to:

$$Q_1(L_1,t) = Q_2(0,t) + Q_3(0,t) \tag{2.8}$$

Alternatively, the flows $Q_1(l_1,t)$, $Q_2(0,t)$, and $Q_3(0,t)$ may be expressed using Fick's first law, and consequently, Equation (2.8) may be rearranged to:

$$-\frac{D_1A_1}{RT}\left(\frac{\partial p_1(x_1,t)}{\partial x_1}\right)_{l_1} = -\frac{D_2A_2}{RT}\left(\frac{\partial p_2(x_2,t)}{\partial x_2}\right)_0 - \frac{D_3A_3}{RT}\left(\frac{\partial p_3(x_3,t)}{\partial x_3}\right)_0 \tag{2.9}$$

In addition, the other two boundary conditions at the common point of the three tubes are as follow:

$$p_1(l_1,t) = p_2(0,t) \tag{2.10}$$

$$p_2(0,t) = p_3(0,t) \tag{2.11}$$

It is important to note that Equations (2.8-2.11) assume that the junction of L1, L2 and L3 has no volume, i.e., there is no accumulation of the gas at this junction. In other words, the junction is treated as a common point of L1, L2 and L3. At the end of the main tube ($x_2 = l_2$) there is no flow, therefore the pressure gradient is always zero:

$$\frac{\partial p_2(l_2,t)}{\partial x_2} = 0 \tag{2.12}$$

The gas flow rate entering the tank may also be expressed using Fick's first law:

$$Q_{tank}(t) = -\frac{D_3A_3}{RT}\left(\frac{\partial p_3(x_3,t)}{\partial x_3}\right)_{l_3} \tag{2.13}$$

Finally, substituting Equation (2.13) into Equation (2.5) yields the sixth boundary condition:

$$\frac{dp_{\text{tank}}(t)}{dt} = -\frac{D_3 A_3}{V}\left(\frac{\partial p_3(x_3,t)}{\partial x_3}\right)_{l_3} \tag{2.14}$$

2.3 Expressions for the time lag in L1, L2 and L3

Application of the Laplace transform to Equation (2.4) along with the initial condition given by Equation (2.6) leads to the following ordinary differential equation:

$$\frac{d^2\bar{p}_i}{dx_i^2} - q_i^2\bar{p}_i + \frac{p_0}{D_i} = 0 \tag{2.15}$$

where, $\bar{p}_i = \bar{p}_i(x_i,s) = \int_0^\infty e^{-st} p_i(x_i,t)\,dt$ and $q_i^2 = \frac{s}{D_i}$. Equation (2.15) has the following particular solution:

$$\bar{p}_i(x_i,s) = M_i \sinh(q_i x_i) + N_i \cosh(q_i x_i) + \frac{p_0}{s} \tag{2.16}$$

The constants M_i and N_i for the three tubes may be determined from the Laplace transforms of the boundary conditions, which are as follows:

For L1 at $x_1 = 0$: $$\left(\frac{d\bar{p}_1}{dx_1}\right)_0 = -\frac{RT}{D_1 A_1}\bar{Q}_1(0,s) \tag{2.17}$$

For L1 at $x_1 = l_1$: $$D_1 A_1\left(\frac{\partial \bar{p}_1}{\partial x_1}\right)_{l_1} = D_2 A_2\left(\frac{\partial \bar{p}_2}{\partial x_1}\right)_0 + D_3 A_3\left(\frac{\partial \bar{p}_3}{\partial x_2}\right)_0 \tag{2.18}$$

For L2 at $x_2 = 0$: $$\bar{p}_2(0) = \bar{p}_1(l_1) \tag{2.19}$$

For L2 at $x_2 = l_2$: $$\left(\frac{\partial \bar{p}_2}{\partial x_2}\right)_{l_2} = 0 \tag{2.20}$$

For L3 at $x_2 = 0$: $$\bar{p}_3(0) = \bar{p}_2(0) \tag{2.21}$$

For L3 at $x_2 = l_3$: $$\left(\frac{\partial \bar{p}_3}{\partial x_3}\right)_{l_3} = -\frac{Vs}{A_3 D_3}\left(\bar{p}_3(l_3) - \frac{p_0}{s}\right) \tag{2.22}$$

It is important to note that Equations (2.18, 2.19) and (2.21) are interchangeable so that each one of them is a valid boundary condition for L1, L2, and L3. For example, in the

above scheme Equation (2.18) is used as a boundary condition for L1; on the other hand, Equation (2.18) could also be used as a boundary condition for L2 and L3.

If $Q_1(0,t)$ follows an ideal step change initiated at t = 0, then $\bar{Q}_1(0,s)=\frac{Q_1(0)}{s}$, where $Q_1(0)$ is constant at $t > 0$. Consequently, substituting Equation (2.16) into Equation (2.17) yields the following expression for M_1:

$$M_1=-\frac{RTQ_1(0)}{sD_1A_1}=-\frac{q_1RTQ_1(0)}{s^2} \tag{2.23}$$

The expressions for the other constants can be obtained by substituting Equation (2.16) into Equations (2.18-2.22) and solving the resulting set of equations. Thus, after some rearrangements the particular solution for L1, L2, and L3 is given by the following expressions:

$$\bar{p}_1-\frac{p_0}{s}=\frac{-M_1}{\cosh(q_1l_1)}\left\{\frac{\begin{array}{l}\sinh\left[q_1(l_1-x_1)\right]+\\ \cosh(q_2l_2)\cosh(q_1x_1)\left[\cosh(q_3l_3)+\frac{Vq_3}{A_3}\sinh(q_3l_3)\right]\end{array}}{\Delta(s)}\right\} \tag{2.24}$$

$$\bar{p}_2-\frac{p_0}{s}=-M_1\frac{\cosh\left[q_2(l_2-x_2)\right]\left[\cosh(q_3l_3)+\frac{Vq_3}{A_3}\sinh(q_3l_3)\right]}{\Delta(s)} \tag{2.25}$$

$$\bar{p}_3-\frac{p_0}{s}=-M_1\frac{\cosh(q_2l_2)\left\{\cosh\left[q_3(l_3-x_3)\right]+\frac{Vq_3}{A_3}\sinh\left[q_3(l_3-x_3)\right]\right\}}{\Delta(s)} \tag{2.26}$$

In which,

$$\begin{aligned}\Delta(s)=&\left[\cosh(q_2l_2)\sinh(q_1l_1)+\frac{A_2}{A_1}\sqrt{\frac{D_2}{D_1}}\sinh(q_2l_2)\cosh(q_1l_1)\right]\times\\ &\left[\cosh(q_3l_3)+\frac{Vq_3}{A_3}\sinh(q_3l_3)\right]+\\ &\frac{A_3}{A_1}\sqrt{\frac{D_3}{D_1}}\cosh(q_2l_2)\cosh(q_1l_1)\left[\sinh(q_3l_3)+\frac{Vq_3}{A_3}\cosh(q_3l_3)\right]\end{aligned} \tag{2.27}$$

With M_1 given by Equation (2.23), Equations (2.24-2.26) may be rearranged to the following form:

$$\bar{p}_i - \frac{p_0}{s} = \frac{f_i(s)}{s^2\Delta(s)} \tag{2.28}$$

in which f_i for L1, L2 and L3 given by:

$$f_1(s) = \frac{q_1 RTQ_1(0)}{\cosh(q_1 L_1)} \left\{ \begin{array}{l} \sinh\left[q_1(l_1 - x_1)\right]\Delta(s) + \\ \cosh(q_2 l_2)\cosh(q_1 x_1)\left[\cosh(q_3 l_3) + \frac{Vq_3}{A_3}\sinh(q_3 l_3)\right] \end{array} \right\} \tag{2.29}$$

$$f_2(s) = q_1 RTQ_1(0)\cosh\left[q_2(l_2 - x_2)\right]\left[\cosh(q_3 l_3) + \frac{Vq_3}{A_3}\sinh(q_3 l_3)\right] \tag{2.30}$$

$$f_3(s) = q_1 RTQ_1(0)\cosh(q_2 l_2)\left\{\cosh\left[q_3(l_3 - x_3)\right] + \frac{Vq_3}{A_3}\sinh\left[q_3(l_3 - x_3)\right]\right\} \tag{2.31}$$

It can be shown that for each tube $f_i(s)/\Delta(s)$ is regular (has a finite value) at $s = 0$. Thus, according to the concept of the asymptotic solution [15], the expression for time lag in each tube can be evaluated from:

$$\theta_i(x_i) = \lim_{s\to 0}\left(\frac{\Delta'(s)}{\Delta(s)} - \frac{f_i'(s)}{f_i(s)}\right) = \lim_{s\to 0}\left(\frac{\Delta'(s)}{\Delta(s)}\right) - \lim_{s\to 0}\left(\frac{f_i'(s)}{f_i(s)}\right) \tag{2.32}$$

Evaluation of Equation (2.32) leads to the following expressions for the time lag:

In L1: $$\theta_1(x_1) = \Phi - \left(1 + 2\frac{V_{total} - A_1 l_1}{A_1(l_1 - x_1)}\right)\frac{(l_1 - x_1)^2}{2D_1} - \frac{l_2^2}{2D_2} - \left(1 + 2\frac{V}{A_3 l_3}\right)\frac{l_3^2}{2D_3} \tag{2.33}$$

In L2: $$\theta_2(x_2) = \Phi - \frac{(l_2 - x_2)^2}{2D_2} - \left(1 + 2\frac{V}{A_3 l_3}\right)\frac{l_3^2}{2D_3} \tag{2.34}$$

In L3: $$\theta_3(x_3) = \Phi - \frac{l_2^2}{2D_2} - \left(1 + 2\frac{V}{A_3(l_3 - x_3)}\right)\frac{(l_3 - x_3)^2}{2D_3} \tag{2.35}$$

where, Φ is a contribution to the time lag, which is independent of the position of the pressure sensor, given by the following expression:

$$\Phi = 2\frac{V}{A_3 l_3}\left(1 - \frac{A_3 l_3 + V}{V_{total}}\right)\frac{l_3^2}{2D_3} + \sum_{i=1}^{3}\frac{l_i^2}{2D_i}\left(1 - \frac{2}{3}\frac{A_i l_i}{V_{total}}\right) \tag{2.36}$$

in which, $$V_{total} = A_1 l_1 + A_2 l_2 + A_3 l_3 + V \tag{2.37}$$

The details of the algebra involved in evaluation of Equation (2.32) are presented in the Appendix.

2.4 Discussion

2.4.1 Verification of the mathematical solution

At the common point of L1, L2 and L3, the respective time lags $\theta_1(L_1)$, $\theta_2(0)$, and $\theta_3(0)$ should be the same. Indeed, substituting $x_1 = l_1$ into Equation (2.33), $x_2 = 0$ into Equation (2.34), and $x_3 = 0$ into Equation (2.35) yields the following expression for the time lag at the common point (θ_{cp}):

$$\theta_{cp} = \theta_1(l_1) = \theta_2(0) = \theta_3(0) = \Phi - \frac{l_2^2}{2D_2} - \left(1 + 2\frac{V}{A_3 l_3}\right)\frac{l_3^2}{2D_3} \tag{2.38}$$

In a special case, in which, $l_2 = l_3 = 0$, that is, the receiver comprises of a single tube L1 and a tank attached to its end, Equation (2.33) simplifies to Equation (2.3). In another special case, in which $l_2 = l_3 = 0$ and $V = 0$, that is the receiver consists of a single tube, Equation (2.33) simplifies to Equation (2.1).

2.4.2 Time lag of the receiver

To facilitate the forgoing discussion, it will be assumed that $A_1 = A_2 = A_3 = A$, and consequently, $D_1 = D_2 = D_3 = D$.

If the receiver comprised of a single tube (the main tube only), the resistance of such a receiver could be represented by the time lag determined from the pressure response monitored at the end of the tube. It thus follows from Equation (2.1) that the time lag of the main tube, $\theta(l) = l^2/6D$, where $l = l_1 + l_2$.

Figure 2.2 presents the numerical values of $l^2/6D$ as a function of l for three different internal diameters of 10.2 mm, 3.86 mm and 1.75 mm corresponding to standard 1/2", 1/4", and 1/8" stainless steel tubes, respectively. The diffusion coefficient in Figure 2.2 is calculated using Equation (2.2) assuming that the gas is nitrogen at 23°C. It is evident that as long as $l < 1$ m, $l^2/6D < 1$s even for the 1/8" tube. The time lag of the main tube will be used as a reference throughout the forgoing discussion.

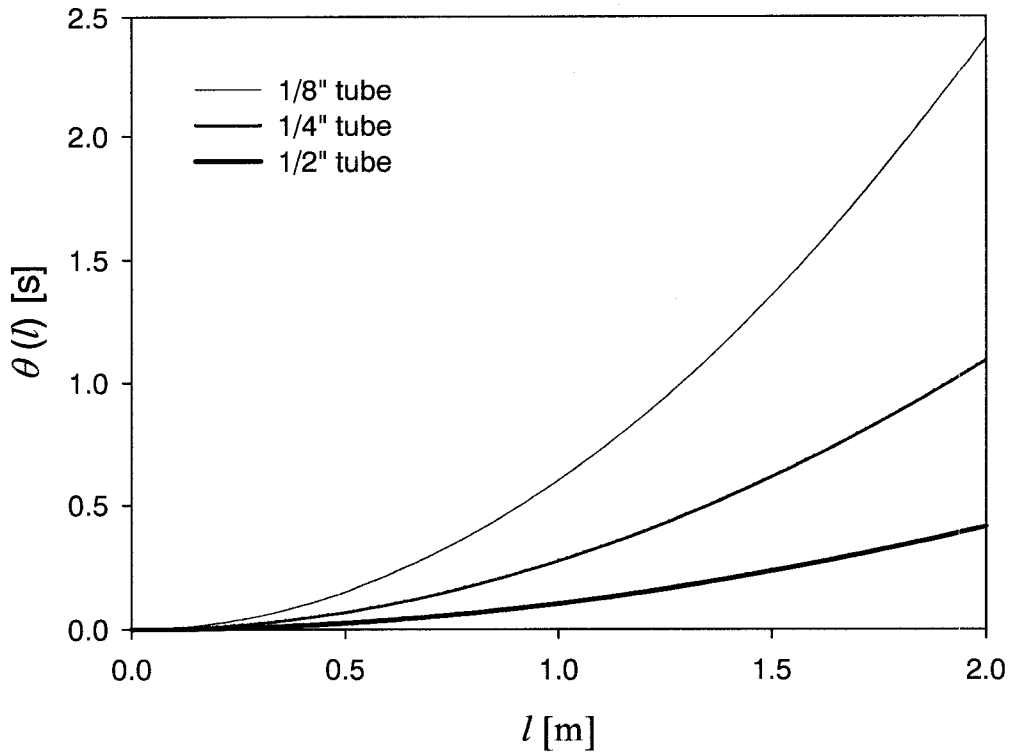

Figure 2.2. Time lag of a tube as a function of its length for different tube diameters.

By analogy, if in addition to the main tube the receiver also consisted of a tank along with a connecting tube, as shown in Figure 2.1, the resistance of such a receiver could be represented by the time lag determined from the pressure response monitored at the end of the main tube. Therefore, the time lag of the receiver depicted in Figure 2.1 can be evaluated using Equation (2.34) with $x_2 = l_2$, i.e.:

$$\theta_2(l_2) = \Phi - \left(1 + 2\frac{V}{Al_3}\right)\frac{l_3^2}{2D} \tag{2.39}$$

To visualize $\theta_2(l_2)$ it is necessary to consider the two terms on the right hand side of Equation (2.39) separately. The first term, Φ, represents a positive contribution to the time lag of the receiver, which appears in every time lag correlation, and which depends on the volume of the tank, the relative position at which the tank is connected to

the main tube (l_1/l), and the length of the connecting tube relative to that of the main tube (l_3/l).

Figure 2.3a presents the dependence of $\frac{\Phi}{l^2/6D}$ on l_1/l and l_3/l in the limiting case, in which $V = 0$. The configuration with $V = 0$, i.e., in which the tank were isolated from the receiver, would be desired if the gas flow rate into the receiver was very low. It is evident that introduction of a side tube L3 to the main tube increases the resistance of the receiver compared to that of the main tube. The maximum increase in the receiver's time lag occurs at $l_1/l = 0$ and 1. At these positions the side tube increases the length of the main tube. For example, for $l_3/l = 0.5$ the length of the main tube becomes $1.5l$ and $\frac{\Phi}{l^2/6D}$ reaches the maximum value of $(1.5)^2 = 2.25$. On the other hand, for $l_3/l = 0.5$, $\frac{\Phi}{l^2/6D}$ reaches the minimum value of 1.75 at $l_1/l = 0.5$. In other words, attaching a side tube to the main tube increases the resistance of the receiver, but the total resistance is never greater than that corresponding to the configuration, in which the side tube is attached to either end of the main tube.

Figure 2.3b presents the dependence of $\frac{\Phi}{l^2/6D}$ on l_1/l and V/lA in another limiting case in which $l_3 = 0$. It is important to note that a short leading tube is usually an integral part of commercially available tanks. In addition, if a tank is to be included to or excluded from the receiver, there should be a valve on L3, and the tubing inside this valve would contribute to l_3. Therefore, in reality the limiting case, in which $l_3 = 0$, does not exist. It is important to emphasize that although the tank has no resistance, its presence increases the resistance of the receiver compared to that of the main tube. Moreover, the dependence of $\frac{\Phi}{l^2/6D}$ on l_1/l in Figure 2.3b is similar to that in Figure 3a, with the maxima at $l_1/l = 0$ and $l_1/l = 1$, and the minimum at $l_1/l = 0.5$. At a given position,

$\frac{\Phi}{l^2/6D}$ increases with V, but this effect is significant only up to $V/lA = 10$. At $l_1/l = 0$ and $l_1/l = 1$, when $V/lA \to \infty$, $\frac{\Phi}{l^2/6D} \to 3$.

Figure 2.3c presents $\frac{\Phi}{l^2/6D}$ as a function of l_1/l for the case in which $l_3/l = 0.2$ and $V/lA = 10$. The solid curve indicates the actual values obtained using Equation (2.36). The dashed curve is obtained by adding the curve for $l_3/l = 0.2$ from Figure 2.3a to the curve for $V/lA = 10$ from Figure 2.3b.

Although except for $l_1/l \approx 0.5$ the dashed curve is above the solid curve in Figure 2.3c, the closeness of the two curves indicates that resistance contributions arising from the presence of the tank and the presence of the connecting tube are additive approximately. In general, while the contribution of Φ to the time lag of the receiver varies considerably depending on l_1/l, l_3/l and V/lA, this contribution in a properly designed system, in which L1 is a 1/2" tube and its length is short, should be less than a second, and thus negligible.

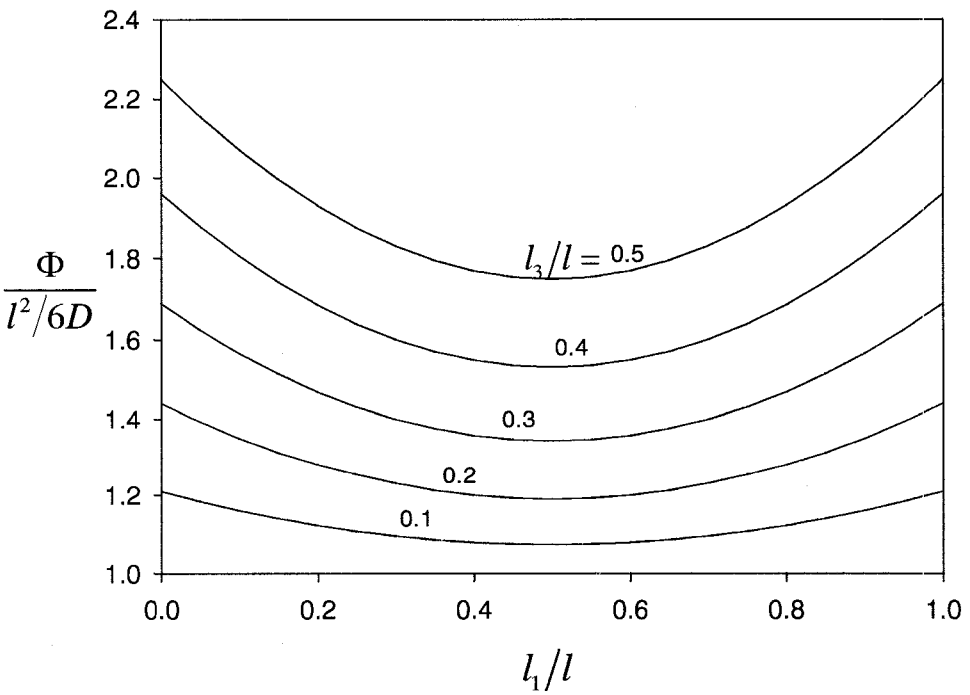

a)

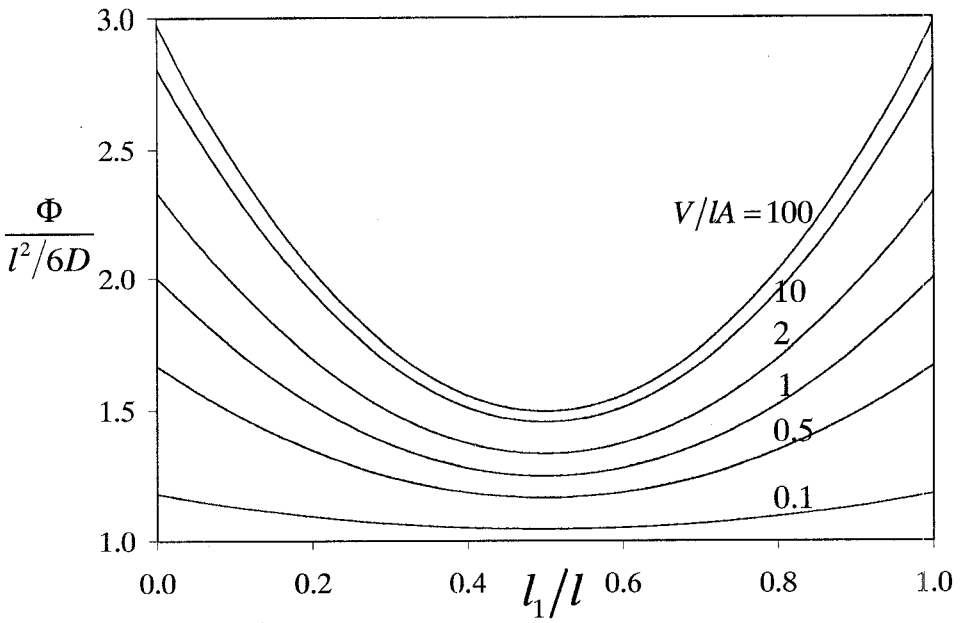

b)

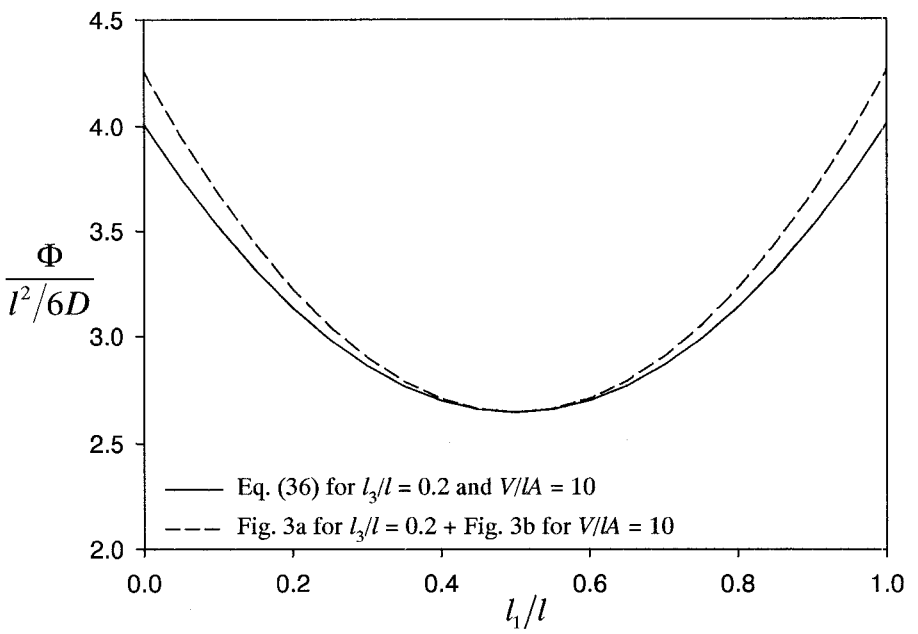

c)

Figure 2.3. Effect of the relative position of the tank (l_1/l) on the relative positive contribution $\left(\frac{\Phi}{l^2/6D}\right)$ for: (a) the limiting case of V/lA = 0; (b) the limiting case of l_3/l = 0; (c) the case of V/lA = 10 and l_3/l = 0.2. The positive contribution Φ evaluated from Equation (2.36) with $A_1 = A_2 = A_3 = A$ and $D_1 = D_2 = D_3 = D$.

Figure 2.4 presents the relative time lag of the receiver, $\frac{\theta_2(l_2)}{l^2/6D}$, as a function of l_3/l and V/lA. The time lag of the receiver, $\theta_2(l_2)$, is evaluated using Equation (2.39) assuming that the tank is connected to the main tube at $l_1/l = 0.2$. It is evident that unless V/lA is of order of unity, the second term on the right hand side of Equation (2.39) has a dominant effect on the numerical value of receiver's time lag. For $V/lA > 10$, the relative time lag of the receiver quickly becomes a large negative number with increase in l_3/l.

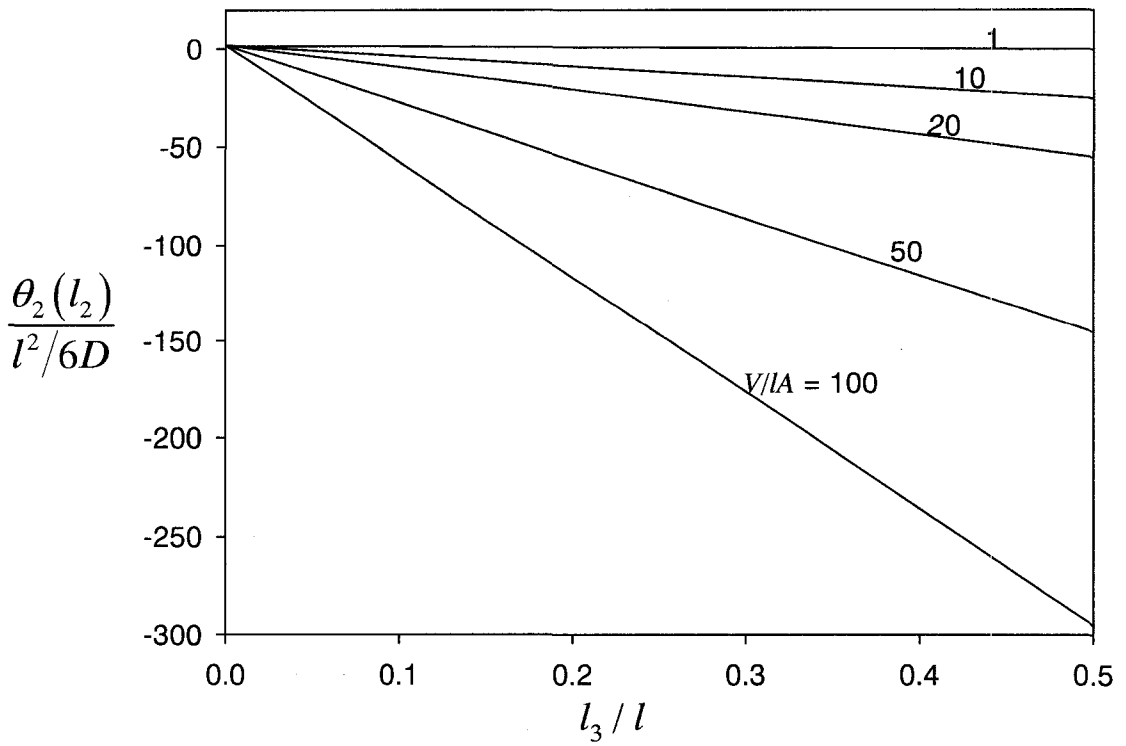

Figure 2.4. Effect of the relative length of the connecting tube (l_3/l) and the relative volume of the tank (V/lA) on the relative time lag of the receiver, $\frac{\theta_2(l_2)}{l^2/6D}$. The time lag of the receiver evaluated from Equation (2.39) with $A_1 = A_2 = A_3 = A$, $D_1 = D_2 = D_3 = D$, and $l_1/l = 0.2$.

The greater the V/lA, the stronger the effect of l_3/l on the relative time lag of the receiver. In turn, the negative time lag of the receiver may lead to underestimation of the time lag of the medium being tested in the system. One way to minimize the possible

negative error is to minimize the length of the connecting tube L3. On the other hand, even when l_3/l is small but $V/lA > 10$, the relative time lag of the receiver might be a large negative number. The safest way of minimizing the possible negative error is to keep $V/lA < 10$, by minimizing the volume of the tank and using the tubes of large cross-sectional area, such as 1/2" tubes. In principle, decreasing the length of the main tube increases V/lA leading to larger negative values for $\frac{\theta_2(l_2)}{l^2/6D}$. At the same time, the time lag of the main tube also decreases as its length decreases. The net effect of decreasing the length of the main tube on $\theta_2(l_2)$ varies depending l_3/l when V/lA.

2.4.3 Optimum position of the pressure sensor in the receiver

In the discussion so far, it was assumed that the pressure sensor is placed at the end of the main tube. However, the pressure sensor can be installed anywhere along L1, L2 and L3, as well as, in the tank.

The effect of the position of the pressure sensor in L2 on the time lag of the receiver can be evaluated from Equation (2.34). At the end of the main tube i.e., at $x_2 = l_2$ in L2, the 2nd term on the right hand side of Equation (2.34), $-(l_2 - x_2)^2/2D$, becomes zero. Thus, as x_2 decreases from l_2 to 0, the time lag in L2, $\theta_2(x_2)$, decreases. If $\theta_2(l_2)$ is negative, $\theta_2(0)$ will be even more negative. Consequently, unless $V/lA < 1$, the optimum position in L2 is at $x_2 = l_2$. However, it is important to note that the difference between the time lags at the two ends of L2 is just $l_2^2/2D$, which should be a fraction of second, unless L2 is long and has a small cross sectional area.

The effect of the position of the pressure sensor in tube L1 on the time lag of the receiver can be evaluated from Equation (2.33). In comparison to Equation (2.39), Equation (2.33) contains two additional negative terms, $-\left(1+2\frac{V_{total}-Al_1}{A(l_1-x_1)}\right)\frac{(l_1-x_1)^2}{2D}$ and $-\frac{l_2^2}{2D}$. The latter term, as already discussed, should be negligible. On the other hand, the former term may be a large negative number.

Figure 2.5a presents the effect of the position of the pressure sensor in L1 (x_1/l_1) on $\frac{\theta_1(x_1)-\theta_{cp}}{l^2/6D}$ for different V/lA. The position at which the tank is connected to the main tube and the length of L3 in Figure 2.5a are fixed at $l_1/l = 0.5$ and $l_3/l = 0.1$, respectively. Since the time lag at the common point θ_{cp} is used as a reference in Figure 2.5, at $x_1/l_1 = 1$ regardless of V/lA, $\frac{\theta_1(x_1)-\theta_{cp}}{l^2/6D} = 0$. It is important to emphasize that θ_{cp}, which is equivalent to $\theta_2(0)$, might be a large negative number. However, even when θ_{cp} is negligible, placing the pressure sensor in L1 may lead to a large negative time lag of the receiver, in particular when the pressure sensor is moved towards the flow source, i.e., when x_1/l_1 decreases. This effect becomes even more evident for large V/lA.

Figure 2.5b illustrates the effect of the position at which the tank is connected to the main tube (l_1/l) and the length of L3 (l_3/l) when the position of the pressure sensor in L1 and the tank's volume are fixed at $x_1/l_1 = 0.5$ and $V/lA = 10$, respectively. It is evident that the time lag of the receiver becomes more negative when l_1/l increases. Therefore, the tank should be connected to the main tube as close as possible to the flow source. Although the possible negative error in time lag of the medium being tested might be minimized by decreasing l_1/l, the pressure sensor should never be installed in L1. For a given l_1/l, the time lag of the receiver becomes more negative when l_3/l increases. However, the effect of l_3/l on the time lag is rather weak.

Considering Equations (2.35) and (2.38); if the pressure sensor is installed in L3, i.e., at $x_3 > 0$, the time lag $\theta_3(x_3)$ becomes greater than θ_{cp} because the negative contribution arising from the term $\left[1+2V/A(l_3-x_3)\right](l_3-x_3)^2/2D$ decreases as x_3 increases. In the limit of $x_3 = l_3$, i.e., when the pressure sensor is installed in the tank, Equation (2.35) becomes:

$$\theta_3(l_3) = \Phi - \frac{l_2^2}{2D} \tag{2.40}$$

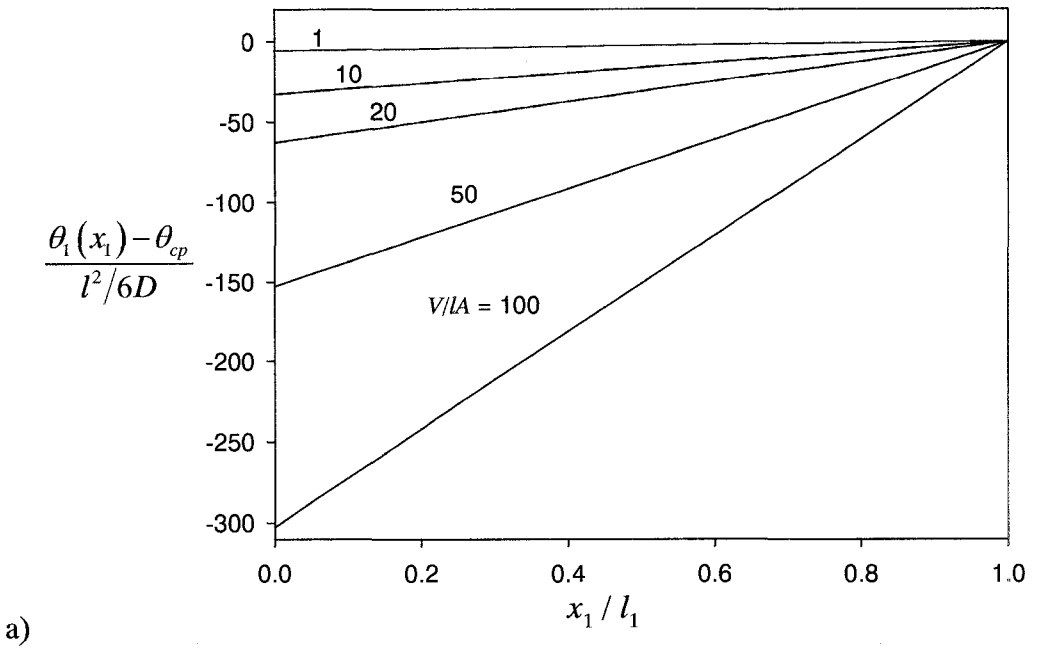

a)

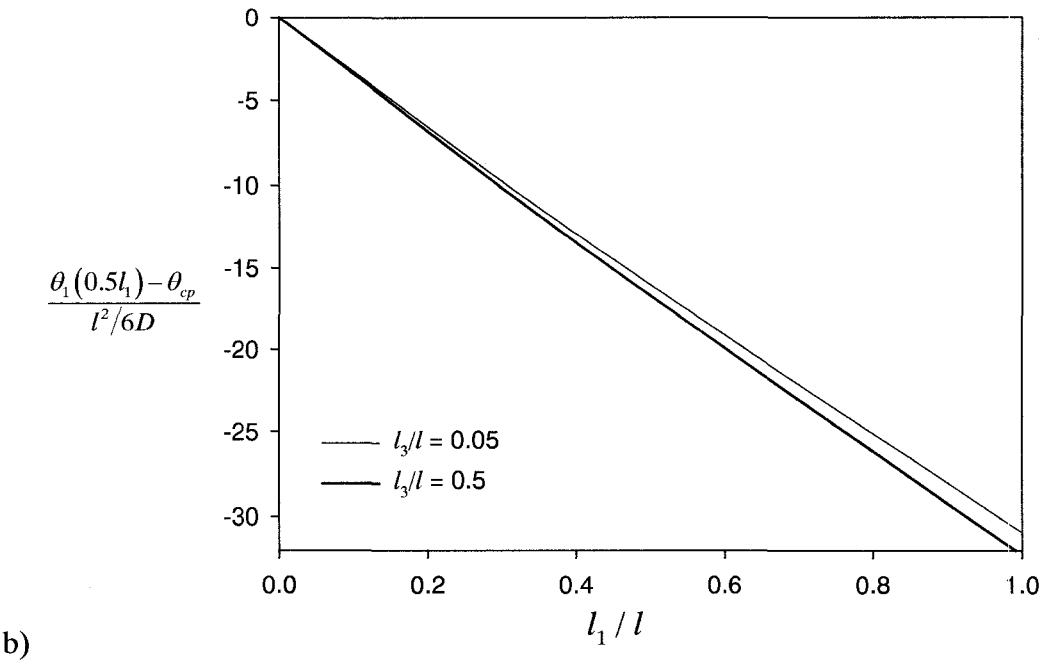

b)

Figure 2.5. The relative time lag of the receiver determined from the pressure response monitored in L1, $\frac{\theta_1(x_1)}{l^2/6D}$, as a function of (a) the relative position of the pressure sensor (x_1/l_1) for different relative volumes of the tank (V/lA) when l_1/l = 0.5 and l_3/l = 0.1; (b) the relative position of the tank (l_1/l) for different relative lengths of the connecting tubes (l_3/l) when x_1/l_1 = 0.5 and V/lA = 10.

As already discussed, in properly designed receiver Φ and $l_2^2/2D$ should not exceed a second each. It is therefore evident, that the best position for the pressure sensor in the receiver's configuration shown in Figure 2.1 is the tank. On the other hand, to allow a wide range of gas flow rates into the receiver, if only one pressure sensor is available, it cannot be installed in the tank, because the tank may or may not be included in the receiver's volume. In this case, the pressure sensor should be installed downstream from the common point, preferably towards the end of the main tube. However, the possibility of a negative time lag of the receiver should be considered.

It is important to keep in mind that all expressions for the time lag derived and discussed in this paper rely on the assumption of a constant diffusion coefficient. In reality, even when the receiver were initially at an ultrahigh vacuum, the conditions for the Knudsen flow regime would quickly disappear because of gas accumulation after initiation of the flow. As shown in Ref. [9], an increase in the diffusion coefficient during the course of a time lag experiment may actually magnify the negative error in the time lag of the tested medium. On the other hand, if the receiver were initially at a moderate vacuum (few mmHg absolute) corresponding to a viscous flow regime, the initial diffusion coefficient would be much greater than the Knudsen diffusion coefficient, leading to a negligible resistance of the receiver even in its least favorable configuration.

2.5 Conclusions

The resistance to gas accumulation in a receiver consisting of a main tube, a tank and a tube connecting the main tube with the tank was investigated theoretically by considering the pressure responses within the receiver to a constant gas flow entering at one end of the main tube. Assuming that gas accumulation is a diffusive process characterized by a constant diffusion coefficient for a given tube diameter, the resistance of the receiver was quantified by using the concepts of the asymptotic solution and the time lag.

Although the resistances of individual tubes in the receiver are very small and the resistance of the tank is negligible, the resistance of the entire receiver might be characterized by a large negative time lag. The time lag of the receiver strongly depends

on the position within the receiver where the pressure response is monitored, as well as, on the volume of the tank and the position where the tank is connected to the main tube.

The following points may be used as guidelines for the design of the receiver's configuration. To minimize the possible errors due to the resistance of the receiver, the volume of the tank should not be much greater than the volume of the main tube; the latter volume should be maximized by using the tubes of large internal diameter (at least 1/2"). The magnifying effect of the tank's volume of the receiver resistance can be diminished by attaching the tank as close as possible to the flow source. Considering the position within the receiver at which the pressure response is monitored, the pressure sensor should never be installed in the main tube before the tank; the closer the pressure sensor to the flow source the more negative the time lag of the receiver. The optimum location of the pressure sensor in the receiver is in the tank. On the other hand, considering that the tank may or may not be included in the receiver's volume, if a single pressure sensor is available, it cannot be installed in the tank. Then, the pressure sensor should be installed towards the end of the main tube, downstream from the point at which the tank is attached to the main tube.

In case of an existing system in which the outflow receiver resembles the configuration considered here, the derived expressions for the time lag may be used to assess if the effects of the resistance to gas accumulation in the receiver are significant or not.

Acknowledgement

The authors gratefully acknowledge the financial support for this project provided by the Natural Science and Engineering Research Council of Canada.

Nomenclature

A: Cross-sectional area of tube (m^2)

D: Diffusion coefficient of gas in tube ($m^2 s^{-1}$)

D_m: Diffusion coefficient of gas in membrane ($m^2 s^{-1}$)

l: Length of tube (m)

L1, L2, L3: Tubes that are part of the receiver with lengths l_1, l_2, l_3, respectively.

M: Molar mass (kg mol^{-1})

p : Pressure (Pa)

P_m: Permeability coefficient of gas in membrane (m^3(STP) $m^{-1}Pa^{-1}s^{-1}$)

p_o: Initial pressure (Pa)

Q: Gas flow rate (kmol s^{-1})

r: Internal radius (m)

R: Gas constant (J $K^{-1}mol^{-1}$)

S_m: Solubility coefficient of gas in membrane (m^3(STP) m^{-3} Pa^{-1})

t: Time (s)

T: Absolute temperature (K)

V: Volume of tank (m^3)

V_{total}: Total volume of the receiver (m^3)

x: Distance from the entrance of a tube (m)

Greek Symbols:

α : Constant defined by Equation (2.A15) (-)

β : Constant defined by Equation (2.A24) (-)

γ_1: Constant defined by Equation (2.A11) (-)

γ_2: Constant defined by Equation (2.A12) (-)

γ_3: Constant defined by Equation (2.A13) (-)

θ: Time lag of receiver (s)

Φ : Positive contribution to the time lag of receiver (s)

References

1. H.A. Daynes, The process of diffusion through a rubber membrane, Roy. Soc. Proc., A97 (1920) 286.
2. E.L. Cussler, "Diffusion Mass Transfer in Fluid Systems", Cambridge University Press, 1984, pp. 78-81.
3. B. Kruczek, H.L. Frisch and R. Chapanian, Analytical solution for the effective time lag of a membrane in a permeate tube collector in which Knudsen flow regime exists, J. Membr. Sci., 256 (2005) 57.
4. J. Crank, The Mathematics of Diffusion, Clarendod Press, Oxford, 1975, pp.49-51.
5. S.W. Rutherford and D.D. Do, Review of time lag permeation technique as a method for characterization of porous media and membranes, Adsorption, 3 (1997) 283.
6. G.E. Favre, N. Morliere, D. Roizard, Experimental evidence and implications of an imperfect upstream pressure step for the time lag technique, J. Membr. Sci., 207 (2002) 59.
7. L.B. Loeb, The Kinetic Theory of Gases, Dover Publications, Inc. New York, 1961, pp 278-300.
8. R. Aris, The Mathematical Theory of Diffusion and Reaction in Permeable Catalysts", Clarendon Press, Oxford, 1975, pp. 20-23.
9. R. Checchetto, N. Bazzanella, B. Patton and A. Miotello, Palladium membranes prepared by r. f. magnetron sputtering for hydrogen purification, Surface and Coatings tech., 177-178 (2004) 73.
10. J. Sanchez, C.L. Gijiu, V. Hynek, O. Muntean, A. Julbe, The application of transient time-lag method for the diffusion coefficient estimation on zeolites composite membranes, Sep. Purification Tech., 25 (2001) 467.
11. B. Kruczek, F. Shemshaki, S. Lashkari, R. Chapanian and H.L. Frisch, Effect of a resistance-free tank on the resistance to gas transport in high vacuum tube, J. Membr. Sci., 280 (2006) 29-36.
12. D.R. Kemp, The Diffusion Time Lag in Heterogeneous Polymer Membranes, PhD Dissertation, University of Texas at Austin, 1972.

13. A. Tabe Mohammadi, T. Matsuura and S. Sourirajan, Design and construction of gas permeation system for the measurement of low permeation rated and permeate compositions, J. Membr. Sci., 98 (1995) 281.
14. W.-H. Lin, R.H. Vora, T.-S. Chung, Gas transport properties of 6FDA-Durene/1,4-phenylenediamine (pPDA) copolyimides, J. Polym. Sci., Part B: Polym. Phys., 38 (2000), 2703.
15. H.S. Carslaw and J.C. Jaeger, Conduction of Heat in Solids, Oxford at the Clarendon Press, 2nd Edition, 1959, p. 402.

Appendix:

Evaluation of Equation (2.32) requires differentiation of Equations (2.27) and (2.29-2.31), which is a very tedious step because of the complexity of the expressions for $\Delta(s)$ and $f_i(s)$. The differentiation step will be illustrated using the example of $f_2(s)$.

First, it is convenient to transform the pertinent differential operators such that:

$$\frac{df_2}{ds} = \frac{df_2}{dq_i}\frac{dq_i}{ds} = \left(\frac{1}{2D_i q_i}\right)\frac{df_2}{dq_i} \tag{2.A1}$$

Also, since $q_2 = q_1\sqrt{D_1/D_2}$ and $q_3 = q_1\sqrt{D_1/D_3}$:

$$\frac{\partial f_2}{\partial q_1} = \sqrt{\frac{D_1}{D_2}}\frac{\partial f_2}{\partial q_2} = \left(\frac{D_1 q_1}{D_2 q_2}\right)\frac{\partial f_2}{\partial q_2} \text{ and } \frac{\partial f_2}{\partial q_1} = \sqrt{\frac{D_1}{D_3}}\frac{\partial f_2}{\partial q_3} = \left(\frac{D_1 q_1}{D_3 q_3}\right)\frac{\partial f_2}{\partial q_3} \tag{2.A2}$$

Thus,

$$f_2'(s) = \frac{1}{(2D_1 q_1)}\left(\frac{f_2(s)}{q_1}\right) + \frac{q_1 RTQ_1(0)}{(2D_1 q_1)}\sqrt{\frac{D_1}{D_2}}q_2(l_2 - x_2)^2\frac{\sinh\left[q_2(l_2 - x_2)\right]}{q_2(l_2 - x_2)}\times$$
$$\left[\cosh(q_3 l_3) + \frac{Vq_3}{A_3}\sinh(q_3 l_3)\right] + \frac{q_1 RTQ_1(0)}{(2D_1 q_1)}\sqrt{\frac{D_1}{D_3}}q_3\cosh\left[q_2(l_2 - x_2)\right]\times$$
$$\left[\left(l_3^2 + \frac{V}{A_3}l_3\right)\frac{\sinh(q_3 l_3)}{q l_3} + \frac{V}{A_3}l_3\cosh(q_3 l_3)\right]$$

Consequently,

$$\lim_{s\to 0}\frac{f_2'(s)}{f_2(s)} = \lim_{s\to 0}\phi_1 + \lim_{s\to 0}\phi_2 + \lim_{s\to 0}\phi_3 \tag{2.A3}$$

where,

$$\phi_1 = \frac{1}{2D_1 q_1^2} \tag{2.A4}$$

$$\phi_2 = \frac{\frac{D_1}{D_2}(l_2 - x_2)^2 \frac{\sinh\left[q_2(l_2 - x_2)\right]}{q_2(l_2 - x_2)}}{2D_1 \cosh\left[q_2(l_2 - x_2)\right]} \tag{2.A5}$$

$$\phi_3 = \frac{\frac{D_1}{D_3}\left[\left(l_3^2 + \frac{V}{A_3}l_3\right)\frac{\sinh(q_3 l_3)}{q_3 l_3} + \frac{V}{A_3}l_3 \cosh(q_3 l_3)\right]}{2D_1\left(\cosh(q_3 l_3) + \frac{Vq_3}{A_3}\sinh(q_3 l_3)\right)} \tag{2.A6}$$

The expressions for ϕ_2 and ϕ_3 can be simplified by using Taylor series expansion. Ignoring the terms with the power of four and greater, the hyperbolic sine and cosine are approximated by:

$$\sinh(y) = y + \frac{y^3}{3!} + \ldots$$

$$\cosh(y) = 1 + \frac{y^2}{2!} + \ldots$$

Thus,

$$\phi_2 = \frac{(l_2 - x_2)^2\left(1 + \frac{q_2^2(l_2 - x_2)^2}{6} + \cdots\right)}{2D_2\left(1 + \frac{q_2^2(l_2 - x_2)^2}{2} + \cdots\right)} \tag{2.A7}$$

$$\phi_3 = \frac{\left(l_3^2 + \frac{V}{A_3}l_3\right)\left(1 + \frac{q_3^2 l_3^2}{6} + \cdots\right) + \frac{V}{A_3}l_3\left(1 + \frac{q_3^2 l_3^2}{2} + \cdots\right)}{2D_3\left[\left(1 + \frac{q_3^2 l_3^2}{2} + \cdots\right) + \frac{Vq_3}{A_3}\left(q_3 l_3 + \frac{q_3^3 l_3^3}{6} + \cdots\right)\right]} \tag{2.A8}$$

Since when $s \to 0$ $q_1, q_2, q_3 \to 0$, substituting Equations (2.A4), (2.A7) and (2.A8) back into Equation (2.A3) leads to:

$$\lim_{s\to 0}\frac{f_2'(s)}{f_2(s)}=\lim_{s\to 0}\frac{1}{2D_1q_1^2}+\frac{(l_2-x_2)^2}{2D_2}+\frac{l_3^2}{2D_3}+\frac{V}{A_3D_3}l_3 \tag{2.A9}$$

Using a similar procedure it can be shown that in general:

$$\lim_{s\to 0}\frac{f_i'(s)}{f_i(s)}=\lim_{s\to 0}\frac{1}{2D_1q_1^2}+\gamma_i \tag{2.A10}$$

where,

$$\gamma_1=\left(1+2\frac{V_{total}-A_1l_1}{A_1(l_1-x_1)}\right)\frac{(l_1-x_1)^2}{2D_1}+\frac{l_2^2}{2D_2}+\left(1+2\frac{V}{A_3l_3}\right)\frac{l_3^2}{2D_3} \tag{2.A11}$$

$$\gamma_2=\frac{(l_2-x_2)^2}{2D_2}+\frac{l_3^2}{2D_3}+\frac{V}{A_3D_3}l_3 \tag{2.A12}$$

$$\gamma_3=\frac{l_2^2}{2D_2}+\left(1+2\frac{V}{A_3(l_3-x_3)}\right)\frac{(l_3-x_3)^2}{2D_3} \tag{2.A13}$$

In addition, the procedure outlined above leads to:

$$\lim_{s\to 0}\frac{\Delta'(s)}{\Delta(s)}=\lim_{s\to 0}\left[\frac{\frac{V_{total}}{A_1}\cosh(q_3l_3)\cosh(q_2l_2)\cosh(q_1l_1)}{(2D_1q_1^2)(\Delta(s)/q_1)}\right]+\alpha \tag{2.A14}$$

where,

$$\alpha=3\frac{V}{A_3l_3}\frac{(A_1l_1+A_2l_2)}{V_{total}}\frac{l_3^2}{2D_3}+\sum_{i=1}^{3}\frac{l_i^2}{2D_i}\left(1-\frac{A_il_i}{V_{total}}\right) \tag{2.A15}$$

It evident that when $s\to 0$, the first term in Equation (2.A10) and in Equation (2.A14) approach to infinity.

Substituting Equations (2.A10) and (2.A14) into Equation (2.32) provides the general expression for the time lag:

$$\theta_i(x_i) = \lim_{s\to 0} \frac{\frac{V_{total}}{A_1}\cosh(q_3 l_3)\cosh(q_2 l_2)\cosh(q_1 l_1)}{(2D_1 q_1^2)(\Delta(s)/q_1)} + \alpha - \lim_{s\to 0}\frac{1}{2D_1 q_1^2} - \gamma_i \quad (2.A16)$$

The two infinity terms in Equation (2.A16) can be combined into a single term:

$$\beta = \lim_{s\to 0}\left[\frac{\frac{V_{total}}{A_1}\cosh(q_3 l_3)\cosh(q_2 l_2)\cosh(q_1 l_1)}{(2D_1 q_1^2)(\Delta(s)/q_1)} - \frac{1}{2D_1 q_1^2}\right] \quad (2.A17)$$

Expressing $\Delta(s)$ with Equation (2.27) and V_{total} with Equation (2.37), the above equation becomes:

$$\beta = \lim_{s\to 0}\frac{1}{(2D_1 q_1^2)(\Delta(s)/q_1)}\left\{\begin{array}{l}\left(l_1 + \frac{A_2}{A_1}l_2 + \frac{A_3}{A_1}l_3 + \frac{V}{A_1}\right)\cosh(q_3 l_3)\cosh(q_2 l_2)\cosh(q_1 l_1) - \\ \left[\cosh(q_3 l_3) + \frac{Vq_3}{A_3}\sinh(q_3 l_3)\right]\left[\begin{array}{l} l_1\cosh(q_2 l_2)\frac{\sinh(q_1 l_1)}{q_1 l_1} + \\ \frac{A_2}{A_1}l_2\frac{\sinh(q_2 l_2)}{q_2 l_2}\cosh(q_1 l_1)\end{array}\right] - \\ \frac{A_3}{A_1}\cosh(q_2 l_2)\cosh(q_1 l_1)\left[l_3\frac{\sinh(q_3 l_3)}{q_3 l_3} + \frac{V}{A_3}\cosh(q_3 l_3)\right]\end{array}\right\}$$

After some rearrangements the expression for β may be presented in the following form:

$$\beta = \lim_{s\to 0}\frac{\sigma}{(\Delta(s)/q_1)} - \lim_{s\to 0}\frac{\tau}{(\Delta(s)/q_1)} \quad (2.A18)$$

In which,

$$\sigma = \frac{1}{2D_1 q_1^2}\left\{l_1\cosh(q_3 l_3)\cosh(q_2 l_2)\left[\cosh(q_1 l_1) - \frac{\sinh(q_1 l_1)}{q_1 l_1}\right] + \frac{A_2}{A_1}l_2\cosh(q_3 l_3)\cosh(q_1 l_1)\left[\cosh(q_2 l_2)\right.\right.$$

$$\left.\left. - \frac{\sinh(q_2 l_2)}{q_2 l_2}\right] + \frac{A_3}{A_1}l_3\cosh(q_2 l_2)\cosh(q_1 l_1)\left[\cosh(q_3 l_3) - \frac{\sinh(q_3 l_3)}{q_3 l_3}\right]\right\} \quad (2.A19)$$

and

$$\tau = \frac{V}{2A_3D_3} l_3 \frac{\sinh(q_3 l_3)}{q_3 l_3} \left[l_1 \cosh(q_2 l_2) \frac{\sinh(q_1 l_1)}{q_1 l_1} + \frac{A_2}{A_1} l_2 \frac{\sinh(q_2 l_2)}{q_2 l_2} \cosh(q_1 l_1) \right] \qquad (2.A20)$$

The expressions for $(\Delta(s)/q_1)$, τ and σ can be expanded using Taylor expansions for the hyperbolic sine and cosine functions:

$$\frac{\Delta(s)}{q_1} = \left\{ l_1 \left(1 + \frac{q_2^2 l_2^2}{2} + \cdots \right) \left(1 + \frac{q_1^2 l_1^2}{6} + \cdots \right) + \frac{A_2}{A_1} l_2 \left(1 + \frac{q_2^2 l_2^2}{6} + \cdots \right) \left(1 + \frac{q_1^2 l_1^2}{2} + \cdots \right) \right\} \times$$
$$\left\{ \left(1 + \frac{q_3^2 l_3^2}{2} + \cdots \right) + \frac{V q_3}{A_3} \left(1 + \frac{q_3^2 l_3^2}{6} + \cdots \right) \right\} + \left\{ \frac{A_3}{A_1} \left(1 + \frac{q_2^2 l_2^2}{2} + \cdots \right) \left(1 + \frac{q_1^2 l_1^2}{2} + \cdots \right) \right\} \times$$
$$\left\{ l_3 \left(1 + \frac{q_3^2 l_3^2}{6} + \cdots \right) + \frac{V}{A_3} \left(1 + \frac{q_3^2 l_3^2}{2} + \cdots \right) \right\}$$

$$\sigma = \frac{1}{2D_1 q_1^2} \left\{ l_1 \left(1 + \frac{q_3^2 l_3^2}{2} + \ldots \right) \left(1 + \frac{q_2^2 l_2^2}{2} + \ldots \right) \left[\left(1 + \frac{q_1^2 l_1^2}{2} + \cdots \right) - \left(1 + \frac{q_1^2 l_1^2}{6} + \cdots \right) \right] \right.$$
$$+ \frac{A_2}{A_1} l_2 \left(1 + \frac{q_3^2 l_3^2}{2} + \ldots \right) \left(1 + \frac{q_1^2 l_1^2}{2} + \ldots \right) \left[\left(1 + \frac{q_2^2 l_2^2}{2} + \cdots \right) - \left(1 + \frac{q_2^2 l_2^2}{6} + \cdots \right) \right]$$
$$\left. + \frac{A_3}{A_1} l_3 \left(1 + \frac{q_2^2 l_2^2}{2} + \ldots \right) \left(1 + \frac{q_1^2 l_1^2}{2} + \ldots \right) \left[\left(1 + \frac{q_3^2 l_3^2}{2} + \cdots \right) - \left(1 + \frac{q_3^2 l_3^2}{6} + \cdots \right) \right] \right\}$$

$$\tau = \frac{V}{2A_3D_3} l_3 \left(1 + \frac{q_3^2 l_3^2}{6} + \ldots \right) \left\{ \begin{array}{l} l_1 \left(1 + \frac{q_2^2 l_2^2}{2} + \ldots \right) \left(1 + \frac{q_1^2 l_1^2}{6} + \ldots \right) + \\ \frac{A_2}{A_1} l_2 \left(1 + \frac{q_2^2 l_2^2}{6} + \ldots \right) \left(1 + \frac{q_1^2 l_1^2}{2} + \ldots \right) \end{array} \right\}$$

Since as $s \to 0$, $q_1, q_2, q_3 \to 0$:

$$\lim_{s \to 0} \frac{\Delta(s)}{q_1} = \left(l_1 + \frac{A_2}{A_1} l_2 \right) + \frac{A_3}{A_1} \left(l_3 + \frac{V}{A_3} \right) = \frac{V_{total}}{A_1} \qquad (2.A21)$$

$$\lim_{s\to 0}\frac{\sigma}{\left(\Delta(s)/q_1\right)}=\frac{\left(l_1^3+\frac{A_2}{A_1}\frac{D_1}{D_2}l_2^3+\frac{A_3}{A_1}\frac{D_1}{D_3}l_3^3\right)}{6D_1\frac{V_{total}}{A_1}} \tag{2.A22}$$

$$\lim_{s\to 0}\frac{\tau}{\left(\Delta(s)/q_1\right)}=\frac{\frac{V}{A_3}l_3\left(l_1+\frac{A_2}{A_1}l_2\right)}{2D_3\frac{V_{total}}{A_1}} \tag{2.A23}$$

Substituting Equations (2.A21-2.A23) back into Equation (2.A18) yields, after some rearrangements, the following expression:

$$\beta=\sum_{i=1}^{3}\frac{l_i^2}{6D_i}\left(\frac{A_i l_i}{V_{total}}\right)-\frac{V}{A_3 l_3}\frac{\left(A_1 l_1+A_2 l_2\right)}{V_{total}}\frac{l_3^2}{2D_3} \tag{2.A24}$$

Introducing a new constant, $\Phi=\alpha+\beta$, the general expression for the time lag becomes:

$$\theta_i\left(x_i\right)=\Phi-\gamma_i \tag{2.A25}$$

where, Φ is obtained by adding Equations (2.A15) and (2.A24), which leads to Equation (2.36), and γ_i for L1, L2, and L3 is given by Equations (2.A11-2.A13), respectively.

Chapter 3

Effect of Resistance to Gas Accumulation in Multi-Tank Receivers on Membrane Characterization by the Time Lag Method. Part I: Reconciliation of the membrane properties

S. Lashkari, Q. Wang, B. Kruczek*

To be submitted to Journal of Membrane Science

Department of Chemical Engineering
University of Ottawa
161 Louis Pasteur Street
Ottawa, ON K1N 6N5, Canada
Fax: (613) 562-5172
Phone: (613) 562-5800 ext. 6302
E-mail: kruczek@eng.uottawa.ca

* **To whom correspondence should be addressed.**

Abstract

Time lag method is a widely used technique in constant volume systems for the determination of the diffusion and permeability coefficients of gases in membrane. This technique relies on the assumption that there is no resistance to gas transport downstream from the membrane, which very often is not the case. To recover the actual permeability and diffusion coefficients, it is necessary to accurately model the position-dependent resistance effects. The resistance to gas accumulation was modeled in a generalized multi-tank receiver of a constant volume system, by solving Fick's 2^{nd} law diffusion, which served as a governing partial differential equation, in each tube of the receiver. The diffusion coefficient appearing in each partial differential equation was evaluated using the empirical model of Knudsen, which allowed investigating the effect of transition from Knudsen regime to the slip flow regime on the apparent properties in membrane characterization. The validity of the developed model was verified by successful Reconciliation of the membrane properties from the data obtained in a high resistance receiver. An optimization procedure based on simplex method was used for reconciliation of data. The actual membrane properties were determined in a specially designed low resistance receiver.

Keywords: Knudsen flow, slip flow, time lag, permeability, diffusion coefficient

3.1 Introduction

The mechanism of gas transport through practical polymeric gas separation membranes is exclusively described by the solution-diffusion mechanism. In this model the permeability coefficient (P_m) is a fundamental property of materials, which is expressed as a product of a thermodynamic factor (S_m) called the solubility coefficient, and a kinetic parameter (D_m) called diffusion coefficient [1,2]

$$P_m = S_m D_m \tag{3.1}$$

The diffusion coefficient of a gas in a homogeneous membrane is determined experimentally using the concept of time lag. A common experimental technique involves the procedure in which the inflow and outflow volumes are evacuated to the absolute vacuum or to the lowest possible pressure so degas initially the membrane. The inflow volume is then instantaneously pressurized and the resulting pressure response at the permeate side of membrane is monitored. If the membrane is initially free from the diffusing gas and after pressurization the concentration of the gas is constant at the feed face of membrane and zero at the permeate face of membrane, D_m is correlated with the time lag of membrane (θ_m) by the following equation:

$$\theta_m = \frac{l_m^2}{6D_m} \tag{3.2}$$

where l_m is the membrane thickness. The time lag of membrane is the intercept of the asymptote of the pressure response curve with the time axis. Equation (3.2) was first deducted by Daynes in 1920 [3].

The slope of the asymptote (Z) is used for the determination of the permeability coefficient of a gas in membrane.

$$P_m = \frac{V v_{STP} l_m}{RTA_m p_f} Z \tag{3.3}$$

The V is the outflow volume, i.e., the volume of the receiver, v_{STP} is the volume of one mole of gas at standard temperature (273.15 K) and pressure (101, 325 Pa), R is the universal gas constant, T is the absolute temperature, A_m is the membrane area, and p_f is the feed pressure. It is important to note that p_f in Equation (3.3) represents the pressure gradient across the membrane. This implies that the pressure at the permeate side of

membrane is the same as the initial pressure (p_o), i.e., equal to zero. Knowing D_m and P_m, allows determination of S_m from Equation (3.1). Thus, the three gas transport coefficients can be evaluated based on the asymptote of the pressure response curve in a single gas permeation experiment [4].

The accuracy of the time lag given by Equation (3.2) depends on the accuracy of the slope of the asymptote. It has been suggested that steady state flow is achieved, to a good approximation, after 2.5 - 3 time lags [5]. However, the actual time corresponding to the three time lags might be very long. To address this problem, Rogers et al. developed the analysis for the determination of the diffusion coefficient from the pressure response before the steady flow is attained [6]. Also, after three time lags the assumption of zero concentration at the permeate face of membrane is no longer valid, in particular when the volume of the receiver is very small. The mathematical solution for the finite volume of the receiver, i.e. when the concentration of the gas at the permeate face of membrane varies with time was obtained by Paul and Dibenedetto [7]. Ash et al., extended time lag analysis to composite membranes consisting of homogeneous layers [8]. In all these amendments of the original time lag analysis the original Daynes assumption of applicability of Henry's law and concentration independent diffusion coefficient had been retained. Extensions of the analysis in which S_m and D_m vary across the membrane have also been developed [8-10] and are now commonly used. Although not explicitly stated, the time lag analysis relies on the assumption that the entire resistance to gas transport during the gas permeation experiment comes from the tested medium. In other words, the pressure within the outflow volume is uniform at a given time.

In our recent publications [11-13], we have challenged this unwritten assumption. First, considering accumulation in a closed cylindrical tube, in which the gas transport is governed by Knudsen diffusion, we have showed that the pressure response right after initiation of the gas flow must depend on the distance from the gas source of the gas flow [11]. This theoretical result was confirmed experimentally; moreover, we have showed both theoretically and experimentally that the presence of a resistance-free tank at the end of the tube dramatically increases the resistance in the tube [12]. Finally, we have

extended the analysis of the effect of the resistance-free tank by theoretically varying its position from the beginning to the end of the tube [13].

The objective of this series of papers is to extend the analysis of the effect of resistance to gas accumulation to complex configurations of real receivers. In Part I, the actual data from the time lag experiments obtained under the conditions of high resistance to gas accumulation are reconciled to extract the actual diffusion, permeability and solubility coefficients of membrane, by means of solving numerically a set of the governing partial differential equations (PDE). Such extracted diffusion and permeability coefficients are then compared with the respective values obtained in a system in which the resistance to gas accumulation is minimized. In Part II, the analysis from Ref. [13] is extended by allowing multiple resistance-free tanks in the outflow volume. This generalization allows modeling of any configuration of the outflow receiver, including the two used in Part I.

3.2 Background

In the solution diffusion model, the diffusion across the membrane is a rate controlling step. Therefore, the gas transport in a homogeneous membrane following a step change in the feed side pressure is governed by the Fick's 2nd law of diffusion:

$$\frac{\partial C(x',t)}{\partial t} = -D_m \frac{\partial^2 C(x',t)}{\partial x'^2} \tag{3.4}$$

where, C is the concentration of a gas in the membrane, x' is the distance along the membrane thickness measured from the feed side of the membrane, and t is the time elapsed from the step change in the feed side pressure. It is important to note that D_m in Equation (3.4) is assumed to be independent of C. In addition, if the membrane is initially free of the diffusing gas, the initial and boundary conditions can be expressed by:

$$\begin{aligned} &t = 0, && C(x',0) = 0 \\ &t > 0, \quad x' = 0, && C(0,t) = C_f \\ &t > 0, \quad x' = l_m, && C(l_m,t) \approx 0 \end{aligned} \tag{3.5}$$

where, C_f is the gas concentration at the upstream face of the membrane. In the solution-diffusion model C_f can be related to the feed pressure (p_f) by the following expression:

$$C_f = p_f S_m = p_f \frac{P_m}{D_m} \tag{3.6}$$

If S_m is independent of pressure, Equation (3.6) corresponds to Henry's law.

Analytical solution of Equation (3.4), subject to the specified initial and boundary conditions, was obtained by separation of variables, is given by the following expression [14]:

$$C(x',t) = \frac{p_f P_m}{D_m}\left(1 - \frac{x'}{l_m}\right) - 2\frac{p_f P_m}{D_m \pi} \times \sum_{n=1}^{\infty} \frac{1}{n} \sin\left(\frac{n\pi x'}{l_m}\right) \exp\left(-\frac{D_m n^2 \pi^2 t}{l_m^2}\right) \tag{3.7}$$

The diffusive flux of the gas within the membrane (N) is given by the Fick's 1st law of diffusion:

$$N(x',t) = -D_m \frac{\partial C(x',t)}{\partial x'} \tag{3.8}$$

Substituting the first derivative of Equation (3.7) with respect to x' into Equation (3.8) and evaluating the obtained expression at $x' = l_m$ yields the equation for the time dependent flux of the gas leaving the membrane:

$$N(l_m,t) = \frac{p_f P_m}{l_m} + \frac{2p_f P_m}{l_m} \times \sum_{n=1}^{\infty} (-1)^n \exp\left(\frac{-n^2 \pi^2 D_m t}{l_m^2}\right) \tag{3.9}$$

Multiplying Equation (3.9) by the membrane area and integrating it with respect to t yields the amount of gas that had accumulated at the permeate side of the membrane at a given time. Assuming applicability of the ideal gas law, the time dependent change in the pressure at the permeate side of the membrane is given by the following equation:

$$p(t) = \frac{A_m p_f P_m RT}{V v_{STP} l_m}\left[t - \frac{l_m^2}{6D_m} + \frac{2l_m^2}{\pi^2 D_m} \times \sum_{n=1}^{\infty} \frac{(-1)^{n+1}}{n^2} \exp\left(-\frac{D_m n^2 \pi^2 t}{l_m^2}\right)\right] \tag{3.10}$$

Figure 3.1 presents a graphical representation of Equation (3.10). The last term on the right-hand side of Equation (3.10) contains an exponential function with a negative argument, which is proportional to t. Consequently as t increases, the last term on the right-hand side of Equation (3.10) disappears and the pressure response becomes a linear function of time.

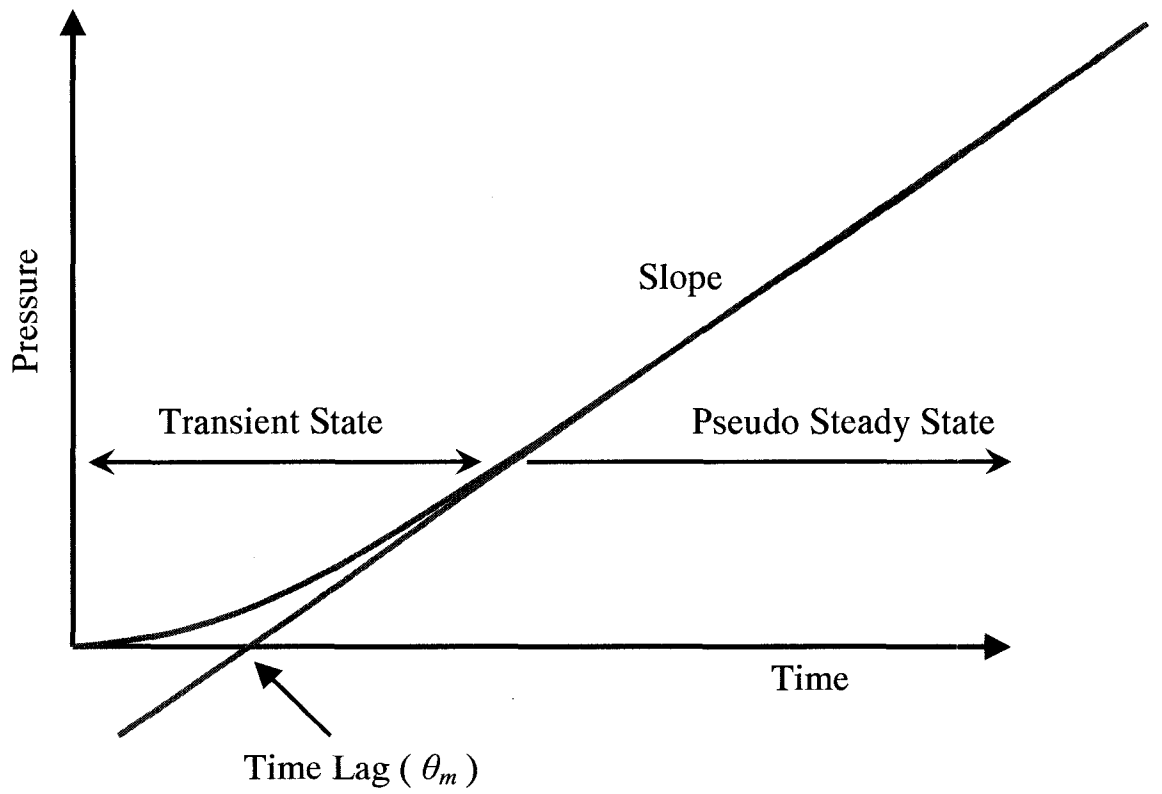

Figure 3.1. Expected pressure response of a pressure sensor installed on the constant volume system.

$$p(t) = \frac{A_m p_f P_m RT}{V v_{STP} l_m}\left[t - \frac{l_m^2}{6D_m}\right] \tag{3.11}$$

The term in front of the bracket in the above equation corresponds to the slope in Figure 3.1, which corresponds to Z in Equation (3.3). The extrapolation of the linear part of the pressure response curve into the time axis represents the time lag (θ_m) of tested membrane. Mathematically, the expression θ_m is obtained by setting $p = p_o$, in Equation (3.11) and solving for t. According to the initial condition, $C(x,0) = 0$ and thus $p_o = 0$, which leads to:

$$t = \theta_m = \frac{l_m^2}{6D_m} \tag{3.12}$$

When the receiver is under vacuum, flow of the gas in a circular tube is governed by Fick's second law [12]:

$$\frac{\partial p}{\partial t} = \frac{\partial}{\partial x}\left(D \frac{\partial p}{\partial x} \right) \tag{3.13}$$

where D is the diffusion coefficient of gas in the tube at pressure p. The actual transport mechanism of the gas in the tube depends on Knudsen number (Kn).

$$Kn = \frac{\lambda}{r} \tag{3.14}$$

where λ and r are the mean free path and the tube radius, respectively. The mean free path of the gas molecules is given by:

$$\lambda = \frac{3\mu}{2p}\sqrt{\frac{\pi RT}{2M}} \tag{3.15}$$

where, μ and M are the dynamic viscosity and the molecular weight of the gas. When $\lambda >> r$, i.e., for $Kn >> 1$, the flow through the tube resembles a plug flow of gas, and the diffusion coefficient in Equation (3.13) becomes the Knudsen diffusion coefficient (D_K), which is evaluated from:

$$D_K = \frac{2}{3} r \sqrt{\frac{8RT}{\pi M}} \tag{3.16}$$

In the other limit, when the density of the gas in the tube is large enough so that the number of collisions with the wall are negligible compared to the number of collisions of molecules with each other ($Kn << 1$), the well-known Hagen-Poiseuille equation is used to describe the flow. The latter equation is developed assuming no slip at the wall. Therefore, there is a transition or slip region in which the Knudsen number is close to unity. Figure 3.2 presents the pressures in 3.175 mm (1/8 in.), 6.35 mm (1/4 in.), and 12.7 mm (1/2 in.) tubes for several gases at which $Kn = 1$. In the transition region, the velocity of the gas at the wall is neither zero, as in the Hagen-Poiseuille regime, nor the flow velocity, as in the Knudsen diffusion. The transition region is still a subject of many studies. Zhdanov and Roldughin published a thorough review in this area [15]. There are several empirical equations for the slip flow regime and the most recent one was proposed by Valougeorgis [16]. Rutherford and Do compared two semi-empirical correlations and presented the effect of using them on the discrepancy in predicting the

experimental results [17]. The effect of this discrepancy on the results of the current study is very small; consequently, any of the available semi-empirical equations for diffusion coefficient in the slip region can be used to simulate the pressure response in the receiver. In the current study, we have adopted the semi-empirical equation reported by Loab [18].

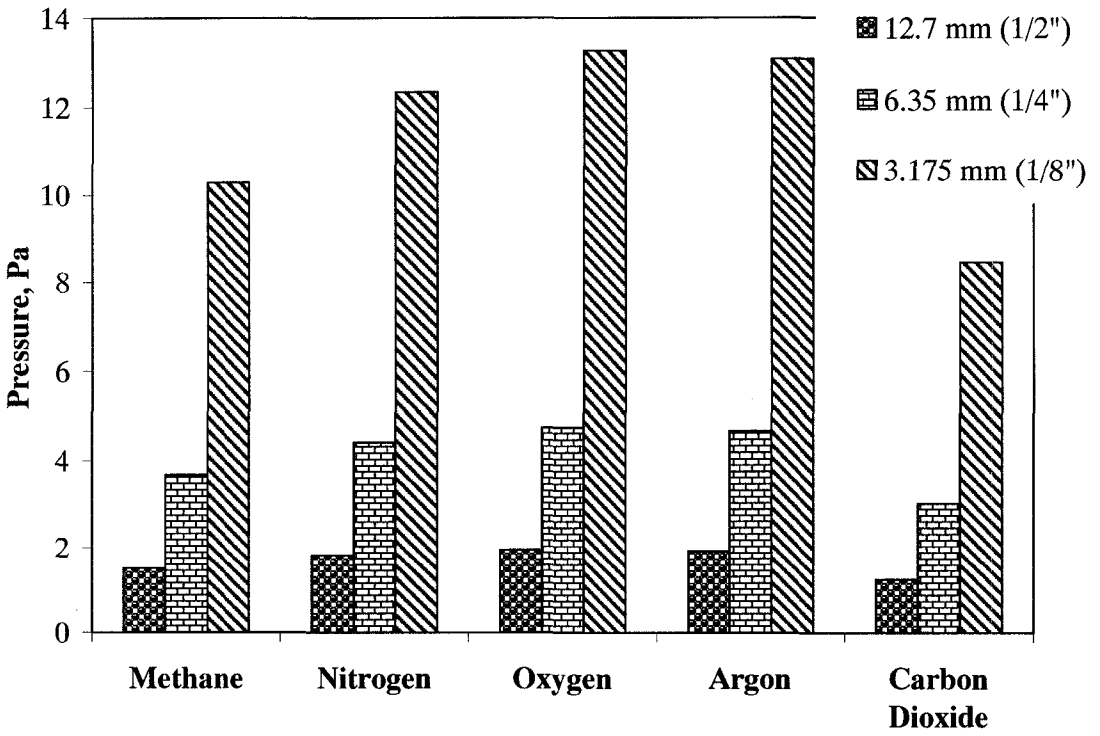

Figure 3.2. Limits of pressure at different tubes for Knudsen number equal to unity.

$$D = \frac{pr^2}{8\eta} + \frac{2}{3} r \sqrt{\frac{8RT}{\pi M}} \left(\frac{1 + C_1 p}{1 + C_2 p} \right) \tag{3.17}$$

where $\frac{C_1}{C_2} = \frac{3\zeta \sqrt{\frac{\pi M}{RT}} p}{8\sqrt{2}\eta}$, $C_2 - C_1 = 0.6117 \sqrt{\frac{M}{RT}} \frac{r}{\eta}$, and $\zeta = \frac{\eta}{p} \sqrt{\frac{\pi RT}{2M}} \left(\frac{2-f}{f} \right)$.

The parameter ζ is the coefficient of slip which gives the ratio of the internal friction of the gas to the external friction at the wall. The parameter f represents the fraction of adsorbed molecules which re-evaporate from the surface at the same temperature. In other words, f is a fraction of gas molecules having elastic collisions with the wall. The reported numerical values of f for He, H_2, air, and O_2 are 1.00, 1.00, 0.98, 0.99,

respectively, [18]. For case of this study, the difference between f = 0.98 and f = 1.00 corresponds to less than 0.01% difference in final results. In all forgoing analysis we adopted f = 1.00.

3.3 Theory

The prediction of the pressure response in the receiver requires solving Equation (3.13) in each element of the receiver. Previously, to simplify the mathematical analysis, the limiting case of Knudsen flow regime in which the diffusion coefficient is independent of pressure was considered [11-13]. However, as the pressure increases, there is a transition from the Knudsen, to slip flow regime, in which the diffusion coefficient depends on pressure. Since the diffusion coefficient depends on pressure, a set of equations derived from Equation (3.13) cannot be solved analytically; it requires a numerical solution. The details related to the numerical solution of Equation (3.13) in different elements of the receiver are presented in the forgoing sections.

3.3.1 Modeling of receiver

Figure 3.3 presents a schematic diagram of a simple multi-tank receiver consisting of two accumulation tanks, a pressure transducer, a vacuum pump, and three valves. The accumulation tanks can be added to or removed from the total volume of the receiver by means of appropriate valves. The pressure transducer is attached to the main line so that it can be used in any configuration of the receiver. The vacuum pump is separated from the receiver by means of another valve. When both tanks are connected to the main line, the entire tubing of the receiver can be divided into 9 different tubes as shown in Figure 3.3. To generalize the analysis, the 9 tubes can have different internal diameters. The prediction of the pressure response in the receiver shown in Figure 3.3 requires simultaneous solution of Equation (3.13) in all 9 tubes subject to appropriate boundary conditions. It is important to emphasize that the configuration shown in Figure 3.3 contains all essential elements to generalize the forgoing discussion to any configuration of a receiver.

The boundary conditions for the receiver shown in Figure 3.3 can be represented by a single, general element shown in Figure 3.4, in which the flow from tube k is

distributed to tube $k+1$, branch n, and volume $k+1$. Application of the continuity requirement to the element presented in Figure 3.4 leads to

$$N_k A_k = N_{k+1} A_{k+1} + N_n A_n + \frac{V_{k+1} + V_{Element}}{RT} \frac{\partial p}{\partial t} \tag{3.18}$$

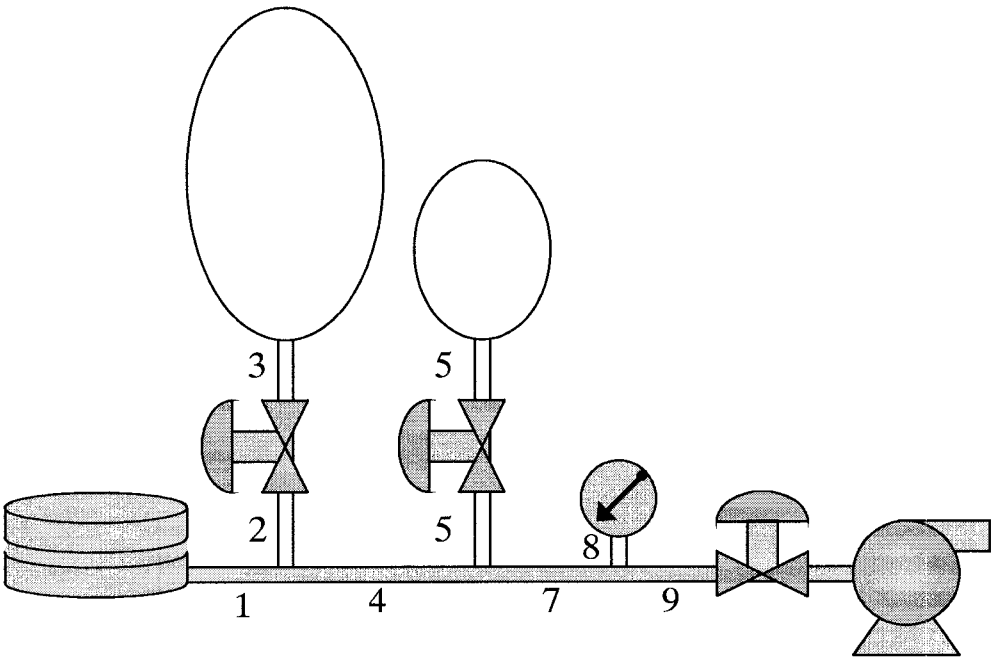

Figure 3.3. Schematic of a typical constant volume system with multiple tanks.

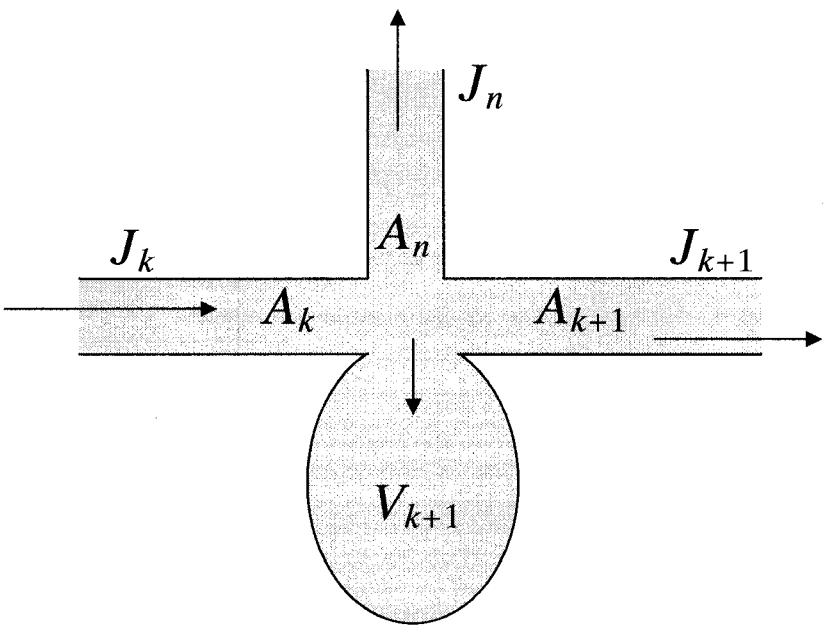

Figure 3.4. Schematic of the general boundary condition for receiver configuration modeling.

It is important to emphasize that volume V_{k+1} is considered to be resistance free. Discrete element, $V_{Element}$, corresponds to the finite volume of the node in finite difference method. As the number of nodes increases this volume decreases. Equation (3.18) represents a general boundary condition for the receiver. Alternatively, since there is no convective flow, the general boundary condition can also be written by applying Fick's law of diffusion [19]

$$-\frac{D_k}{RT}\frac{\partial p}{\partial x}\bigg|_{k^-} A_k = -\frac{D_{k+1}}{RT}\frac{\partial p}{\partial x}\bigg|_{k^+} A_{k+1} - \frac{D_n}{RT}\frac{\partial p}{\partial x}\bigg|_{n^+} A_n + \frac{V_{k+1}+V_{element}}{RT}\frac{\partial p}{\partial t} \tag{3.19}$$

In addition, based on the finite difference approximation, the pressure in the element shown in Figure 3.4 can be represented by a single value, which is the pressure of the node that represents this element.

$$p|_{k^-} = p|_{k^+} = p|_{k^{+n}} = p|_{V_{k+1}} \tag{3.20}$$

Equations (3.18-3.20) can be used to define all boundary conditions for the 9 tubes in Figure 3.3, except for the boundary condition at the interface between the membrane and the 1st tube. The latter boundary condition is given by Equation (3.9).

$$-\frac{D}{RT}\frac{\partial p}{\partial x}\bigg|_{x=0^+}\frac{A_0}{A_m} = N(l_m,t) = \frac{p_f P_m}{l_m}\left[1+2\sum_{n=1}^{\infty}(-1)^n \exp\left(\frac{-n^2\pi^2 D_m t}{l_m^2}\right)\right] \tag{3.21}$$

Finally, the initial condition in all tubes of the receiver is given by

$$p(t=0,x) = p_0 \tag{3.22}$$

3.3.2 Numerical solution

The governing PDE given by Equation (3.13) can be solved by an implicit finite difference method. This method requires the governing PDE, and the boundary and initial conditions to be rewritten in dimensionless form and discretized [25].

There are four variables in Equation (3.13). These are: pressure (p), time (t), position (x), and diffusion coefficient (D). These variables can be converted into the following dimensionless variables:

$$y = \frac{p-p_0}{p_0} \qquad \eta = \frac{D_0 t}{L_0^2} \qquad z = \frac{x}{L_k} \qquad \phi = \frac{D}{D_0} \tag{3.23}$$

where D_0 is an arbitrary reference diffusion coefficient; in our case D_0 corresponds to the Knudsen diffusion coefficient in the first tube downstream from the membrane cell at initial time; L_0 is the length of the first tube downstream from the membrane and L_k is the length of tube k.

Figure 3.5 presents discretization of different elements of the receiver, including a straight tube (Figure 3.5a) and different boundary conditions (Figures 3.5b-d). The end of a tube with a cross sectional area A_k can be seen as half of the element shown in Figure 3.5a. Alternatively, it can be represented by Figure 3.5b in which $V = 0$. If $V > 0$, Figure 3.5b corresponds to the end of a tube connected to a resistance-free tank. Figure 3.5c corresponds to any valve in the receiver. In this case, V represents a dead volume of the valve, which is also considered to be resistance-free. Figure 3.5d corresponds to any tee in the receiver. It is important to emphasize all sketches shown in Figure 3.5 are obtained by simplification of the general element of the receiver presented in Figure 3.4.

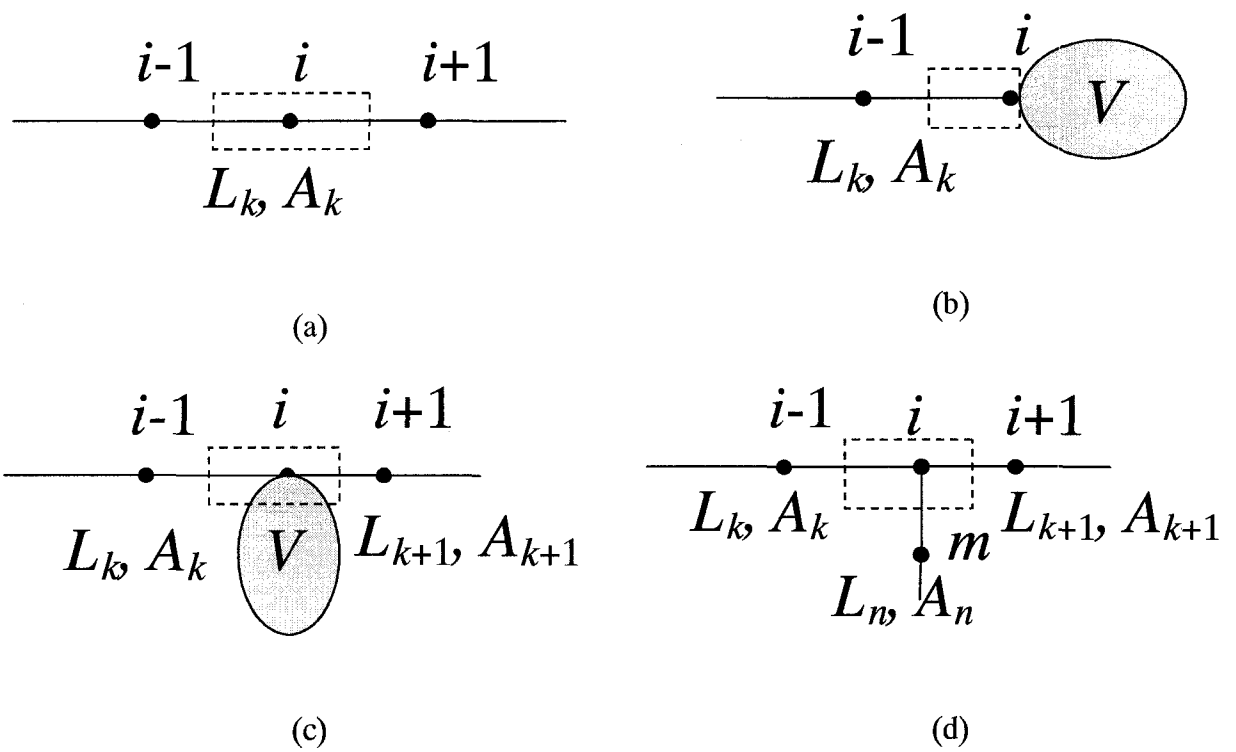

Figure 3.5. Various boundary conditions which could happen in a receiver configuration modeling. a) In a tube, b) Entrance of a volume, c) A volume on a tube, d) A branch

Using the dimensionless variables defined by Equation (3.23), Equation (3.13) can be converted into dimensionless form.

$$\frac{\partial y}{\partial \eta} = \left(\frac{L_0}{L_k}\right)^2 \frac{\partial}{\partial z}\left(\phi \frac{\partial y}{\partial z}\right) \tag{3.24}$$

or

$$\frac{\partial y}{\partial \eta} = \left(\frac{L_0}{L_k}\right)^2 \left[\left(\frac{p_0}{D_0}\frac{dD}{dp}\right)\left(\frac{\partial y}{\partial z}\right)^2 + \phi \frac{\partial^2 y}{\partial z^2}\right] \tag{3.25}$$

The term dD/dp is evaluated analytically from Equation (3.17). Discretization of Equation (3.25) for the node i presented in Figure 3.5a and the time interval j leads to:

$$y_{i-1}^j - \frac{\xi + 2\phi_i^j}{\phi_i^j + \psi\left(y_{i-1}^j - y_{i+1}^j\right)} y_i^j + \frac{\phi_i^j - \psi\left(y_{i-1}^j - y_{i+1}^j\right)}{\phi_i^j + \psi\left(y_{i-1}^j - y_{i+1}^j\right)} y_{i+1}^j = \frac{-\xi}{\phi_i^j + \psi\left(y_{i-1}^j - y_{i+1}^j\right)} y_i^{j-1} \tag{3.26}$$

where $\xi = \left(\frac{L_k}{L_0}\right)^2 \frac{(\Delta z)^2}{\Delta \eta}$ $\qquad \psi = \frac{p_0}{4D_0}\frac{dD}{dp}\Big|_i^j$.

Similarly, all boundary conditions can be rewritten in a dimensionless form and descretized. For example, the boundary condition existing at the end of a tube with a cross sectional area A_k is given by:

$$-\phi \frac{\partial y}{\partial z}\Big|_{k^-} = \left(\frac{L_k}{L_0}\right)^2 \left(\frac{V}{A_k L_k} + \frac{dz}{2}\right)\frac{\partial y}{\partial \eta} \tag{3.27}$$

Discretization of Equation (3.27) gives,

$$y_{i-1}^j - \left[1 + \frac{1}{\phi_i^j}\left(\frac{L_k}{L_0}\right)^2 \frac{\Delta z}{\Delta \eta}\left(\frac{V}{A_k L_k} + \frac{\Delta z}{2}\right)\right] y_i^j = -\frac{1}{\phi_i^j}\left(\frac{L_k}{L_0}\right)^2 \frac{\Delta z}{\Delta \eta}\left(\frac{V}{A_k L_k} + \frac{\Delta z}{2}\right) y_i^{j-1} \tag{3.28}$$

In case of a tube with a valve at its end, the appropriate boundary condition in a dimensionless form is given by:

$$-\phi \frac{\partial y}{\partial z}\Big|_{k^-} = -\phi \frac{\partial y}{\partial z}\Big|_{k^+} \frac{A_{k+1}}{A_k}\frac{L_k}{L_{k+1}} + \left(\frac{L_k}{L_0}\right)^2 \left[\frac{V}{A_k L_k} + \left(1 + \frac{A_{k+1}L_{k+1}}{A_k L_k}\right)\frac{dz}{2}\right]\frac{\partial y}{\partial \eta} \tag{3.29}$$

or in a discretized form:

$$y_{i-1}^j - \left\{\zeta - 1 + \frac{\phi_{i^+}^j}{\phi_{i^-}^j}\frac{A_{k+1}}{A_k}\frac{L_k}{L_{k+1}}\right\} y_i^j + \frac{\phi_{i^+}^j}{\phi_{i^-}^j}\frac{A_{k+1}}{A_k}\frac{L_k}{L_{k+1}} y_{i+1}^j = -\zeta y_i^{j-1} \tag{3.30}$$

where, $\zeta = \frac{1}{\phi_{i^-}^j}\left(\frac{L_k}{L_0}\right)^2 \frac{\Delta z}{\Delta \eta}\left[\frac{V}{A_k L_k} + \left(1 + \frac{A_{k+1}L_{k+1}}{A_k L_k}\right)\frac{dz}{2}\right]$.

Similarly, for a tube with a tee at its end, the appropriate boundary condition in a discretized form is given by:

$$y_{i-1}^j - \left(1 + \frac{\phi_{i^+}^j}{\phi_{i^-}^j}\frac{A_{k+1}L_k}{A_k L_{k+1}} + \frac{\phi_{i^+m}^j}{\phi_{i^-}^j}\frac{A_n L_k}{A_k L_n} + \beta\right) y_i^j + \frac{\phi_{i^+}^j}{\phi_{i^-}^j}\frac{A_{k+1}L_k}{A_k L_{k+1}} y_{i+1}^j + \frac{\phi_{i^+m}^j}{\phi_{i^-}^j}\frac{A_n L_k}{A_k L_n} y_m^j = -\lambda y_i^{j-1} \qquad (3.31)$$

where, $\beta = \frac{1}{2\phi_{i^-}^j}\left(\frac{L_k}{L_0}\right)^2 \left(1 + \frac{A_{k+1}L_{k+1}}{A_k L_k} + \frac{A_n L_n}{A_k L_k}\right)\frac{(\Delta z)^2}{\Delta \eta}$.

3.3.3 Data reconciliation

The main objective of this paper is to examine the possibility of extracting the actual diffusion and permeability coefficients of a membrane from the time lag data obtained in a CV system having a non-negligible resistance to gas accumulation. To accomplish this, the objective function is defined as a sum of the square residuals of the measured and simulated pressure responses. The latter are obtained by simultaneously solving Equation (3.13) in all tubes of the actual receiver. To obtain the simulated pressure responses, the permeability and diffusion coefficients of the gas in the membrane are assumed to be independent on the gas concentration in the membrane. In addition, it is assumed that the effect of the permeate pressure on the membrane properties is negligible. Consequently, to describe the gas flow into the receiver following the step change in feed pressure, we can use Equation (3.21). The objective function is minimized by optimizing the permeability and diffusion coefficients using a simplex method, available in MATLAB (Version 7.2 R2006).

3.4 Experimental

A polyphenylene oxide membrane was prepared from a 10% solution in trichloroethylene by means of spin coating over a silicon wafer. To increase the membrane thickness, the wafer was coated four times. After each coat the membrane on the wafer was allowed to solidify. The final average thickness of the membrane was 93.6 μm. To stabilize the gas transport properties, the membrane was pre-aged using the

following procedure. The free standing final membrane was heated in vacuum oven, which was thoroughly purged by nitrogen, to 230°C (15°C above its glass transition temperature). The membrane was kept at 230°C for 45 minutes. Then, the temperature of the oven was decreased to 200°C, and the membrane remained at this temperature for 24 hours.

After pre-aging, the membrane was installed in a stainless steel cell equipped with an O-ring for complete sealing. The same membrane in the same cell was used in all experiments, which involved two different constant volume (CV) systems and various configurations of the receiver in each system. Before each test, the receiver and the membrane cell were tested for possible leaks by two procedures. First, the system was pressurized by helium to 274 kPa (25 psig), and all elements of the system were checked using a Matheson leak detector with sensitivity of $1.0\times10^{-5}\ cm^3/s$ for helium. Then the system was evacuated and left for at least 24 hours at vacuum to record any pressure rise in the system, which would indicate a leak. The experiments were started only if there was no detectable pressure rise in the system.

The feed pressure was controlled by means of a large tank upstream from the membrane cell, which was pressurized to the desired level prior to start of a time lag experiment. The actual experiment was started by opening a valve separating the upstream tank from the membrane cell. Because of a large volume of the feed tank, the feed pressure remained constant during all time lag experiments. The data from a pressure transducer installed on the feed tank and those installed in the receiver were collected using an analog to digital converter with speed of 7 Hz and 16 bit resolution.

The two CV systems used in this study are referred to as low resistance (LR) and high resistance (HR) systems and are described in the following sub-sections.

3.4.1 Low resistance CV system (LR)

The low resistance CV system was designed to minimize the resistance to gas accumulation in the receiver. More specifically, the length of tubing in the receiver was minimized for the physical dimensions of the accumulation tanks, pressure transducers and valves. Moreover, whenever possible, 12.7 mm (1/2 in.) rather than 6.35 mm (1/4 in.) tubes were used. The latter were used only in connections to the membrane cell and

to the accumulation tanks. Most of the tube joints were welded to decrease the possibility of leaks, while all the other joints were sealed using VCR gaskets. The position of the two pressure transducers and the location of accumulation tanks in the receiver were determined following the guidelines from our previous publication [13].

A schematic diagram of the LR receiver, which includes all the tube dimensions and the location of the pressure transducers and accumulation tanks, is shown in Figure 3.6. The two pressure transducers used in the receiver were identical (MKS 627B11TBC1B) with the measurement range from 0 to 10 mmHg. One of the pressure transducers was connected close to the end of the main tube, where the potential resistance effects should be smaller that in other part of the system [13]. The other pressure transducer is installed to the end of the last volume. The three cylindrical accumulation tanks, whose specification are summarized in Table 3.1, were connected to the main tube by means of high-pressure diaphragm-sealed valves (Swagelok SS-DSVCR4).

Table 3.1. Specifications of tanks that were used in constant volume systems.

CVS	Volume, cm^3	Inner diameter, mm	Length, mm
LR	150	33.2	173
	300	46.2	179
	500	46.2	298
HR	2250	91.6	341
	3785 (1 Gal)	91.6	574

3.4.2 High resistance CV system (HR)

The second CV system used in this study, which is referred to as a high resistance system, was designed by Tabe-Mohamadi et al. [20]. The system was employed in several studies to measure the permeation rate through the membranes [21-27]; it was not used for the measurement of the diffusion coefficient.

The schematic diagram of the HR system with all the relevant dimensions is shown in Figure 3.7. The system consists of two large accumulation tanks with volumes of 2250 and 3780 cm^3, which can be incorporated into the total volume of the receiver.

When the tanks are excluded from the system, the volume of the receiver is 70 cm^3. The specifications of these two tanks are presented in Table 3.1. The original system consists of three cells in parallel in order to increases the flow rate of gas when characterizing membranes with very low permeability coefficients. The presence of three cells in the system is associated with an additional length of tubes in the receiver. All tubes are 6.35 mm (1/4 in.) stainless steel tubes. There are many additional connections and tubing in the receiver to make the system more flexible. For example, there is a connection to a gas chromatograph, a connection to additional high-range pressure transducer, and several valves to allow evacuation of one, two, or all three permeation cells at the same time.

To utilize the HR system in the current study, the two pressure transducers used in the LR system, which are denoted here as PT1 and PT2, were installed at the locations shown in Figure 3.7. The original pressure transducer associated with the HR system, denoted as PT3, was left in the same position as in previous studies [21-27].

3.5 Results and discussion

The unwritten assumption associated with a time lag method suggests the same results regardless of the position of the pressure transducer or the system configuration. Using the recommended procedure for the time lag measurement [14,28], Figure 3.8 presents the example of a typical test performed in the HR receiver, in which the pressure response to a step change in the feed pressure was monitored simultaneously by the PT1, PT2, PT3 located as shown in Figure 3.7. The time lags evaluated based on the asymptotes determined from the pressure rise detected at the respective locations are: 2.4, -6.3, -0.2 min. The enormous differences in the experimental time lags as well as the negative time lags arise from the resistance to gas accumulation in the HR receiver. However, rather than focusing on the magnitude of the differences between different locations, which was the subject of our previous paper [12], our main objective is use the apparent time lags and slopes to recover the actual diffusion and permeability coefficients of the studied membrane.

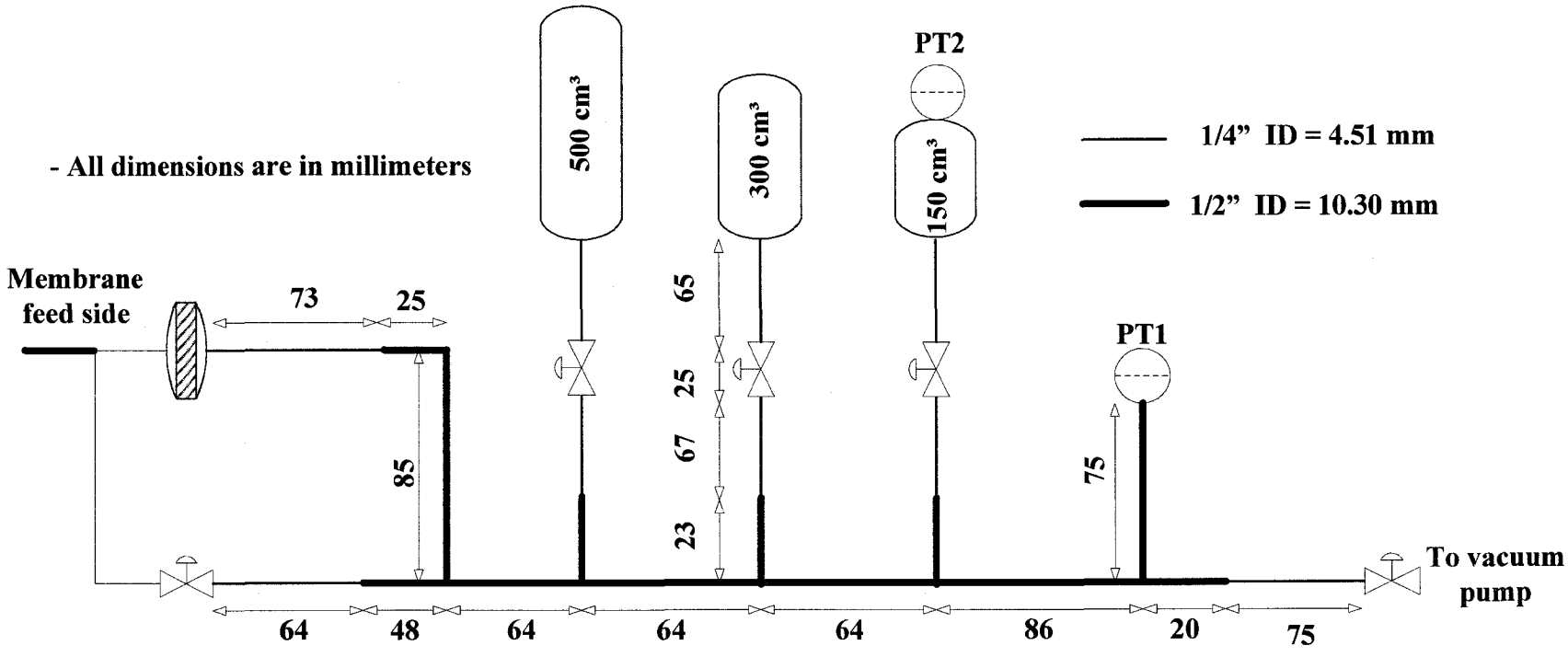

Figure 3.6. Low resistance (LR) receiver configuration.

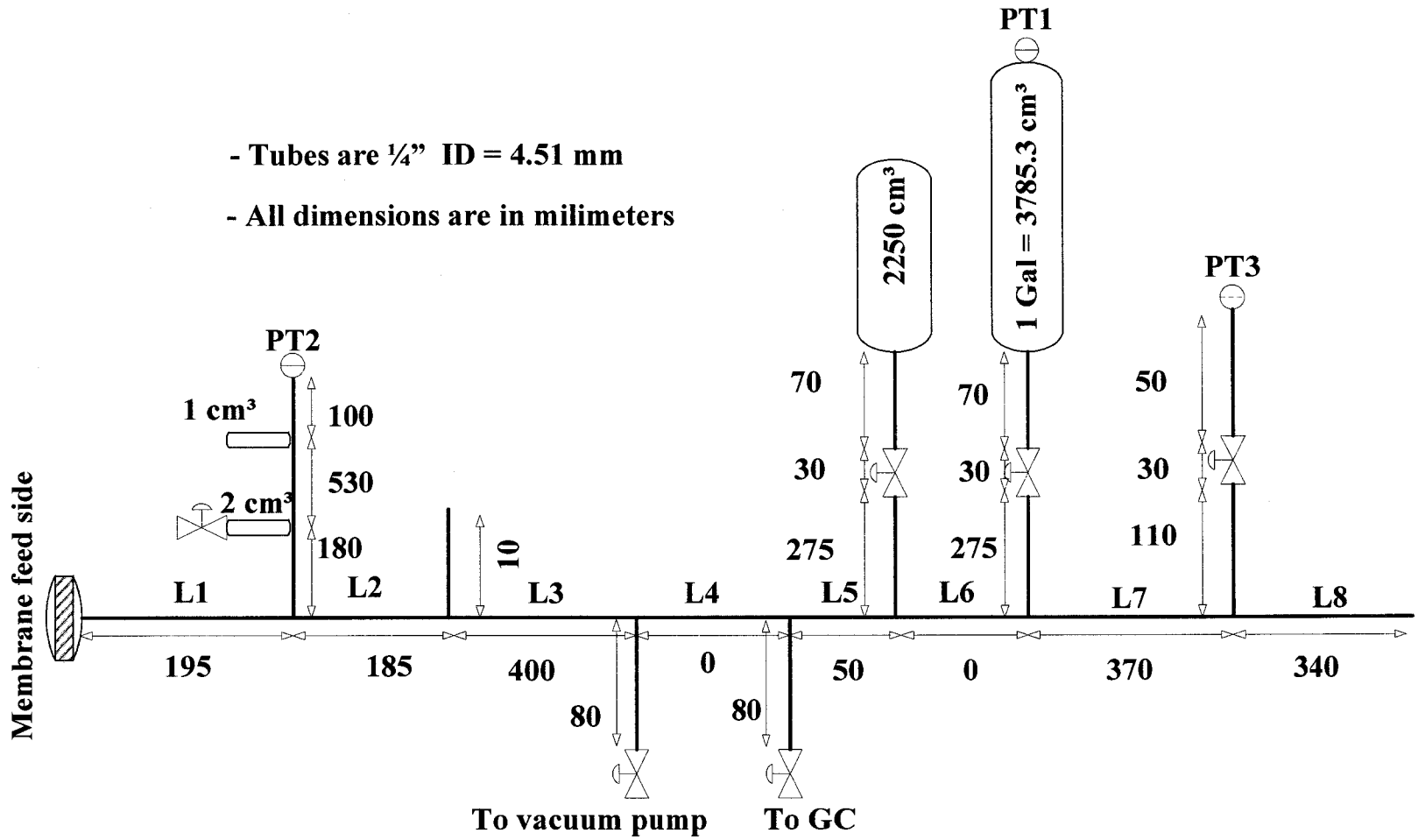

Figure 3.7. High resistance (HR) receiver configuration.

In total, 36 time lag experiments were performed, 21 in the LR receiver and 16 in the HR receiver. The apparent time lags along with the corresponding diffusion coefficients and the apparent slopes along with the corresponding permeability coefficients from all the experiments are summarized in Tables 3.2-3.5. Tables 3.2 and 3.3 present the results obtained using nitrogen and oxygen as a feed in the LR system, respectively. For the tests with nitrogen, four different configurations of the LR receiver were used while for the tests with oxygen one additional configuration was also considered. In addition, for a given configuration, the tests were performed at different feed pressures. The results of the tests with nitrogen and oxygen performed in four different configurations of the HR receiver are presented in Tables 3.4 and 3.5, respectively.

To evaluate the accuracy of the apparent diffusion and permeability coefficients, some experiments were repeated. For example, two tests at similar feed pressures (2.37 and 2.39 bars) were performed with oxygen in the LR receiver with the smallest tank (150 cm^3) attached to the system (Table 3.2). In the HR receiver, two tests at similar feed pressures (3.92 and 3.98 bars) were performed with oxygen with both accumulation tanks attached (Table 3.4), and also two tests at similar feed pressures (7.08 and 7.11 bars) were performed with nitrogen when only the larger accumulation tank was attached. For the repeated tests in the LR receiver, the apparent time lags differ by not more than 3 s. On the other hand, in the HR receiver the apparent time lags in the repeated experiments differ by not more than 8 s. The corresponding differences in the slope of asymptotes are much smaller than those in the apparent time lags; the former differ only by a third significant digit.

As anticipated, the differences between the apparent diffusivities and permeabilities determined from the pressure responses recorded by different pressure transducers are much smaller in the LR receiver than in the HR receiver. For the LR receiver, the difference between the apparent time lags determined from PT1 and PT2, respectively, are within an experimental error, except for the tests with oxygen at the three lowest feed pressures in configuration with the smallest tank (150 cm^3) attached to the receiver (Table 3.2).

Table 3.2. Results of LR system for oxygen with several feed pressure and various configurations of the receiver.

Additional volume	Total volume cm^3	Feed pressure bar	Pressure transducer position	Time lag s	D x 10^{12} m^2/s	Slope Pa/s	Permeability x 10^{17} $m^3(STP)/m/s/Pa$	Permeability Barrer
500, 300, 150 cm^3	1009.07	2.73	PT1	81.14	18.00	0.0519	16.30	21.73
		1.70		82.73	17.65	0.0326	16.42	21.89
		1.20		83.13	17.56	0.0232	16.57	22.09
		0.33		86.80	16.82	0.0058	14.85	19.79
		2.73	PT2	81.74	17.86	0.0522	16.40	21.87
		1.70		84.39	17.30	0.0328	16.51	22.01
		1.20		82.08	17.79	0.0234	16.66	22.22
		0.33		86.15	16.95	0.0057	14.93	19.91
500, 150 cm^3	707.83	2.41	PT1	86.12	16.96	0.0646	16.13	21.50
		2.41	PT2	92.67	15.76	0.0650	16.23	21.63
300, 150 cm^3	507.83	2.40	PT1	82.46	17.71	0.0879	15.78	21.03
		2.40	PT2	89.65	16.29	0.0884	15.87	21.15
150 cm^3	206.59	2.39	PT1	82.41	17.72	0.2047	15.00	20.00
		2.37		85.14	17.15	0.1990	14.73	19.64
		0.80		111.71	13.07	0.0533	11.73	15.64
		0.52		123.31	11.84	0.0320	10.71	14.28
		0.33		136.57	10.69	0.0190	10.23	13.63
		2.39	PT2	83.50	17.49	0.2056	15.07	20.09
		2.37		85.69	17.04	0.1999	14.80	19.73
		0.80		121.69	12.00	0.0536	11.81	15.74
		0.52		147.74	9.88	0.0322	10.78	14.37
		0.33		168.62	8.66	0.0191	10.30	13.73

Table 3.3. Results of LR system for nitrogen with several feed pressure and various configurations of the receiver.

Additional volume	Total volume cm^3	Feed pressure bar	Pressure transducer position	Time lag s	D x 10^{12} m^2/s	Slope Pa/s	Permeability x 10^{17} m^3(STP)/m/s/Pa	Permeability Barrer
500, 300, 150 cm^3	1009.07	4.00	PT1	279.79	5.219	0.01535	3.287	4.383
		3.09		279.67	5.221	0.01204	3.338	4.450
		0.99		261.32	5.588	0.00408	3.520	4.693
		0.79		255.84	5.707	0.00329	3.587	4.782
		0.54		250.13	5.838	0.00229	3.644	4.858
		4.00	PT2	281.16	5.193	0.01546	3.311	4.414
		3.09		279.42	5.226	0.01211	3.358	4.478
		0.99		263.57	5.540	0.00414	3.571	4.761
		0.79		259.47	5.628	0.00332	3.619	4.825
		0.54		251.34	5.809	0.00231	3.663	4.884
500, 150 cm^3	707.83	3.98	PT1	270.18	5.404	0.02180	3.287	4.382
		3.98	PT2	272.15	5.365	0.02196	3.310	4.414
300, 150 cm^3	507.83	3.98	PT1	285.25	5.119	0.02955	3.202	4.269
		3.98	PT2	286.04	5.105	0.02973	3.221	4.295
150 cm^3	206.59	3.98	PT1	286.40	5.098	0.06790	2.990	3.987
		1.40		286.44	5.098	0.02518	3.155	4.207
		3.98	PT2	286.99	5.088	0.06830	3.008	4.011
		1.40		287.52	5.078	0.02534	3.175	4.233
500 cm^3	556.59	0.49	PT1	245.71	5.943	0.00384	3.723	4.964

Table 3.4. Results of HR system for oxygen with several feed pressure and various configurations of the receiver.

Additional volume	Total volume cm^3	Feed pressure bar	Pressure transducer position	Time lag s	D x 10^{12} m^2/s	Slope Pa/s	Permeability x 10^{17} $m^3(STP)/m/s/Pa$	Permeability Barrer
2250, 3785 cm^3	6095.58	3.98	PT1	107.18	13.62	0.0123	15.98	21.30
		3.92		106.75	13.68	0.0122	16.06	21.42
		3.18		110.57	13.21	0.0099	16.09	21.45
		2.49		108.36	13.48	0.0078	16.22	21.63
		1.82		109.78	13.30	0.0057	16.22	21.63
		1.19		141.36	10.33	0.0029	12.73	16.97
		3.98	PT2	-332.39	-4.39	0.0113	14.70	19.59
		3.92		-336.20	-4.34	0.0112	14.77	19.70
		3.18		-360.29	-4.05	0.0091	14.81	19.74
		2.49		-384.56	-3.80	0.0072	14.99	19.99
		1.82		-403.76	-3.62	0.0053	15.15	20.20
		1.19		-376.59	-3.88	0.0028	12.28	16.37
		3.98	PT3	-30.78	-47.43	0.0110	14.35	19.13
		3.92		-32.04	-45.58	0.0109	14.43	19.24
		3.18		-35.13	-41.57	0.0089	14.48	19.30
		2.49		-41.04	-35.58	0.0070	14.61	19.48
		1.82		-41.68	-35.03	0.0052	14.65	19.54
		1.19		-11.51	-126.87	0.0027	11.64	15.52
3785 cm^3	3844.22	3.88	PT1	96.39	15.15	0.0189	15.88	21.17
		3.88	PT2	-171.40	-8.52	0.0179	15.03	20.04
		3.88	PT3	-8.25	-176.92	0.0171	14.33	19.10
2250 cm^3	2308.92	3.84	PT2	-30.31	-48.18	0.0306	15.61	20.82
		3.84	PT3	47.30	30.87	0.0286	14.61	19.48
---	57.56	3.81	PT2	94.66	15.43	0.7767	9.96	13.28
		3.81	PT3	91.32	15.99	0.7034	9.02	12.03

Table 3.5. Results of HR system for nitrogen at various configurations of the receiver contains repeated experiments.

Additional volume	Total volume cm^3	Feed pressure bar	Pressure transducer position	Time lag s	D x 10^{12} m^2/s	Slope Pa/s	Permeability x 10^{17} m^3(STP)/m/s/Pa	Permeability Barrer
2250, 3785 cm^3	6095.58	7.31	PT1	307.44	4.749	0.00458	3.240	4.320
		7.14		310.88	4.697	0.00445	3.220	4.293
		7.31	PT2	-171.69	-8.505	0.00434	3.069	4.091
		7.14		-174.53	-8.366	0.00420	3.042	4.055
		7.31	PT3	166.25	8.783	0.00415	2.937	3.916
		7.14		170.41	8.569	0.00402	2.912	3.883
3785 cm^3	3844.22	7.11	PT1	302.89	4.821	0.00697	3.245	4.326
		7.08		295.10	4.948	0.00695	3.202	4.269
		7.11	PT2	-10.15	-143.91	0.00667	3.102	4.135
		7.08		-12.17	-120.02	0.00666	3.070	4.093
		7.11	PT3	188.91	7.729	0.00631	2.937	3.916
		7.08		182.38	8.006	0.00629	2.901	3.867
2250 cm^3	2308.92	7.17	PT2	148.88	9.807	0.01147	3.176	4.234
		6.97		143.62	10.167	0.01127	3.167	4.223
		7.17	PT3	248.60	5.873	0.01071	2.967	3.956
		6.97		241.94	6.035	0.01051	2.954	3.938
---	57.56	7.15	PT2	299.63	4.873	0.29486	2.041	2.722
		6.97		304.87	4.789	0.28492	1.997	2.662
		7.15	PT3	295.08	4.948	0.26770	1.853	2.471
		6.97		300.66	4.856	0.25840	1.811	2.415

3.5.1 Estimation of the diffusion and permeability coefficients

Knowing the exact configuration of the LR and HR receivers with the details depicted in Figures 3.6 and 3.7, it is possible to use the optimization procedure explained in previous sections to reconcile the actual diffusion and permeability coefficients from the pressure rise data obtained anywhere within the receiver. Although in general, the differences between the apparent diffusion and permeability coefficients determined from PT1 and PT2 fall within the experimental errors, the optimization procedure was also applied to the data obtained from the LR receiver.

Figure 3.9 presents the example of a plot of pure error variance of the pressure versus D_m and P_m for the experiment performed with oxygen at the feed pressure 2.73 bar in the system with the LR receiver, using the pressure rise recorded by PT1. Figure 3.9a shows the above plot in a 3-D format, while Figure 3.9b as a 2-D counter plot. It is evident, in particular from the counter plot, that there exist multiple minima, which are close to the global minimum. The latter, which was found by multiple runs using different initial values, corresponds to $D_m = 15.11\times10^{-12}$ m^2/s and $P_m = 19.02\times10^{-17}$ $m^3(STP)/m\ s\ Pa$ or 25.4 Barrer. The optimized D_m is 19% smaller, while the optimized P_m is 16% greater than the respective experimental values. Table 3.6 presents the optimization results for 25 runs coming from 17 different experiments.

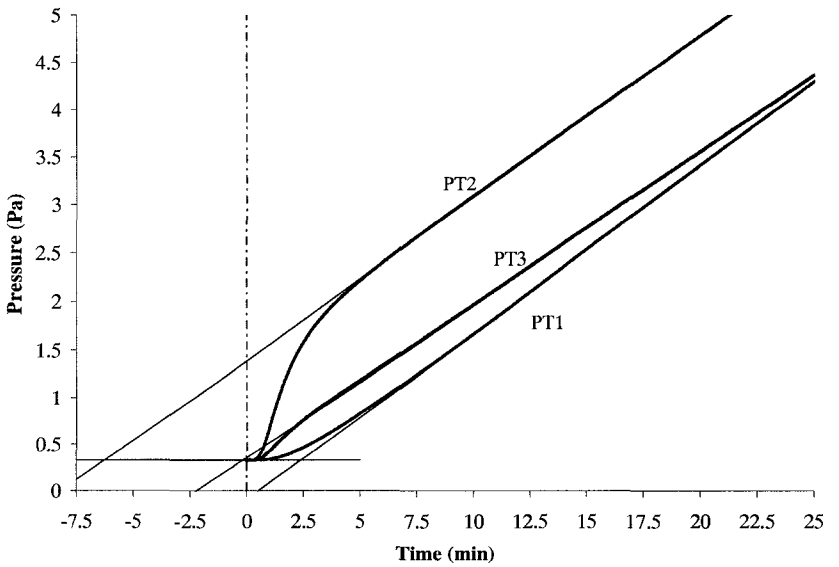

Figure 3.8. Experiment for oxygen at 1.19 bar feed pressure executed with HR system to which both extra volumes are connected.

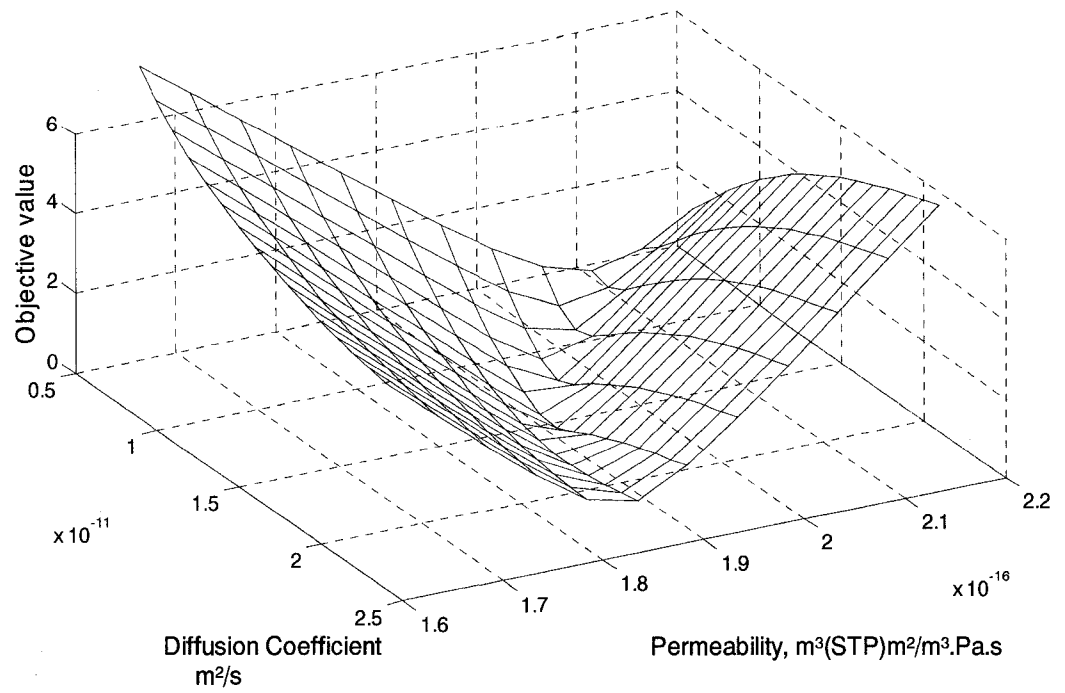

a)

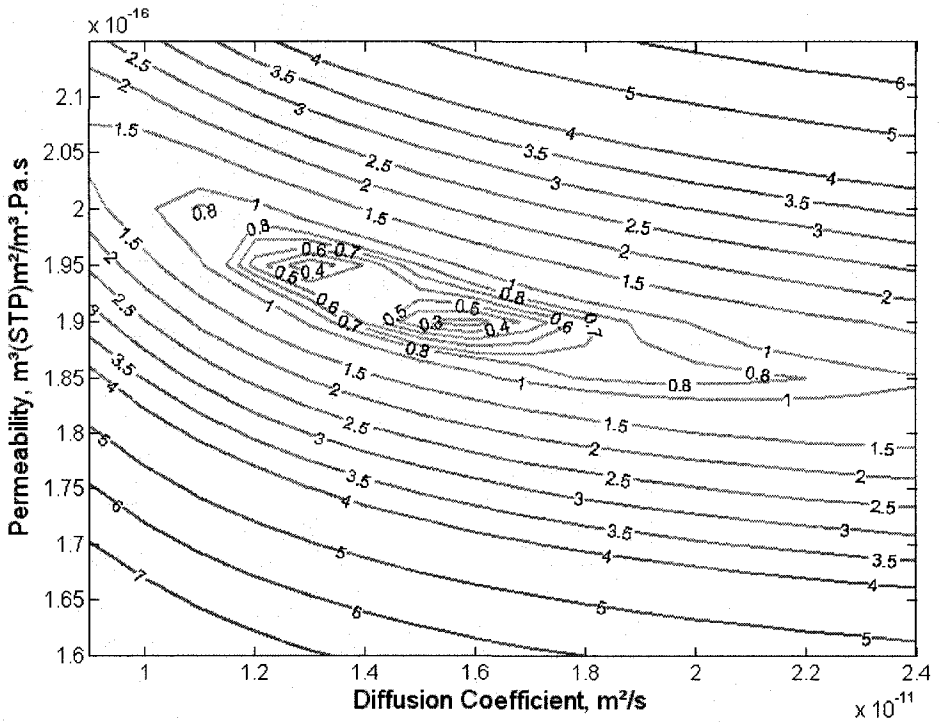

b)

Figure 3.9. Plot of objective value for PT1 versus optimization parameters for experiment with oxygen performed in LR system at 2.73 bar feed pressure. a) Three dimensional presentation, b) The same graph in contour form.

Table 3.6. Experimental and optimized values for selected results.

System	Gas	Feed pressure bar	Pressure transducer position	Experimental				Optimized			
				Time lag s	D x 10^{12} m^2/s	Permeability x 10^{17} m^3(STP)/m/s/Pa	Permeability Barrer	Time lag s	D x 10^{12} m^2/s	Permeability x 10^{17} m^3(STP)/m/s/Pa	Permeability Barrer
LR	O_2	2.73	PT1	81.14	18.00	16.30	21.73	96.62	15.11	19.02	25.36
LR	O_2	0.33	PT1	86.80	16.82	14.85	19.79	97.38	14.99	16.31	21.74
LR	O_2	0.33	PT2	86.15	16.95	14.93	19.91	93.83	15.56	16.43	21.90
HR	O_2	3.98	PT1	107.18	13.62	15.98	21.30	83.30	17.53	15.90	21.20
HR	O_2	3.98	PT2	-332.39	-4.39	14.70	19.59	112.83	12.94	15.49	20.65
HR	O_2	3.98	PT3	-30.78	-47.43	14.35	19.13	86.87	16.81	14.67	19.56
HR	O_2	3.92	PT2	-336.20	-4.34	14.77	19.70	113.11	12.91	16.34	21.78
HR	O_2	3.18	PT2	-360.29	-4.05	14.81	19.74	113.81	12.83	17.57	23.42
HR	O_2	2.49	PT2	-384.56	-3.80	14.99	19.99	114.50	12.75	17.66	23.54
HR	O_2	1.82	PT2	-403.76	-3.62	15.15	20.20	115.17	12.68	17.84	23.79
HR	O_2	1.19	PT2	-376.59	-3.88	12.28	16.37	117.29	12.45	18.05	24.06
HR	O_2	3.88	PT2	-171.40	-8.52	15.03	20.04	129.66	11.26	15.86	21.15
HR	O_2	3.84	PT2	-30.31	-48.18	15.61	20.82	114.41	12.76	16.82	22.42
HR	O_2	3.81	PT2	94.66	15.43	9.96	13.28	106.64	13.69	15.68	20.91
LR	N_2	4.00	PT1	279.79	5.22	3.29	4.38	280.69	5.20	3.24	4.32
LR	N_2	4.00	PT2	281.16	5.19	3.31	4.41	282.00	5.18	3.25	4.33
LR	N_2	0.99	PT1	261.32	5.59	3.52	4.69	277.41	5.26	3.38	4.51
LR	N_2	0.99	PT2	263.57	5.54	3.57	4.76	274.60	5.32	3.39	4.52
LR	N_2	0.79	PT1	255.84	5.71	3.59	4.78	273.75	5.33	3.42	4.56
LR	N_2	0.79	PT2	259.47	5.63	3.62	4.83	275.55	5.30	3.42	4.56
LR	N_2	0.54	PT1	250.13	5.84	3.64	4.86	268.94	5.43	3.48	4.64
LR	N_2	0.54	PT2	251.34	5.81	3.66	4.88	266.41	5.48	3.49	4.65
HR	N_2	7.14	PT2	-174.53	-8.37	3.04	4.06	310.34	4.71	3.09	4.12

In case of tests with oxygen in the LR receiver, the optimized diffusion (except for run 1 depicted in Figure 3.9) and permeability coefficients are higher than the apparent values. On the other hand, in case of tests with nitrogen in the LR receiver, the optimized diffusion and permeability coefficients are slightly lower than the apparent values. The differences between the optimized and apparent diffusion and permeability coefficients of LR system are sufficiently small to consider these values as a reference in assessing the optimized values from the HR system.

Runs 6, 7 and 8 in Table 3.6 show the apparent and optimized diffusion and permeability coefficients from the test with oxygen performed at the feed pressure of 3.98 bar in the HR receiver with both tanks attached to the system. The recovered diffusion coefficients range from 12.94×10^{-12} m^2/s for PT2 to 17.53×10^{-12} m^2/s for PT1. On the other hand, the corresponding recovered diffusion coefficients from the tests with nitrogen in the LR receiver range from 14.92×10^{-12} m^2/s to 15.56×10^{-12} m^2/s. It is therefore evident that the optimization procedure is capable to recover reasonable diffusion coefficients from all pressure transducers in the HR receiver, including PT2 and PT3, which originally lead to meaningless negative apparent diffusion coefficients. Based on the apparent diffusion coefficients, the position corresponding to PT2 in the HR receiver is associated with a higher resistance than the positions corresponding to PT1 and PT3. Since the recovery of the actual diffusion and permeability coefficients from a given experimental run took at least 2 days of computation, the optimization procedure in the HR receiver was limited to the "worst case", i.e. to the data recorded by the PT2.

Considering the runs 7 and 9-16 the apparent time lag varies, depending on the configuration of the receiver and feed pressure, from -403.8 s to 94.7 s. Despite these huge variations, the recovered diffusion coefficient of oxygen in PPO varies only from 11.26×10^{-12} m^2/s to 13.69×10^{-12} m^2/s. The recovered diffusion coefficients of O_2 from the experimental runs in the HR receiver are roughly 15% lower than those recovered from the experimental runs in the LR receiver. It is important to emphasize that while on the schematic diagram in Figure 3.7 all tubes appear straight; some of them were bent to accommodate the system on a laboratory bench. These bends could contribute to some uncertainty in the effective length of different tubes and consequently to uncertainty in the actual position of the accumulation tanks and pressure transducers. As we have shown

in our previous paper [12], the resistance to gas accumulation in a tube is greatly magnified in the presence of a resistance-free volume attached to the tube. Consequently, a small uncertainty in the actual position of PT2 in the presence of large accumulation tanks could translate into a systematic, error in the apparent time lag. This hypothesis is supported by the fact that the optimized diffusion coefficient from run 16, in which the accumulation tanks were not incorporated into the HR receiver volume, is closest to the recovered diffusion coefficients from the LR receiver.

Focusing on permeability coefficients in runs 7 and 9-16, the apparent values vary from 13.3 to 20.8 Barrer. On the other hand, the recovered permeability coefficients are always greater than the corresponding apparent values, and vary from 20.9 to 24.1 Barrer. The latter values compare well to the recovered permeability coefficient of oxygen from the LR receiver.

3.5.2 Effect of pressure dependent diffusion coefficient in tubes

The major advantage of the numerical approach used in the present study is to allow for the variation of the diffusion coefficient with pressure, which occurs in a slip-flow regime. The assumption of constant diffusion coefficient, which is required in the analytical approach is valid only in Knudsen flow regime [11-13], and although typically the condition for Knudsen diffusion exist at the beginning of a time lag experiment, as the receiver's pressure increases, there is a transition from Knudsen to the slip flow regime.

Because of a non-negligible resistance to gas accumulation in the receiver, as the gas starts to permeate through the membrane a pressure gradient develops downstream from the membrane, as shown in Figure 3.8. In absence of resistance to gas accumulation, following a step change in feed pressure, the steady state flow through a membrane is achieved, to a good approximation, after 2.5 - 3 time lags [5]. However, this rule, as shown in Figure 3.8, may not apply when there is high resistance to gas accumulation. Moreover, because of pressure-dependent diffusion coefficient downstream from the membrane, the slope of the asymptote at a given position within the receiver may change with time. This is because in the slip flow regime, as the pressure increases the diffusion coefficient increases according to Equation (3.12). Consequently, the resistance to gas

accumulation decreases, which leads to a decrease of the pressure gradient within the receiver.

Figure 3.10 illustrates implications of the pressure-dependent diffusion coefficient on the apparent slope and time lag in gas permeation experiments performed in the LR and HR receivers. Figure 3.10a presents the effect of the time on the slope of the asymptote in one of the experiments performed in the LR receiver. The experimentally determined slopes are compared with the theoretical ones predicted using the optimized values of the diffusion and permeability coefficients for this particular run and the pressure-dependent diffusion coefficient downstream from the membrane evaluated using Equation (3.12). Except for the first set of experimental slopes, which are determined significantly before the time corresponding to the three time lags of the membrane, the slopes determined after 5 minutes from the initiation of the experiment are practically constant, which indicate negligible resistance effects. On the other hand, the theoretically predicted slopes in Figure 3.10a, after the first five minutes, decrease slightly with time. In other words, the model seems to over predict the resistance effects in the LR receiver. This over prediction is better seen in Figure 3.10b, in which the corresponding experimental and theoretical time lags are compared. The time lag is obtained by extrapolation of the asymptote to the time axis, and consequently even a very small variation in slope of the asymptotes may be translated into significant variation in the corresponding time lags.

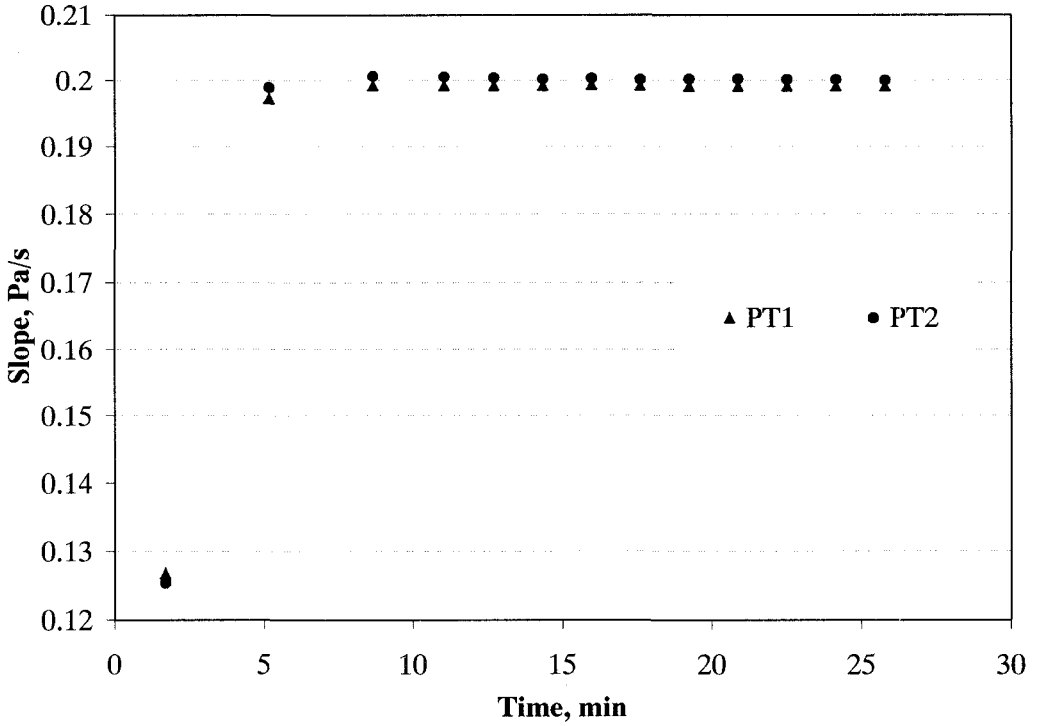

a)

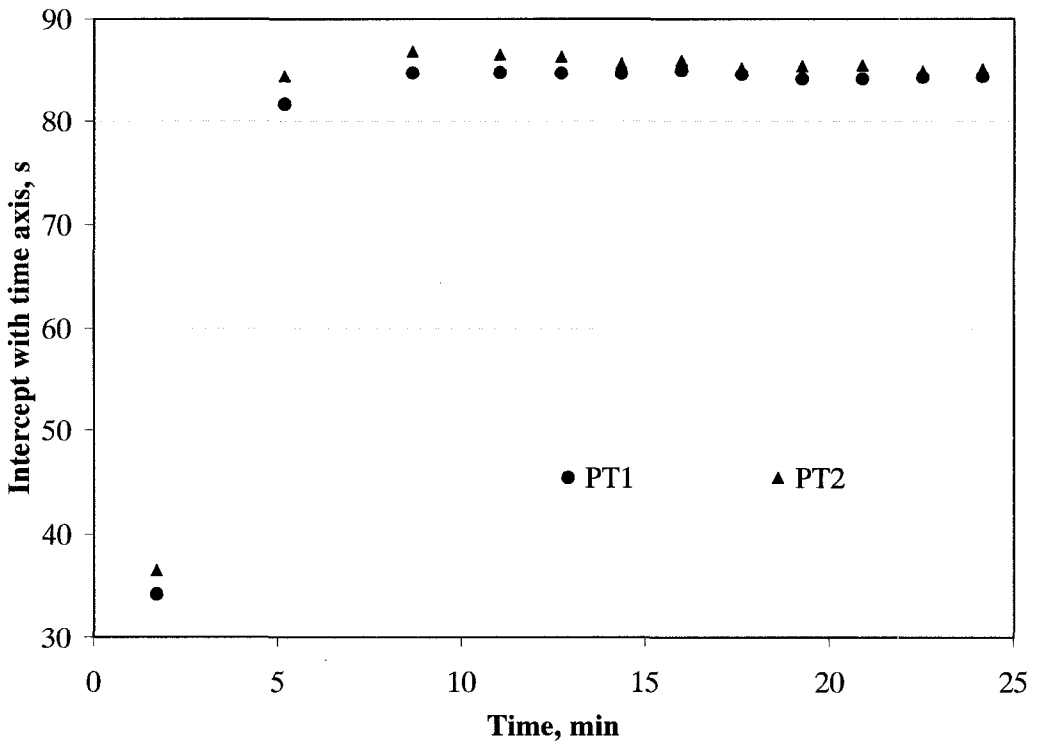

b)

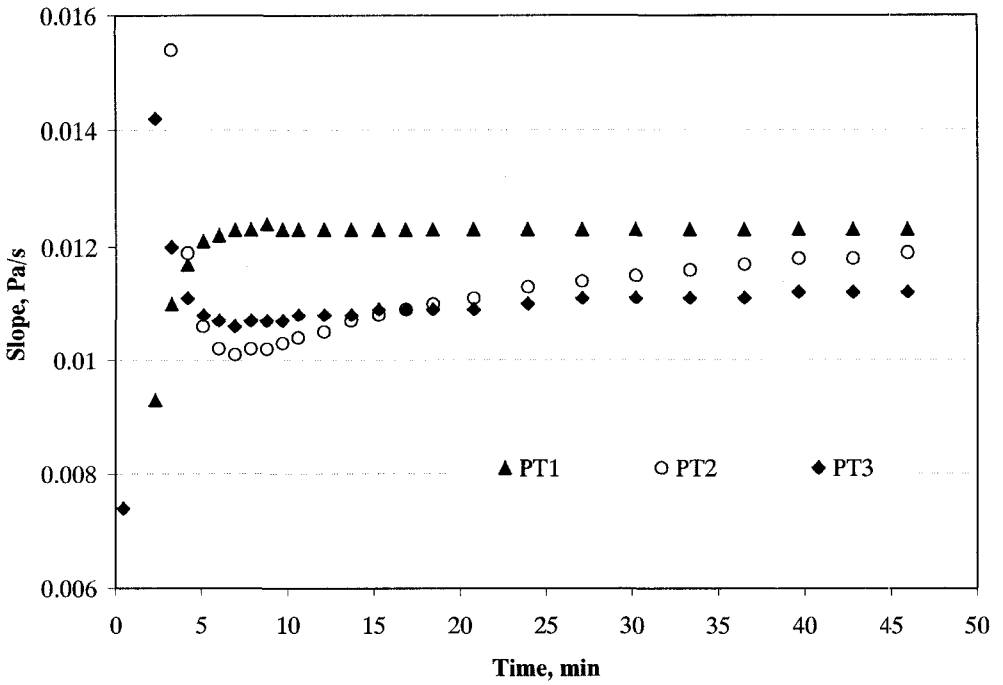

c)

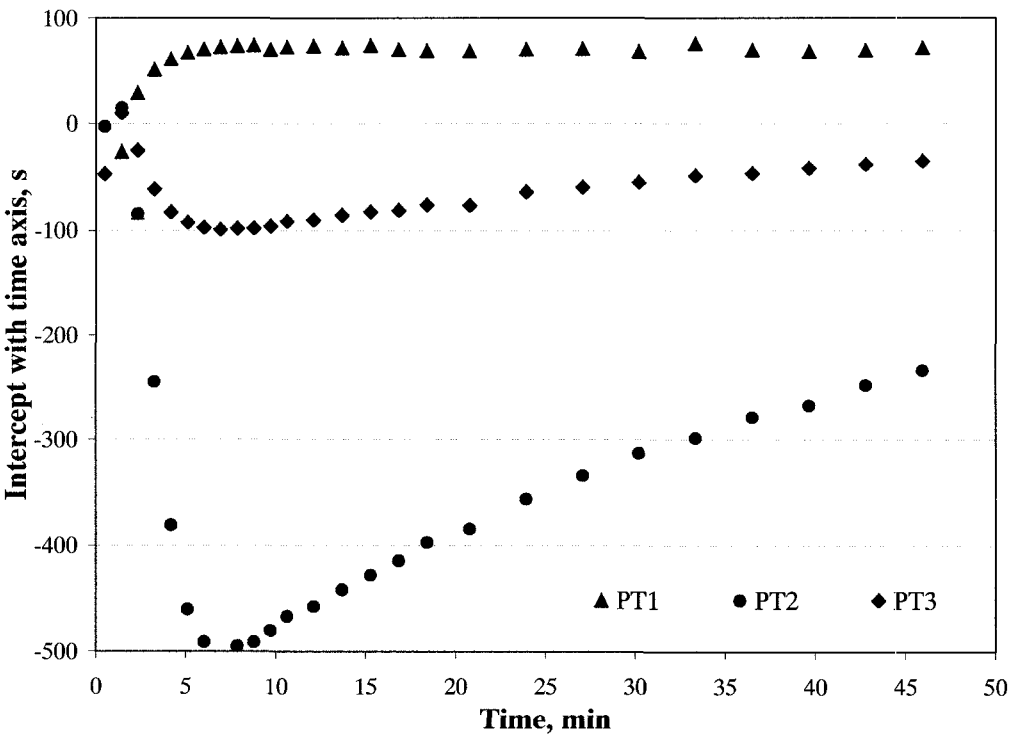

d)

Figure 3.10. Comparison between intercept with time axis and slope of HR and LR CVS. a,b) LR CVS for oxygen feed pressure of 2.37 bar when volume of receiver is 206.59 cm^3 (Table 3.2). c,d) HR CVS for oxygen feed pressure of 3.98 bar when volume of receiver is 6095.58 cm^3 (Table 3.4).

Focusing on the effect of time on the slope of the asymptote in a gas permeation experiment performed in the HR receiver, it can be noticed that for PT1 and PT3 it takes more time than the equivalent of three time lags of the membrane to reach a constant slope. In case of the pressure response at PT2, even after 45 minutes from the initiation of the experiment, both the experimental and theoretical slopes continue to increase with time. The resistance to gas accumulation at a given position can be quantified by the difference between the apparent and the actual time lags at that position. Consequently, for the positions corresponding to the three pressure transducers in the HR receiver with both accumulation tanks attached to the system, the resistance increases in the following order: PT1 < PT3 < PT2. This order is consistent with the time required to reach the constant slope at these positions. The latter is even more evident in Figure 3.10d, which shows the variation in the apparent time lag at a given position with time. Generally, the time required for the slope to reach a constant value, which is better reflected by the time required for the time lag to become independent of time, is another measure of the resistance at a given position. It is important to emphasize that unlike the LR receiver, in case of the HR receiver the theoretical variation in the slope and in the intercept with the time axis follow well the experimentally observed dependence of these parameters on time.

Ideally, the pressure transducer should be installed at a point at which the apparent time lag and the recovered time lag are the same. At such a position both the apparent diffusion and permeability coefficients would reflect the actual values. A question arises, where is such a position within the receiver? The numerical approach could allow finding this position, however, would be an extremely tedious task. While the numerical approach allows recovering the actual properties of membrane from a pressure response anywhere with in the system, it is not the best tool for optimization of the position of the pressure transducer. The latter is a subject of Part II of this series.

3.5.3 Effect of feed pressure

One of the assumptions behind Equation (3.21), which is used as a boundary condition in this analysis, is that the permeability coefficient is independent of feed pressure. This assumption might not be correct, particularly for a glassy polymer such as

PPO. On the other hand, regardless of the dependence of the actual permeability coefficient on pressure, the apparent permeability coefficient must depend on pressure, unless it is evaluated from the pressure response at a "non-zero" position. This dependence is conveniently expressed by the dependence of the intercept with the time axis (the apparent time lag) on the time from the initiation of the experiment. Figure 3.11 presents the effect of the feed pressure on the intercept with the time axis, from which it is evident that at a low feed pressure of 1.19 bar, the apparent time lag is a weak function of time. On the other hand, as the feed pressure increases, the apparent time lag shows a stronger dependence on time. The above can be explained on the basis of transition of the diffusion coefficient from Knudsen to the slip flow regime. At low feed pressures, the flow of the gas through the membrane is relatively low and consequently, during the first 35 min of the experiment, the diffusion remains almost constant. As the feed pressure increases, leading to a higher permeation rate through the membrane, the transition to the slip flow regime occurs faster, and the apparent time lag becomes a smaller negative number as time progresses. The fact that the apparent time lag becomes a smaller negative number at a given time after initiation of the experiment is a direct consequence of an increase in the diffusion coefficient with pressure and a stronger dependence of the apparent permeability coefficient on time. It is evident that the effect of feed pressure on the intercept of the asymptote with the time axis is well captured by the theoretical model, in particular at lower feed pressures.

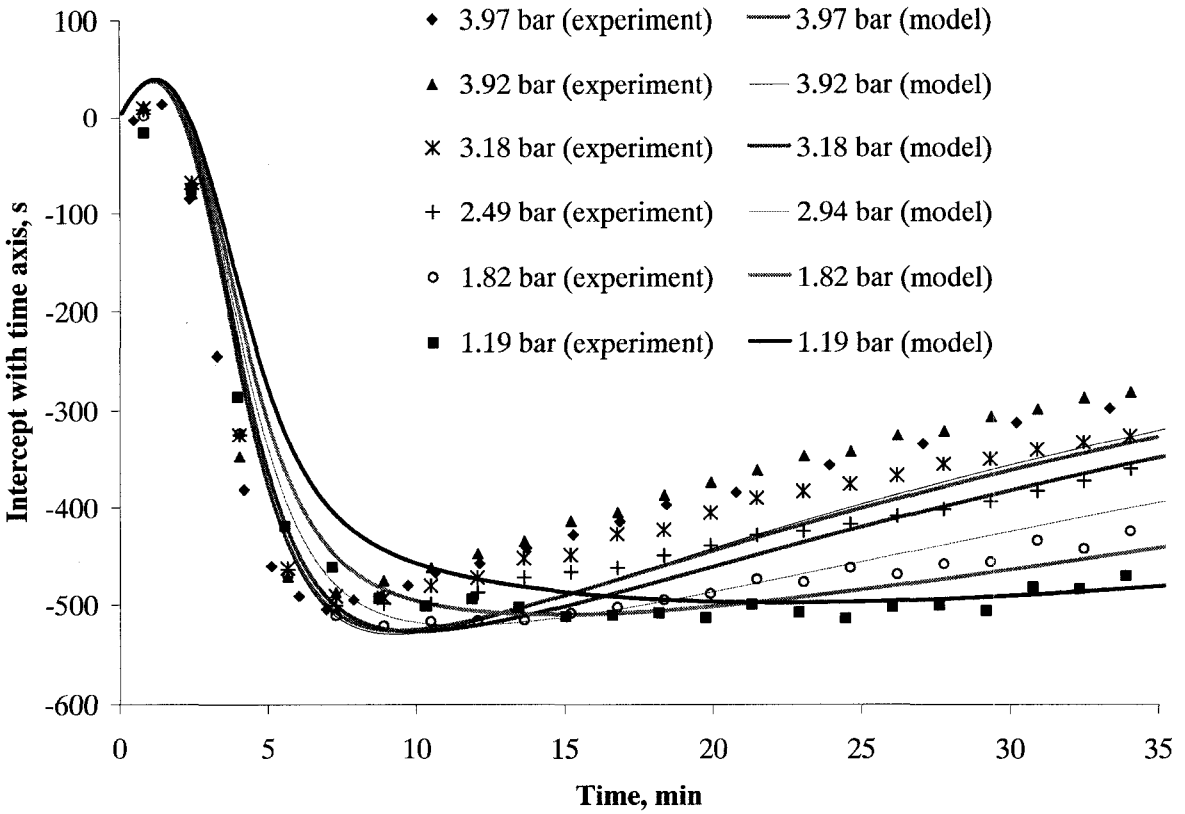

Figure 3.11. Change of intercept with time axis, which the final value would be time gas, measured by PT2 at HR CVS for different feed pressure of oxygen. Points are calculated from experimental response of PT2 and lines are model based on optimized values reported in Table 3.6.

3.6 Conclusions

The resistance to gas accumulation was modeled in a generalized multi-tank receiver of a constant volume system, by solving Fick's 2nd law, subject to appropriate initial and boundary conditions, in each tube of the receiver. The diffusion coefficient appearing in each partial differential equation was evaluated using the empirical model of Knudsen, which allowed investigating the effect of transition from Knudsen to the slip flow regime. The experimental data for the comparison with the model was obtained in two constant volume systems, one having a low resistance receiver and the other one having a high resistance receiver. The former system served the purpose of a reference for the evaluation of the recovered diffusion and permeability coefficients from the data collected in the high resistance receiver, using an optimization procedure based on a simplex method. The reconciled diffusion and permeability coefficients compared very well with the experimental coefficients determined in a constant volume system with a low resistance receiver. Consequently, the developed procedure can be used for the estimation of the membrane properties from the any configuration of the receiver, provided that the geometry and all the relevant dimensions of the receiver are known. Ultimately, regardless of the complexity and of the receiver, it is recommended to install or reinstall a pressure sensor as close as possible to the position corresponding to the minimum resistance to gas accumulation within the receiver. This approach would allow obtaining the actual diffusion and permeability coefficients without a necessity of a tedious and time consuming optimization procedure. However, the numerical solution combined with an optimization procedure, is not an appropriate tool for the optimization of the position of a pressure transducer in the receiver. The problem of optimization of the location for the pressure transducer in addressed in Part II of this series.

Acknowledgement

The authors gratefully acknowledge the financial support for this project provided by the Natural Science and Engineering Research Council of Canada.

Nomenclature

A: Cross-sectional area of tube (m^2)

A_m: Area of the membrane (m^2)

C: Concentration of gas in the membrane (mol L^{-1})

C_1, C_2: Constants defined in Equation (3.17)

D: Diffusion coefficient of gas in tube ($m^2\ s^{-1}$)

D_m: Diffusion coefficient of gas in membrane ($m^2\ s^{-1}$)

f: Friction coefficient of adsorbed gas molecules

Kn: Knudsen number (Equation 3.14)

l_m: Thickness of membrane (m)

L: Length of tubes (m)

M: Molar mass (kg mol^{-1})

N : Volume flux ($cm^3\ s^{-1}\ m^{-2}$)

p : Pressure (Pa)

P_m: Permeability coefficient of gas in membrane (m^3(STP) $m^{-1}Pa^{-1}s^{-1}$)

p_o: Initial pressure (Pa)

r: Internal radius (m)

R: Gas constant (J $K^{-1}mol^{-1}$)

S_m: Solubility coefficient of gas in membrane (m^3(STP) $m^{-3}\ Pa^{-1}$)

t: Time (s)

T: Absolute temperature (K)

v_{STP}: Volume of one mole of gas at standard temperature and pressure (m^3)

V: Volume of tank, Volume of the receiver (m^3)

x: Distance from the entrance of a tube (m)

x': Distance from the entrance of membrane (m)

y : Dimensionless pressure (Equation 3.23)

z : Dimensionless length (Equation 3.23)

Z : Slope of the asymptote (Pa s^{-1})

Greek Symbols:

β : Constant defined in Equation (3.31)

λ : Mean free path of gas molecule (m) (Equation 3.15)

μ: Dynamic viscosity (cP)

η : Dimensionless time (Equation 3.23)

ϕ : Dimensionless diffusion coefficient (Equation 3.23)

θ_m: Time lag of membrane (s)

ζ: Coefficient of slip, dimensionless

ξ : Constant defined in Equation (3.26)

ψ : Variable defined in Equation (3.26)

Subscripts:

i, j, k: Tube number

m: membrane

n: Branch number

f: feed

References

1. R. Zolandz and G.K. Fleming, Gas Permeation, in H. Sirkar (Ed.), Membrane Handbook, Van Nostrand Reinhold, New York, 1992.
2. W.J. Koros, G. K. Fleming, Membrane-based gas separation, J. Membr. Sci., 83, 1 (1993).
3. H.A. Daynes, The process of diffusion through a rubber membrane, Roy. Soc. Proc., 97 (1920) 286-307.
4. R.M. Barrer, Permeation, diffusion and solution of gases in organic polymers, Trans. Farad. Soc., 35 (1939) 628-643.
5. G.J. van Amerongen, The permeability of different rubbers to gases and its relation to diffusivity and solubility, J. Appl. Phys., 17 (1946) 972-985.
6. W.A. Rogers, R.S. Buritz and D Alpert, Diffusion coefficient, solubility, and permeability for helium in glass, J. Appl. Phys., 257 (1954) 868-875.
7. D.R. Paul and T. DiBenedetto, Diffusion in amourphous polymers, J. Polym. Sci. Part C, 10 (1965) 17.
8. R. Ash, R.M. Barrer and D.G. Palmer, Diffusion in multiple laminates, Br. J. Appl. Phys., 16 (1965) 873-884.
9. J.H. Petropoulos and P.P. Roussis, Study of "non-fickian" diffusion anomalies through time lags. V. Simple distance-dependent anomalies in laminated media, J. Chem. Phys., 51 (1969) 1332-35.
10. H.L. Frisch and S. Prager, Time lag and fluctuations in diffusion through an inhomogeneous material, J. Chem. Phys., 63 (1971) 1451-53.
11. B. Kruczek, H.L. Frisch, R. Chapanian, Analytical solution for the effective time lag of a membrane in a permeate tube collector in which Knudsen flow regime exists, J. Membr. Sci. 256 (2005) 57-63
12. B. Kruczek, F. Shemshaki, S. Lashkari, R. Chapanian, H.L. Frisch, Effect of a resistance-free tank on the resistance to gas transport in high vacuum tube, J. Membr. Sci. 280 (2006) 29-36
13. S. Lashkari, B. Kruczek, H.L. Frisch, General solution for the time lag of a single-tank receiver in the Knudsen flow regime and its implications for the receiver's configuration, J. Membr. Sci. 283 (2006) 88–101

14. J. Crank, Mathematics of Diffusion, 2nd Edition, Clarendon Press, Oxford, 1975.
15. V.M. Zhdanov, V.I. Roldughin, Kinetic phenomena in the diffusion of gases in capillaries and porous bodies, Colloid J. 64(1) (2002) 1-24.
16. D. Valougeorgis, The friction factor of a rarefied gas flow in a circular tube, Physics of Fluids 19(9) (2007) 091702 1-4.
17. S.W. Rutherford, D.D. Do, Knudsen, slip, and viscous permeation in a carbonaceous pellet, Ind. Eng. Chem. Res. 38 (1999) 565-570.
18. L. B. Loab, "The Kinetic Theory of Gases" 3rd ed., Dover Publication, Inc., New York (1961) pp. 278-300.
19. R.B. Bird, W.E. Stewart and E.N. Lightfoot, Transport Phenomena, 2nd Ed., John Wiley & Sons, New York, 2001.
20. A. Tabe-Mohammadi, T. Matsuura, S. Sourirajan, Design and construction of gas permeation system for the measurement of low permeation rates and permeate compositions, J. of Membr. Sci., 98 (3) (1995) 281-286.
21. A. Alsari, B. Kruczek, T. Matsuura, Effect of pressure on the aging of dense (PPO) membranes, Sep. Sci. Tech., 42 (12) (2007) 2567-2582.
22. K.C. Khulbe, F. Hamad, C. Feng, T. Matsuura, T. Gumi, C. Palet, Characterization of the poly(phenylene oxide) dense membrane prepared at different temperatures, Sep. Pur. Tech., 36 (1) (2004) 53-62.
23. J.P.G. Villaluenga, A. Tabe-Mohammadi, Effects of pressure ratio and pressure difference on the gas permeation properties of rubbery and glassy membranes, J. Polym. Eng., 23 (3) (2003) 209-223.
24. B. Kruczek, T. Matsuura, Limitations of a constant pressure-type testing system in determination of gas transport properties of hydrophilic films, J. Membr. Sci., 177 (2000) 129-142.
25. B. Kruczek, T. Matsuura, Effect of metal substitution of high molecular weight sulfonated polyphenylene oxide membranes on their gas separation performance, J. Membr. Sci., 167 (2) (2000) 203-216.
26. K.C. Khulbe, T. Matsuura, G. Lamarche, H.J. Kim, The morphology characterisation and performance of dense PPO membranes for gas separation, J. Membr. Sci., 135 (1997) 211-223.

27. K.C. Khulbe, G. Chowdhury, B. Kruczek, R. Vujosevic, T. Matsuura, G. Lamarche, Characterization of the PPO dense membrane prepared at different temperatures by ESR, atomic force microscope and gas permeation, J. Membr. Sci., 126 (1997) 115-122.
28. S.W. Rutherford, D.D. Do, Review of time lag permeation technique as a method for characterisation of porous media and membranes, Adsorption, 3(4) (1997) 283-312.

Chapter 4

Effect of Resistance to Gas Accumulation in Multi-Tank Receivers on Membrane Characterization by the Time Lag Method. Part II: Analytical Approach for Optimization of the Position of the Pressure Sensor

S. Lashkari[1], B. Kruczek[1]*

To be submitted to Journal of Membrane Science

[1] Department of Chemical Engineering
University of Ottawa
161 Louis Pasteur Street
Ottawa, ON K1N 6N5, Canada
Fax: (613) 562-5172
Phone: (613) 562-5800 ext. 6302
E-mail: kruczek@eng.uottawa.ca

* **To whom correspondence should be addressed.**

Abstract

The distribution resistances to gas accumulation in multi-tank receivers, which are typical in constant volume systems, were analyzed assuming that gas transport in the receiver is governed by Knudsen diffusion. The final equations for the position-dependent time lag were derived by solving the governing set of partial differential equations using Laplace transforms and the concept of asymptotic solution. The obtained analytical solutions compared well with the experimental results reported in Part I of this series, in particular with those obtained in the experiments performed at relatively low feed pressures. The derived analytical solutions allow for optimization of the position of the pressure transducer in the receiver, that is, finding a "zero time lag" position in any configuration of a multi-tank receiver. Regardless of the actual configuration the "zero time lag" position always occurs in the tube connecting the largest tank to the main line of the receiver, very close to the tank. The developed model suggests using multiple smaller tanks rather than one large tank. Moreover, for a given number of tanks, the model suggests using tanks having the same, preferably small volume, rather than tanks having different volumes. While the use of multiple tanks make the configuration of the receiver more complex, the resistance to gas accumulation is minimized provided that the length of extra tubing is minimized, while their diameter is not smaller than 6.35 mm (1/4 in.)

Keywords: Constant volume system, Knudsen flow, time lag, permeability, diffusion coefficient

4.1 Introduction

Constant volume (CV) systems have been used for the characterization of gas permeation through semi-permeable membranes since the introduction of the latter in the mid nineteenth century [1, 2]. The principle of using CV systems for the measurement of gas permeation is based on ideal gas law. The volume of a receiver, i.e. the volume downstream from the membrane, is constant; as a result, when the gas permeates through the membrane the receiver's pressure increases. Consequently, gas flow measurement methods, which utilize CV systems, are often referred to as variable-pressure methods or barometric methods. Since the introduction of a time lag method by Daynes nearly a century ago [3], which was brought to the prominence by Barrer [4], CV systems are also widely used for the evaluation of membrane diffusivity.

Over the years the CV systems have evolved considerably. However, a CV system used in the most recent Standard Test Method for determining gas permeation rates by the variable-pressure method [5], still utilizes a simple Dow gas transmission cell, originally developed in late 1950s [6]. In general, the Dow cell is representative of the early designs of CV systems. In the Standard Test Method for determining gas permeation rates [5], the gas is accumulated directly under the tested membrane and the volume of the receiver is varied by means of an adapter. It is important to emphasize that the requirement of "constant volume" is not strictly observed in the Dow's cell, because the pressure increase due to gas permeation is measured using a mercury manometer, and as the pressure of the accumulated gas increases, the mercury in the capillary leg is being displaced. Interestingly, although high accuracy, low-range pressure transducers are commercially available for several decades, the standard procedure described above still relies on the "old fashion" pressure measurement.

Implementation of pressure transducers for measuring the pressure downstream form the membrane, however, is not the only difference between the Dow's cell and modern CV systems. Generally, in case of the modern systems, the permeating gas is no longer accumulated directly under the tested membrane. The configurations of the receiver in modern CV systems can be divided into two groups, systems with a single accumulation tank and systems with multiple accumulation tanks.

The example of a CV system with a single accumulation tank is described by O'Brian et al. [7]. In this system, depending on the anticipated permeation rate, the tank with appropriate volume can be used. However, the range of tank volumes, the length and size of tubing used downstream from the membrane are not reported. The system described in Ref. 7 was modified by Costello and Koros to allow for its use at elevated temperatures; the accumulation tank used in modified system has volume of 1000 mL [8]. Recently, Al-Juaied and Koros [9] reported using 6.35 mm (1/4 in.) and 3.175 mm (1/8 in.) tubes and the total receiver volume of 1029 mL. Assuming the same size of the accumulation tank in Ref. [8] and in Ref. [9], 29 mL corresponds to the volume of 6.35 mm (1/4 in.) and 3.175 mm (1/8 in.) tubes as well as the volume associated with valves and fittings downstream from the membrane. CV systems with a single accumulation tank are also used by other research groups [10-12].

Unlike the systems with a single accumulation tank, in systems with multiple accumulation tanks the receiver volume can be changed without exposing the system to atmosphere. The latter is not desirable, because re-evacuation of the receiver might be very time consuming. For example, Huvard et al. reported two weeks as a minimum evacuation time before performing any gas permeation experiments [13]. One of the earliest examples of a system with multiple accumulation tanks, but without any detailed specifications, is provided by Stern et al. [14]. Based on the schematic diagram provided in this reference, the system consists of three accumulation tanks arranged in parallel. Another example of a three-tank system is described Kemp [15], in which two of the tanks are arranged in parallel, while the third tank is in series with the other two. As a result, the volume downstream from the membrane can have five discrete values ranging from 4.77 mL to 108.7 mL [15]. The system reported by Huvard et al. consists of four accumulation tanks arranged in parallel and 6.35 mm (1/4 in.) tubes [13]. While the volumes of the accumulation tanks are not reported, according to the schematic diagram, each tank has a different volume. Therefore, the volume of the receiver in that system can have 16 discrete values. Multiple accumulation tanks are also used in CV system described by Lin et al [16] and Mohammadi et al. [17].

As we have shown in Part I of this series [18], the combination high vacuum, tubes with small diameter and accumulation tanks may lead to very large errors in the

diffusion and permeability coefficients determined by the variable-pressure method. On the other hand, the resistance to gas accumulation leads, depending on the position of a pressure sensor, to under or overestimation of the time lag of the tested membrane [19-21]. This implies that regardless of the actual resistance to gas accumulation, there is always a specific location within the receiver at which the time lag of the tested membrane could be measured accurately. In other words, the position of the pressure transducer can be optimized to minimize the errors due to resistance to gas accumulation. The approach used in Part I of this series to retrieve the actual values of diffusivity and permeability [18], could also be used for the optimization of the position of a pressure sensor in the receiver. However, this would require a trial and error procedure, which could be very time consuming. Therefore, the objective of Part II of this series is to develop a tool for quick optimization of the position of pressure transducer in any configuration of the receiver. Using the data from the optimized location of the pressure transducer would greatly facilitate the data reconciliation approach presented in Part I of this series.

4.2 Background - concept of "zero time lag"

The resistance to gas transport through a homogeneous membrane leads to a delayed response at the low pressure side of the membrane to a change in pressure at the high pressure side of the membrane. This delay, which is typically quantified by a time lag of the membrane (θ_{ml}), allows for the determination of the membrane diffusivity (D_m). In the simplest case, in which the membrane is initially completely degassed, the pressure at the feed side after a step change remains constant and the pressure at the permeate side despite gas permeation remains negligible, the sorption at the high pressure side and desorption at the low pressure side are instantaneous, and the solubility of the gas in membrane obeys Henry's law, the diffusion coefficient and the time lag are correlated by Sannett [2].

$$\theta_{ml} = \frac{l_m^2}{6D_m} \tag{4.1}$$

where l_m is the membrane thickness. In many cases, rather than monitoring the pressure response at the low pressure side it might be more convenient to monitor the pressure

changes at the high pressure side, while the permeate side is continuously evacuated. In this case, the corresponding expression for the time lag is given by [22]:

$$\theta_{m0} = -\frac{l_m^2}{3D_m} \tag{4.2}$$

To distinguish between the time lags given by Equations (4.1) and (4.2), the former is referred to as an outflow time lag and the latter as an inflow time lag. The fact that the inflow time lag is always negative while the outflow time lag is always positive suggests that there is a position within a membrane associated with a zero time lag.

In our previous publications, we have extended the concept of time lag to characterize the resistance to gas accumulation in various simple configurations [19-21]. In the simplest case in which the gas flows into a cylindrical tube at one end while the other end of the tube closed, we have showed, assuming a constant diffusion coefficient of the gas in the tube (D), that the time lag in the pressure response depends on the distance from the flow source (x) [19].

$$\theta(x) = \frac{l^2}{6D} - \frac{(l-x)^2}{2D} \tag{4.3}$$

where l is the length of the tube. The requirement of constant diffusion coefficient in a tube exists when the mean free path of gas molecules is much larger than the diameter of the tube, i.e., at very high vacuum and/or in tubes of very small diameter; and the corresponding Knudsen diffusion coefficient is evaluated from [23]:

$$D = \frac{2}{3} r \sqrt{\frac{8RT}{\pi MW}} \tag{4.4}$$

where r is the tube radius, R is the universal gas constant, T is the absolute temperature, and M is the molecular weight of the gas.

Going back to Equation (4.3), for $x = 0$, the corresponding time lag, θ_0, becomes identical to the inflow time lag given by Equation (4.2), while for $x = l$, the corresponding time lag, θ_l, becomes identical to the outflow time lag given by Equation (4.1). Also, it follows from Equation (4.3) that for $x/l = 0.423$, $\theta(x) = 0$. This means, if the membrane time lag experiment were performed in a CV system whose receiver consisted of only a single tube described above, the pressure sensor should be located at $x/l = 0.423$ from the

flow source (membrane), in order to avoid the error arising from the resistance to gas accumulation in the receiver.

The position of the "zero time lag" in a tube changes when a resistance-free tank is attached to the tube [20-21]. In a resistance-free tank, the probability of finding a gas molecule, which is entering the tank, is the same anywhere within the tank. Since typical accumulation tanks have an internal diameter of at least 50.8 mm (2 in.), the corresponding Knudsen diffusion coefficient is relatively large. This, in combination with a short axial dimension of typical accumulation tanks allows considering them as resistance-free. In the limiting case in which as an accumulation tank is attached to the end of the tube, which is opposite from the source of the gas flow, the expression for the position-dependent time lag in the tube becomes [20]:

$$\theta(x)=\frac{\frac{l^2}{D}\left(\frac{l}{6}+\frac{V}{2A}\right)}{l+\frac{V}{A}}-\frac{(l-x)^2}{2D}-\frac{V(l-x)}{AD} \tag{4.5}$$

where V is the volume of the tank and A is the internal cross sectional area of the tube. Setting $\theta(x)=0$ in Equation (4.5) and solving for x/l leads to:

$$\frac{x}{l}=1-\sqrt{\left(\frac{V}{Al}\right)^2+\frac{2(l/6+V/2A)}{l+V/A}}+\frac{V}{Al} \tag{4.6}$$

It follows from Equation (4.6) that for $V \rightarrow 0$, $x/l \rightarrow 0.423$ and for $V \rightarrow \infty$, $x/l \rightarrow 1$. In other words, the presence of the resistance-free tank at the end of tube pushes the "zero time lag" position towards the end of the tube. Moreover, as the volume of the resistance free tank increases, the magnitude of the negative time lag upstream from the "zero time lag" position dramatically increases.

In our recent publication [21], to generalize the analysis on the effect of a resistance free tank, we allowed the tank to be attached to the receiver anywhere along the main tube by means of a connecting tube (L3), which is shown graphically in Figure 4.1. Consequently, the main tube was split into two parts, L1 upstream from L3 and L2 downstream from L3. Allowing each tube to have different internal diameters and consequently different cross-sectional areas and the diffusion coefficients, the

corresponding expressions for the position-dependent time lag in each tube are given by [21].

In L1:
$$\theta_1(x_1) = \Phi - \left(1 + 2\frac{V_{total} - A_1 l_1}{A_1(l_1 - x_1)}\right)\frac{(l_1 - x_1)^2}{2D_1} - \frac{l_2^2}{2D_2} - \left(1 + 2\frac{V}{A_3 l_3}\right)\frac{l_3^2}{2D_3} \tag{4.7}$$

In L2:
$$\theta_2(x_2) = \Phi - \frac{(l_2 - x_2)^2}{2D_2} - \left(1 + 2\frac{V}{A_3 l_3}\right)\frac{l_3^2}{2D_3} \tag{4.8}$$

In L3:
$$\theta_3(x_3) = \Phi - \frac{l_2^2}{2D_2} - \left(1 + 2\frac{V}{A_3(l_3 - x_3)}\right)\frac{(l_3 - x_3)^2}{2D_3} \tag{4.9}$$

The parameter Φ represents the contribution to the time lag, which is independent of the position of the pressure transducer, and is by:

$$\Phi = 2\frac{V}{A_3 l_3}\left(1 - \frac{A_3 l_3 + V}{V_{total}}\right)\frac{l_3^2}{2D_3} + \sum_{i=1}^{3}\frac{l_i^2}{2D_i}\left(1 - \frac{2}{3}\frac{A_i l_i}{V_{total}}\right) \tag{4.10}$$

in which,
$$V_{total} = A_1 l_1 + A_2 l_2 + A_3 l_3 + V \tag{4.11}$$

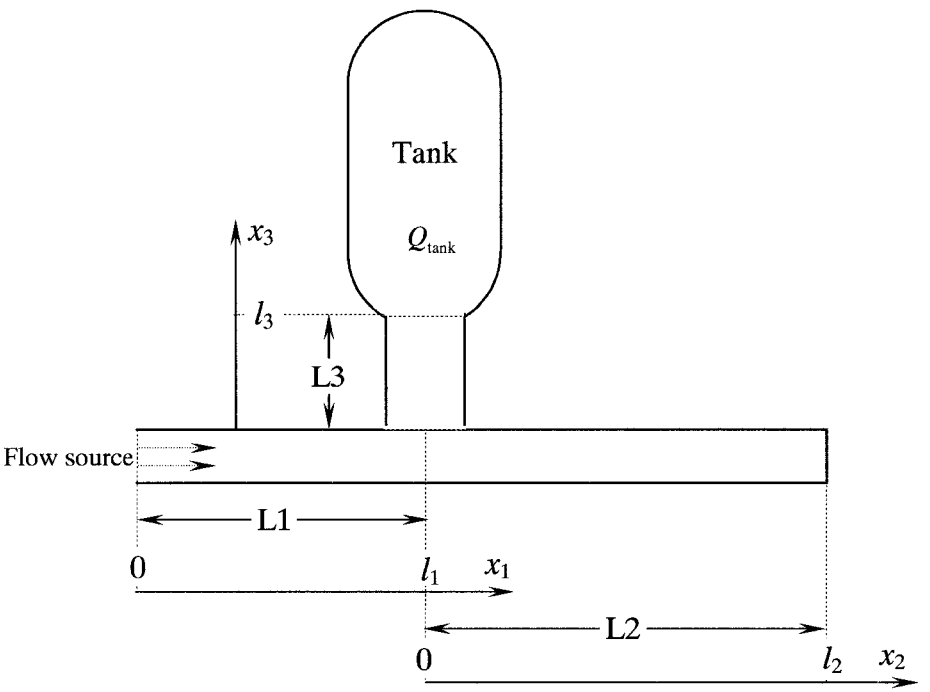

Figure 4.1. Schematic representation of a single-tank receiver of CV system. Simplified configuration of an outflow receiver for the modeling purposes.

The "zero time lag" positions in L1, L2 and L3 are not immediately apparent from the respective equations. Therefore, to illustrate application of these equations, we will assume, referring to Figure 4.2, that the volume of the accumulation tank is 1000 cm^3, the length of the main tube (L1 + L2) is 30 cm, the length of side tube (L3) is also 30 cm, and the side tube is attached to the main tube 10 cm from the flow source so that L1 = 10 cm and L2 = 20 cm. Furthermore, all tubes are assumed to be standard 6.35 mm (1/4 in.) tubes. With these specifications Figure 4.2 presents the position-dependent time lag in each tube. It is evident that there are no "zero time lag" positions in L1 and L2. Moreover, $\theta_1(x_1)$ and $\theta_2(x_2)$ are always negative, and $\theta_1(x_1)$ is more negative than $\theta_2(x_2)$.

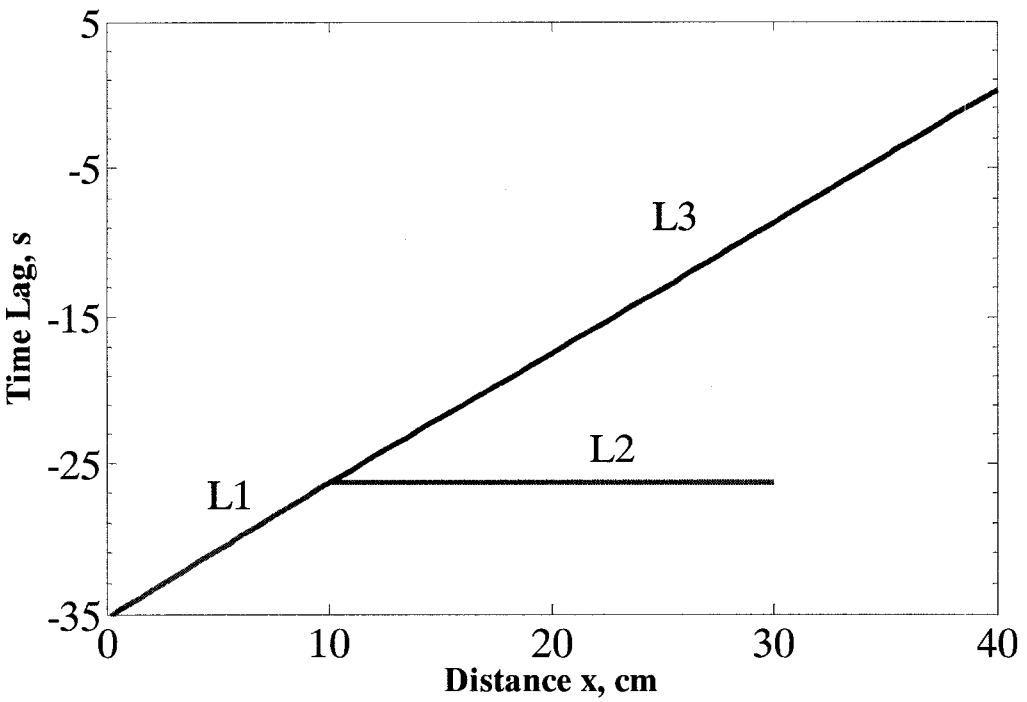

Figure 4.2. Application of the solution for a single-tank receiver. Tank volume V = 1000 cm^3, L_1 = 10 cm, L_2 = 20 cm, L_3 = 30; all tubes are standard 6.35 mm (1/4 in.) tubes.

While the magnitude of the negative time lags in L1 and L2 depends on the diameter and the length of the tubes, as well as the volume of the accumulation tanks, the negative time

lags in L1 and L2 will exists as long as V/A_3L_3 is greater than unity, which practically would always be the case. The zero time lag position in Figure 4.2 exists only in L3 very close to the accumulation tank. In general, as the volume of the tank increases, the "zero time lag" position is shifted towards the accumulation tank, which is consistent with Equation (4.6).

In reality, as the pressure downstream from the membrane increases, there might be a transition from the Knudsen flow to the slip flow regime, in which the diffusion coefficient becomes a function of pressure. As a result, the analytically predicted "zero time lag" position may not be completely accurate. Nevertheless, installing the pressure transducer at the analytically predicted "zero time lag" position, could still be considered as an optimized position for the pressure sensor in the receiver.

4.3 General solution for receivers with multiple tanks

To generalize the analysis of the "zero time lag" position, it is necessary to expand the configuration shown in Figure 4.1 to consider receivers with multiple tanks. Figure 4.3 presents a generalized multiple tank configuration, in which *n-1* tanks are connected to the main line by means of *n - 1* connecting tubes with different lengths but equal diameters. Consequently, the main line can be split into *n* tubes. The length and diameter of connecting tubes can be different from the main line. Similarly to our previous analysis for a single tank receiver, the diffusion coefficient in each tube is constant and can be evaluated using Equation (4.4); the diffusion coefficient in each tank is assumed sufficiently large to consider tanks as resistance-free. With a constant diffusion coefficient, the gas transport in each tube can be described by Fick's second law

$$\frac{\partial p_i}{\partial t} = D_i \frac{\partial^2 p_i}{\partial x^2} \tag{4.12}$$

where p_i is the pressure in tube i, t is time, x is the position in the tube, and D_i is the Knudsen diffusion coefficient defined by Equation (4.4). At the entrance to the main tube ($x = 0$), the boundary condition is expressed in terms of the gas flow rate entering the tube and Fick's first law:

$$\frac{\partial p_1(0,t)}{\partial x} = -\frac{RT}{D}\frac{Q_1(0,t)}{A} = -\frac{\alpha}{D} \tag{4.13}$$

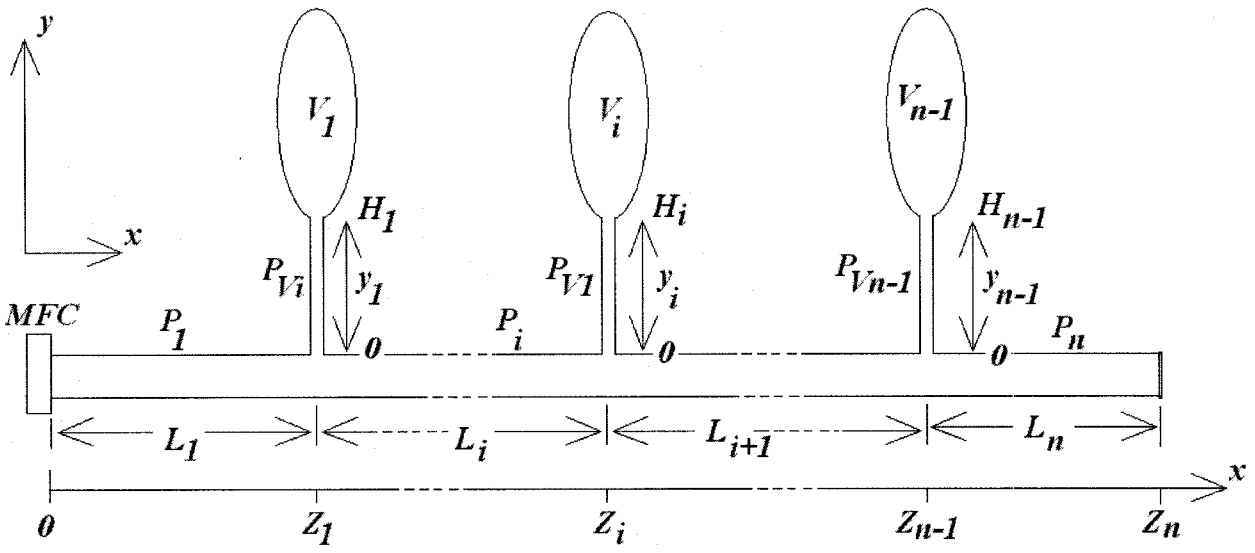

Figure 4.3. Schematic representation of a multi-tank receiver of CV system for the modeling purposes.

While the gas flow into the first tube corresponds to the rate of gas permeation across the membrane, for example in a membrane time lag test, Q_1 will be assumed constant. It can be resembled by having a mass flow controller in the beginning of the tubes. Therefore $\alpha = RTQ_1(0,t)/A$ is constant. It is important to emphasize that as shown in our previous publications [20,21], when the diffusion coefficient is constant, the resistance to gas accumulation is independent of the gas flow rate. The concept of a general boundary condition for the receiver introduced in Part I of this series [18], is also applicable in this analysis. Consequently, each junction in the receiver shown in Figure 4.3 can be characterized by at least one of the following equations.

$$D_i A_i \left(\frac{\partial p_i}{\partial x}\right)\Big|_{x=Z_i^-} = D_{i+1}A_{i+1}\left(\frac{\partial p_{i+1}}{\partial x}\right)\Big|_{x=Z_i^+} + D_{Vi}A_{Vi}\left(\frac{\partial p_{Vi}}{\partial y_i}\right)\Big|_{y=0} + V_i \frac{\partial p_{Vi}}{\partial t}\Big|_{y=H_i} \tag{4.14}$$

$$p_i|_{x=Z_i^-} = p_i|_{x=Z_i^+} = p_{Vi}|_{y=0^+} = p_{Vi}|_{V_i} \tag{4.15}$$

There are three types of junctions in Figure 4.3. At a point where the connecting tube is attached to the main tube, the last term in Equations (4.14, 4.15) disappears. On the other hand, at a point where the connecting tube is attached the tank, the 2nd and 3rd terms

disappear. Finally, at the end of the main tube, terms 2-4 in Equation (4.14) are zero and consequently.

$$\frac{\partial p_n(Z_n,t)}{\partial x}=0 \tag{4.16}$$

The above equation is also applicable at a point where the connecting tube is attached the tank when the volume of the tank is zero. The initial condition in each tube is given by:

$$p_i(x,0)=p_{Vi}(y,0)=p_0=const. \tag{4.17}$$

The method of solution of the governing PDE subject to the initial and boundary conditions specified by Equations (4.13-4.17) is similar to that in Ref. [21]. Consequently, only the key steps will be shown in the current paper. Application of the Laplace transform to Equation (4.12) along with the initial condition given by Equation (4.17) allows conversion of time-domain to s-domain, thus reducing the governing PDE into the following ordinary differential equation:

$$s\bar{p}_i-p_0=D_i\frac{\partial^2\bar{p}_i}{\partial x^2} \tag{4.18}$$

which has the following particular solution:

$$\bar{p}_i(x_i,s)=M_i\sinh(q_ix_i)+N_i\cosh(q_ix_i)+\frac{p_0}{s} \tag{4.19}$$

where $q_i=\sqrt{\frac{s}{D_i}}$ and M_i and N_i, which can be determined from the Laplace transform from the boundary conditions applicable for a given tube. To simplify the following analysis, we will assume that all tubes in the main line have the same diameter and consequently, the same diffusion coefficient (D). This will allow dropping subscripts for the main tube in the final solutions and write the solution in a compact form of equations.

For a tube in the main line the application of the boundary conditions leads to:

$$\bar{p}_i-\frac{p_0}{s}=\frac{\frac{\alpha q}{s^2}\left(\cosh(q(Z_n-x_i))+\sum_{j=i}^{n-1}\lambda_j\frac{M_{Vj}}{M_n}\sinh(qZ_n)\sinh\left(q\left(Z_j-x_i\right)\right)\right)}{\sinh(qZ_n)+\sum_{j=1}^{n-1}\lambda_j\frac{M_{Vj}}{M_n}\sinh(qZ_n)\cosh\left(qZ_j\right)} \tag{4.20}$$

On the other hand, for a connecting tube, Equation (4.19) after application of the boundary conditions becomes:

$$\overline{p}_{Vi} - \frac{p_0}{s} = \frac{\alpha q}{s^2}\left(\frac{\cosh\left(q\left(Z_n - Z_i\right)\right) + \sum_{j=i+1}^{n-1}\lambda_j\left(\frac{M_{Vj}}{M_n}\sinh\left(qZ_n\right)\right)\sinh\left(q\left(Z_j - Z_i\right)\right)}{\sinh\left(qZ_n\right) + \sum_{j=1}^{n-1}\lambda_j\left(\frac{M_{Vj}}{M_n}\sinh\left(qZ_n\right)\right)\cosh\left(qZ_j\right)}\right)\times \left(\frac{\cosh\left(q_{Vi}\left(H_i - y_i\right)\right) + \frac{V_i q_{Vi}}{A_{Vi}}\sinh\left(q_{Vi}\left(H_i - y_i\right)\right)}{\cosh\left(q_{Vi}H_i\right) + \frac{V_i q_{Vi}}{A_{Vi}}\sinh\left(q_{Vi}H_i\right)}\right) \tag{4.21}$$

where:

$$\frac{M_{Vi}}{M_n}\sinh\left(qZ_n\right) = q\frac{\delta_i}{q}\left(\cosh\left(q\left(Z_n - Z_i\right)\right) + \sum_{j=i+1}^{n-1}\lambda_j\left(\frac{M_{Vj}}{M_n}\sinh\left(qZ_n\right)\right)\sinh\left(q\left(Z_j - Z_i\right)\right)\right) \tag{4.22}$$

$$M_n = \frac{-\alpha q/s^2}{1 + \sum_{j=1}^{n-1}\lambda_j\frac{M_{Vj}}{M_n}\cosh\left(qZ_j\right)} \tag{4.23}$$

$$\delta_i = \frac{\sinh\left(q_{Vi}H_i\right) + \frac{V_i q_{Vi}}{A_{Vi}}\cosh\left(q_{Vi}H_i\right)}{\cosh\left(q_{Vi}H_i\right) + \frac{V_i q_{Vi}}{A_{Vi}}\sinh\left(q_{Vi}H_i\right)} \tag{4.24}$$

$$\lambda_i = \frac{D_{Vi}A_{Vi}q_{Vi}}{DAq} = \frac{A_{Vi}}{A}\sqrt{\frac{D_{Vi}}{D}} \tag{4.25}$$

It can be shown that Equations (4.20, 4.21) can be rewritten in the following form:

$$\overline{p}_i - \frac{p_0}{s} = \frac{f_i(s)}{s^2\,\Delta(s)} \tag{4.26}$$

$$\overline{p}_{Vi} - \frac{p_0}{s} = \frac{f_{Vi}(s)}{s^2\,\Delta(s)} \tag{4.27}$$

Moreover, both Equations (4.26) and (4.27) are regular at $s = 0$, i.e., they take a finite value:

$$\lim_{s\to 0}\frac{f_i(s)}{\Delta(s)} = \lim_{s\to 0}\frac{f_{Vi}(s)}{\Delta(s)} = \frac{\alpha}{Z_n + \sum_{j=1}^{n-1}\left(\frac{A_{Vj}}{A}H_j + \frac{V_j}{A}\right)} = \frac{\alpha A}{V_{total}} \tag{4.28}$$

Therefore, according to the concept of the asymptotic solution [24], the expression for time lag in each tube can be evaluated from:

$$\theta_i(x_i) = \lim_{s\to 0}\left(\frac{\Delta'(s)}{\Delta(s)} - \frac{f_i'(s)}{f_i(s)}\right) = \lim_{s\to 0}\left(\frac{\Delta'(s)}{\Delta(s)}\right) - \lim_{s\to 0}\left(\frac{f_i'(s)}{f_i(s)}\right) \tag{4.29}$$

Evaluation of Equation (4.29) for the tubes in the main line and for the connecting tubes leads to the following expressions for the position-dependent time lag:

- Tubes in the main line:

$$\frac{\theta_i}{\theta_0} = \frac{\Upsilon}{\theta_0} + \frac{\Psi}{\theta_0} - 3\left(\frac{Z_n - x}{Z_n}\right)^2 - 6\sum_{j=i}^{n-1}\left(\frac{A_{Vj}H_j + V_j}{AZ_n}\right)\left(\frac{Z_j - x}{Z_n}\right) \tag{4.30}$$

- Branch connecting tubes:

$$\frac{\theta_{Vi}}{\theta_0} = \frac{\theta_i(x = Z_i)}{\theta_0} + 3\frac{D}{D_{Vi}}\frac{H_i\left(H_i + 2\dfrac{V_i}{A_{Vi}}\right)}{Z_n^2} - 3\frac{D}{D_{Vi}}\left(\left(\frac{H_i - y_i}{Z_n}\right)^2 + 2\frac{V_i}{A_{Vi}Z_n}\frac{(H_i - y_i)}{Z_n}\right) \tag{4.31}$$

where:

$$\theta_0 = \frac{Z_n^2}{6D} \tag{4.32}$$

$$\frac{\theta_i(x = Z_i)}{\theta_0} = \frac{\Upsilon}{\theta_0} + \frac{\Psi}{\theta_0} - 3\left(\frac{Z_n - Z_i}{Z_n}\right)^2 - 6\sum_{j=i+1}^{n-1}\left(\frac{A_{Vj}H_j + V_j}{AZ_n}\right)\left(\frac{Z_j - Z_i}{Z_n}\right) \tag{4.33}$$

$$\frac{\Upsilon}{\theta_0} = \frac{AZ_n}{V_{total}} - 6\sum_{j=1}^{n-1}\frac{DA_{Vj}H_j}{D_{Vj}V_{total}}\left(\frac{1}{3}\left(\frac{H_j}{Z_n}\right)^2 + \frac{V_jH_j}{A_{Vj}Z_n^2} + \left(\frac{V_j}{A_{Vj}Z_n}\right)^2\right) + 3\sum_{j=1}^{n-1}\left(\frac{A_{Vj}H_j}{V_{total}} + \frac{V_j}{V_{total}}\right)\left(\frac{Z_j^2 + (Z_n - Z_j)^2}{Z_n^2}\right) \tag{4.34}$$

$$\frac{\Psi}{\theta_0} = 6\frac{V_{total}}{AZ_n}\sum_{j=1}^{n-1}\left(\frac{A_{Vj}H_j + V_j}{V_{total}}\right)\sum_{k=j+1}^{n-1}\left(\frac{A_{Vk}H_k + V_k}{V_{total}}\right)\left(\frac{Z_k - Z_j}{Z_n}\right) \tag{4.35}$$

4.4 Discussion

4.4.1 Verification of the model

It can be shown that in the limiting case, in which there is only one accumulation tank attached to the main line, Equation (4.30) becomes Equation (4.7) for the tube

upstream from the junction point. Similarly, in this limiting case Equation (4.31) becomes Equation (4.9) for the connecting tube and Equation (4.8) for the tube downstream from the connection point. This proves consistency between the model for a multiple-tank receiver developed in this study and the previously developed model for the receiver with a single tank [21]. The following configuration will provide the result:

$$\begin{array}{lllll} n=3 & L_1=l_1 & L_2=L_3=0 & H_1=l_2 & H_2=l_3 \\ A=A_1 & A_{V1}=A_2 & A_{V2}=A_3 & V_1=0 & V_2=V \end{array} \tag{4.36}$$

The asymptotic solutions are applicable to a steady state system, i.e., when the pressure response anywhere within the receiver becomes a linear function of time. Consequently, using Equations (4.30) and (4.31) the expression for the gas flow rate entering the receiver should be obtained. Using the *final value theorem* the steady state flow rate at any position within the receiver is given by [25]:

$$Q_{i\infty}(x_i)=\lim_{s\to 0} s\overline{Q_i}(x_i,s)=\lim_{s\to 0}\left(-s\frac{DA}{RT}\frac{d\,\overline{p}_i}{d\,x_i}\right) \tag{4.37}$$

Application of Equation (4.37) to any point in the main line, leads to the following expression for the dimensionless flow rate:

$$\frac{Q_{i\infty}(x_i)}{Q_1(0,t)}=\frac{(Z_n-x_i)+\sum_{j=i}^{n-1}\frac{A_{Vj}}{A}\left(H_j+\frac{V_j}{A_{Vj}}\right)}{Z_n+\sum_{j=1}^{n-1}\frac{A_{Vj}}{A}\left(H_j+\frac{V_j}{A_{Vj}}\right)}=\frac{(Z_n-x_i)A+\sum_{j=i}^{n-1}\left(A_{Vj}H_j+V_j\right)}{V_{total}} \tag{4.38}$$

Similarly, at any point in the connecting tube, the dimensionless steady state flow rate is given by:

$$\frac{Q_{Vi\infty}(y_i)}{Q_1(0,t)}=\frac{\frac{V_i}{A}}{Z_n+\sum_{j=1}^{n-1}\frac{A_{Vi}}{A}\left(H_i+\frac{V_i}{A_{Vi}}\right)}=\frac{V_i}{V_{total}} \tag{4.39}$$

Equations (4.38) and (4.39) show that at steady state, the flow rate at any point within the receiver is proportional to the ratio of the volume downstream from that point to the total volume of the receiver. In addition, applying the continuity equation to any point within the receiver, leads to:

$$\frac{\partial p}{\partial t} = -RT\frac{d\left(\frac{Q_{i\infty}(x)}{A}\right)}{dx} = \frac{\alpha}{Z_n + \sum_{j=1}^{n-1}\frac{A_{Vj}}{A}\left(H_j + \frac{V_j}{A_{Vj}}\right)} = \frac{Q_1(0,t)RT}{V_{total}} \tag{4.40}$$

Equation (4.40) proves that if the diffusion coefficient were constant, the gas flow into the receiver could be evaluated from the pressure rise at any point within the receiver. However, since as the gas accumulates in the receiver, the diffusion coefficient becomes a function of pressure, the actual flow rate determined from Equation (4.40) might be associated with an error. The larger the position-dependent time lag the larger the error in the measured flow rate from the pressure rise and the longer the time for this error to disappear. In other words, installing a pressure sensor at the zero-time lag position increases the reliability of the gas flow rate determined from the rate of pressure rise.

4.4.2 Comparison of the experimental data and the model results

Another way to verify the correctness of the developed model is to compare the theoretical results obtained using Equations (4.30, 4.31) with the experimental data. In Part I of this series we presented apparent diffusivity coefficients in a PPO membrane determined from the pressure responses recorded simultaneously by two or three pressure transducers in two CV systems, one having a high resistance (HR) receiver and one having a low resistance (LR) receiver [18]. To facilitate the discussion the schematic diagrams of the LR and HR receivers are shown in Figures 4.4 and 4.5, respectively. In terms of a generalized multiple-tank configuration shown in Figure 4.3, the LR receiver consists of three parallel tanks and two parallel branches attached to the main line. The first branch corresponds to the tube connecting the outflow volume with the inflow volume. The second branch corresponds to the tube connecting the pressure transducer PT1 to the main line. Alternatively, these two branches can be treated as tubes connecting "zero volume" tanks to the main line. Similarly, the HR receiver can be represented by the generalized multiple-tank configuration shown in Figure 4.3. In case of the LR receiver the differences between the membrane time lags were relatively small, therefore to illustrate the application of the model we will use the data from the HR receiver.

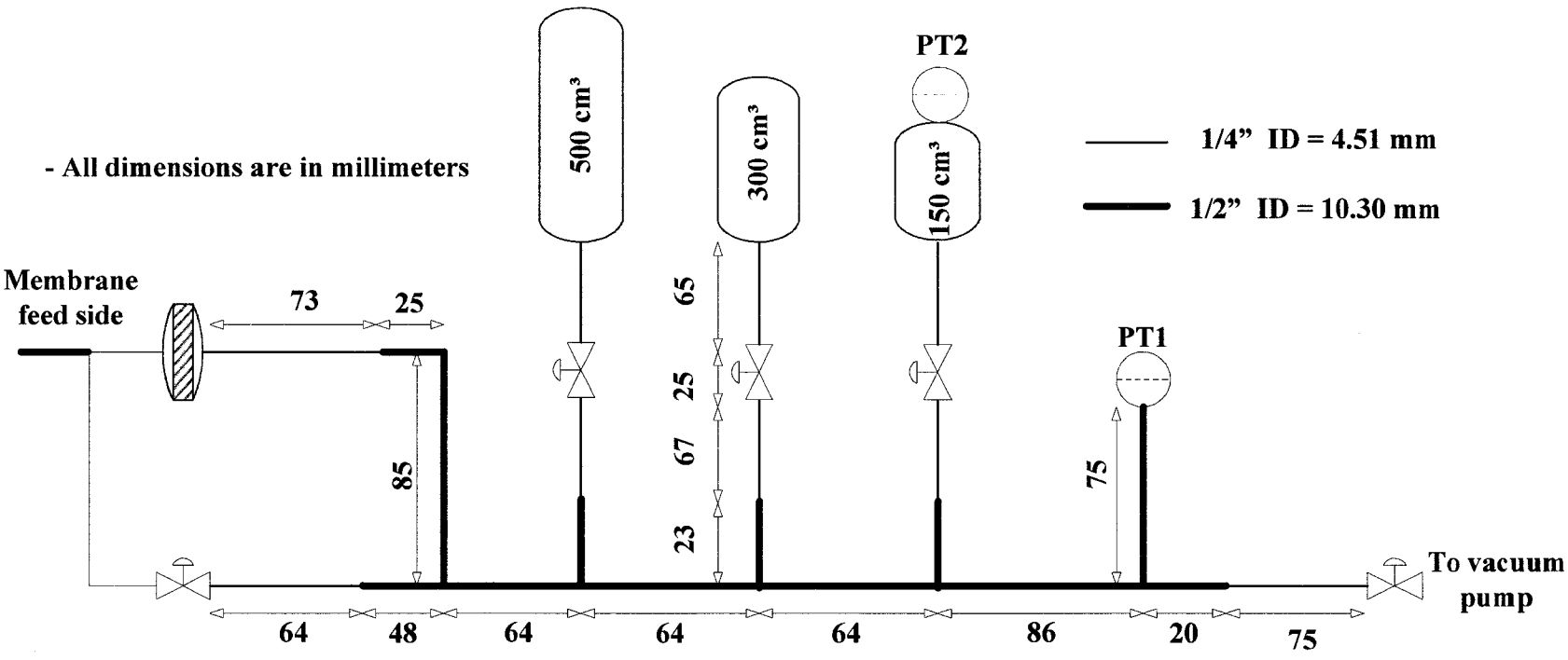

Figure 4.4. Low resistance (LR) receiver configuration.

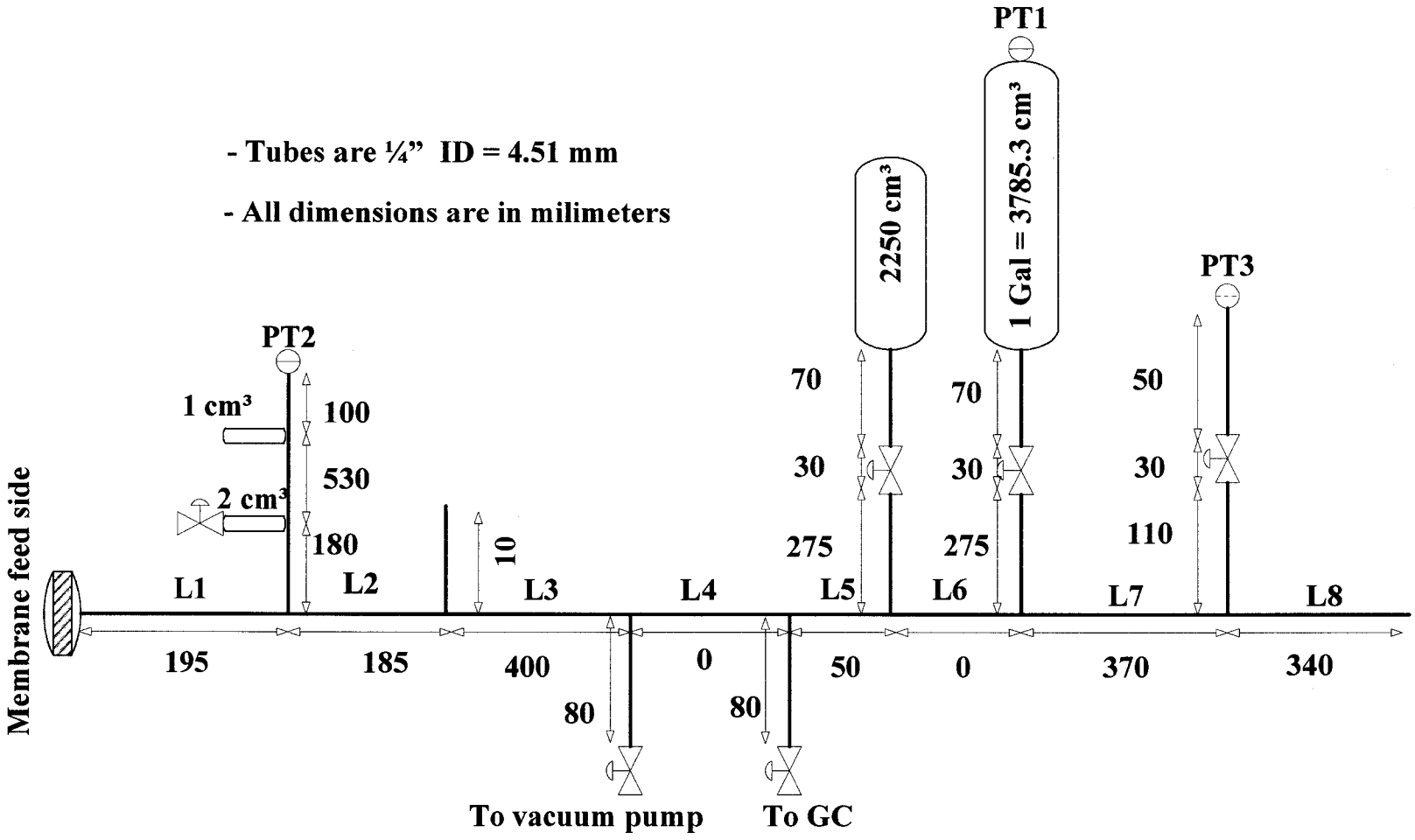

Figure 4.5. High resistance (HR) receiver configuration.

Table 4.1 presents the differences between the experimental time lags in the PPO membrane determined from PT1 and PT2 and from PT3 and PT2 in two different configurations of the HR receiver, one with both accumulation tanks and the other with only the larger accumulation tank incorporated to the receiver. The experimental differences between the time lags in the PPO membrane are compared with the theoretical differences in the time lags at the respective positions of the pressure transducers in the two configurations of the HR receiver. The theoretical model is independent of the permeation rate of the gas through the membrane, therefore, for a given configuration and the set of two pressure transducers only one theoretical value is provided. The theoretical model is presented graphically in Figure 4.6 for the test with oxygen.

Table 4.1. Comparison of the analytical model to experimentally observed differences in time lag of a PPO membrane within a HR receiver [18].

Additional Volume	Total volume cm^3	Feed pressure bar	Experimental (sec)		Theoretical (sec)	
			PT1-PT2	PT3-PT2	PT1-PT2	PT3-PT2
			Nitrogen			
2250, 3785 cm^3	6095.58	7.31	479.13	337.94	465.37	340.39
		7.14	485.41	344.94		
3785 cm^3	3844.22	7.11	313.04	199.06	339.10	214.12
		7.08	307.27	194.55		
			Oxygen			
2250, 3785 cm^3	6095.58	3.98	439.57	301.61	497.38	363.80
		3.92	442.95	304.16		
		3.18	470.86	325.16		
		2.49	492.92	343.52		
		1.82	513.54	362.08		
		1.19	517.95	365.08		
3785 cm^3	3844.22	3.88	267.79	163.15	362.42	228.85

Figure 4.6a shows the distribution of the position-dependent time lag when both accumulation tanks are attached to the receiver, while Figure 4.6b shows the analogous results when only the larger tank is incorporated into the receiver.

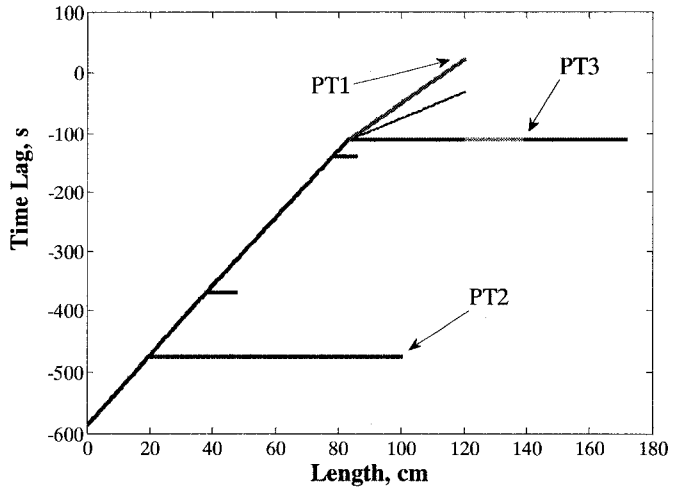

a)

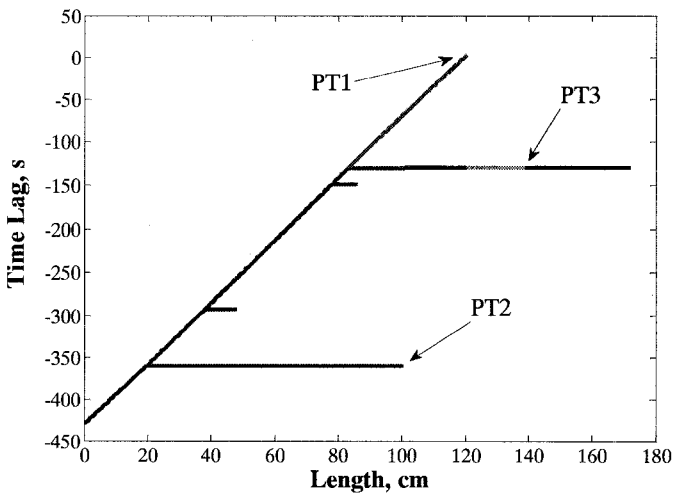

b)

Figure 4.6. Position-dependent time lag in the HR receiver for the experiments with oxygen: a) both tanks (2250, 3785 cm^3) incorporated in the receiver volume; b) large tank (3785 cm^3) incorporated in the receiver volume.

Considering the configuration with both accumulation tanks included in the receiver, the theoretical PT1 - PT2 and PT3 – PT2 are in the range of the experimentally observed differences. Although the latter varies with feed pressure, the consistency

between the experimental and theoretical differences is evident, in particular in case of test with oxygen. In case of the configuration with only the larger tank incorporated into the receiver, the theoretical PT1 - PT2 and PT3 – PT2 are greater than the corresponding experimental differences. However, the experiments in this configuration were carried out only at relatively high feed pressures for each gas. On the other hand, as shown for the tests with oxygen with both tanks incorporated into the receiver, the experimental differences in the membrane time lags increase with a decrease in the feed pressure. Consequently, the differences between the theoretical and experimental data could be smaller or even disappear if the experiments with one accumulation tank in the receiver were also performed at lower feed pressures.

A better consistency between the theoretical and experimental differences, when the latter are obtained at low feed pressures can be justified as follow. At lower feed pressures, the gas flow rate passing through the membrane and entering the receiver decreases. Therefore, the receiver's pressure stays in, or close to the Knudsen region during the measurement, which is the major assumption underlying the analytical approach. As a result, the measured time lags are more consistent with the theoretical values. It is important to emphasize that a decrease in the difference between the experimental time lags at higher feed pressures is not an indication of the lower resistance of the receiver, since the experimental time lags at higher feed pressures are very sensitive to the time frame used for the evaluation of the time lag.

4.4.3 Application of the model in design of the receiver

To illustrate the application of the analytical solution the LR receiver will be used as a case study. It is import to emphasize that to minimize the resistance to gas accumulation in the LR receiver the length of tubing was minimized for the physical dimensions of the accumulation tanks, pressure transducers and valves. Whenever possible, 12.7 mm (1/2 in.) rather than 6.35 mm (1/4 in.) tubes were used, and most importantly, the accumulation tanks having relatively low volumes were utilized. However, despite these efforts, as shown in Part I of this series, the apparent membrane properties determined from the pressure responses recorded simultaneously by PT1 and PT2 were slightly different [18].

Figure 4.7 presents the effect of incorporation of accumulation tanks on the position-dependent time lag in the receiver. To facilitate the discussion, the time lag at the position corresponding to PT1, which as shown in Figure 4.4 is located downstream from the last junction point, will be used. When no accumulation tank is attached to the receiver (Figure 4.7a), the time lag at PT1 is roughly 0.03 s. Such a negligible resistance in the configuration with no accumulation tanks is a result of using 12.7 mm (1/2 in.) tubes in the main line and minimization of the length of the main line. Incorporation of any accumulation tank into the systems results in a negative time lag at PT1, which increases as the number of the attached tanks increases. More specifically, when only a 150 cm^3 tank is attached (Figure 4.7b), the time lag at PT1 is -1.5 s; when 150 cm^3 and 300 cm^3 tanks are attached (Figure 4.7c), the time lag at PT1 is -3.0 s; when all three tanks are attached, the time lag at PT1 is -4.8 s (Figure 4.7d). On the other hand, regardless of the number of the tanks attached to the receiver, the difference between the time lags at PT2 (pressure transducer installed on the 150 cm^3 tank) and PT1 is the same. In other words, a change in the configuration upstream from a given point results in a change of time the lag downstream from that point, but the magnitude of this change is the same anywhere downstream from that point.

It is important to note that the strongest dependence of the time lag on the position occurs in the tube connecting the largest tank to the main line. In fact, the slope of the time lag versus the position in the tube is proportional to the volume at the end of tube. In the limiting case of "zero volume" at the end of a tube, that is, for a closed tube, it may appear in Figure 4.6 as if the time lag was independent of the position. In reality, the time lag in the closed tube increases with the distance from the tube entrance (x) according to: $-(l-x)^2/2D$, but for short tubes, which are not 3.175 mm (1/8 in.) diameter or smaller, the magnitude of the change with the position is very small as shown in Figure 4.7a. Consequently, while the presence of connecting tubes in the receiver complicates the mathematical analysis, the contribution of these tubes to the resistance of the receiver is negligible, unless they are used as connectors to active accumulation tanks.

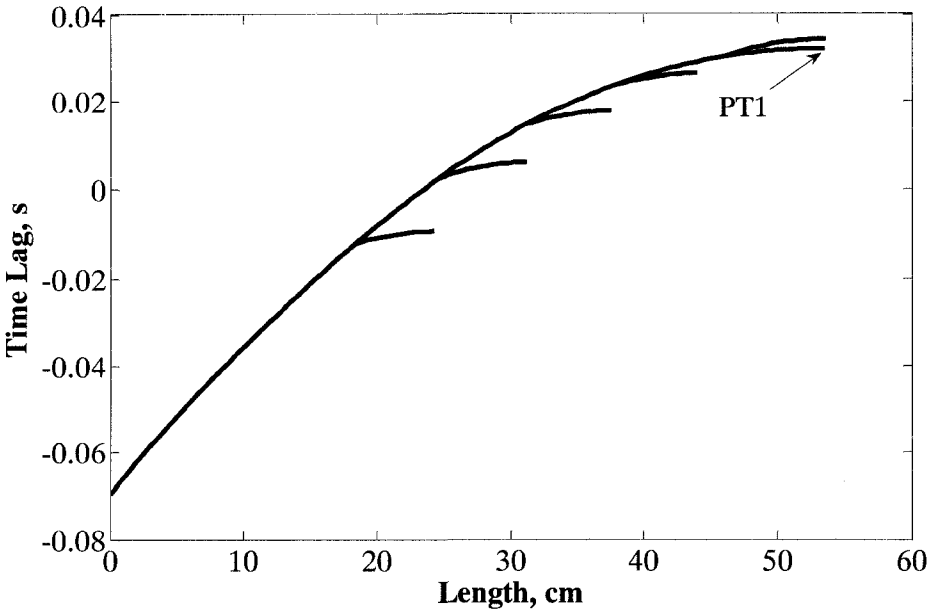

a)

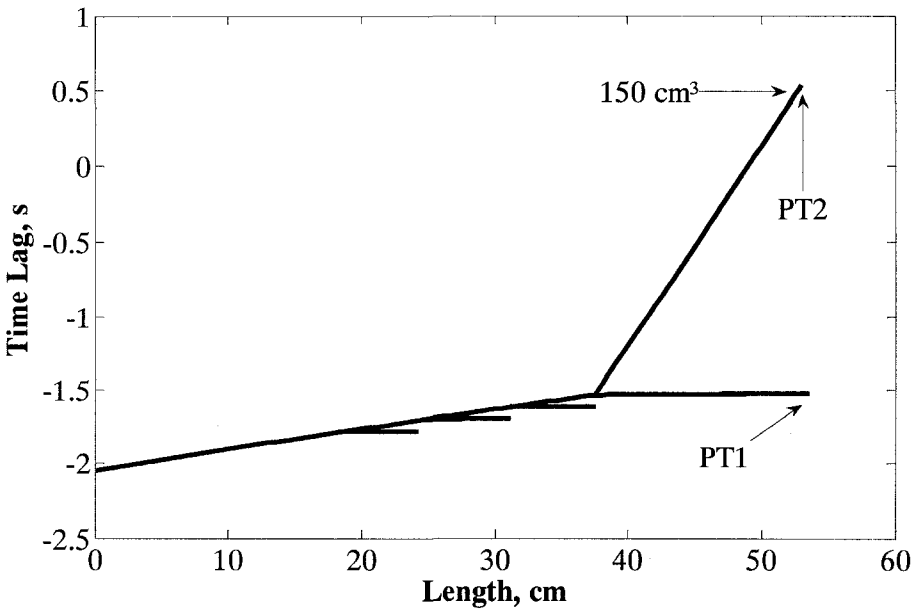

b)

c)

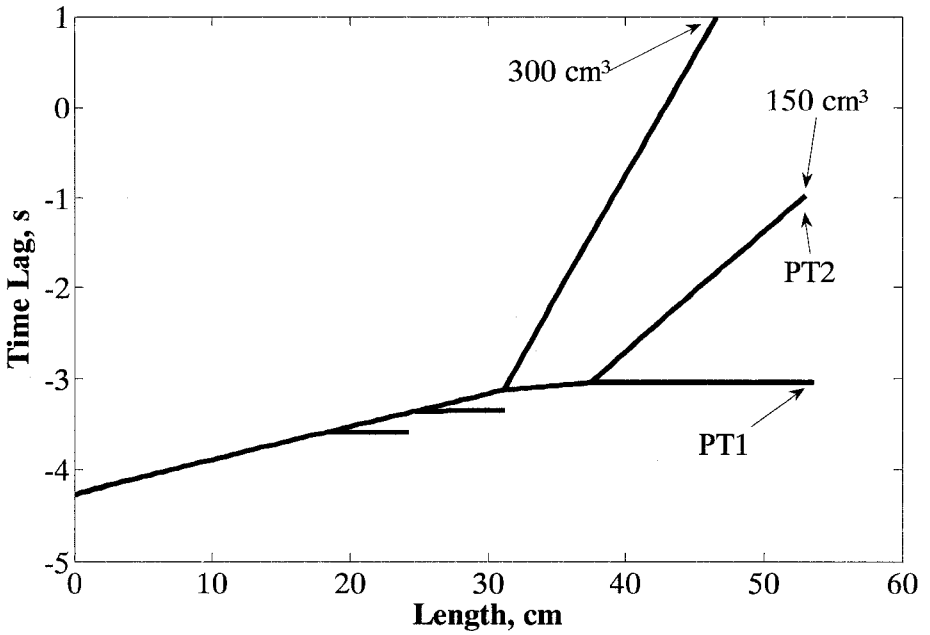

d)

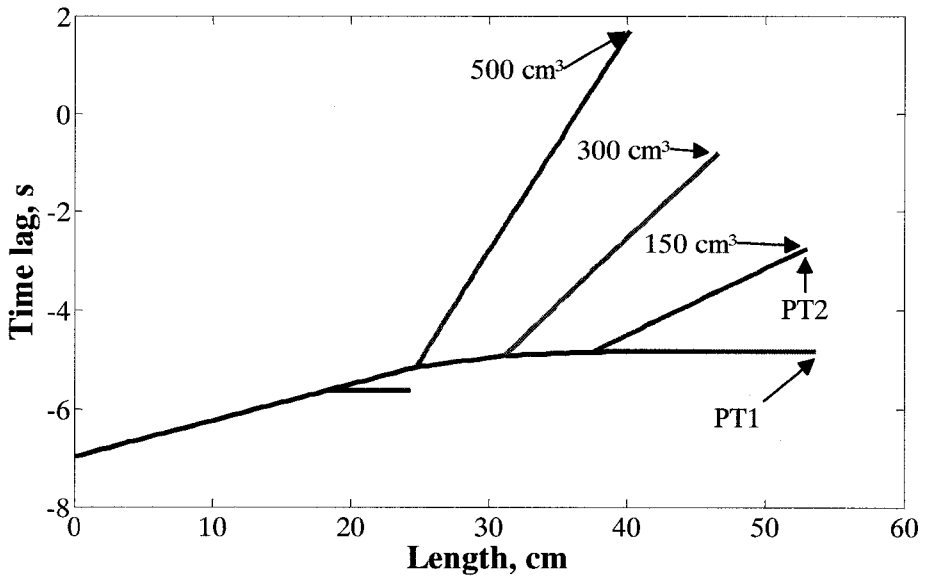

Figure 4.7. Effect of adding volume on time lag of LR receiver. a) No volume is added, b) 150 cm^3 volume is added, b) 150 cm^3 and 300 cm^3 volumes are added, d) 150, 300, 500 cm^3 volumes are added.

Considering the four configurations of the LR receiver in Figure 4.7, it can be noticed that in each configuration there is only one "zero time lag" position in the receiver, which changes with the configuration of the system. However, regardless of the configuration the "zero time lag" position always occurs in the tube connecting the largest tank to the main line, very close to the tank.

It is important to emphasize that while the negative time lag at PT1 increases with incorporation of additional tanks, for the total volume of 950 cm^3 distributed among the three tanks in Figure 4.7d, the corresponding time lag of -4.8 s is a smaller negative number than for a hypothetical case in which this volume was contained in a single tank. In the latter case, the actual time lag at PT1 would depend on the position of the tank. If this hypothetical 950 cm^3 tank were installed in place of the 150 cm^3 tank, the corresponding time lag at PT1 would be -12.4 s. Consequently, from the point of view of minimizing the resistance to gas accumulation in the receiver, it is advantageous to use several smaller tanks rather than a large, single tank.

The advantage of using multiple tanks in the receiver is further illustrated in Figure 4.8, in which the tanks are incorporated into the receiver in a different sequence than in Figure 4.7. More specifically, Figure 4.8a presents the position-dependent time lag with only the largest tank (500 cm^3) attached to the receiver. The corresponding time lag at PT1 in Figure 4.8a is -6.3 s. This time lag decreases to -5.4 s in Figure 4.8b when the volume of the receiver is increased by attaching the second tank of volume 300 cm^3. Moreover, when all three tanks are attached to the system (Figure 4.8c), the time lag at PT1 decreases to -4.8 s. Consequently, in the sequence in which the tanks of gradually decreasing volumes are attached in parallel to the main line, the actual negative time lag at PT1 decreases.

Figure 4.9 presents the position-dependent time lag in the LR receiver with all volumes attached to the main line in two hypothetical cases. In the first case (Figure 4.9a) the positions of the 150 cm^3 and 500 cm^3 are exchanged compared to Figure 4.7d. It is evident, that despite this exchange, the time lag at PT1 of -4.8 s is the same as in Figure 4.7d. Similarly, in the second case (Figure 4.9b), in which the 150 cm^3 and 300 cm^3 tanks are exchanged, the time lag at PT1 remains the same as before. This indicates that for given volumes of the accumulation tanks and the positions at which these tanks can be

attached to the main line of the receiver, the order in which they are attached does not affect the time lag in the main line downstream from the last junction point.

Figure 4.10 presents another hypothetical case in which the total volume of 950 cm^3 is distributed in three identical tanks of volume 316.7 cm^3, and the tanks are gradually attached to the main line of the receiver. It is evident that the negative time lag at PT1 in Figure 4.10 is smaller than that in Figure 4.9a and 4.9b. This suggests that to minimize the resistance to gas accumulation, the volume of the largest tank should be minimized, which can be achieved when all tanks have the same volume. Consequently, to increase the volume the receiver, it is better to attach a new tank to the main line rather than to increase the volume of one of existing tanks. At the same time, the length of the tube connecting the additional tank to the main line should be minimized while its diameter should be maximized.

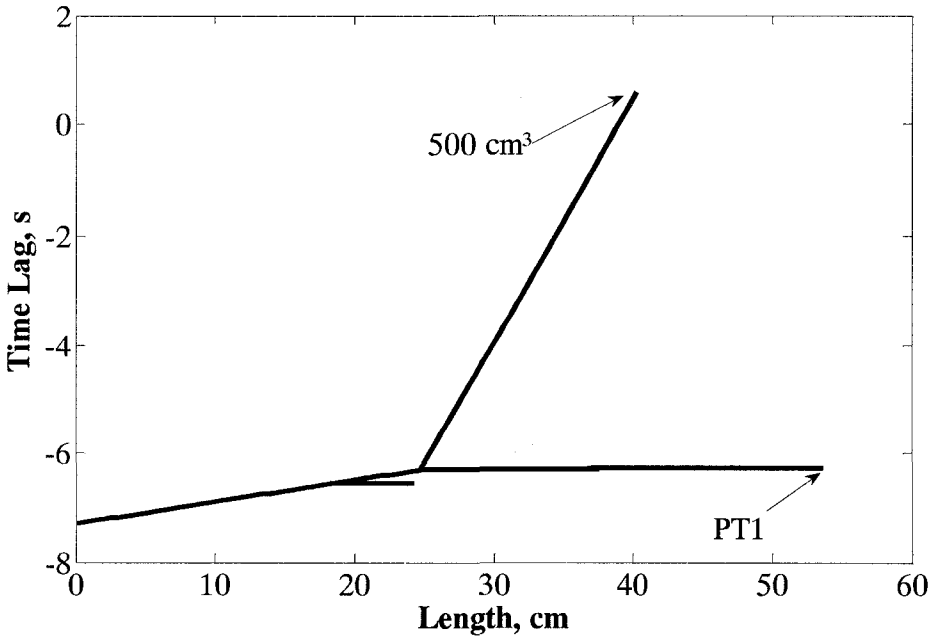

a)

b)

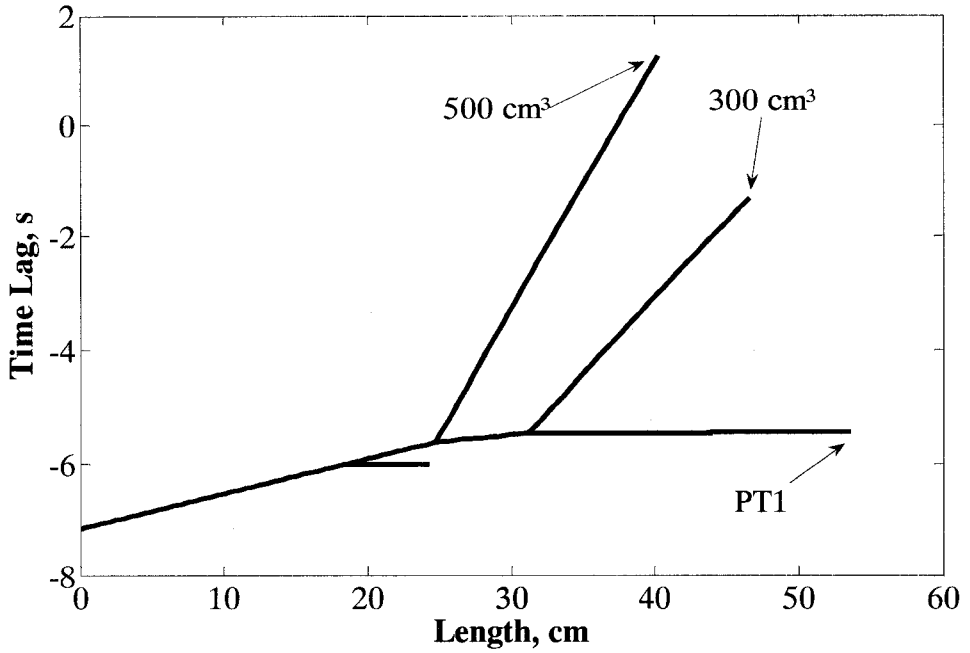

c)

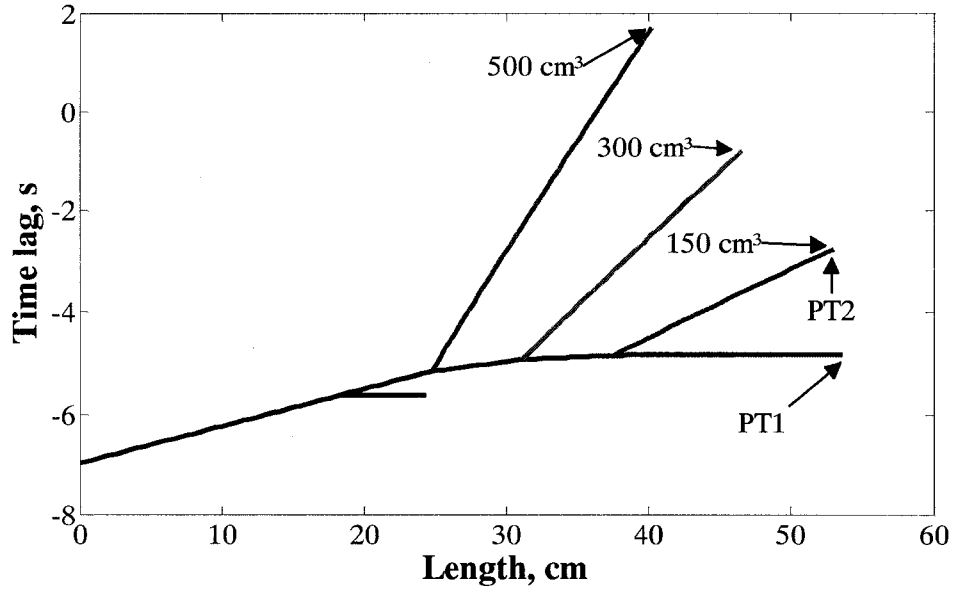

Figure 4.8. Effect of adding volume on time lag of LR receiver. a) 500 cm^3 volume is added, b) 500 cm^3 and 300 cm^3 volumes are added, d) 150, 300, 500 cm^3 volumes are added.

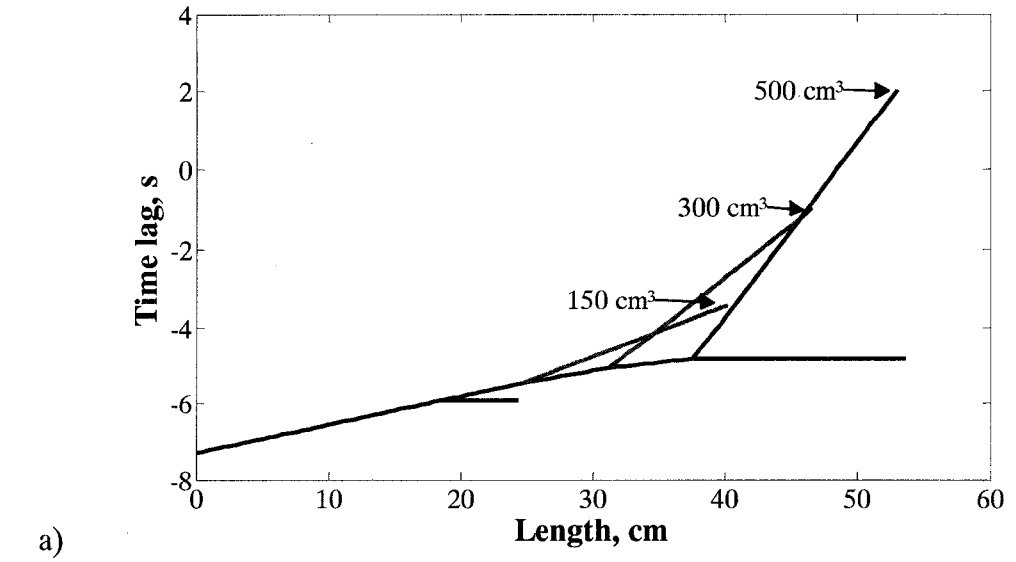

a)

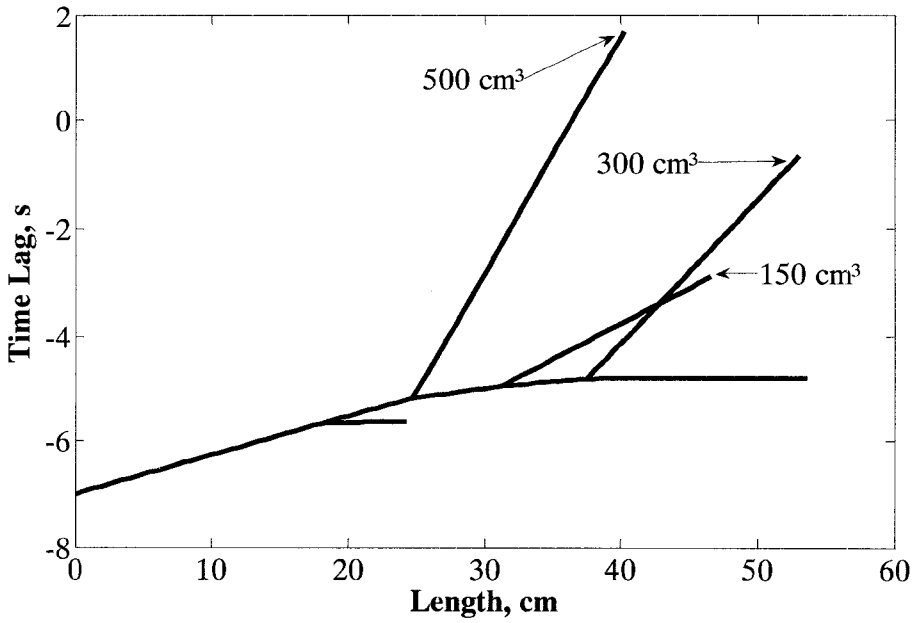

b)

Figure 4.9. Effect of position of volume on time lag of LR receiver. a) Higher volume at the end, b) Higher volume at the beginning.

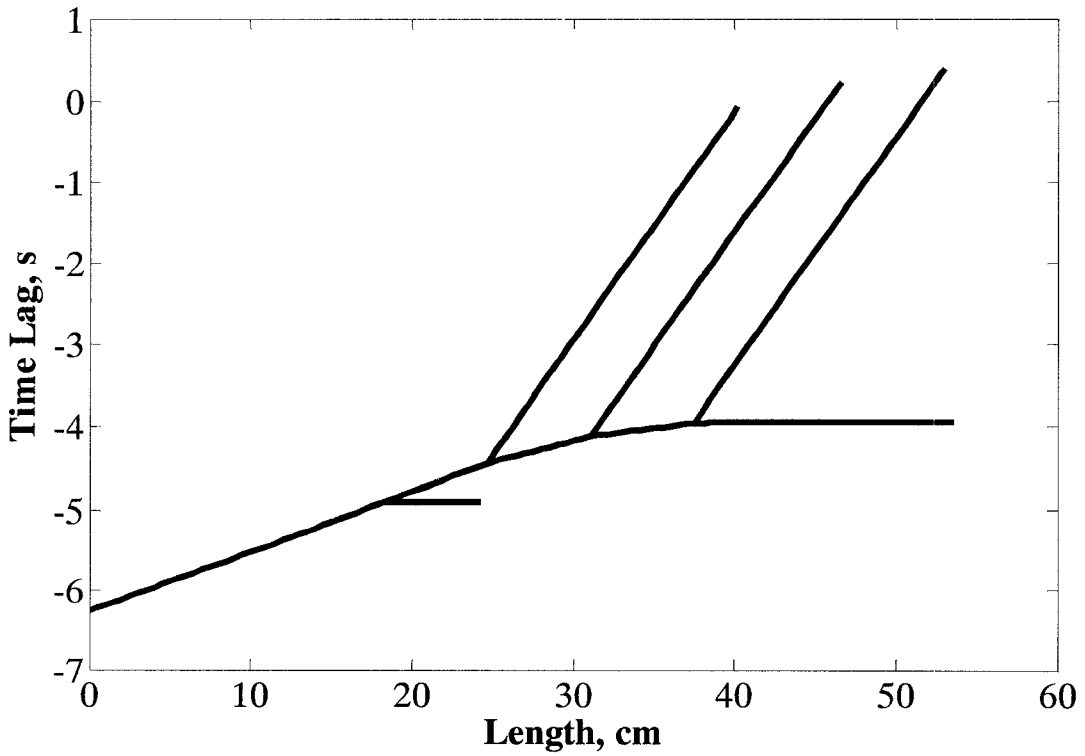

Figure 4.10 Time lag of LR receiver when the total volume (150+300+500 cm^3) distributed equally between three volumes each 950/3 cm^3.

4.5 Conclusions

The position-dependent time lag in multi-tank receivers, in which the tanks are attached to the main line in parallel, were evaluated using the concept of the asymptotic solution. The obtained solutions were applied for the prediction of differences in the position-dependent time lags in a high resistance receiver in two different configurations. The comparison with the theoretical differences with the experimental values, show that the theoretical differences are generally greater than the experimental value. However, as the feed pressure in the actual time lag experiments decreases, the experimental differences are approaching the theoretically predicted values. A better consistency between the theoretical and experimental differences in the position-dependent time lags at low feed pressures arise from the fact at low feed pressures the assumption of constant diffusion coefficient in the receiver is more realistic than at high feed pressures. The

analytical model also allows for a quick retrieval of approximate membrane properties from the data obtained under the conditions high resistance to gas accumulation.

The derived analytical solutions also allow for optimization of the position of the pressure transducer in the receiver, that is, finding a "zero time lag" position in any configuration of a multi-tank receiver. Regardless of the actual configuration the "zero time lag" position always occurs in the tube connecting the largest tank to the main line of the receiver, very close to the tank. The developed model suggests using multiple smaller tanks rather than one large tank. Moreover, for a given number of tanks, it suggests using tanks having the same, preferably small volume, rather than tanks having different volumes. While the use of multiple tanks make the configuration of the receiver more complex, the resistance to gas accumulation is minimized provided that the length of extra tubing is minimized, while their diameter is not smaller than 6.35 mm (1/4 in.).

Acknowledgement

The authors gratefully acknowledge the financial support for this project provided by the Natural Science and Engineering Research Council of Canada.

Nomenclature

A: Cross-sectional area of tube (m^2)

D: Diffusion coefficient of gas in tube ($m^2 s^{-1}$)

D_m: Diffusion coefficient of gas in membrane ($m^2 s^{-1}$)

H: Length of connection to the volume (m)

l: Length of tube (m)

l_m: Thickness of membrane (m)

L1, L2, L3: Tubes that are part of the receiver with lengths l_1, l_2, l_3, respectively.

M, N: Coefficients (Equation 4.19)

MW: Molar mass (kg mol^{-1})

p : Pressure (Pa)

p_o: Initial pressure (Pa)

q: Defined as $q_i = \sqrt{\frac{s}{D_i}}$ (Equation 4.19)

Q: Gas flow rate (kmol s^{-1})

R: Gas constant (J $K^{-1}mol^{-1}$)

s: Laplace domain

t: Time (s)

T: Absolute temperature (K)

V: Volume of tank (m^3)

V_{total}: Total volume of the receiver (m^3)

x: Distance from the entrance of a tube (m)

Z : Distance in the main tube from the entrance of the receiver

Greek Symbols:

α : Constant defined as $\alpha = RTQ_1(0,t)/A$ (Equation 4.13)

δ : Defined as Equation (4.24)

λ : Defined as Equation (4.25)

θ: Time lag of receiver (s)

θ_m: Time lag of membrane (s)

Φ : Position independent contribution to time lag of receiver (s) (Equations 4.10)

Υ : Position independent contribution to time lag of receiver (s) (Equations 4.34)

Ψ: Position independent to time lag of receiver (s) (Equation 4.35)

Subscripts:

i, j, k: Tube number

l: Permeate side of membrane

n: Branch number

References

1. K. Ghosal and B.D. Freeman, Gas separation using polymer membranes: an overview, Polymers for Advanced Technologies, 5 (1994) 673-697.
2. V.T. Sannett, The transport of gases in synthetic polymeric membranes — a historic perspective, J. Membrane Sci. 3(2) (1978) 97-115.
3. H. A. Daynes, The process of diffusion through a rubber membrane, Proceedings of the Royal Society of London, Series A, 97 (685) (Jun. 1, 1920) 286-307.
4. R.M. Barrer, Permeation, diffusion and solution of gases in organic polymers, Trans. Farad. Soc., 35 (1939) 628.
5. ASTM Standard Methods, Standard test method for determining gas permeability characteristics of plastic film and sheeting, ASTM D 1434 - 82(2003).
6. D.R. Paul and T. DiBenedetto, Diffusion in amourphous polymers, J. Polym. Sci. Part C, 10 (1965) 17-44.
7. K.C. O'Brien, W.J. Koros, T.A. Barbari, E.S. Sanders, A new technique for the measurement of multicomponent gas transport through polymeric films, J. Membr. Sci., 29 (1986) 229-238.
8. L.M. Costello and W.J. Koros, Temperature dependence of gas sorption and transport properties in polymers: measurement and applications, Ind. Eng. Chem. Res., 31 (1992) 2708-2714.
9. M. Al-Juaied, W.J. Koros, Performance of natural gas membranes in the presence of heavy hydrocarbons, J. Membr. Sci., 174 (206) 227-243.
10. A.M. Shishatskii, Yu.P, Yampol'skii, K.-V Peinemann, Effects of film thickness and density on gas permeation parameters of glassy polymers, J. Membr. Sci., 112 (1996) 275-285.
11. A. Bos, I.G.M. Pünt, M. Wessling and H. Strthmann, Plasticization-resistanct glassy polyimide membranes for CO_2/CH_4 separations, Sep. Pur. Tech., 14 (1998) 27-39.
12. Y.M. Lee, S.Y. Ha, Y.K. Lee, D.H. Suh, S.Y. Hong, Gas separation through conductive polymer membrane. 2. Polyaniline membranes with O_2 selectivity, Ind. Eng. Chem. Res. 38 (1999) 1917.

13. G.S. Huvard, V.S. Stannett, W.J. Koros and H.B. Hopfenberg, The pressure dependence of CO_2 sorption and permeation in poly(acrylonitrile), J. Membr. Sci., 6 (1980) 185-201.
14. S.A. Stern, P.J. Gareis, T.F. Sinclair and P.H. Mohr, Performance of a versatile variable-volume permeability cell. Comparison of gas permeability measurements by the variable-volume and variable-pressure methods, J. Appl. Polym. Sci., 7 (1963) 2035-2051.
15. D. R. Kemp, The diffusion time lag in heterogeneous polymer membranes, PhD Dissertation, University of Texas at Austin, 1972.
16. W.-H. Lin, R.H. Vora, T.-S. Chung, Gas transport properties of 6FDA-Durene/1,4-phenylenediamine (pPDA) copolyimides, J. Polym. Sci., Part B: Polym. Phys., 38 (2000), 2703.
17. A. Tabe Mohammadi, T. Matsuura and S. Sourirajan, Design and construction of gas permeation system for the measurement of low permeation rated and permeate compositions, J. Membr. Sci., 98 (1995) 281.
18. S. Lashkari, Q. Wang, B. Kruczek, Effect of Resistance to Gas Accumulation in Multi-Tank Receivers on Membrane Characterization by the Time Lag Method. Part I: Reconciliation of the membrane properties, to be submitted to J. Membr. Sci.
19. Kruczek, B., H. L. Frisch, and R. Chapanian, "Analytical solution for the effective time lag of a membrane in a permeate tube collector in which Knudsen flow regime exists", J. Membrane Sci., 256, (2005) 57-63.
20. B. Kruczek, F. Shemshaki, S. Lashkari, R. Chapanian and H.L. Frisch, Effect of a resistance-free tank on the resistance to gas transport in high vacuum tube, J. Membr. Sci., 280 (2006) 29-36.
21. Lashkari, S., B. Kruczek, and H. L. Frisch, "General solution for the time lag of a single-tank receiver in the Knudsen flow regime and its implications for the receiver's configuration", J. Membr. Sci., 283 (2006) 88-101.
22. S.W. Rutherford and D.D. Do, Review of time lag permeation technique as a method for characterization of porous media and membranes, Adsorption, 3 (1997) 283.

23. L.B. Loeb, The Kinetic Theory of Gases, Dover Publications, Inc. New York, 1961, pp 278-300.
24. H.S. Carslaw and J.C. Jaeger, Conduction of Heat in Solids, Oxford at the Clarendon Press, 2nd Edition, 1959, p. 402.
25. R.A. Siegel, A Laplace Transform technique for calculating diffusion time lags, J. Membr. Sci. 26 (1986) 251-262.

Part II

Constant Pressure System

This part focuses on an investigation of the phenomena of back diffusion and back permeation in a traditional constant pressure system. Two papers are presented in this Part. The first one is a detailed explanation of a fully-automated flowmeter, which was designed and constructed in this thesis. The second paper provides the theoretical and experimental data related to the phenomena of back diffusion and back permeation. Additional results, which were not included in the second paper, are presented in Appendix C. Chronologically, these additional results, which are consistent with those presented in the second paper, were the first results on the combined phenomena of back diffusion and back permeation. However, for the sake of brevity, the first set of the experimental results was removed from the body of the thesis. In addition, Appendix C presents examples of dynamic experiments, which may be published at a later date.

Chapter 5

Development of a Fully Automated Soap Flowmeter for Micro Flow Measurements

S. Lashkari, B. Kruczek*

Flow Measurement and Instrumentation, 19 (2008) 397- 403

Department of Chemical Engineering
University of Ottawa
161 Louis Pasteur Street
Ottawa, ON K1N 6N5, Canada
Fax: (613) 562-5172
Phone: (613) 562-5800 ext. 6302
E-mail: bkruczek@uottawa.ca

* **To whom correspondence should be addressed.**

Abstract

A soap flowmeter is commonly used for measuring of low flow rates of gases. In order to have accurate measurements using this instrument, the diameter and the length of the flowmeter tube should be selected on the basis of the expected flow rate [1]. However, there are restrictions when reducing the diameter of the tube or increasing its length. The objective of this study is to find alternative ways to improve the accuracy of the existing flowmeters in the range of micro flow rates. To accomplish this objective a fully automated system for making soap bubbles was developed and implemented with different commercial soap flowmeters. In addition, a computerized data acquisition was developed to improve the accuracy of the time measurement. The final product is capable of performing hands-free measurements even in isolated areas. Gas flow rates ranging from 5 to 100 μL/min were successfully measured and suggestions for more improvements in the accuracy of flow measurements are proposed. Since the automated bubble maker allows controlling the size of the soap bubbles, the modified soap flowmeter is also suitable for the investigation of free foam films in vertical tubes.

Keywords: Gas flow measurement, Micro flow, Soap flowmeter, Soap bubble, Foam film, Bubble maker

5.1 Introduction

Although the application of soap flowmeters to measure gas flow rates has a long history, the scientific description of these instruments was first revealed by Exner [2] and Barr [3]. Since then, soap flowmeters have been widely utilized for the calibration of other gas flowmeters [4-6]. In addition, soap flowmeters have been applied for the manual measurements of gas flow rates, especially for low flow rates such as those in gas chromatography and membrane characterization. The main advantage of a soap flowmeter is that it operates based on measurement of primary units, the time and volume. As a result, there is no correlation which could change over time and thus, there is no need to recalibrate the instrument over time. Recently, a soap flowmeter has also been employed to study free foam films, which are of growing interest in diverse industrial applications [7,8].

Figure 5.1 represents a schematic diagram of a typical soap flowmeter. In order to describe the performance of this instrument, it is important to distinguish four parts of the soap flowmeter. The bottom part accommodates a rubber bulb containing soap, a side aperture for the gas influx, and a smooth intersection to hold a small residual of soap from which the bubble is formed. The purpose of this part is to create a bubble and to transfer it to the main tube. There are other possible configurations for this part such as those described by Barr [2]. The second part is a part of the tube above the side aperture for the gas influx where the created bubble accelerates and reaches a constant velocity. The length of this part depends on the gas flow rate as well as on the diameter of the tube. In most flowmeters this part is very short compared to the length of the main tube. The third part is a graduated tube where the actual measurement takes place. The bubble moving in the calibrated tube should have a constant velocity, which requires a constant pressure difference across the bubble. A smooth glass wall, which is well lubricated with a soap falling down, provides a frictionless path for the soap bubble to rise. The last part is the end section of the tube, in which the bubbles break up thus creating the falling liquid soap which lubricates the tube walls. According to Czubryt and Gesser [9] and Guo and Heslop [10], back diffusion of air may significantly affect the velocity of the bubble in the end section; therefore, this part should not be used for the measurement purposes.

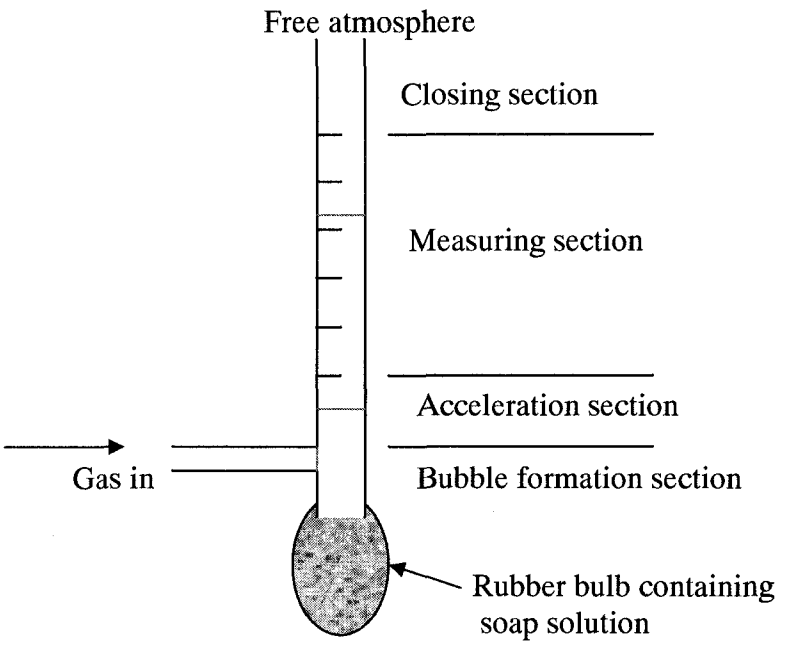

Figure 5.1. Schematic of a typical soap flowmeter.

The physics of soap bubbles is well documented in books dedicated to study the soap bubbles experimentally, analytically, and numerically [11,12]. Growing number of applications of soap films, especially in studies of gas-liquid interface, was the motivation of the work performed at the University of Cambridge on simulation of a soap film moving in vertical tube [7,8].

The current study is aimed on improving the existing soap flowmeters to make the measurements of low flow rates of gases both automated and more accurate. To accomplish this, two of the four parts in the soap flowmeters are modified, the bubble maker and the calibrated tube. The details of these modifications as well as the performance of the automated soap flowmeters are presented and discussed in this paper.

5.2 Description of the automated soap flowmeter

5.2.1 Bubble maker apparatus

In order to produce a bubble in a typical soap flowmeter shown in Figure 5.1, the rubber bulb must be squeezed to push the liquid soap into the tube. When the liquid level is above the inlet gas tube, the liquid is held for a short time to wet the glass, after which the rubber bulb is released leaving some residual liquid at the intersection with the gas inlet and this residual liquid is pushed inside the main tube forming a bubble. The produced bubble must be thin, yet strong enough to pass through the calibrated part of the tube without breaking up. There are several parameters affecting the properties of the bubble. One of the parameters is the properties of the soap solution. The common solution is a mixture of glycerol, distilled water, and a surfactant. The influence of soap properties on the flow measurement are discussed in the literature [7,13]. The holding time of liquid is another parameter, which however has not been adequately investigated.

Figure 5.2 presents a schematic diagram of an automated bubble making device developed in this study. In order to make the process fully automated, a computer-controlled three way solenoid valve, a needle valve, a low pressure regulator and a sealed soap container are used. When the three way valve is opened by a computer signal, a low external pressure, less than 108 kPa (1 psig), is applied on the surface of the soap liquid in the sealed container. To avoid a sudden pressurization of the liquid soap, which would cause a jump and splash of the liquid on the tube walls, a needle valve is installed between the low pressure regulator and the three way solenoid valve. This allows pushing slowly the soap liquid inside the flowmeter tube and forming a soap bubble in front of the gas inlet to the main tube. The final height of the liquid in the tube depends on the applied pressure and the ratio of the area of the liquid soap container to the cross sectional area of the tube. Then, the solenoid valve is closed and the pressure on the liquid soap is released through the vent. This allows removing excess liquid from the tube back to the soap container.

It is generally believed that to make a thin bubble the time interval for holding the liquid in the tube should be very short, and by increasing the holding time, the curvature of the produced bubble will increase. In turn, the greater the curvature of the bubble the more liquid will be carried out by the bubble. Experimental data and equations relating

the amount of liquid with the diameter of the bubble in vertical tubes are presented and discussed in the literature [8,13,14]. On the other hand, Heslop et al. [15] showed that there is a range of the liquid amount from which meta-stable bubbles can be formed.

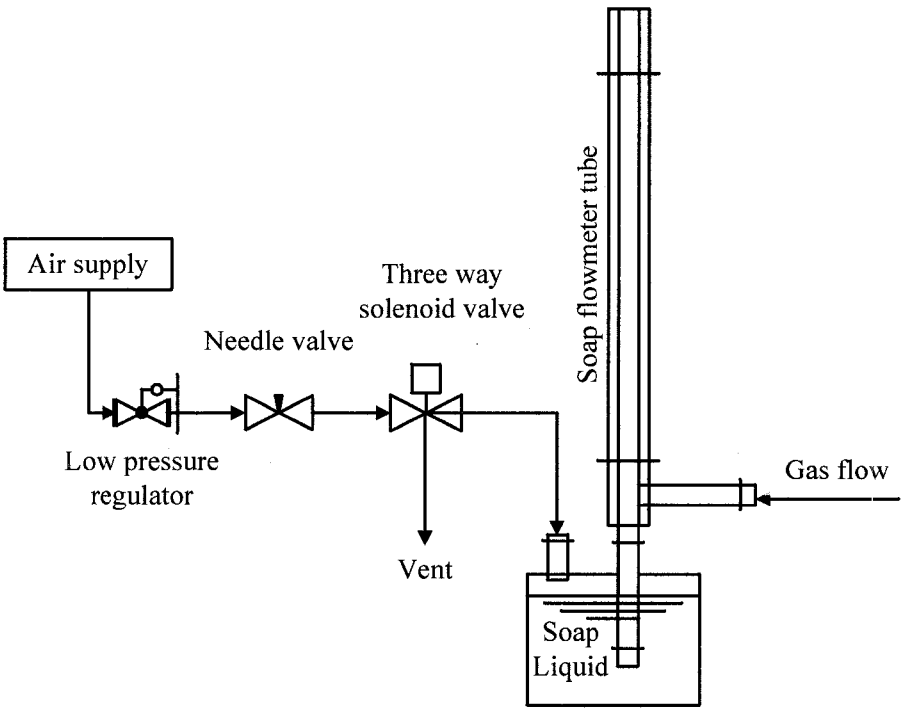

Figure 5.2. Schematic diagram of a traditional CP system with an automated soap bubble maker apparatus.

Using a computer controlled instrument makes it possible to adjust the time interval for holding liquid inside the tube. Consequently the bubbles can be produced in the same way in all the experiments. This is one of the human errors, which can easily be eliminated using the bubble maker developed in this study. According to our experience, in a 500 μL flowmeter, 0.3 second is a sufficient residence time for the soap liquid in the tube to make a thin, yet strong, layer of soap at the gas entrance. It is important to note that such a short residence time would not be attainable if the bubble were made manually by squeezing a rubber bulb. Moreover, since opening and closing of the solenoid valve is controlled by a computer program, the measurements of the flow rate can be executed automatically in a pre-scheduled routine.

The only commercial bubble making apparatus is available with SF-1/2, an automated flowmeter supplied by STEC. The bubble making mechanism in SF-1/2 is based on the principle discussed by Bailey et al. [16], which utilizes another type of a soap bubble flowmeter described by Barr [2]. Essentially, the bubble is made by pushing the liquid to touch the bottom of the flowmeter tube. This mechanism is suitable for much higher flow rates (0.2-1000 mL/min) than those which are of interest in the current work. The advantage of the mechanism described in the current study is the speed and the accuracy of making the same bubble every time. In addition, having a pneumatic instrument with a supply pressure as low as 108 kPa (1 psig), makes it versatile and portable, as well as fully automated and hands-free.

5.2.2 Sensors setup for continuous measurement of gas flow rates

Levy [1], who studied the accuracy of soap flowmeters, concluded that the uncertainty of using a stop watch for the time measurement is ±0.2 s, and this is the most important contributor to the uncertainty in the flow rate measurement by this technique. He suggested that employing an electro-optical circuit reported later by Hunter [17] might improve the accuracy. Arenas et al. [18] described these optical sensors for an automatic detection of soap bubble passing through the flowmeter; these sensors were commercialized more than a decade ago. SF-1/2 and Optiflow supplied by STEC and Supelco, respectively, utilize a timer-trigger mechanism for bubble detection. Optiflow Flowmeter has various models which cover the range of flow between 0.1-5000 mL/min with 3% accuracy of any reading.

In addition, Arenas et al. [18] provided recommendations for measuring the flow rates as low as 1 mL/min with an uncertainty of less than 1.5%, and these recommendations have been adapted in this work to design a continuous and automated measurement of gas flow rates in a soap flowmeter. In the current study, a digitalized data acquisition is employed in order to reach a better accuracy by analyzing data. As shown later, by analyzing the data collected from the sensors, we have expanded the range of the flow measurements to 0.005 mL/min, which is much lower than 0.1 mL/min specified by Supelco for their Optiflow flowmeters. To our best knowledge, the lowest commercially available manual soap bubble flowmeter, which is supplied by SGE, has

the nominal size of 50 μL, and allows measurements between 0.005 – 0.5 mL/min. We have reached the lower end of the measurement range with an order of magnitude greater nominal size of the bubble flowmeter.

Figure 5.3 presents a schematic of light emitting diodes (LEDs) and their corresponding photo diode sensors installed on a 500 μL Supelco soap flowmeter. The dimensions of this and other soap flowmeters used in this project are provided in Table 5.1. The distance between any two adjacent sensors is restricted by the size of the photodiodes, and in Figure 5.3 this distance is approximately 1/2". The passage for the light to the photodiode is about 1/16". When a bubble passes through the light the photodiode voltage reduces because the curvature of the bubble meniscus disperses the light. As a result, the photodiode receives less light. The luminance of the light emitting diodes is 1000 mCd. This luminance gives the best response for the setup configuration and the tube dimensions in this study. A gray PVC support in Figure 5.3 is designed to hold the LEDs and photodiodes in a fixed position. In addition, the gray PVC body acts as an opaque barrier for the light to eliminate the interference between the light produced by the adjacent LEDs. Instead of using a time-trigger circuit, output of photodiodes are digitalized and sent to a computer for further analysis. Employing computerized data acquisition system allows for a greater accuracy. A 20 Hz analog to digital converter is used in this study; however, for more accurate measurements a real time data acquisition with a greater speed could be utilized. Figure 5.4 presents sample responses from a bubble passing through the tube of the system shown in Figure 5.3.

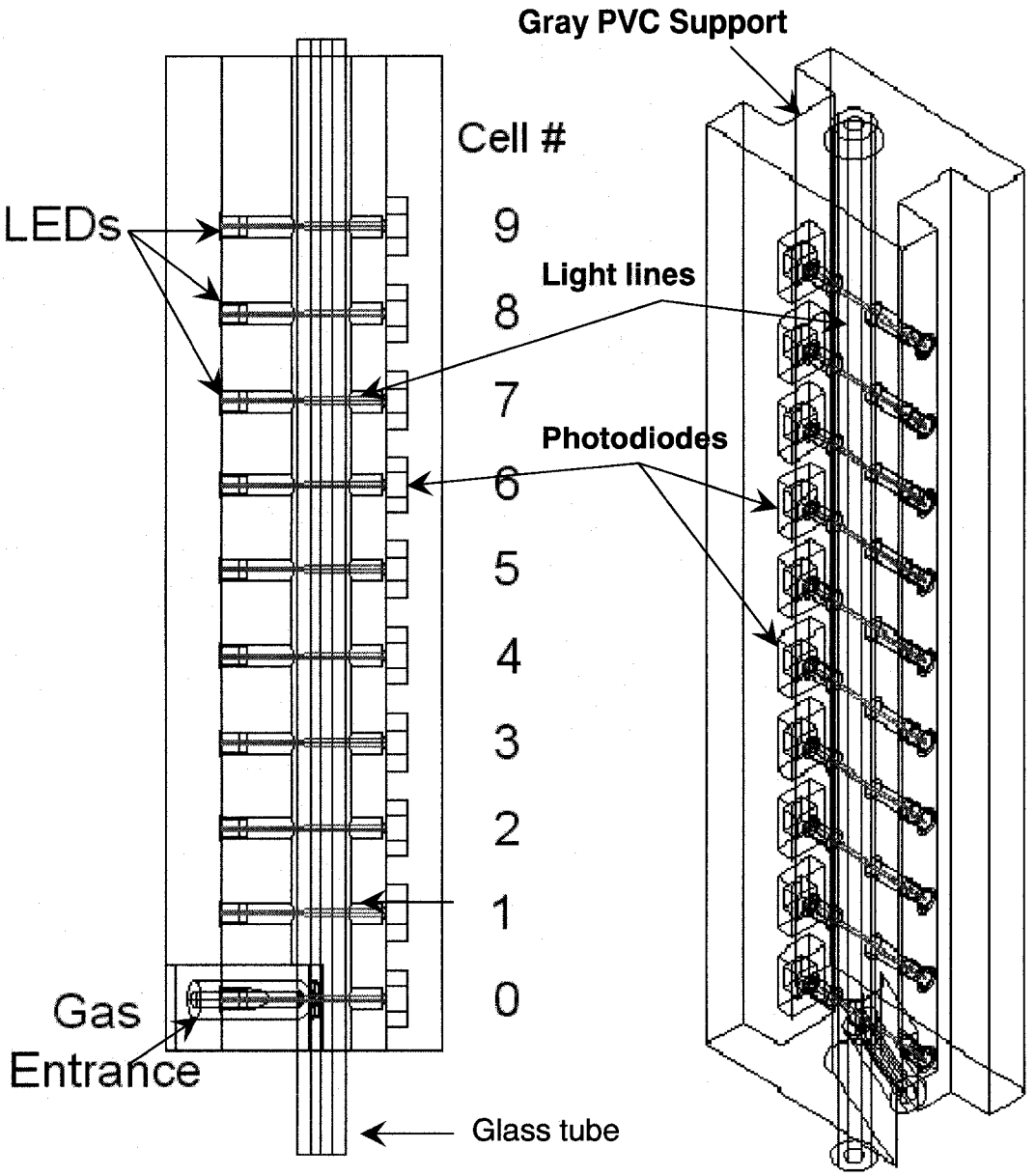

Figure 5.3. Position of sensors installed on a 500 µL Supelco flowmeter. Left is a front view of an the isometric view on right.

Table 5.1. Soap flowmeter tube specifications

Nominal size	500 μL	500 μL	100 μL
Vendor	Supelco	SGE	SGE
Recommended range	0.05 – 5	0.05 – 5	0.01 – 1
Tube inner Diameter (mm)*	2.821	3.257	1.457
Scale Length (mm)	80	60	60
Length of the barrel (mm)	165	125	125
No of measurement intervals (based on installed	8	4	2

* SEG tube characteristics provided by manufacturer and Supelco characteristics measured by a digital vernier.

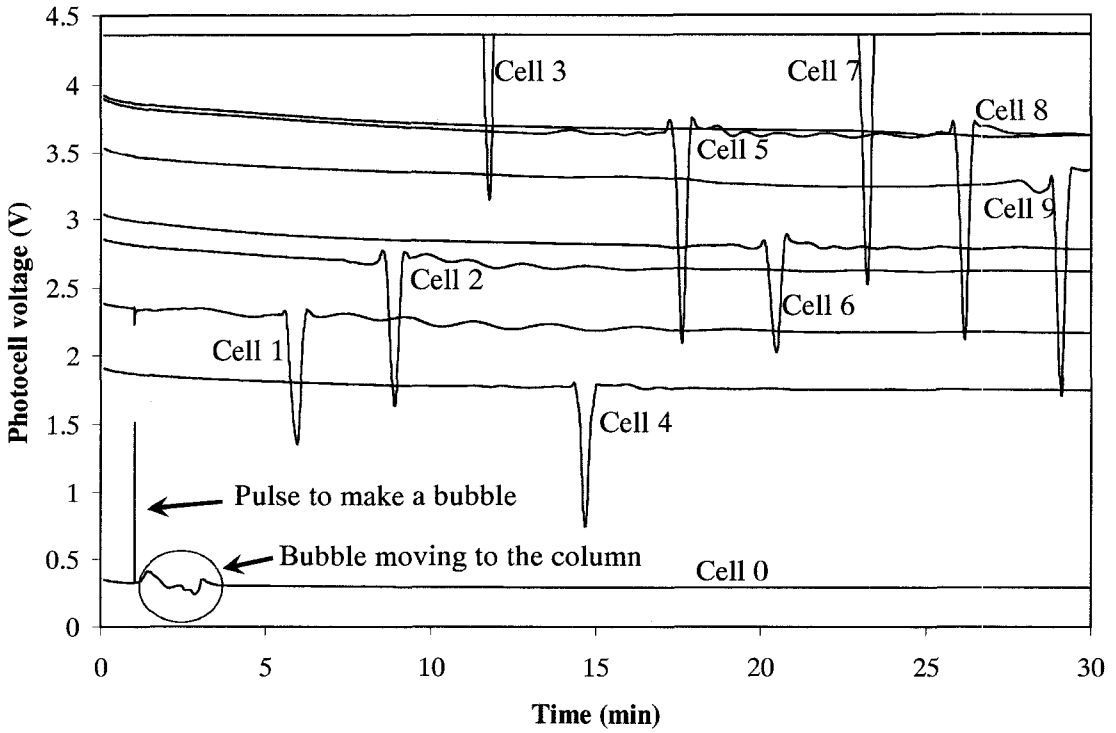

Figure 5.4. Responses of photo diodes to a bubble passing through a 500 μL Supelco soap flowmeter tube equipped with 9 photodiodes positioned for the flow measurement. The gas flow rate as measured based on the above responses is 27.1 μL/min.

5.2.3 Signal analysis

When dealing with low gas flow rates, the time for a bubble to pass in front of a photodiode is orders of magnitude greater than the accepted uncertainty of ±0.2 s for the time measurement. In this case it is very difficult, if not impossible, to get accurate time intervals using a stop watch. Levy [1] and Arenas et al. [18] investigated this problem and suggested that reducing the tube diameter to increase the speed of the bubble would solve the problem. However, because there is a critical tube radius below which the bubble cannot form, the radius of the tube cannot be freely decreased. Employing a timer-trigger described by Arenas et al. [18] would not improve the result satisfactorily too. This can be explained by analyzing Figure 5.4. In a timer-trigger, the sensor will yield 0 when its voltage goes below a pre-specified value. It is evident from Figure 5.4 that because of the different levels of the initial voltage, i.e., when there is no bubble in the tube, whatever the pre-specified voltage, different photodiodes will not to reach it in the same phase of their pulses. If the peaks are very sharp, this will not affect adversely the accuracy of the measurement. At the same time, some photodiodes may have responses significantly below or above the pre-specified voltage so that they would not participate in the flow measurement. The initial voltage can be changed or adjusted by the area of light passage as well as by changing the corresponding LED luminance. Even a small movement of the flowmeter or any obstacle to the light will result in a change of the initial voltage. The error produced by this effect can be analyzed on the basis of the total time of a pulse over the time interval between two pulses. Arenas et al. [18] analyzed this effect and recommended that the volume between two adjacent photodiodes should be at least 2 cm^3, which in case of the flowmeter used in Figure 5.3 would require 32 cm between two adjacent photodiodes, and the time for taking one measurement for the flow rate of 10 μL/min would be even more than three hours!

To improve the accuracy of the time measurement without increasing the time for the measurement or decreasing the radius of the tube, we have employed a signal analysis to find the minimum voltage of every pulse. These minima are determined by an interpolation using a 4^{th} order Spline equation fitted to the experimental points. Then by comparing the minimum values for two subsequent photodiodes, the time interval can be extracted. By increasing the number of experimental points the accuracy will increase as

long as the resolution of an analog to digital converter is high enough. Based on current technology, the time that can be measured by a computer directly is in order of milliseconds; however, the real time instruments can provide a much higher accuracy. As a result, having a more advanced real time data acquisition apparatus would provide a more precise measurement of the time intervals allowing increasing the accuracy of the flow measurement.

5.3 Experimental

The experimental setup consists of an automated bubble making system (Figure 5.2), photodiodes and LEDs (Figure 5.3), analog-digital converters, a gas cylinder along with a regulator, a cell hosting a gas separation membrane, and a computer.

5.3.1 Materials

To make soap solution, a Liqui-Nox detergent from Alconox was diluted by distilled water. The density of the diluted solution measured by a DMA 48 Density meter was ρ = 1022 kg/m^3 and its surface tension measured by a Krüss K12 was σ = 28 mN/m. The characteristics of all flowmeters used in this study are summarized in Table 5.1. Photodiodes OPT101 were purchased from Texas Instrument. Ultra miniature two-stage diaphragm pressure regulator was purchased from Beswick Engineering; it can provide stable pressures as low as 105 kPa (0.5 psig). This regulator was used in both the bubble maker setup and the control of the membrane feed pressure, when the latter had to be less than 136 kPa (5 psig). A pressure transducer with an accuracy of 1.7 kPa (±0.25 psi) for the range of 14.7-790 kPa (0-100 psig) was purchased from Cole-Parmer. Digital-analog converters with a 16 bit resolution, sampling rate of 20 per second, and the accuracy of ±0.05% were acquired from ADLINK Technology Inc.

5.3.2 Methods

In order to test the flowmeter in the range of μL/min, a constant flow had to be generated. Based on our best knowledge, there is no commercial flow controller for this range of flow rates. Therefore, to produce constant flow rates in this range a gas (nitrogen or oxygen) was permeated through a poly phenylene oxide gas separation membrane

mounted in a gas permeation cell. The flow rates were adjusted by means of a pressure gradient across the membrane. The experiments with nitrogen were carried out for four months and the experiments with oxygen were carried out for three months.

5.4 Results and discussion

The performance of the system shown in Figure 5.3 is presented in Figure 5.4. A passage of a single bubble through the entire tube allows for 8 flow measurements, and consequently it gives the possibility to analyze the error associated with the measurements of steady flows. Cell 0, which is positioned at the entrance to the main tube, does participate in flow measurement, but allows detecting the formed bubble. First, when the liquid is pushed inside the main tube, a positive pulse is observed. Then the bubble is transferred from the inlet to the main tube, which results in fluctuation of the light detected by the first photodiode (cell 0) in Figure 5.4.

Another noticeable feature in Figure 5.4 is a fluctuation after the bubble passes each cell except cells 3 and 7. The latter cells had the initial light signal higher than a threshold of the photodiode cells. The observed fluctuations may be explained by the concept, proposed by Helslop et al. [15]. Considering the static and dynamic pressures of a bubble in a vertical tube, they concluded that by adding more liquid to the existing bubble the pressure will increase but the bubble will remain stable. This suggests that the amount of liquid for a stable bubble is a range of values rather than a specific value. Since the bubbles eventually break up, there is some liquid soap falling on the walls, and this liquid can be absorb by a raising bubble until the bubble becomes unstable. When this happens, the bubble will start releasing the extra liquid to attain its initial stable conditions, after which it may start absorbing again the falling liquid. The fluctuations seen in Figure 5.4 were not observed in all experiments; therefore, this phenomenon might also depend on other parameters such as, for example, the amount of the falling liquid on the wall.

The gas flow rates measured using a soap flowmeter may be affected by the diffusion of the gas through the bubble, which is particularly evident in case of some gases such as helium, argon and carbon dioxide [9]. To overcome this problem, Guo and Heslop [10], who thoroughly investigated the phenomenon of the diffusion of gases

through soap bubbles, recommended producing multiple bubbles and/or increasing the length of the flowmeter tube. The bubble maker developed in this study allows creating multiple bubbles with the same properties. Figure 5.5 presents the result of two bubbles passing through a 500 μL SEG flowmeter equipped with five photodiodes. After break up of the bubble the liquid falling on the tube walls is recognized by the last cell, i.e., the one nearest to open end of the tube. Unlike a soap bubble, which because of the meniscus produces a negative pulse, the liquid passing in front of a photodiodes produces positive pulse.

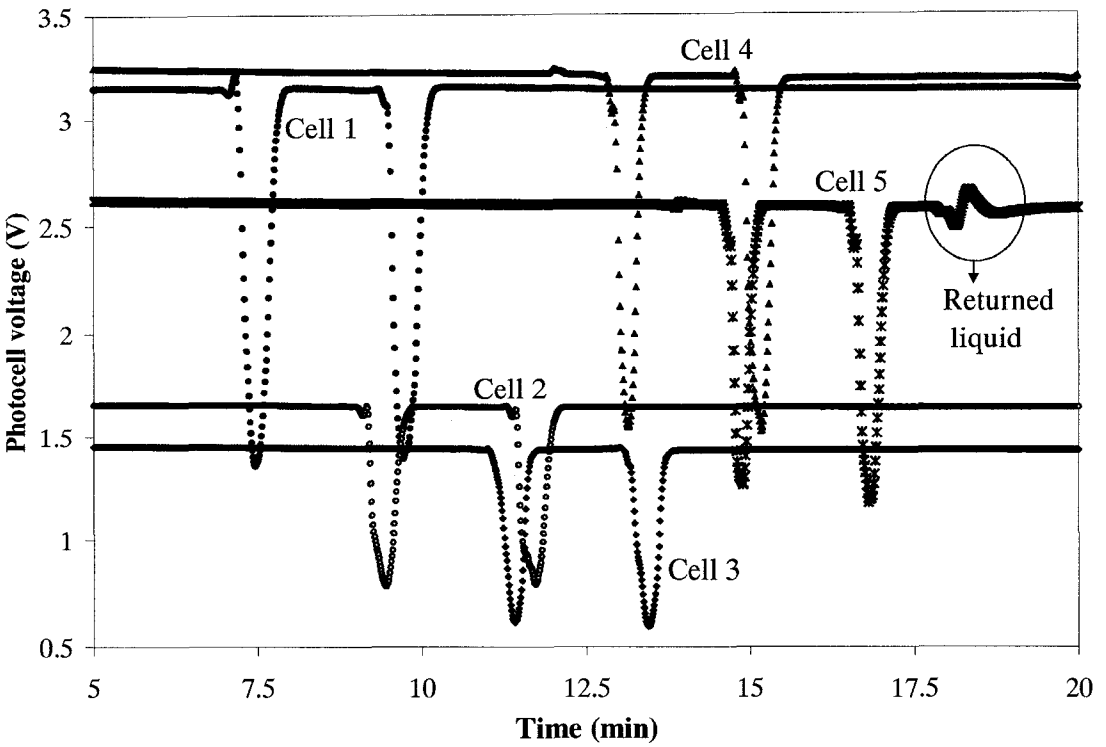

Figure 5.5. Responses of photo diodes to two bubbles passing simultaneously through a 500 μL SEG flowmeter equipped with 5 photodiodes positioned for the flow measurement. The gas flow rate as measured based on the above responses is (provide the number) 53.3 μL/min.

The critical tube radius, R_{cr}, is a minimum radius of the tube in which a bubble can form. When the tube radius is less than R_{cr}, a small column of liquid is formed instead of a bubble. The critical tube radius (R_{cr}) is related to the critical Bond number (B_{cr}):

$$B_{cr} = \frac{\rho g R_{cr}^2}{\sigma}$$

where ρ and σ are the density and the surface tension of the soap liquid solution, and g is the gravity constant. For fully wetting liquids in a vertical capillary tube, Concus [19] calculated the critical Bond number to be $B_{cr} = 0.842$. Although this value is applicable for a liquid column, it has been also used for free bubbles. For the soap solution used in this work and the above critical Bond number, the calculated critical radius is 1.53 mm. It is important to note that despite the fact that a 500 μL Supleco flowmeter has a radius of 1.41 mm, i.e., smaller than the estimated R_{cr}, the bubbles were formed in this flowmeter. This could be because in his calculations Concus [19] considered the interface of two fluids in a capillary, and the existence of a small lamella could reduce the critical Bond number.

On the other hand, as expected, the bubbles did form in a SGE 500 μL flowmeter having the radius of 1.63 mm, and did not form in a 100 μL SGE flowmeter having the radius of 0.73 mm. Despite the fact that the bubbles did not form in the smaller tube, this flowmeter was still successfully used for the flow measurements as shown in Figure 5.6. The only difference between the responses of the bubble and the liquid column is the shape of the pulse. In the latter case, because the liquid column has no significant curvature, the pulse is positive.

5.4.1 Experimental results

To our best knowledge, there is no commercial flow controller capable of controlling the flow rates that were of interest in this study. Therefore, the flow rates that were subsequently measured by the flowmeter systems developed in this study were generated by permeation of gases through semi-permeable membranes under different trans-membrane pressures.

Typical results from a series of experiments involving measurement of low flow rates of nitrogen using a 500 μL Supleco flowmeter are presented in Figure 5.7.

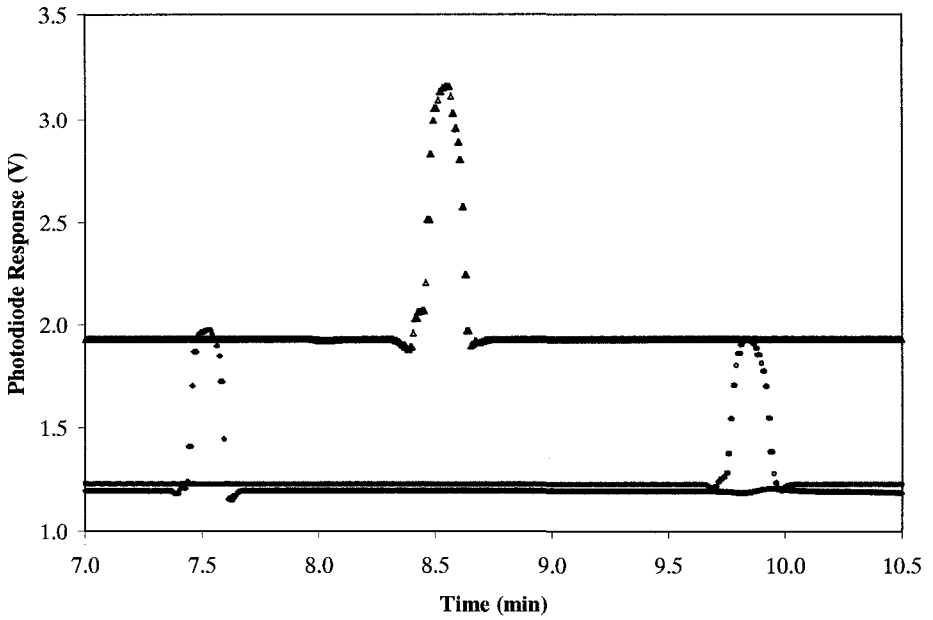

Figure 5.6. Responses of photo diodes to column of liquid passing though a 100 μL SEG flowmeter equipped with 3 photodiodes positioned for the flow measurement. The gas flow rate as measured based on the above responses is 36 μL/min.

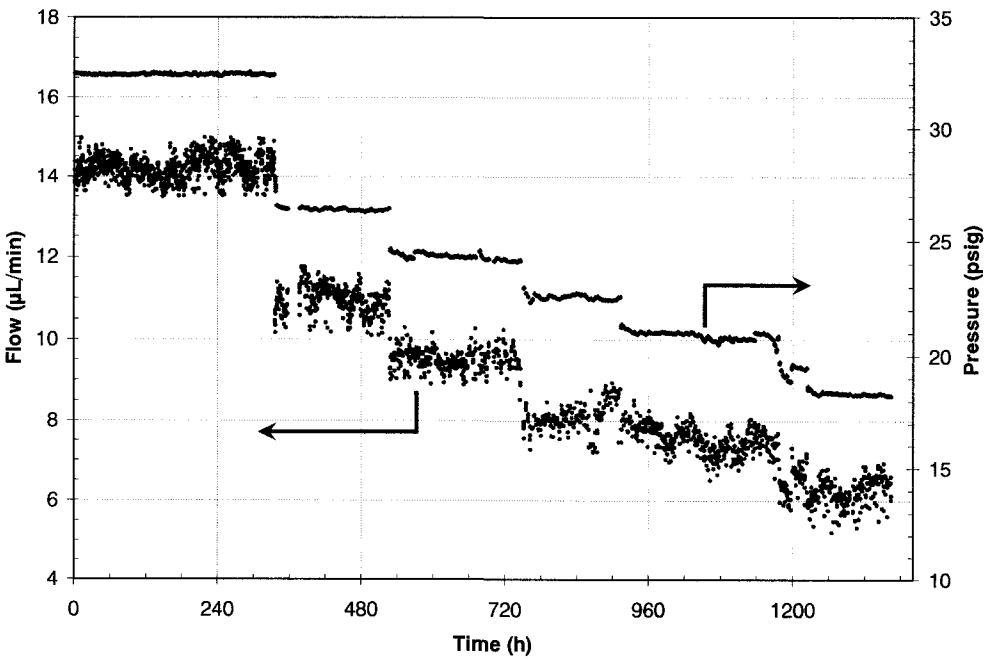

Figure 5.7. Typical nitrogen permeation rate measurements through a poly phenylene oxide membrane, subjected to different trans-membrane pressures, using a 500 μL Supelco flowmeter.

In addition to the measured flow rates, the corresponding feed pressures are also shown in the same figure. The membrane used to generate the data in Figure 5.7 was exposed to a given feed pressure for at least one week and sometimes for two weeks. It is evident that the measured flow rates fluctuate considerably. On the other hand, for a given feed pressure the average flow rate generally does not depend on the time frame used for its evaluation, provided that the time frame is sufficiently long, e.g. one day. This suggests that the fluctuations in the measured flow represent a random rather than a systematic error.

The observed fluctuations could arise from a variation in ambient temperature and pressure in the laboratory where the measurements were performed. In case of very low flow rates such as those depicted in Figure 5.7, the pressure difference across the bubble is very small [14,15]; therefore, even a movement of a person around the flowmeter would produce a draft for the bubble inside the tube resulting in fluctuations of its movement. This type of random error could easily be eliminated by performing the flow measurements in a controlled environment, which would be necessary if the purpose of the flow measurements were to calibrate other instruments. Another easy way to minimize this error would be to connect a long tube to the end of the flowmeter, which would also minimize the effects of back diffusion of air [10].

The other source of fluctuations in Figure 5.7 could be the actual flow rate of the gas. As seen in Figure 5.7, there are small fluctuations in the feed pressure and since the flow rate is directly proportional to the feed pressure, the fluctuations in the feed pressure should lead to the fluctuations in the actual flow rate. A closer examination of Figure 5.7 reveals that despite a significant difference magnitude, the fluctuations in the measured flow rate generally follow the fluctuations in the feed pressure.

Figure 5.8 presents the summary of all experimental results along with the standard deviations for the pressure and flow. Dashed lines in Figure 5.8 are just guides to follow the change in the flow rate with the change in the feed pressure. The details of the results for oxygen are also summarized in Table 5.2. The flow and pressure deviations are calculated based on the number of the experimental points when the permeation rate for a given feed pressure seems to reach a steady state. Some experiments were repeated

in different time periods, and generally an excellent repeatability of the flow measurements was observed.

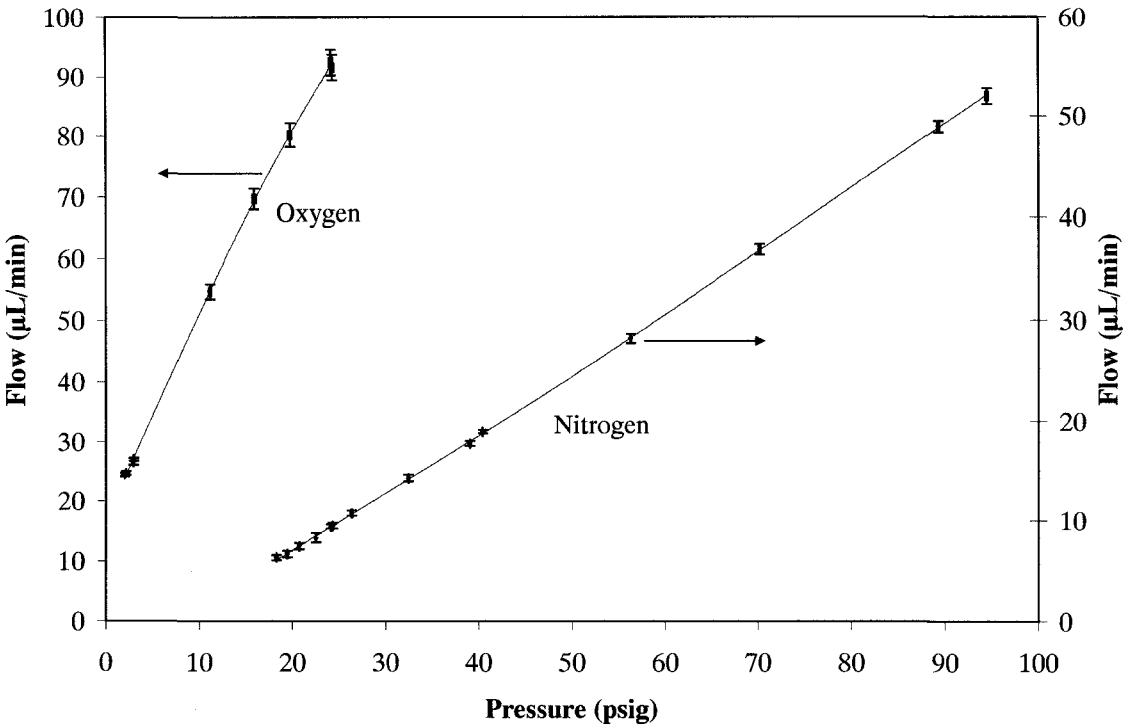

Figure 5.8. The effect of trans-membrane pressure of the average permeation rates of nitrogen and oxygen through a poly phenylene oxide membrane. All permeation rates were measured using a 500 µL Supelco flowmeter. The bars indicate the deviation of flow and pressure from the respective average values. The trend lines are indicated by the dashed lines.

For low feed pressures, because of employing a low pressure regulator, the deviation in the feed pressure and consequently in the measured flows rate is an order of magnitude lower than in higher pressure runs. This signifies the contribution of the fluctuations in feed pressure to the observed fluctuations in the measured flow rate. It is important to mention however, that the relative flow deviations remain almost constant regardless of the feed pressure as shown in Table 5.2. The apparent curvature of the dashed line in Figure 5.8 is most likely related to the membrane properties and this effect is currently under investigation.

Table 5.2. Summary of oxygen permeation measurements through a polyphenylene oxide membrane.

Flow (μL/min)	Pressure (kPa)	Pressure (psig)	Flow Deviation (μL/min)	Pressure Deviation (kPa)	Pressure Deviation (psi)	No. of points
91.54	269	24.31	2.07	1.0	0.14	330
92.39	268	24.13	2.13	1.3	0.19	420
80.21	238	19.79	1.97	1.3	0.19	570
69.72	211	15.94	1.66	1.3	0.19	300
54.67	178	11.14	1.18	0.7	0.10	25
27.02	122	2.95	0.29	0.1	0.01	250
26.59	122	2.93	0.49	0.1	0.01	620
24.69	116	2.13	0.34	0.1	0.01	240
24.40	115	2.01	0.30	0.1	0.01	360

5.4.2 Thickness of meniscus

The shape of the bubble has been a long time subject of study by physicists, mathematicians and engineers. Barigou et al. [7,8] reported the results of an extensive study on the shape of bubbles in vertical tubes. They measured the dimensions of bubbles produced by hand squeezing of a soap bulb and reported the meniscus thickness of 3.5 mm. In the current study the meniscus thickness was measured to see if the bubble thickness change as it passes through the tube, including the experiments in which the gas flow rate was very low and it required up to two hours for a single bubble to pass through the entire flowmeter tube.

The comparison of the thickness of a single bubble at different heights is presented in Figure 5.9, in which all of the pulses appearing in Figure 5.4 are normalized and then matched by their minima. Based on the measured flow rate, which in case of Figure 5.9 is 27.1 μL/min, the time can be converted to the length, and thus the thickness of the bubble can be estimated. It is evident from Figure 5.9 that except for cell 3, the bubble thickness is generally constant when it rises inside the tube. It is important to note that cell 3 was associated with a high luminance of the LED, higher than in other cells. The literature bubble thickness of 3.5 mm [7,8] is also shown in Figure 5.9 for comparison.

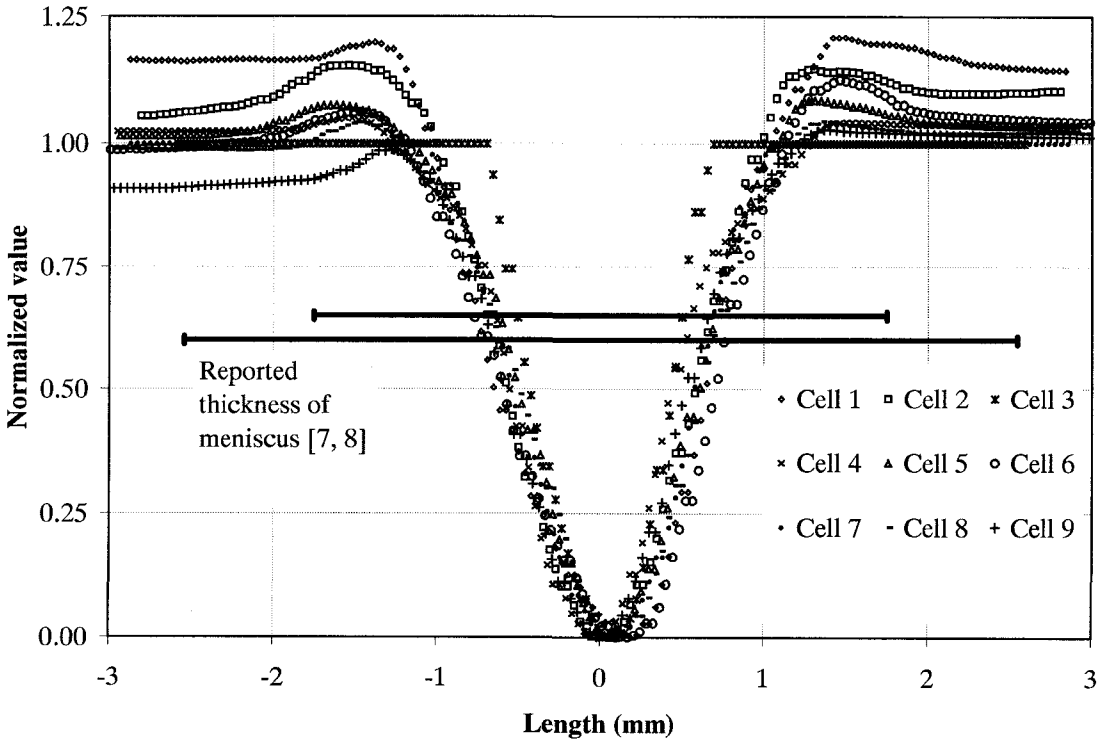

Figure 5.9. Comparison of the meniscus thickness as determined from the responses from different photodiodes shown in Figure 5.4. The reported literature value, 3.5 mm, of the meniscus thickness is included for comparison.

In addition, since the diameter of passage in front of the photodiode is 1/16", this distance is added to 3.5 mm, and the resulting value, 5.1 mm, is also shown in Fig 9 for comparison. It is evident from Figure 5.9 that there is a good agreement between the meniscus thickness observed in this study and the literature value of 3.5 mm.

5.5 Conclusions

The objective of this work was to adopt commercially available soap flowmeters for accurate measurements of gas flow rates in the range of μL/min. Such low flow rates are common in gas chromatography and in characterization of gas separation membranes. While the commercially available flowmeters could be used for a direct measurement of flow rates in the range of μL/min, the measurements would be associated with uncertainties significantly greater ±1%, that is, the accepted accuracy of soap flowmeters.

To achieve the above accuracy without increasing the required time for the flow measurement, a fully automated bubble maker, capable of producing similar bubbles at any time interval and of working with any commercial soap flowmeter, was developed. The soap flowmeters used in this work were equipped with a system consisting of several LEDs and photodiodes for the detection of bubbles passing along the calibrated part of the tube, which was also developed in this project. To collect and analyze the signals from the photodiodes, a data acquisition was developed, which allows for more accurate time measurements compared to manual measurements with a stop watch and those involving electronic timer-trigger circuits. The low flow rates required in this study were generated by permeation of gases through semi-permeable membranes under different trans-membrane pressures. The actual gas flow rates were controlled by means of the feed pressure.

The commercial soap flowmeters modified according to the above criteria successfully measured gas flow rates ranging from 5 to 100 μL/min with a reasonable accuracy. Moreover, the flow measurements were fully automated and were carried out hands-free for extended periods of time. The major source of random error in the measured flow rates were fluctuations in ambient temperature and pressure. However, since the flowmeters developed in this study are for hands-free operation, this source of error can be easily eliminated by performing measurements in isolated, fully controlled environments. Alternatively, the effect of environmental fluctuations could be minimized by connecting a long tube to the end of the flowmeter tube. The modified soap flowmeter systems allowed also for the measurement of the size of the bubbles meniscus. It appears that this size remains constant regardless of the amount of liquid carried out by the bubble. However, the determination of the metastable range for the bubbles would require more investigation.

Acknowledgement

The authors gratefully acknowledge the financial support for this project provided by the Natural Science and Engineering Research Council of Canada.

Nomenclature

B	Bond number $B = \frac{\rho g R^2}{\sigma}$, dimensionless
g	Gravity, 9.81 m/s^2
R	Radius of the tube, m, mm
ρ	Density, kg/m^3
σ	Surface tension, mN/m

References

1. A. Levy, The accuracy of the bubble meter method for gas flow measurements, J. Sci. Instrum. 41 (1964) 449-453.
2. F. Exner, Über den Durchgang der Gase durch Flüssigkeitslamellen, Pogg. Ann. phys. Chem. 231 (1875) 321.
3. G. Barr, Two designs of flow-meter, and a method of calibration, J. Sci. Instrum. 11 (1934) 321-324.
4. T.J.S. Brian, Reference standards for gas flow measurement, Measurement and Control 11 (August 1978) 283-288.
5. W.C. Pursley, The calibration of flowmeters, Measurement and Control 19 (5) (1986) 37-45, (special issue).
6. J. Waaben, D.B. Stokke, and M.M. Brinkløv, Accuracy of gas flowmeters determined by the bubble meter method, Br. J. Anaesth. 50 (1978) 1251-1255.
7. M. Barigou and J.F. Davidson, Soap film drainage: Theory and experiment, Chem. Eng. Sci. 49 (11) (1994) 1807-1819.
8. M. Barigou, N.S. Deshpande and F.N. Wiggers, Numerical simulation of the steady movement of a foam film in a tube, Trans IChemE, Vol 81, Part A (July 2003) 623-630.
9. J.J Czubryt, H.D. Gesser, Part I-Inaccuracy of the moving bubble flowmeter in the low flow rate region, J. Gas Chromat. 6 (1968) 528-530.
10. J. Guo and M.J. Heslop, Diffusion problems of soap-film flowmeter when measuring very low-rate gas flow, Flow Measurement and Instrumentation 15 (2004) 331-334.
11. K.J. Mysels, K. Shinoda and S. Frankel, Soap films: studies of their thinning, and a bibliography, Pergamon Press, London (1959).
12. D. Lovett, Demonstrating science with soap films, Institue of Physics Publishing, Bristol (1994).
13. F.N. Wiggers, N.S. Deshpande and M. Barigou, The flow of foam in vertical tubes, Trans IChemE, Vol 78, Part A (July 2000) 773-778.
14. M. Barigou and J.F. Davidson, The fluid mechanics of the soap film meter, Chem. Eng. Sci. 48 (14) (1993) 2587-2597.

15. M. J. Heslop, G. Mason and A. Provatas, Comments on the pressure produced by a soap film meter, Chem. Eng. Sci. 50 (15) (1995) 2495-2497.
16. B.J. Bailey, J.A. Ferguson, J.L1 Moses, "Two Flowmeters Using Electronic Timing", Journal of Scientific Instruments (Journal of Physics E) Series 2 Volume 1 (1968) 562-563.
17. J.J Hunter, Photoelectric timer for the bubble meter method of gas flow measurement, J. Sci. Instrum. 42 (1965) 175.
18. A. Arenas, L. Victoria, and J.A. Ibañez, A time-integration-based measurement circuit for a soap bubble flow-meter using optical fibre sensors, Mass. Sci. Technol. 6 (1995) 435-436.
19. Paul Concus, Static menisci in a vertical right circular cylinder, J. Fluid Mech. 34, part 3 (1968) 481-495.

Chapter 6

Effect of Back Diffusion and Back Permeation of Air on Membrane Characterization in Constant Pressure System

S. Lashkari, A. Tran, B. Kruczek*

Journal of Membrane Science, 324 (2008) 162-172

Department of Chemical Engineering
University of Ottawa
161 Louis Pasteur Street
Ottawa, ON K1N 6N5, Canada
Fax: (613) 562-5172
Phone: (613) 562-5800 ext. 6302
E-mail: kruczek@eng.uottawa.ca

* **To whom correspondence should be addressed.**

Abstract

Constant pressure (CP) testing systems are often used in characterization of gas separation membranes. Unlike constant volume (CV) systems, the membrane tested in a CP system is exposed to atmosphere via a flow metering device. Consequently, as long as the permeating gas has a composition different from that of the atmosphere, there is a driving force for diffusion of atmospheric gases towards the membrane. Moreover, if as a consequence this there is a nonzero partial pressure of the back diffusing gases at the permeate side of the membrane, there will be a driving force for the permeation of these gases from the permeate side to the feed side of the membrane (back permeation), which could affect the permeation rate of the tested gas.

This paper presents a mathematical model that allows estimation of an error arising from back diffusion and back permeation in CP systems. The model is derived from the first principles assuming that there are no interactions between the forward and back permeating gases with each other and with the membrane. The theoretical predictions are then compared with experimental results obtained in a specially designed, fully-automated CP system, using poly-2,6-dimethyl-1,4-phenylene oxide (PPO) films in single gas permeation tests involving nitrogen and oxygen. The experimental results confirm theoretically predicted trends resulting from the phenomena of back diffusion and back permeation. However, the influence of these phenomena on the experimentally determined permeability coefficients is greater than that predicted by the model.

Keywords: Membrane characterization, Back diffusion, Back permeation, Constant pressure system, Solution diffusion model

6.1 Introduction

Gas separation membranes have received extensive attention in the last three decades because of their economic advantages compared to the other gas separation methods, and different aspects related to their formation, characterization and application have been summarized in several excellent reviews [1-4]. Membrane characterization in laboratory-scale systems is an important step in the membrane development process. However, transport properties of gas separation membranes reported in the literature are often not reproducible [5]. Generally, characterization of gas separation membranes involves evaluation of three fundamental transport parameters of the gas in membrane, namely the permeability (P_i), diffusion (D_{iM}), and solubility (S_i) coefficients. Essentially, there are two methods that are employed for the membrane characterization. These are constant pressure (CP) and constant volume (CV) techniques. In a CP system, the permeate side of membrane is open to atmosphere, or swept with a gas at atmospheric pressure, and thus gas permeation tests are performed at a constant trans-membrane pressure. On the other hand, in a CV system the permeate side of membrane is initially at vacuum, and as the gas permeates through the membrane, the pressure at the permeate side increases. Consequently, the gas permeation tests in the CV system are executed at a variable trans-membrane pressure. Although most membrane laboratories use CV systems, a quick review of the latest membrane articles shows that CP systems are also commonly used for the membrane characterization [6-12].

Since a CP system is open to atmosphere, the air components which are not present in the gas permeating through the membrane, may diffuse towards the membrane (back diffusion) and then permeate to the feed side of the membrane (back permeation). Tran, who studied gas permeation properties of modified polyphenylene oxide (PPO) membranes in a CP system equipped with a bubble flowmeter, observed unusually high permeability ratios for CO_2/CH_4 and O_2/N_2, and speculated that these unusual values resulted from underestimation of the permeability coefficients of the slower gases, i.e., N_2 and CH_4 due to back diffusion and back permeation phenomena [13]. Although these phenomena are inherent to CP systems, they are not adequately addressed in the literature. The only work on back permeation in the field of gas separation was reported by Mason [14], who considered microporous membranes, in which gas transport is

governed by the Knudson diffusion. Vallieres et al. considered the effect of back permeation of sweep gas in a pervaportion experiment performed below the atmospheric pressure; however, they did not observe any significant effects of back permeation on their measurements [15]. To our best knowledge there is no systematic study concerning back permeation of gases and vapors in nonporous membranes. At the same time, it should be noted that the phenomenon of back permeation gained more attention in liquid separations, in particular those involving bio-membranes [16,17] and water treatment [18].

In this paper a simple mathematical model was presented which allows estimation of an error arising from back diffusion and back permeation in CP systems. The model is derived from the first principles and then verified experimentally in a specially designed, fully-automated CP system, using poly-2,6-dimethyl-1,4-phenylene oxide (PPO) films in single gas permeation tests involving nitrogen and oxygen.

6.2 Theoretical Background

Gas transport in nonporous membranes is commonly described by a solution-diffusion model, in which the gas transport consists of three independent steps. First, a gas is dissolved in a membrane at a high pressure (feed) side, then the gas diffuses across the membrane according to Fick's law of diffusion, and finally the gas evaporates from the membrane at a low pressure (permeate) side. Assuming applicability of Henry's law, which is a reasonable approximation in case of dilute solutions, the three steps of the solution-diffusion model are described by the following equations:

Step 1: $$C_{i,f} = S_i\, p_{i,f} \tag{6.1}$$

Step 2: $$J_i = -D_{iM} \frac{dC_i}{dz} \tag{6.2}$$

Step 3: $$C_{i,p} = S_i\, p_{i,p} \tag{6.3}$$

where: C_i is the concentration of component i inside the membrane, p_i is the partial pressure of i in the gas phase, J_i is the diffusive flux, and z is the distance from the feed surface of the membrane. The subscripts f and p refer to the feed and permeate side, respectively.

Assuming that Step 2 is a rate controlling step, and D_{iM} and S_i are pressure independent, the solution-diffusion model simplifies to:

$$N_i = \frac{P_i}{L_M}\left(p_{i,f} - p_{i,p}\right) \tag{6.4}$$

where: $P_i = D_{iM}S_i$, L_M is the membrane thickness, and N_i is the permeate flux of an i-th component, which in this case is equal to the diffusive flux of this component. Equation (6.4) may also be rearranged to:

$$P_i = \frac{N_i L_M}{p_{i,f} - p_{i,p}} \tag{6.5}$$

In case of an experiment with a single gas, P_i is easily evaluated because N_i is represented by the total gas flux through the membrane and $p_{i,f} - p_{i,p}$ is represented by the gauge pressure of the feed stream. The selective properties of a membrane are often evaluated on the basis of a permeability ratio (α_{ij}) using the permeability coefficients determined in separate, single gas permeation experiments:

$$\alpha_{ij} = \frac{P_i}{P_j} \tag{6.6}$$

6.2.1 Concept of back diffusion and back permeation

Figure 6.1 presents a schematic diagram of a typical CP system used for measuring the permeation rate of gas A through a membrane. The gas permeation rate is evaluated based on the gas flow rate measured by a soap bubble flowmeter, which is attached to the permeate side of the membrane. The soap bubble is introduced at the entrance of a calibrated column and is picked up by the flowing gas. Because of negligible weight of the soap bubble, the speed of the bubble through the calibrated column can be correlated to the volumetric flow rate of the permeating gas. In the system depicted in Figure 6.1, the membrane is open to atmosphere of gas B, which is typically air. However, in a CP system with sweep, B can be any gas. If A and B are different gases, B may diffuse towards the membrane and then permeate through the membrane. Since the direction of the diffusion and permeation of B is opposite to the direction of the

permeation and flow of A, the diffusion and permeation of B are referred to as back diffusion and back permeation, respectively.

Treating the membrane in Figure 6.1 as a "black box", that is, assuming that the permeability coefficient of A (P_A) is not affected by the presence of B and the permeability coefficient of B (P_B) is not affected by the presence of A in the membrane; the respective fluxes, N_A and N_B, are expressed using Equation (6.4):

$$N_A = \frac{P_A}{L_M}\left(p_{A,f} - p_{A,p}\right) = \frac{P_A}{L_M}\left(p_f - p_p\left(x_A\right)_P\right) \tag{6.7}$$

$$N_B = \frac{P_B}{L_M}\left(p_{B,f} - p_{B,p}\right) = \frac{P_B}{L_M}\left(0 - p_p\left(1-\left(x_A\right)_P\right)\right) = -\frac{P_B}{L_M}p_p\left(1-\left(x_A\right)_P\right) \tag{6.8}$$

where: $\left(x_A\right)_P$ is the mole fraction of gas A at the permeate side of the membrane. It is important to note that Equation (6.7) assumes that the mole fraction of A at the feed side of membrane is equal to unity. This is a reasonable assumption, especially when the feed side is swept with A.

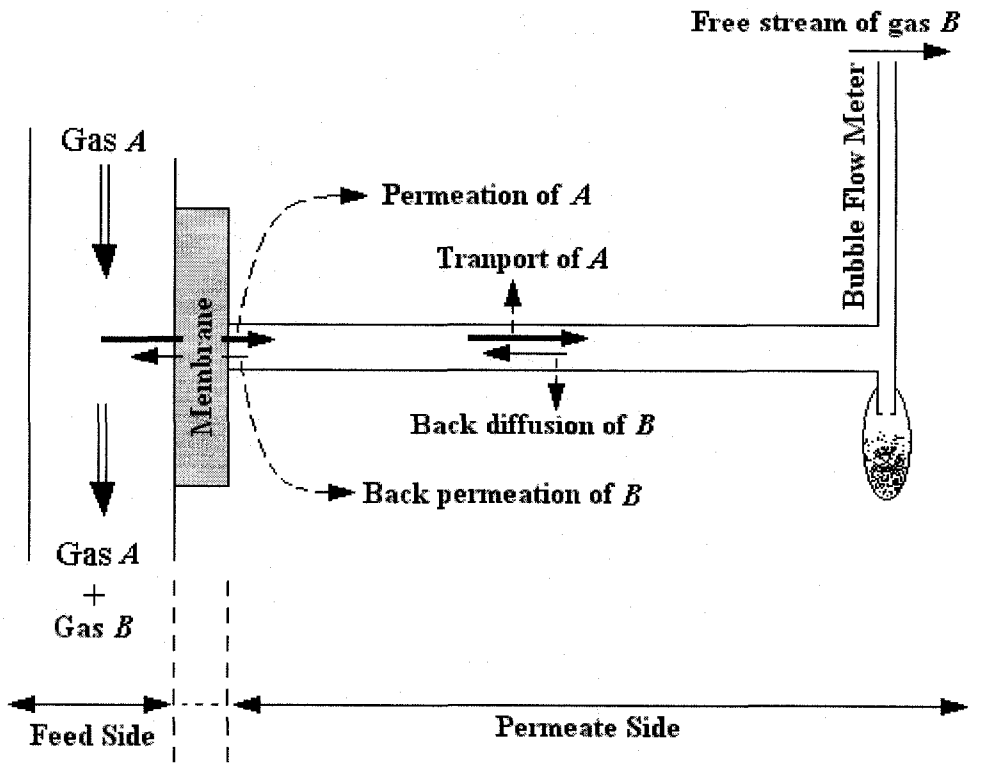

Figure 6.1. Measurement of the permeation rate of a gas through a membrane in a constant pressure system.

The expression for the permeability coefficient, given by Equation (6.5), can be rewritten in a slightly different form, which follows from Equation (6.7):

$$P_A = \frac{L_M N_A}{p_p\left(\frac{p_f}{p_p} - (x_A)_P\right)} \tag{6.9}$$

In case of a single gas permeation test in a CP system, the composition of the permeating gas is not measured, and although not explicitly stated, it is simply assumed that $(x_A)_P$ is equal to unity. Moreover, it is assumed that the experimentally measured gas flux through the membrane (N) corresponds to N_A. With these assumptions, the expression for the permeability coefficient given by Equation (6.9) becomes:

$$P_A\big|_{app} = \frac{L_M N}{p_p\left(\frac{p_f}{p_p} - 1\right)} \tag{6.10}$$

To distinguish between the permeability coefficients given by Equations (6.9) and (6.10), the former will be referred to as the actual permeability coefficient and the latter as the apparent permeability coefficient. In situation, in which back diffusion and back permeation of B exist, $N \neq N_A$, and $(x_A)_P < 1.0$, consequently $P_A \neq P_A\big|_{app}$.

To evaluate the error associated with the apparent permeability coefficient when the phenomena of back diffusion and back permeation are present, it is necessary to realize that for the system depicted in Figure 6.1, the experimentally measured gas flux is given by:

$$N = N_A + N_B = Cu \tag{6.11}$$

where: u is the gas velocity and $C = \sum C_i$ is the total gas concentration. Substitution of Equations (6.7) and (6.8) into Equation (6.11) leads, after rearrangements, to:

$$P_A = \frac{L_M N}{p_p\left(\frac{p_f}{p_p} - (x_A)_P - \alpha_{BA}\left(1 - (x_A)_P\right)\right)} \tag{6.12}$$

where: $\alpha_{BA} = P_B / P_A$. Dividing Equation (6.10) by Equation (6.12) yields the following expression:

$$\frac{P_A|_{app}}{P_A} = 1 + (1 - \alpha_{BA}) \frac{1 - (x_A)_P}{\frac{p_f}{p_p} - 1} \tag{6.13}$$

When $p_f > p_p$, it follows from Equation (6.13) that:

$$\text{if } \alpha_{BA} < 1 \quad \Rightarrow \quad P_A|_{app} > P_A$$

$$\text{if } \alpha_{BA} > 1 \quad \Rightarrow \quad P_A|_{app} < P_A$$

In the limiting case when $p_f >> p_p$, regardless of α_{BA}, $P_A|_{app} \rightarrow P_A$.

In case of polyphenylene oxide, the permeability coefficients decrease in the following order, $P(CO_2) > P(O_2) > P(CH_4) > P(N_2)$ [19]. Hence, when CP system is open to atmosphere, in the tests in which A is N_2 or CH_4, $\alpha_{BA} > 1$, and the apparent permeability coefficients will underestimate the actual permeability coefficients of these gases. On the other hand, in the tests in which A is O_2 or CO_2, $\alpha_{BA} < 1$, and the apparent permeability coefficients will overestimate the actual permeability coefficients of these gases.

6.2.2 Modeling of back diffusion

To quantify Equation (6.13) it is necessary to evaluate the composition of the gas at the permeate side of the membrane. This requires modelling of back diffusion and the knowledge of the mechanism by which the gas is transported through the membrane. In the following analysis the transport equations describing the phenomenon of back diffusion are developed by assuming that the membrane can be treated as a "black box". The derivation of the transport equations for back diffusion relies on basic transport phenomena concepts discussed, for example, by Bird et al. [20].

For the purpose of modeling the CP system presented in Figure 6.1 is generalized in Figure 6.2. Tube 1 represents a bubble flowmeter. The bubble is made at z_1 and moves towards z_0. Tube 2 is a connecting tube between the membrane cell and the bubble flowmeter. There can be more than two tubes between the membrane and the atmosphere, but for the purpose of modeling the case with two tubes will be sufficiently representative.

Since there is no velocity field except in longitudinal, z-direction, the continuity equation for a constant density fluid is reduced to:

$$\frac{du}{dz}=0 \tag{6.14}$$

where z is distance from the free stream of B (air), i.e. from the outlet of the bubble flowmeter tube.

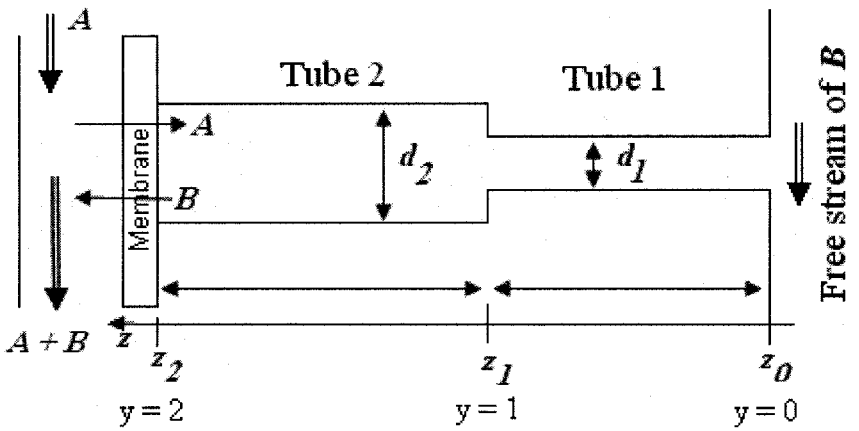

Figure 6.2. Schematic representation of a CP system for the purpose of modeling of back diffusion and back permeation.

It is important to emphasize that for typical velocities in gas permeation experiments the pressure drop through the tubes does not affect the velocity field. This can be verified by applying Bernoulli's equation for typical velocities associated with membrane gas permeation. Since the velocity in a tube of constant diameter is constant, the continuity equation yields:

$$u_1\left(\frac{\pi d_1^2}{4}\right)=u_2\left(\frac{\pi d_2^2}{4}\right)=u_M A_M \tag{6.15}$$

where d is the tube diameter, subscripts 1, 2 and M indicate the tube numbers and the membrane, respectively, and A_M is the membrane area available for gas permeation. The velocity across the membrane can be calculated from:

$$u_M = \frac{\sum_i (N_i)_M}{C} \tag{6.16}$$

Combining Equations (6.15) and (6.16) leads to:

$$u_1 = u_M \frac{A_M}{\left(\frac{\pi d_1^2}{4}\right)} = \frac{\sum_i (N_i)_M}{C} \frac{A_M}{\left(\frac{\pi d_1^2}{4}\right)} \tag{6.17}$$

Assuming that air consists only of N_2 and O_2, gas permeation experiments with single N_2 and O_2 will represent the examples of back diffusion and back permeation in binary systems. In the experiment with O_2, A = O_2 and B = N_2. For the components A and B in a binary system the continuity equations are:

$$\frac{d(N_A)}{dz} = 0 \qquad \frac{d(N_B)}{dz} = 0 \tag{6.18}$$

Applying Fick's first law, the total flux of A in tube k is given by:

$$(N_A)_k = -CD_{AB}\frac{dx_A}{dz} + x_A(Cu_k) \tag{6.19}$$

or:

$$\frac{dx_A}{dz} = \frac{u_k}{D_{AB}}(x_A - \xi_A) \tag{6.20}$$

where ξ_A is a position independent dimensionless parameter defined by Equation (6.21), and subscript k indicates the tube number.

$$\xi_A = \frac{(N_A)_k}{(N_A)_k + (N_B)_k} = \frac{(N_A)_k}{Cu_k} \tag{6.21}$$

To obtain the composition profile in the tubes, $x_A(z)$, and thus the gas composition at the permeate side of the membrane, $(x_A)_P$, Equation (6.20) must be solved for all tubes. The solution in each tube requires one boundary condition. The composition of the free stream B, which is the composition of air, represents the boundary condition for tube 1. Solving Equation (6.20) for tube 1 allows evaluation of the gas composition at z_1, $(x_A)_1$, which represents the boundary condition for tube 2, with which Equation (6.20) may be solved in tube 2. Treating the membrane as a black box, ξ_A may be expressed in terms of N_A evaluated from Equations (6.7) and (6.8) as:

$$\xi_A = \frac{\frac{p_f}{p_p} - (x_A)_P}{\frac{p_f}{p_p} - (x_A)_P - \alpha_{BA}\left(1-(x_A)_P\right)} \tag{6.22}$$

Therefore, for a binary system and a two-tube configuration presented in Figure 6.2 the following equation becomes applicable:

$$\frac{\xi_A - (x_A)_P}{\xi_A - (x_A)_0} = \exp\left(-\frac{u_1}{D_{AB}}\left(L_1 + L_2\left(\frac{d_1}{d_2}\right)^2\right)\right) \tag{6.23}$$

It is important to note that u_1 in Equation (6.23) represents the net velocity of the gas in the bubble flowmeter, a positive number, which can be measured experimentally. In general:

$$\frac{\xi_A - (x_A)_P}{\xi_A - (x_A)_0} = \exp\left(-\frac{u_j}{D_{AB}}L_e\right) = \exp(-Pe) \tag{6.24}$$

where Pe is the Peclet number ($Pe = u_j L_e / D_{AB}$) in which L_e is an equivalent length of the connecting tubes. For n tubes in series including bubble flowmeter as tube j, the general equation for L_e is given by:

$$L_e = \sum_{k=1}^{n} L_k \left(\frac{d_j}{d_k}\right)^2 \tag{6.25}$$

Equations (6.22) and (6.24) can be simultaneously solved for the two unknowns $(x_A)_P$ and ξ_A, and then $P_A|_{app}/P_A$ can be evaluated using Equation (6.13).

6.3 Experimental

6.3.1 Experimental apparatus

Arenas et al. suggested using optical sensors for an automatic measurement of the gas velocity in soap bubble flowmeters [21]. This concept has been adapted in the current study to design a system for gas flow measurements, which is shown schematically in Figure 6.3. To make the measurements fully automated, a bubble is formed by applying a low external pressure on the surface of a soap liquid reservoir by means of opening of a solenoid valve, which is controlled by a computer. The flowmeter column (500 μL from Supleco) of the total length of 16.5 cm and the cross sectional area of 0.0625 cm^2 is

equipped with multiple light sensors to detect the bubble moving along the column. The automated bubble flow meter used in this study is capable of measuring the flow rates as low as 5 μL/min with accuracy greater than 2%; details of the automated bubble flowmeter are described elsewhere [22].

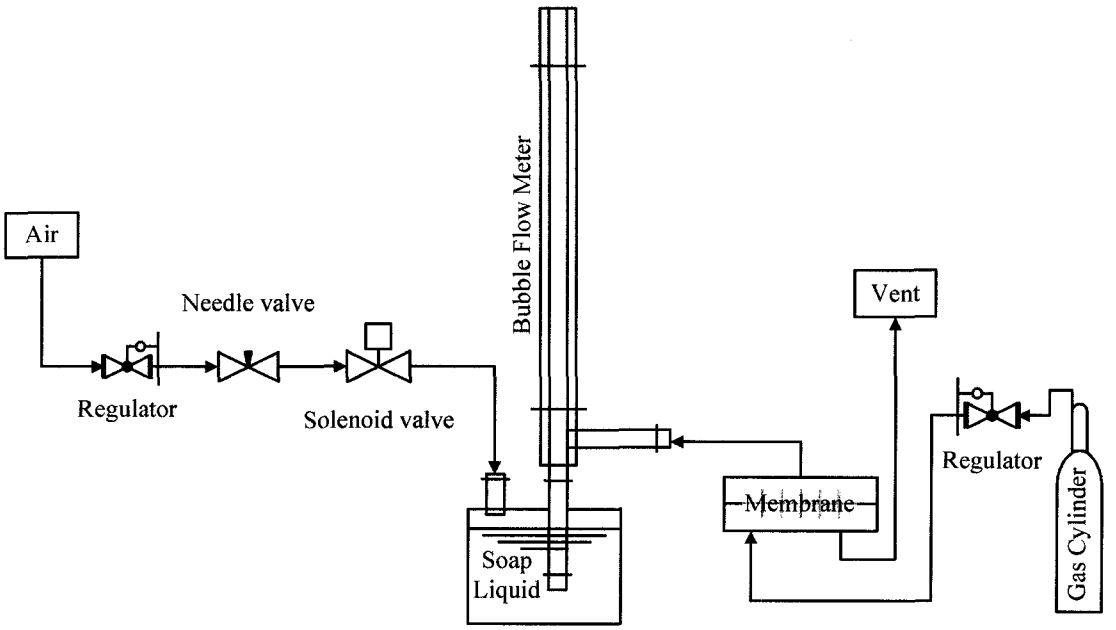

Figure 6.3. Schematic diagram of the experimental of CP system with a fully automated soap bubble flowmeter.

The entire system consists of four membrane cells connected via 6.35 mm (1/4 in.) and 3.175 mm (1/8 in.) vinyl tubes to four fully automated 500 μL Supleco bubble flowmeters. To improve the accuracy of the flow measurements, additional length of tubing is attached to the outlet of each bubble flowmeter [23]. To eliminate possible leaks Swagelok hose connectors and sleeves are used in all connections between the tubes. In addition, sampling points equipped with septa are installed to measure the composition of permeate at three different distances from each membrane cell.

The feed pressure is adjusted by two different regulators, one for high pressures (>70 kPag) and one for low pressures (5-70 kPag). In addition, the feed pressure is monitored continuously, and an average value corresponding to each time interval for the

flow measurement is determined. The ambient temperature during gas permeation experiments is also monitored continuously.

6.3.2 Preparation of membranes

The membranes were prepared by a spin coating technique using a 10% poly(2,6-dimethyl-1,4-phenylene oxide) (PPO) solution in trichloroethylene on a rotating 6.35 mm (4 in.) diameter silicon wafer. To vary the thickness of the final membranes different spinning speeds were used. After the removal from the wafer, each membrane was heat treated in a vacuum oven, which had been previously purged with N_2. First, the membranes were heated to 230°C (15°C above their glass transition temperature) for at about 40 minutes, then cooled down to 200°C and kept at that temperature for 24 hours. During the heat treatment, the membranes were free standing, thus they were allowed to freely shrink or expand [24]. The thickness of the final membranes was evaluated on the basis of their weight, surface area, and density; the latter was assumed to be 1.07 cm^3/g [25]. In total four homogeneous PPO membranes of different thickness (3.5, 10.5, 12, and 17 μm) were prepared.

6.3.3 Gas permeation tests

After the membranes were put in their respective cells, they were purged with helium at 345 kPag for five days. During this time every connection, as well as, the area around each membrane cell was checked for possible leaks and all discovered leaks were fixed. For leak detection, a Matheson leak detector with sensitivity of $1.0\times10^{-5}\ cm^3/s$ or $0.6\ \mu L/\text{min}$ for helium was utilized.

Three membranes with thicknesses of 3.5, 10.5, 17μm were tested with O_2 as a feed, while a 12μm-thick membrane was simultaneously tested with N_2. The equivalent length of tubing for each cell used for O_2 tests was L_e = 136 cm, whereas for the cell used for N_2 test the equivalent length of tubing was L_e = 84 cm. The membranes were tested at different feed pressures. For a given feed pressure, the gas permeation test was carried out for one month. This allowed using at least 300 points at steady state conditions for the determination of the average and standard deviation values for the permeation rate and the feed pressure. During the gas permeation tests the temperature was 24 ± 1.5°C. For

the determination of permeate composition 25 μL samples, taken using Hamilton gastight syringes, were analyzed using a GOW-MAC 580 gas chromatograph equipped with a molecular sieve 5A column. To minimize flow disturbances, the samples were taken only once a day. For a given sampling point, five or more samples at steady state were used for the evaluation of the average and deviation of the permeate composition.

6.4 Results and Discussion

Figure 6.4 presents the effect of feed pressure on the apparent permeability coefficient of N_2 in a 12 μm PPO membrane. The horizontal line in Figure 6.4, corresponding to 3.81 Barrer, represents the permeability coefficient of N_2 in PPO reported by Ilinitch [26], to which the apparent permeabilities appear to approach.

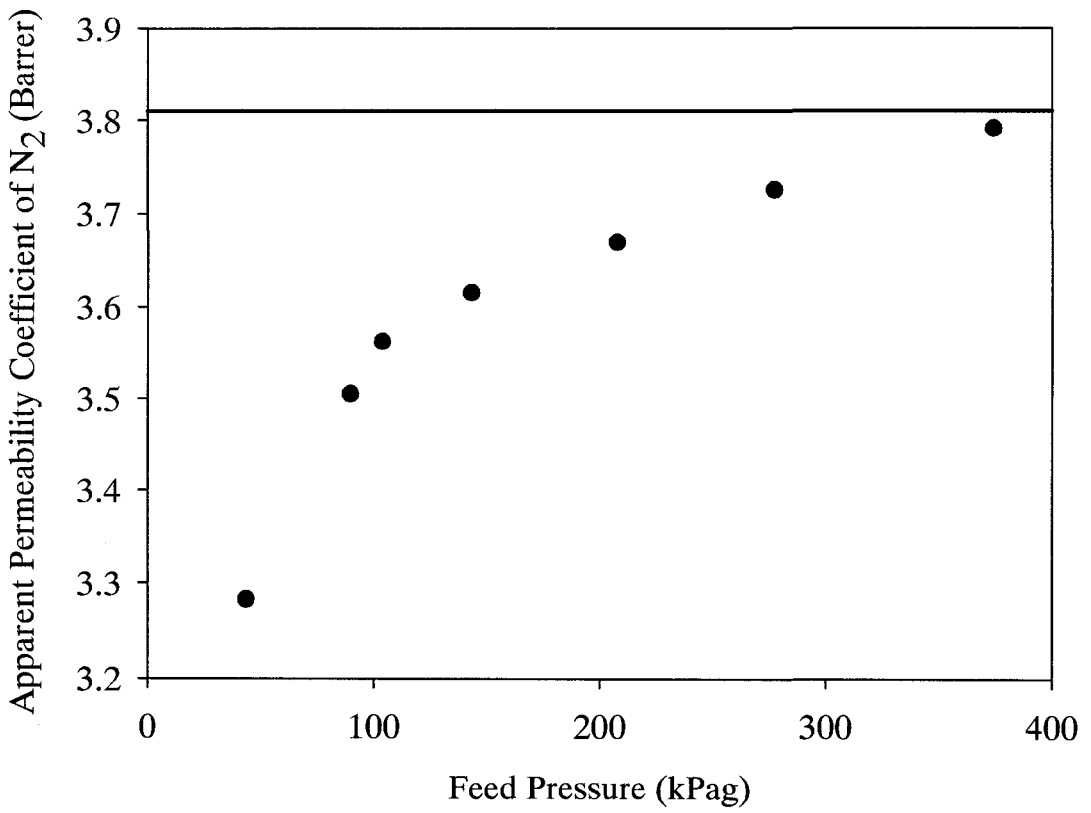

Figure 6.4. Effect of feed pressure on the apparent permeability coefficient of N_2 in 12 μm-thick PPO membrane. Horizontal line corresponds to the permeability coefficient of N_2 in PPO reported in Ref. [26].

It is well known that permeability of gases in glassy polymers such as PPO may vary with feed pressure. This dependence arises from a dual mode sorption, which occurs in glassy polymers. If one side of a glassy film is exposed to pure gas A at a pressure p_A while the other side is exposed to vacuum, the permeability coefficient P_A is related to p_A through the following equation [27]:

$$P_A = D_D\left(k_{DA} + F\frac{C'_{HA}b_A}{1+b_A p_A}\right) \tag{6.26}$$

Where: D_D is the diffusivity of A in Henry's sites, k_{DA} is the Henry's law constant, C'_{HA} is hole saturation constant, b is the hole affinity constant, and $F = D_H/D_D$, in which D_H is the diffusivity of A in Langmuir sites. The literature values of D_D, k_{DA}, C'_{HA}, b, and F for N_2 in PPO [28] are listed in Table 6.1. In case of our gas permeation experiments the permeate side of the membranes was at atmospheric pressure rather than vacuum so that Equation (6.26) might not be directly applicable. Nevertheless, replacing p_A with the feed gauge pressure and using the literature values from Table 6.1 it can be shown that for the pressure range in Figure 6.4 the P_{N2} in PPO should decrease by roughly 2%, while in reality it increases by 16%. It is therefore clear, that the observed increase in the apparent permeability coefficient of N_2 in PPO cannot be explained on the basis of dual mode sorption.

Table 6.1. Reported transport properties of oxygen and nitrogen in PPO membranes.

Gas	$k_D \times 10^6$ $\frac{m^3(STP)}{m^3.Pa}$	C'_H $\frac{m^3(STP)}{m^3}$	$b \times 10^6$ Pa^{-1}	$D_D \times 10^{11}$ m^2/s	$F = \frac{D_H}{D_D}$	Reference
Nitrogen	1.18	7.1	0.395	2.02	0.14	[28]
Oxygen	2.47	11.0	0.715	1.53	0.28	[29]

Similarly to Figure 6.4, Figure 6.5 presents the effect of feed pressure on the apparent permeability coefficient of O_2 in three PPO membranes of different thickness. The horizontal line in Figure 6.5 corresponding to 13.2 Barrer represents the permeability

coefficient of O_2 in PPO reported by Ilinitch [26]. It can be noticed that the thicker the membrane the greater the apparent permeability coefficient at a given feed pressure, which is particularly evident at very low feed pressures. However, as the feed pressure increases the difference between the apparent permeability coefficients decrease and they all seem to approach to a single value, which is close to the permeability reported by Ilinitch [26.]. If one considers the dual mode sorption represented by Equation (6.26) and the literature values of D_D, k_{DA}, C'_{HA}, b, and F for O_2 in PPO [29], which are also listed in Table 6.1, for the pressure range in Figure 6.5 the permeability coefficient of O_2 in PPO should decrease by 4%. On the other hand, the observed decrease in the apparent permeability coefficients varies, depending on the membrane thickness from 40% for the 3.5 μm membrane to 58% for the 17 μm membrane. It is therefore clear that the observed decrease in the apparent permeability coefficient cannot be solely explained on the basis of dual mode sorption.

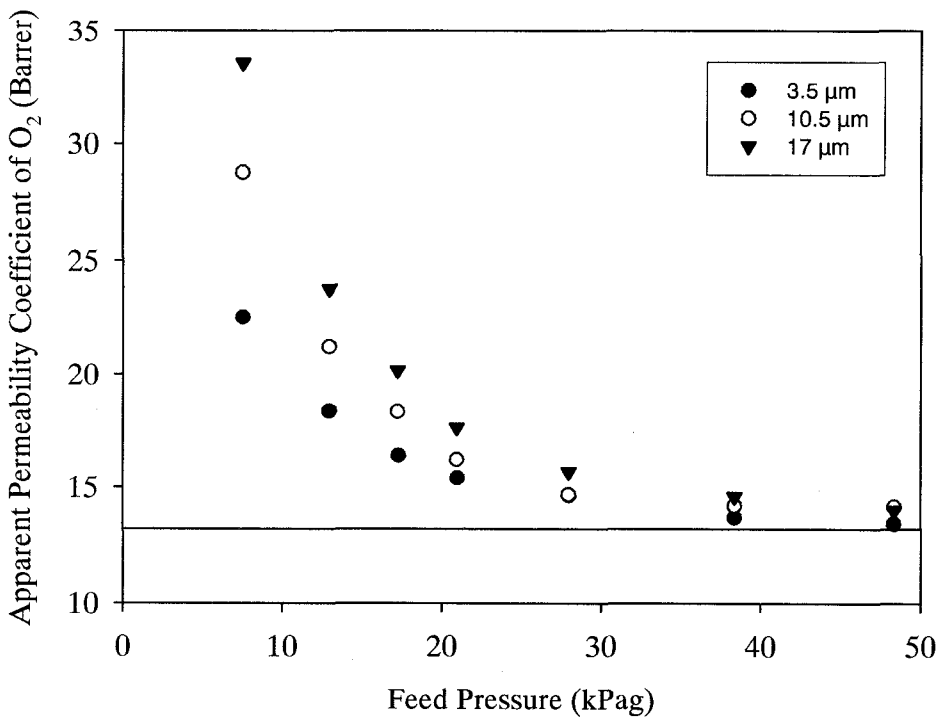

Figure 6.5. Effect of feed pressure on the apparent permeability coefficient of O_2 in three PPO membranes of different thicknesses. Horizontal line corresponds to the permeability coefficient of O_2 in PPO reported in Ref. [26].

From a practical point of view the results shown in Figures 6.4 and 6.5 indicate that if the respective single gas permeation tests with N_2 and O_2 are performed at low feed pressures, one could report a considerably greater permeability ratio for these two gases than the actual value.

6.4.1 Application of the model

If one considers the possible influence of back diffusion on the apparent permeability coefficient, the observed effect of membrane thickness in Figure 6.5 is logical, because the thicker the membrane the lower the flux at a given feed pressure allowing back diffusion to have a greater influence on the transport of the forward permeating gas. In the following discussion the mathematical model describing the combined effects of back diffusion and back permeation, which was developed in Section 2, will be confronted with the experimental data.

To compare the model with the experimental data the apparent permeability coefficients shown in Figures 6.4 and 6.5 are presented in a dimensionless form as $P_i|_{App}/P_i$, in which P_i represents the actual permeability coefficient. Considering Figures 4 and 5 it appears reasonable to use for P_i the respective permeability coefficients of N_2 and O_2 reported by Ilinitch [26].

Figures 6.6 and 6.7 present the comparison of the experimental and theoretical $P_i|_{App}/P_i$ at different feed pressures for the gas permeation tests with N_2 and O_2, respectively. The experimental $P_i|_{App}/P_i$ in these figures are shown with the error bars. The latter were evaluated using the following equation [30]:

$$\varepsilon_{P_A|_{app}} = \sqrt{\left(\frac{\partial P_A|_{app}}{\partial N}\varepsilon_N\right)^2 + \left(\frac{\partial P_A|_{app}}{\partial(p_f - p_p)}\varepsilon_{(p_f-p_p)}\right)^2} \tag{6.27}$$

where ε_i is the precision of parameter i.

Generation of the theoretical $P_i|_{App}/P_i$ using Equation (6.13) requires the composition of the gas in contact with the permeate side of the membrane $(x_i)_p$. This, in

turn requires simultaneous solving of Equations (6.22) and (6.24) and the specification of D_{AB} and α_{BA}, which appear in these equations. For D_{AB}, the experimental value of 0.22 cm^2/s at 20°C [31] was used. As far as α_{BA} is concerned, it was evaluated on the basis of the permeability coefficients of N_2 and O_2 in PPO reported by Ilinitch [26].

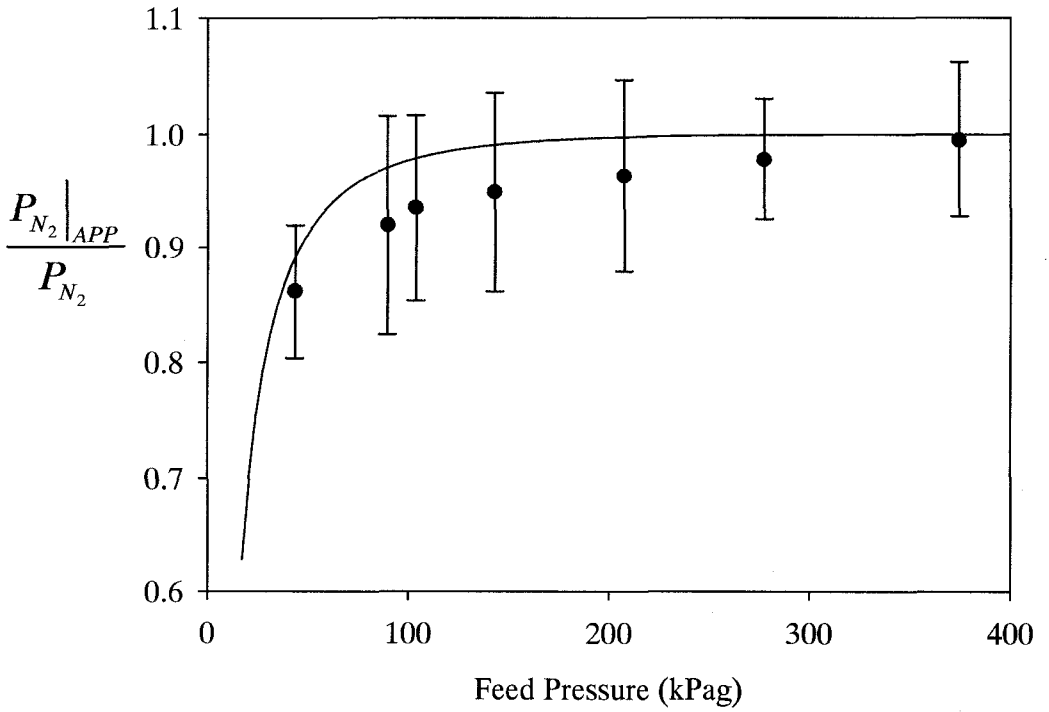

Figure 6.6. Effect of feed pressure on the experimental (symbols) and theoretical (lines) relative permeability coefficients of N_2 in a 12 μm-thick PPO membrane.

Focusing on Figure 6.6 it is evident that for the experiment with N_2 the model (solid line) overestimates $P_{N_2}|_{App}/P_{N_2}$. On the other hand, for the experiments with O_2 (Figure 6.7) the model overestimates the values of $P_{O_2}|_{App}/P_{O_2}$. Since $P_{O_2}|_{App}/P_{O_2}$ is generally greater than unity while $P_{N_2}|_{App}/P_{N_2}$ is generally smaller than unity, it can be concluded that the model underestimates the effects of back diffusion. It is important to emphasize that despite discrepancies between the theoretical and experimental values in Figures 6.6 and 6.7 the theoretical line shows a similar trend as the experimental data.

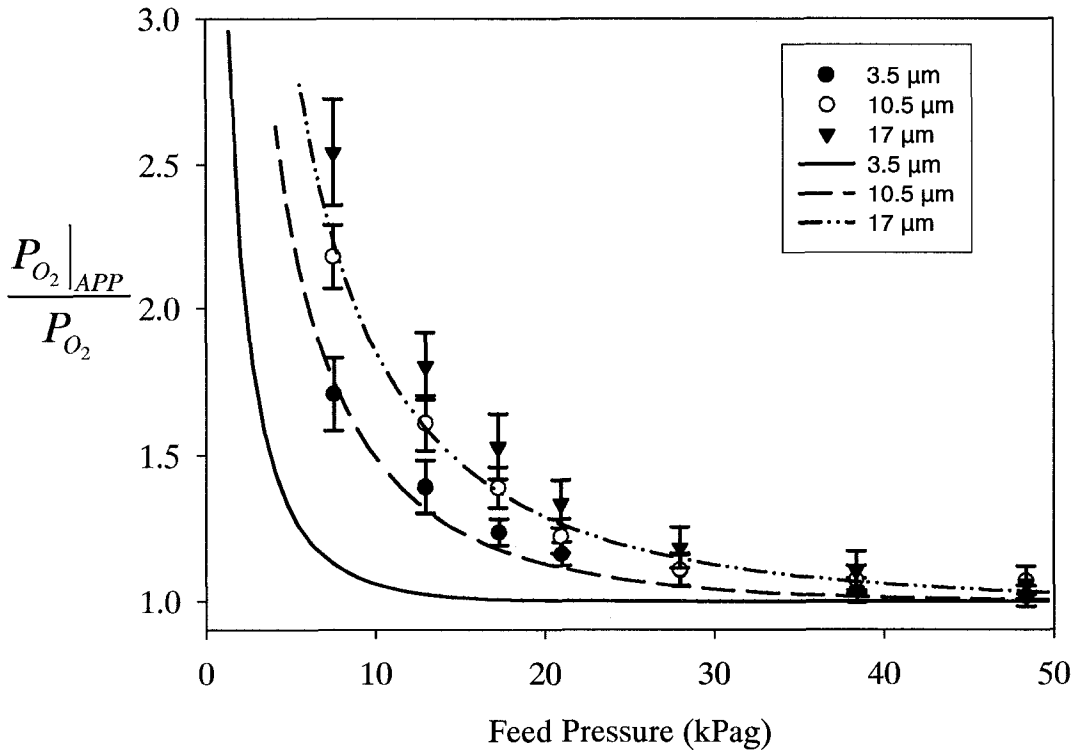

Figure 6.7. Effect of feed pressure on the experimental (symbols) and theoretical (lines) relative permeability coefficients of O_2 in three PPO membranes of different thicknesses.

As already discussed, back permeation and back diffusion may lead, depending whether α_{BA} is smaller or greater than unity, to an increase or decrease in the apparent permeability coefficient. On the other hand, regardless of the numerical value of α_{BA}, the greater the effects of back permeation and back diffusion the smaller the concentration of the forward moving gas at membrane/permeate interface $(x_A)_P$.

Figure 6.8 compares the experimentally determined concentrations of oxygen in the permeate stream at three different distances from the free stream with the theoretical concentration profiles. The experiments performed in Figure 6.8 were performed at feed pressure of 48.3 kPag performed using three membranes of different thicknesses. The experimental concentrations of oxygen in the permeate stream increase as the distance from the free stream increases, i.e. as the distance from membrane decreases, which is

consistent with the theoretical concentration profiles. Also, at a given distance from the free stream, the concentration of oxygen increases as the membrane thickness decreases, which is again consistent with the theoretical effect of membrane thickness on the concentration of oxygen in the permeate stream. On the other hand, the experimental concentrations of oxygen are significantly lower than the theoretical values, and generally, the thinner the membrane the greater the discrepancy between the theoretical and experimental concentrations.

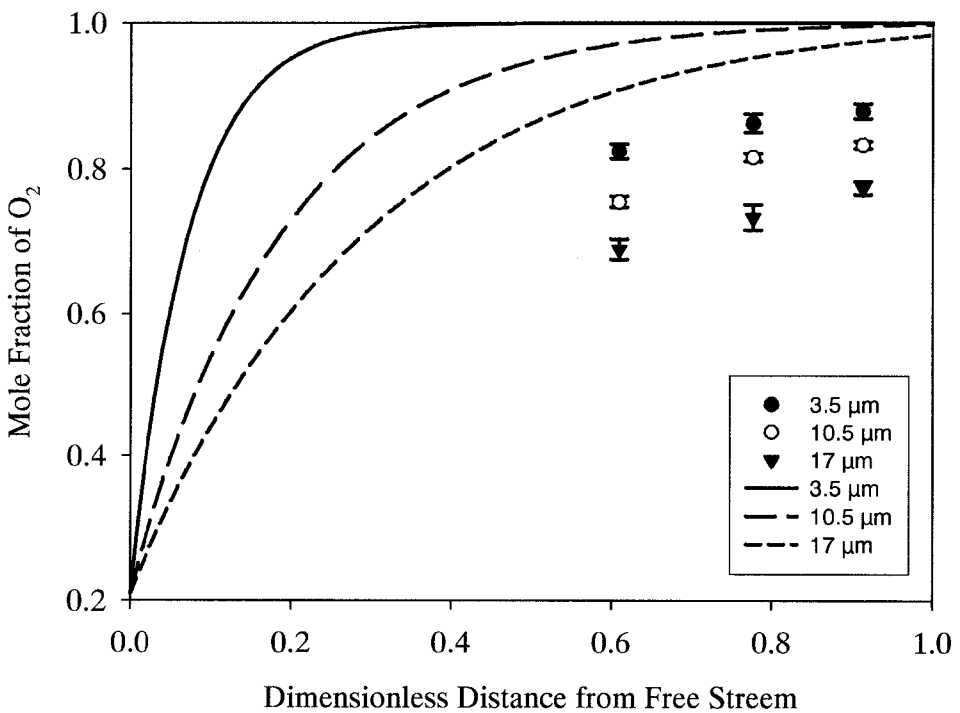

Figure 6.8. Comparison of the experimental mole fractions of O_2 at three different distances from the free stream (symbols) with the model predictions (lines) in gas permeations tests with pure O_2 performed at feed pressure of 48.3 kPag using three PPO membranes of different thicknesses.

The effect of feed pressure on the concentration of the forward permeating gas at the sampling point closest to the membrane (dimensionless distance from the free stream $y = 0.91$) is shown in Figures 6.9 and 6.10 for the experiments with oxygen and nitrogen respectively. As the feed pressure increases, the respective experimentally measured concentrations of oxygen and nitrogen in the permeate stream increase, which is consistent with the theoretical model. On the other hand, similarly to Figure 6.8 while the experimental concentrations follow the theoretical trend, the experimental concentrations are lower than the theoretical values. However, the differences between the experimental data and the model predictions are greater in tests with oxygen than those in tests with nitrogen. In the case of the tests with oxygen, discrepancy between the experimental and theoretical concentrations appears to increase with a decrease in the membrane thickness.

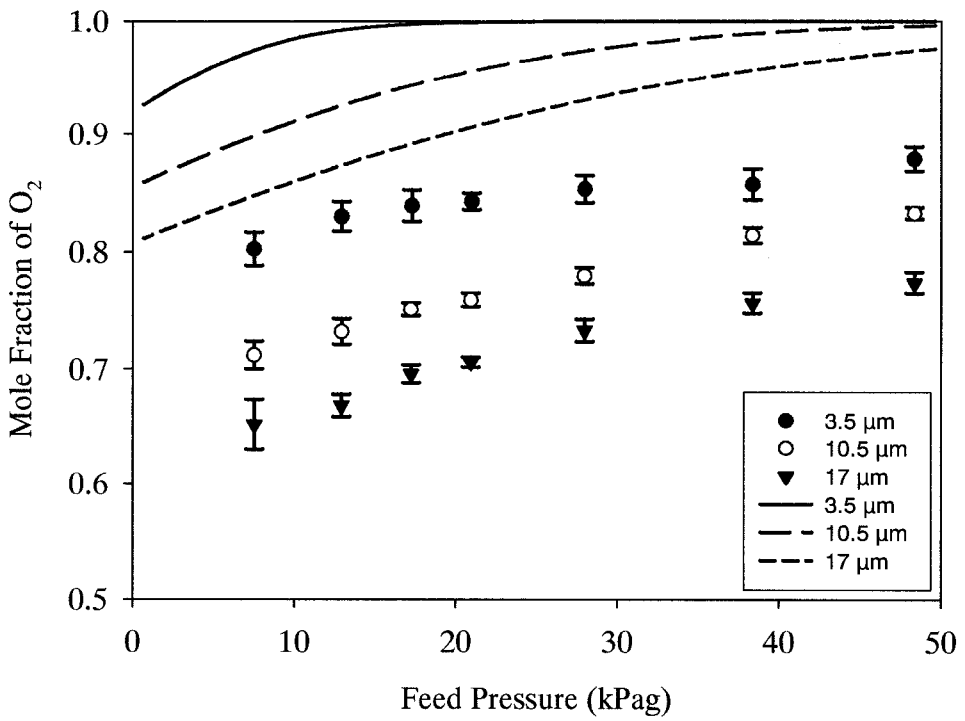

Figure 6.9. Effect of feed pressure on the experimental (symbols) and theoretical (lines) mole fractions of O_2 at the dimensionless distance from the free stream of 0.91 in single gas permeation tests with O_2 using three PPO membranes of different thickness.

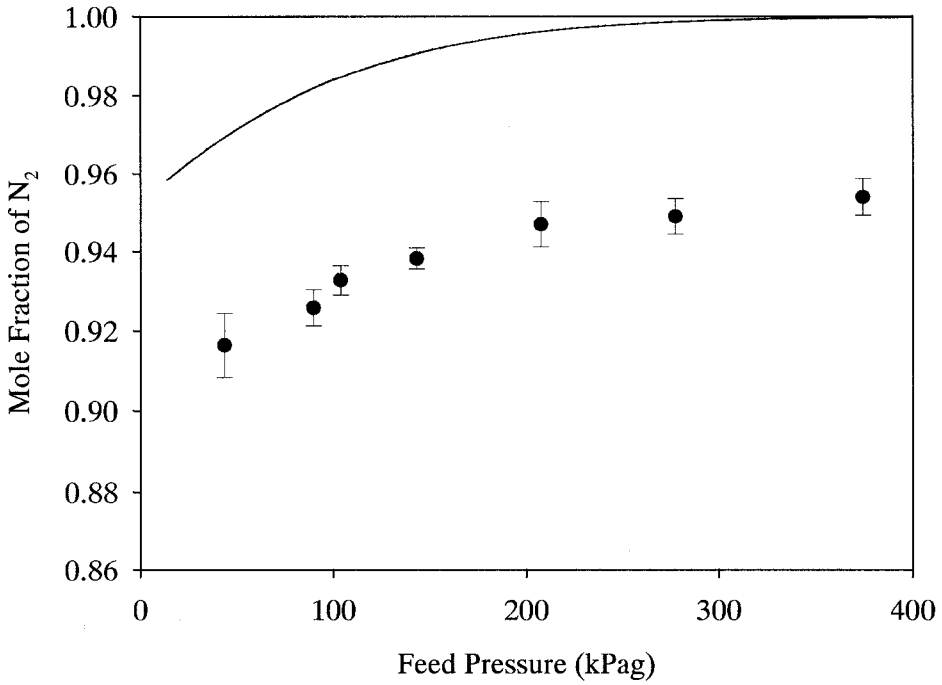

Figure 6.10. Effect of feed pressure on the experimental (symbols) and theoretical (solid line) mole fractions of N_2 at the dimensionless distance from the free stream of 0.91 in single gas permeation tests with N_2 using a 12 μm-thick PPO.

6.4.2 Quantification of discrepancy between experimental and theoretical results

Figures 6.8-6.10 confirm that underestimation of the effects of back diffusion and back permeation evident in Figures 6.6 and 6.7 can, to a large part, be due to overestimation of the concentration of the forward permeating gas in contact with the permeate side of the membrane $(x_i)_P$. In turn, the latter is calculated by simultaneous solution of Equations (6.22) and (6.24). These two equations can be used to predict the concentration of the forward permeating at any distance from the membrane by using the appropriate equivalent length (L_e) in Peclet number. Considering Equation (6.24), an overestimation of the concentration of the forward permeating could result from an overestimation of Pe number. Conversely, to fit the theoretical concentrations of the forward permeating gas to the experimental data, Equation (6.24) can be modified as follow:

$$\frac{\xi_A - (x_A)_P}{\xi_A - (x_A)_0} = \exp(-\beta Pe) \tag{6.28}$$

Where β is a dimensionless correction factor; for β = 1, Equation (6.28) becomes Equation (6.24). The numerical value of β can be used to quantify the discrepancy between the theoretical and experimental results; the smaller the β the greater the discrepancy between the two. Moreover, β can also be used to quantify the discrepancy the experimental and theoretical values of $P_i|_{App}/P_i$ since the latter, which is determined from Equation (6.13), requires $(x_A)_p$.

Using a MATLAB simplex method the value of β was optimized by minimizing the least square difference between the theoretical and experimental values of x_A at y = 0.91 i.e., at the sampling point closest to the membrane, and the difference between the theoretical and experimental values of $P_i|_{App}/P_i$ as a function of pressure.

Figures 6.11 and 6.12 present the examples of comparison of the theoretical model modified using the optimized values of β with the experimental $P_i|_{App}/P_i$ for the 17 μm membrane tested with oxygen, and with x_A at y = 0.91 for the 10.5 μm membrane tested with oxygen, respectively. The respective values of β in Figures 10.11 and 10.12 are 0.777 and 0.253. It is evident that using the optimized β the modified theoretical models follow closely the experimental data.

Table 6.2 presents the summary the optimized β values for all tested membranes. There are two interesting observations which must be emphasized. First, is the fact that for a given membrane β based on $P_i|_{App}/P_i$ is considerably greater than that based on x_A. This means that Equation (6.13), from which the theoretical $P_i|_{App}/P_i$ is calculated, diminishes the discrepancy between the model and experimental data.

In other words, if $(x_A)_p$ required for Equation (6.13) were determined by simultaneous solving of Equations (6.22) and (6.24) using experimental x_A at y = 0.91 as a boundary condition and the corresponding L_e, the $P_i|_{App}/P_i$ would overestimate rather than underestimate the back diffusion effects.

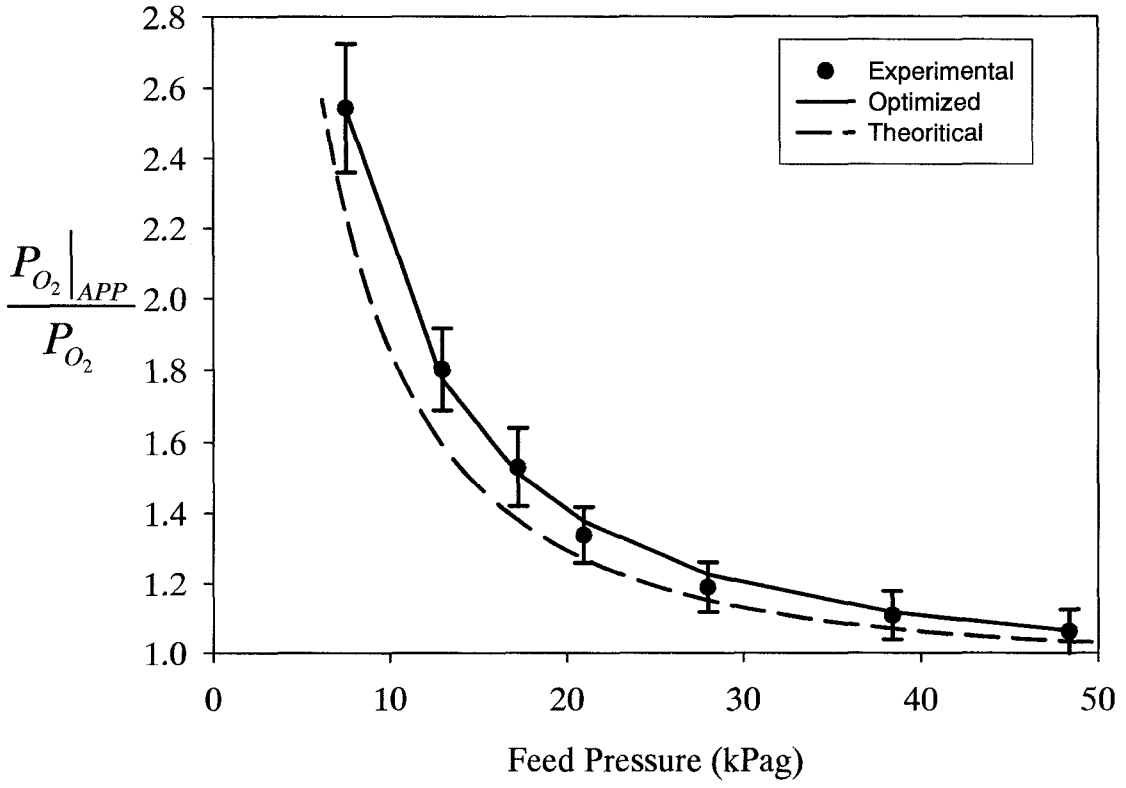

Figure 6.11. Comparison of the experimentally observed effect of feed pressure on the relative permeability coefficient of O_2 in single gas permeation tests performed using a17 μm-thick PPO membrane (symbols) with the model (dashed line) and the optimized model predictions.

Table 6.2. Summary of the optimized β values for all tested membranes.

Membrane Thicknesses (μm)	Test Gas	β values based on:	
		Permeability	Composition
17	O_2	0.777	0.301
12	N_2	0.697	0.262
10.5	O_2	0.638	0.253
3.5	O_2	0.321	0.133

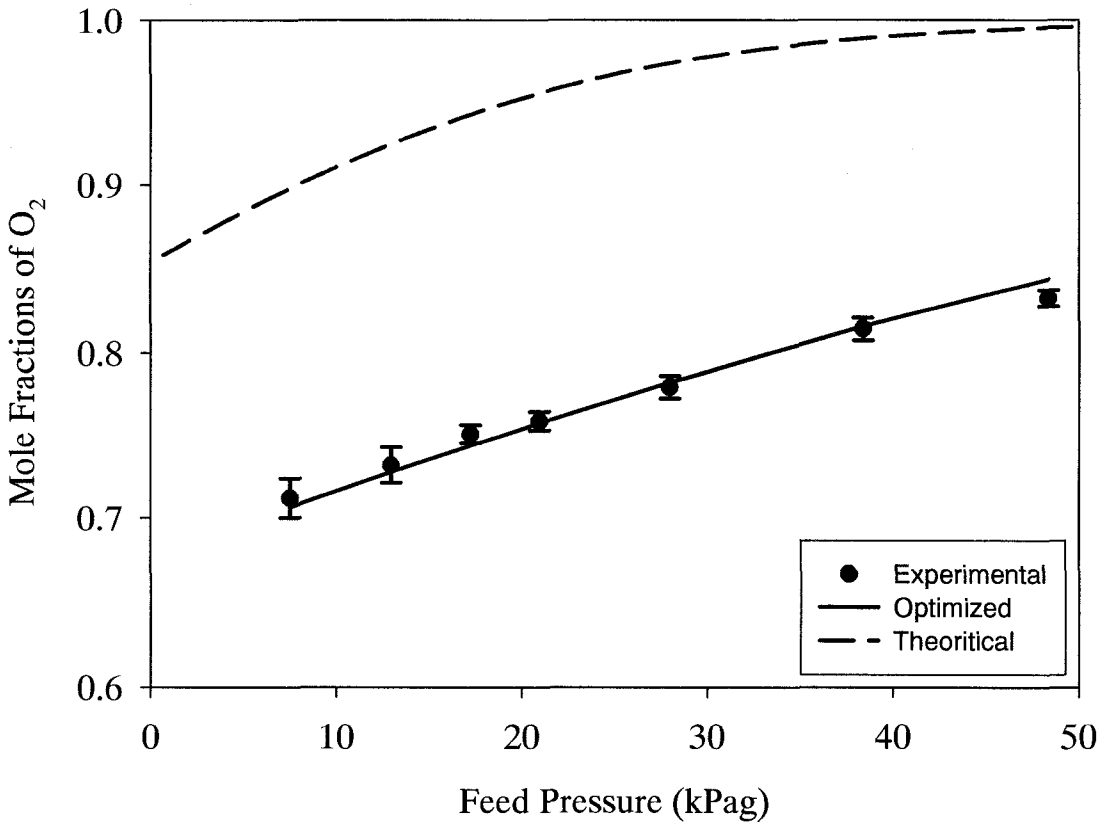

Figure 6.12. Comparison of the experimentally observed effect of feed pressure on the mole fractions of O_2 at the dimensionless distance from the free stream of 0.91 in single gas permeation tests performed using a 10.5 μm-thick PPO membrane (symbols) with the model (dashed line) and the optimized model (solid line) predictions.

Another important observation from Table 6.2 is an increase of β with an increase in the membrane thickness, which indicates that the thinner the membrane the greater the discrepancy between the theoretical and experimental data. As already stated, overestimation of the concentration of the forward permeating gas downstream from the membrane could result from overestimation of Pe number. In turn, considering the definition of Pe its overestimation could result from overestimation of the velocity measured in the flow meter column (u_j), and/or overestimation of the effective length (L_e), and/or underestimation of the binary diffusion coefficient (D_{AB}). However, out of

these three parameters, the only one which could, in principle, be associated with a significant error is u_j. Consequently, if u_j were responsible for a discrepancy between the theoretical and experimental data, one would expect this discrepancy to increase with the membrane thickness, because the flow rate is inversely proportional to the membrane thickness. On the other hand, as shown in Table 6.2, β increases rather than decreases with the membrane thickness.

While the dimensionless parameter β provides a convenient way to assess the discrepancy between the theoretical and experimental results, it is clear that the numerical values of β in Table 6.2 cannot be explained on the basis of overestimation of Pe number in Equation (6.24). Therefore, overestimation of $(x_A)_p$ must arise from the dimensionless parameter ξ_A, which as shown by Equation (6.21), is defined in terms of the fluxes of the forward (N_A) and back (N_B) diffusing gases. Since these fluxes cannot be measured directly, Equation (6.21) was converted to Equation (6.22) by assuming no interactions between the forward and back permeating gases with each other and with the membrane. The latter equation contains α_{BA}, which, as already discussed, was evaluated by the actual permeabilities of the backward and forward permeating gases.

It is widely accepted that the transport of a binary gas mixture through a glassy polymeric membrane is influenced by sorption coupling, which is a consequence of dual mode sorption in glassy polymer. For a binary gas mixture Equation (6.26) becomes [32]:

$$P_A = D_D\left(k_{DA} + F\frac{C'_{HA}b_A}{1+b_Ap_A+b_Bp_B}\right) \tag{6.29}$$

It is important to emphasize that Equation (6.29) represents the simplest departure from the concept of a "black box membrane"; it simply recognizes that gas molecules are sorbed into by Henry's sites and Langmuir sites, while it still assumes no interactions between gas molecules and the membrane. Moreover, it is applicable when the transport of species A and B occurs in the same direction and the permeate side of the membrane is under vacuum. Nevertheless, the above example illustrates the importance of the gas transport model in the membrane on the actual effect of back diffusion and back permeation phenomena.

It is therefore clear that the discrepancies between the theoretical and experimental data evident in Figures 6.6-6.10 must primarily arise from a lack of the

adequate model describing the gas transport in the membrane. To our best knowledge, while there are numerous models for the transport of binary gas mixtures, there is no model for the transport of species in the opposite directions in glassy polymeric membranes.

6.5 Conclusions

A model to describe the phenomenon of back diffusion and back permeation, which are inherent to membrane gas permeation in systems open to atmosphere, has been developed assuming a binary system, i.e., a single forward and a single back permeating gas, no interactions between the forward and back permeating gases and no interactions between the gases and the membrane. According to this model, for the system in which back permeating gas is more permeable than the forward permeating gas, the experimentally measured permeability coefficient of the forward permeating gas will be lower than the actual permeability coefficient. If the forward permeating gas is more permeable than the back permeating gas, the experimentally measured permeability coefficient of the forward permeating gas will be greater than the actual permeability coefficient. According to the model, the error in the measured permeability coefficient for either system quickly decreases as the feed pressure increases. The developed model also allows prediction of the composition of the gas in a tube connecting the membrane cell with the flow meter at any distance from the membrane.

To verify the developed model for back diffusion and back permeation single gas permeation experiments with oxygen and nitrogen were performed using homogeneous PPO membranes in a constant pressure system equipped with fully automated soap bubble flow meters capable of measuring the flow rates as low as 5 μL/min. The experimental system also allowed sampling of the permeating gas at three different distances from the membrane in order to compare the experimentally determined gas compositions with the model-predicted values.

The experimental results for the apparent permeability and the composition of the permeating gas as a function of feed pressure have confirmed the theoretical trends. However, the experimentally observed effects of back permeation and back diffusion are considerably greater than the theoretically predicted effects. The discrepancy between the

experimental and theoretical results has been quantified by a dimensionless correction factor determined by minimizing the least square difference between the theoretical and experimental values using a MATLAB simplex method. These analyses have showed that the discrepancy based on the composition of permeate is greater than that based on the permeability coefficients; also the discrepancy appears to increase with a decrease in the membrane thickness. It is believed that the major reason for the observed discrepancies between the experimental and theoretical data is the assumption of no interactions between the forward and back permeating gases as well as no interactions between the gases and the membrane.

While at present there is no adequate model for the gas transport in opposite directions in glassy membranes, the observed discrepancies between the model and experimental data indicate that the phenomenon of back permeation and back diffusion might influence membrane characterization in constant pressure systems, in particular permeability ratios determined based on single gas permeation experiments, over much wider range of testing conditions than originally thought.

Acknowledgement

The authors gratefully acknowledge the financial support for this project provided by the Natural Science and Engineering Research Council of Canada.

Nomenclature

$Area_M$	Cross section area of membrane, m^3, cm^3
B	The hole affinity constant, Equation (6.26)
C	Total concentration defined as $C = \sum C_i$, mol/cm^3
C_i	Concentration, mol/cm^3
C'_{HA}	The hole saturation constant, mol/cm^3
D	Diameter of tube, cm
D_D	The diffusivity in Henry's sites, Equation (6.26), cm^2/s
D_H	The diffusivity in Langmuir sites, Equation (6.26), cm^2/s

D_{ij}	Diffusivity of component i in presence of component j, cm^2/s
D_{iM}	Diffusivity of component i in membrane, cm^2/s
F	$F = D_H/D_D$, Equation (6.26), dimensionless
J_i	Diffusive flux of component i defined by Equation (6.2), $mol/cm^2.s$
k_D	The Henry's law constant, Equation (6.26)
L_k	Length of the tube k, cm
L_M	Thickness of membrane, cm, μm
N	Number of tubes
N_i	Transport flux of component i, $mole/cm^2.s$
P	Pressure, kPa
P_i	Permeability of component i defined as $P_i = D_{iM} S_i$, mol/cm.Bar.s, Barrer
Pe	The Peclet number ($Pe = u_j L_e / D_{AB}$), Equation (6.24)
S_i	Solubility of component I defined in Equation (6.1), $mole/m^3.Bar$
U	Velocity, cm/s
x_i	Composition of component i
Y	Dimensionless distance from free stream based of equal length of tubes
Z	Distance, cm

Greek letters:

α_{ij}	Selectivity between components i and j defined by Equation (6.6), dimensionless
β	Dimensionless correction factor, Equation (6.28)
ε_i	The precision of parameter i, Equation (6.27)
ξ	Dimensionless parameter introduced in Equation (6.21)
Π	3.1415

Subscripts:

0	At free stream
A, B	Components in a binary gas mixture
App	Apparent , used for permeability in Equation (6.10)

F	Membrane feed side
I	Component i
K	Tube index
M	Inside the membrane
P	Membrane permeate side

References

1. W.J. Koros and G.K. Fleming, Review: Membrane-based gas separation, J. Membr. Sci., 83 (1993) 1.
2. V. Stannett, Review: The transport of gases in synthetic polymeric membranes-a historic perspective, J. Membr., Sci. 3 (1978) 97.
3. P. Pandey and R.S. Chauhan, Membranes for gas separation, Prog. Polym. Sci., 26 (2001) 853.
4. R.W. Baker, Future directions of membrane gas separation technology, Ind. Eng. Chem. Res. 41 (2002) 1393.
5. J.Y. Park and D.R. Paul, Correlation and prediction of gas permeability in glassy polymer membrane materials via modified free volume based group contribution method, J. Membr. Sci., 125 (1997) 23.
6. Michael C. Villet, George R. Gavalas, Measurement of concentration-dependent gas diffusion coefficients in membranes from a psuedo-steady state permeation run Michael C. Villet, George R. Gavalas, J. Membr. Sci. 297 (2007) 199–205.
7. Jamal Kurdi, Ashwani Kumar, Performance of PEI/BMI semi-IPN membranes for separations of various binary gaseous mixtures, Separation and Purification Technology 53 (2007) 301–311.
8. M. Pourafshari Chenar, M. Soltanieh, T. Matsuura, A. Tabe-Mohammadi, K.C. Khulbe, The effect of water vapor on the performance of commercial polyphenylene oxide and Cardo-type polyimide hollow fiber membranes in CO_2/CH_4 separation applications, J. Membr. Sci. 285 (2006) 265–271.
9. Junya Okazaki, David A. Pacheco Tanaka, Margot A. Llosa Tanco, Yoshito Wakui, Fujio Mizukamia, Toshishige M. Suzuki, Hydrogen permeability study of the thin Pd–Ag alloy membranes in the temperature range across the α–β phase transition, J. Membr. Sci. 282 (2006) 370–374.
10. Jamal Kurdi, Ashwani Kumar, Formation and thermal stability of BMI-based interpenetrating polymers for gas separation membranes, J. Membr. Sci. 280 (2006) 234–244.

11. A.P. Korikov, P.B. Kosaraju, K.K. Sirkar, Interfacially polymerized hydrophilic microporous thin film composite membranes on porous polypropylene hollow fibers and flat films, J. Membr. Sci. 279 (2006) 588–600.
12. S.K. Ryi, J.S. Park, S.H. Kim, S.H. Cho, J.S. Park, D.W. Kim, Development of a new porous metal support of metallic dense membrane for hydrogen separation, J. Membr. Sci. 279 (2006) 439–445.
13. A. Tran, Development of and Gas Permeation Study of Homo and Copolymers from the Family of Polyphenylene Oxides, MASc Thesis, University of Ottawa, Ottawa, ON, 2003.
14. E.A. Mason and H.K. Lonsdale, Statistical mechanical theory of membrane transport, J. Membr. Sci., 51 (1990) 1.
15. C. Vallieres, E. Favre, X.A.D. Roizard, Separation of binary mixture by dense membrane processes: influence of inert gas entrance under variable downstream pressure conditions, Chem. Eng. Sci. 58 (2003) 2767-2775.
16. J.C. Shah, Application of kinetic model to in vitro percutaneous permeation of drugs, Int. J. Pharm., 133 (1996) 179.
17. R.G. Males, P.S. Phillips and F.G. Herring, Equations describing passive transport through vesicular membranes, Biophys. Chem., 70 (1998) 65.
18. Y. Fang, L.W. Clapp, R.M. Hozalski, P.J. Novak, M.J. Semmens, Membrane gas transfer under conditions of creeping flow: modeling gas composition effects, Water Research, 38 (2004) 2489-2498.
19. M. Aguilar-Vega and D.R. Paul, Gas transport properties of polyphenylene ethers, J. Appl. Polym. Sci., 31 (1993) 1577.
20. R.B. Bird, W.E. Stewart and E.N. Lightfoot, Transport Phenomena, 2nd Ed., John Wiley & Sons, NY, 2001.
21. A. Arenas, L. Victoria and J.A. Ibañez, A time-integration-based measurement circuit for a soap bubble flow-meter using optical fiber sensors, Meas. Sci. Technol., 6 (1995) 435.
22. S. Lashkari, B. Kruczek, Development of a fully automated soap flowmeter for micro flow measurements, Flow Measurement and Instrumentation, 19 (2008) 397- 403.

23. Jia Guo and Mark J. Heslop, Diffusion problems of soap-film flowmeter when measuring very low-rate gas flow, Flow Measurement and Instrumentation 15 (2004) 331-334.
24. Y. Huang, D.R. Paul, Experimental methods for tracking physical aging of thin glassy polymer films by gas permeation, J. Membr. Sci. 224 (2004) 167-178.
25. G.A. Polotskaya, S.A. Agranova, N.V. Gazdina, Yu.P. Kuznetsov, V.V. Nesterov, Effect of molecular weight parameters on gas transport properties of poly(2,6-dimethyl-1,4-phenylene oxide), J. Appl. Polym. Sci. 62 (1996) 2215-2218.
26. O.M. Ilinitch, Gas permeation through the films of polyphenylene oxides, in G. Chowdhury, B. Kruczek, T. Matsuura (Eds.), Polyphenylene Oxide and Modified Polyphenylene Oxide Membranes, Kluwer Academic Publishers, Boston, 2001, p. 29-30.
27. R. M. Barrer, R. R. Fergusson, Diffusion of Benzene in Rubber and Polythene, Transactions of the Faraday Society 54 (1958) 989-1000.
28. K. Toi, G. Morel, and D.R. Paul, Gas sorption and transport in poly(phenylene oxide) and comparisons with other glassy polymers, , J. Appl. Polym. Sci., 27 (1982) 2997-3005.
29. H. Kumazawa and M. Yoshida, Mechanism of gas transport of NH_3-plasma-treared poly(phenylene oxide) membranes, J. Appl. Polym. Sci., 78 (2000) 1845-1852.
30. S. Tavoularis, Measurement in fluid mechanics, Cambridge University Press, New York, (2005).
31. J.O. Hirschfelder, C.F. Curtiss, R.B. Bird, Molecular theory of gases and liquids, 2nd corrected printing, Wiley, New York (1964), p. 579.
32. W.J. Koros, Model for Sorption of Mixed Gases in Glassy Polymers, J. Polym. Sci., Polym. Phys. Ed., 18 (5) (1980) 981-992.

Part III

Constant Pressure System with Sweep Gas

This part is an application of Part II and consists of one paper.

Chapter 7

A Novel Technique for the Measurement of Diffusion Coefficient of Forward Permeating Gas in Presence of Back Permeation

S. Lashkari, Q. Wang, B. Kruczek*

To be submitted to Journal of Membrane Science

Department of Chemical Engineering
University of Ottawa
161 Louis Pasteur Street
Ottawa, ON K1N 6N5, Canada
Fax: (613) 562-5172
Phone: (613) 562-5800 ext. 6302
E-mail: bkruczek@.uottawa.ca

* **To whom correspondence should be addressed.**

Abstract

A procedure for evaluation of the diffusion coefficient of single gases in membrane in the presence of back permeation was developed and successfully employed using a specially designed constant pressure system. In this method a step change in feed pressure is executed while permeate side of the membrane is swept by a gas mixture containing at least one gas not present in the feed stream. Using this method the diffusion coefficient of nitrogen in a PPO membrane was determined in the presence of back permeating oxygen and methane, respectively; also, the diffusion coefficient of oxygen in the presence of back permeating nitrogen and the diffusion coefficient of methane in the presence of back permeating nitrogen were measured. The results indicate that the diffusion coefficients of nitrogen and oxygen increase when another gas is present in the membrane matrix, but diffusion coefficient of methane decreases in the presence of nitrogen in the membrane matrix. The effect of composition of the sweep gas on the diffusion coefficient of the forward permeating gas is very strong whenever methane is either forward or back permeating gas. The novel technique developed in this work may prove to be a very useful tool in fundamental studies on transport mechanism in gas separation membranes.

Keywords: Time lag, Diffusion coefficient, Back permeation, Sweep gas

7.1 Introduction

Glassy polymers have a great potential as membrane materials for separation of gases and vapours, and the industry for gas and vapour separation membranes has been developing rapidly in the last decade. However, the competing processes, such as cryogenic distillation and adsorption, are also improving along. These processes are very popular and, unlike membranes, are more established and thoroughly studied. For the membranes to further compete with the traditional separation processes, they must offer an increasing economical benefit. The latter cannot be achieved without a better understanding of transport mechanisms of gases and vapours in membranes, which helps to design and optimize more cost effective membrane-based processes.

There are many researches to modify the existing membranes or to create new ones to achieve better performances in comparison to upper bound lines [1,2]. The upper bound lines are the correlations of the selectivity versus permeability for gas mixtures. The permeability, which is the pressure and thickness normalized flux, is an indicator of the membrane productivity of a membrane. The separation factor is defined as:

$$\alpha_{A/B} = \frac{w_{A,p}/w_{B,p}}{w_{A,f}/w_{B,f}} \tag{7.1}$$

where w is the composition, usually on the molar basis, subscripts A and B represent the components and subscripts p and f denote the permeate and feed side of the membrane, respectively. The separation factor defines the efficiency of a membrane for the separation of a mixture of A and B. In most cases the separation factor is approximated by an ideal selectivity, which is the ratio of permeabilities of A and B, measured in single gas experiments. This way, one can avoid sophisticated measurements of gas mixture properties. Since the permeability is considered as a product of the solubility, S, and the diffusion, D, coefficients, the separation factor can be approximated as:

$$\alpha_{A,B} \approx \frac{P_A}{P_B} = \left(\frac{S_A}{S_B}\right)\left(\frac{D_A}{D_B}\right) \tag{7.2}$$

In order to have a better membrane performance for the separation of A and B, either the solubility or diffusivity ratio should increase [3]. To study these ratios or their

improvement upon a change in membrane characteristics, permeability, selectivity, and diffusion coefficient should be measured accurately.

There are several mechanisms to explain the transport of gases in glassy polymeric membranes. Two major models are the dual-mode sorption and matrix models. In the dual-mode sorption two different populations of gas molecules are considered, those sorbed according to Henry's law and those sorbed according to Langmuir's isotherm. The transport of the two populations is then characterized by two distinct diffusion coefficients. The ratio of these populations is an adjustable parameter. The matrix model is based on interactions of the gas molecules with the polymer matrix. The presence of gas molecules in the polymer matrix perturbs the membrane matrix. This alteration of the membrane matrix changes the transport potential of the gas molecule. The dependence of the gas diffusion coefficient on the concentration of foreign gases in the membrane matrix can be modeled and correlated with the experimental data. Klopffer and Flaconnèche [4] reviewed and compared the dual mode sorption and matrix models.

The common method for the measurement of the diffusion coefficient of individual gases from a gas mixture, which permeates the membrane, is described by Flaconnèche et al. [5]. In this method, the gas mixture is instantaneously introduced at the feed side of the membrane, which was initially purged by an inert gas, and the composition changes in the permeate stream are measured using a mass spectrometer. The inert gas can be any gas that has no peak conflict in the mass spectrometer with the permeating gases and has no influence on the characteristics of the membrane matrix. For example, nitrogen and argon were recommended for the CH_4/CO_2 mixture at the feed side. The effect of the inert gas on the diffusion coefficients of individual gases from the feed mixture was mostly ignored or assumed to be negligible Flaconnèche et al. [5].

On the other hand, in our recent study we observed a strong influence of back permeating nitrogen and the forward permeating oxygen and back permeating oxygen on the forward permeating nitrogen [6]. In that study, the back permeating gases reached the membrane surface by back diffusion of air components through a bubble flow meter and a connecting tube. To model the combined phenomena of back diffusion and back permeation it was assumed that the forward and back permeating gases do not interact with each other and with the membrane matrix, and it was speculated that this assumption

was responsible for under prediction of the effect of back diffusion on the apparent permeability coefficient of the forward permeating gas. The difference between the experimental and predicted data was qualitatively explained on the bases of dual mode sorption model extrapolated to the case of back permeation [6]. Lack of information on interactions between oxygen and nitrogen prevented using a more realistic transport model of gases in the membrane in our previous study.

The objective of this study is to develop a novel method to measure the diffusion coefficient of single gases under the influence of back permeation. Unlike our previous study in which back permeation was a consequence of back diffusion and could not be directly controlled [6], in the current study back diffusion is controlled by the composition of the sweep gas, which is directly in contact with the permeate side of the membrane. The diffusion coefficient of the forward permeating gas is evaluated from the analysis of the time-dependent flux following a step change in feed pressure of the forward permeating gas. Different approaches for the evaluation of the diffusion coefficient arising from the approach originally proposed by Zeigel et al. [7] are compared and discussed. The effects of back permeating nitrogen on the diffusion coefficient of oxygen, back permeating oxygen on the diffusion coefficient of nitrogen, back permeating nitrogen on the diffusion coefficient of methane, and the back permeating methane on the diffusion coefficient on nitrogen are presented and discussed.

7.2 Background - evaluation of diffusion coefficient in a constant pressure system

Zeigel et al. [7] introduced a method for the measurement of the diffusion coefficient in a constant pressure system. This method, which relies on measuring of the gas permeation through the membrane following a step change in composition of the feed stream, provides the basis for the current study. In the following derivation of the expressions for the diffusion coefficient the applicability of the solution-diffusion mechanism is assumed. In addition, the membrane is assumed to have a homogeneous structure.

7.2.1 Fundamentals

The gas transport in polymeric membranes is a diffusive process, thus at the steady state the gas flux within the membrane is governed by the Fick's 1st law of diffusion

$$J = -D\frac{dC}{dx} \tag{7.3}$$

where J is the gas flux, x is the distance from the feed face of membrane, C is the concentration of the gas in membrane at x; and D is the diffusion coefficient of the gas in membrane. If D is independent of C, the concentration profile at steady state is a linear function of x, and the expression for the gas flux becomes,

$$J = D\frac{(C_0 - C_L)}{L} \tag{7.4}$$

where L is the membrane thickness, C_0 is the concentration of the gas at the feed face of membrane, i.e., at $x = 0$, and C_L is the concentration of the gas at the permeate face of membrane, i.e., at $x = L$.

Assuming applicability of Henry's law, Equation (7.4) can be rewritten using the solubility coefficient,

$$J = DS\frac{(p_0 - p_L)}{L} \tag{7.5}$$

where p_0 is the partial pressure at the feed face of membrane, and p_L is the pressure at the permeate face of membrane. In the solution-diffusion model, the product DS represents the permeability coefficient (P). Rearrangement of Equation (7.5) provides the expression for the permeability coefficient in terms of the steady state gas flux,

$$P = \frac{JL}{p_0 - p_L} \tag{7.6}$$

7.2.2 Gas flux after step change in feed pressure

The solution-diffusion model assumes that when the feed pressure changes the new equilibrium concentration at the feed face of membrane is established instantaneously [8]. Consequently, a step change in the feed pressure from p_0 to p_1 leads to a step change in the equilibrium concentration at the feed face of membrane from C_0 to C_1. Since it is assumed that D is independent of C, the concentration response within the

membrane resulting from step change in feed pressure is governed by the Fick's 2nd law of diffusion,

$$\frac{\partial C}{\partial t} = D\frac{\partial^2 C}{\partial x^2} \tag{7.7}$$

where t is the time elapsed from the step change in feed pressure. Before the step change in feed pressure, the gas concentration in the membrane is a linear function of the position.

$$C(x, t=0) = C_0 - (C_0 - C_L)\frac{x}{L} \tag{7.8}$$

Equation (7.8) is the initial condition for Equation (7.7). The two boundary conditions required for the solution of Equation (7.7) are given by the following equations,

$$C(x=0, t>0) = C_1 \tag{7.9a}$$

$$C(x=L, t) = C_L \tag{7.9b}$$

Solving Equation (7.7) by the method of separation of variables leads to,

$$C = C_1 - (C_1 - C_L)\frac{x}{L} - \frac{2(C_1 - C_0)}{\pi}\sum_{n=1}^{\infty}\frac{1}{n}\sin\left(\frac{n\pi x}{L}\right)\exp\left(-n^2\pi^2\frac{Dt}{L^2}\right) \tag{7.10}$$

Differentiating Equation (7.10) with respect to x and substituting the resulting expression into Equation (7.3) yields the expression for the gas flux within the membrane as a function of time and position,

$$J(x,t) = D\frac{(C_1 - C_L)}{L} + 2D\frac{(C_1 - C_0)}{L}\sum_{n=1}^{\infty}\cos\left(\frac{n\pi x}{L}\right)\exp\left(-n^2\pi^2\frac{Dt}{L^2}\right) \tag{7.11}$$

Setting $x = L$ provides the final expression for the transient gas flux leaving the membrane,

$$J(L,t) = D\frac{(C_1 - C_L)}{L} + 2D\frac{(C_1 - C_0)}{L}\sum_{n=1}^{\infty}(-1)^n\exp\left(-n^2\pi^2\frac{Dt}{L^2}\right) \tag{7.12}$$

7.2.3 Expressions for the diffusion coefficient

As t increases the gas flux approaches to a new steady state (J_∞). The expression for J_∞ is obtained by setting $t = \infty$ in Equation (10),

$$J_\infty = J(L, t\to\infty) = D\frac{(C_1 - C_L)}{L} \tag{7.13}$$

The initial gas flux (J_0), which exists before the step change in the feed pressure, is given by Equation (7.4),

$$J_0 = J(L, t=0) = D\frac{(C_0 - C_L)}{L} \tag{7.14}$$

Equations (7.12-7.14) can be combined as follows,

$$\phi = \frac{J - J_\infty}{J_0 - J_\infty} \tag{7.15}$$

The parameter ϕ in Equation (7.15) is dimensionless. Moreover, since J changes from J_0 to J_∞, ϕ changes from 1 to 0, respectively. It is important to emphasize that $J = Q/A$, where Q is the gas permeation rate, and A is the membrane area. Therefore, replacing J, J_0 and J_∞ in Equation (7.15) by the respective Q, Q_0 and Q_∞ would lead to the same ϕ. The latter approach is more practical because the gas permeation rate is a measurable parameter. Substituting Equations (7.12-7.14) into Equation (7.15) leads to,

$$\phi = -2\sum_{n=1}^{\infty}(-1)^n \exp\left(-n^2\pi^2\tau\right) \tag{7.16}$$

where $\tau = Dt/L^2$ is a dimensionless time.

A semi-log plot of ϕ versus τ is presented in Figure 7.1. It can be noticed that for $\tau > 0.15$ which corresponds to $\phi < 0.45$, ϕ decreases linearly with τ in Figure 7.1. This is because for $\tau > 0.15$ the second term of the series becomes less than 1% of the absolute value from the first term of the series, and Equation (7.16) is approximated by,

$$\phi = 2\exp\left(-\pi^2\tau\right) \tag{7.17}$$

Equation (7.17) is represented by a dashed line in Figure 7.1. Using the analogy with time lag analysis in constant volume systems the dashed line is considered as an asymptote to the dimensionless permeation rate, and the intersection of the asymptote with $\phi = 1$ is considered as a dimensionless time lag (θ_{cp}') [8]. It follows from Equation (7.17) that:

$$\theta_{cp}' = \frac{\ln(2)}{\pi^2} \tag{7.18}$$

On the other hand, the slope of the asymptote in Figure 7.1 (σ') is given by,

$$\sigma' = -\pi^2 \tag{7.19}$$

In practice one cannot plot ϕ versus τ, unless the diffusion coefficient is known. On the other hand, since $\tau = Dt/L^2$, the plot of ϕ versus t will have the same shape as the plot of ϕ versus τ depicted in Figure 7.1. The corresponding expressions for the dimensional time lag (θ_{cp}) and the dimensional slope (σ) when plotting ϕ versus t will be,

$$\theta_{cp} = \frac{\ln(2)}{\pi^2}\frac{L^2}{D} \tag{7.20}$$

$$\sigma = -\frac{\pi^2 D}{L^2} \tag{7.21}$$

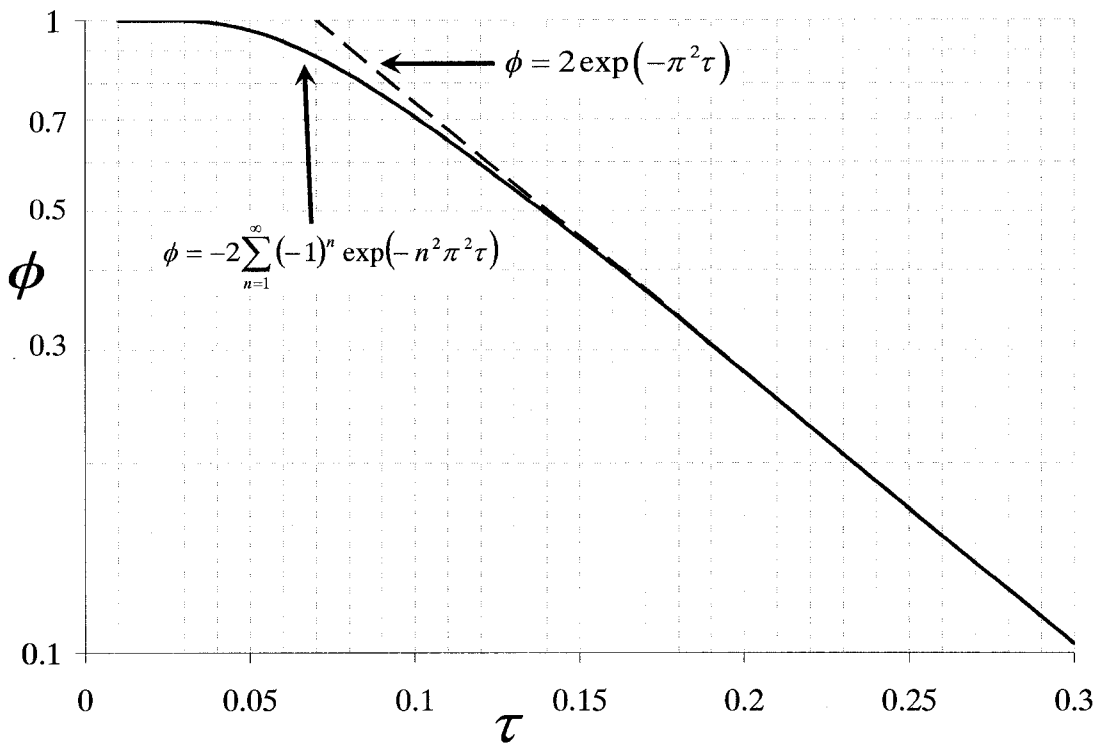

Figure 7.1. Semi-logarithmic plot of dimensionless flux versus dimensionless time for the purpose of evaluation of the diffusion coefficient.

Thus the diffusion coefficient of the gas in membrane can be determined from the plot of ϕ versus t using either the dimensional time lag,

$$D = \frac{\ln(2)}{\pi^2}\frac{L^2}{\theta_{cp}} = 0.0702\frac{L^2}{\theta_{cp}} \tag{7.22}$$

or the dimensional slope,

$$D = -\frac{\sigma L^2}{\pi^2} \tag{7.23}$$

The accuracy of the diffusion coefficient determined from the time lag depends on the accuracy of recording the zero time, that is, the time when the step change in the feed pressure occurs. Moreover, the true step change in feed pressure is required. The problem of non-instantaneous pressurization of the inflow volume in a constant volume system was investigated by Favre et al., who concluded this problem exists only in case of vapors [8].

Unlike the time lag-based diffusion coefficient, the slope-based diffusion coefficient given by Equation (7.23) is not affected by the error in recording the zero time. Its accuracy depends on the range of ϕ taken for the determination of the slope and evaluation of initial and final flow rates.

Zeigel et al. [7] used the time required to reach one-half of the ultimate steady-state value. Figure 7.2 presents their approach for determining the diffusion coefficient by using a half time, that is, time required for ϕ to decrease from 1.0 to 0.5, and by the slope at point of inflection. By substituting $\phi = 0.5$ into Equation (7.16), $\tau_{1/2} = 0.1388$ or

$$D = \frac{L^2}{7.205\tau_{1/2}} \tag{7.24}$$

To find the point of inflection, the second derivative of Equation (7.16) must be zero; then the dimensionless time lag related to this point becomes $\tau_S = 0.091752$ and corresponding dimensionless flux is $\phi = 0.75576$. The slope at the inflection point is given by:

$$\left.\frac{d\phi}{d\tau}\right|_{\tau_S} = 2\sum_{n=1}^{\infty}(-1)^n n^2\pi^2 \exp\left(-n^2\pi^2\tau_S\right) = -5.92205 \tag{7.25}$$

Consequently, the diffusion coefficient can be evaluated from the slope at the inflection point using

$$D = \frac{L^2}{5.922\, t_S} \tag{7.26}$$

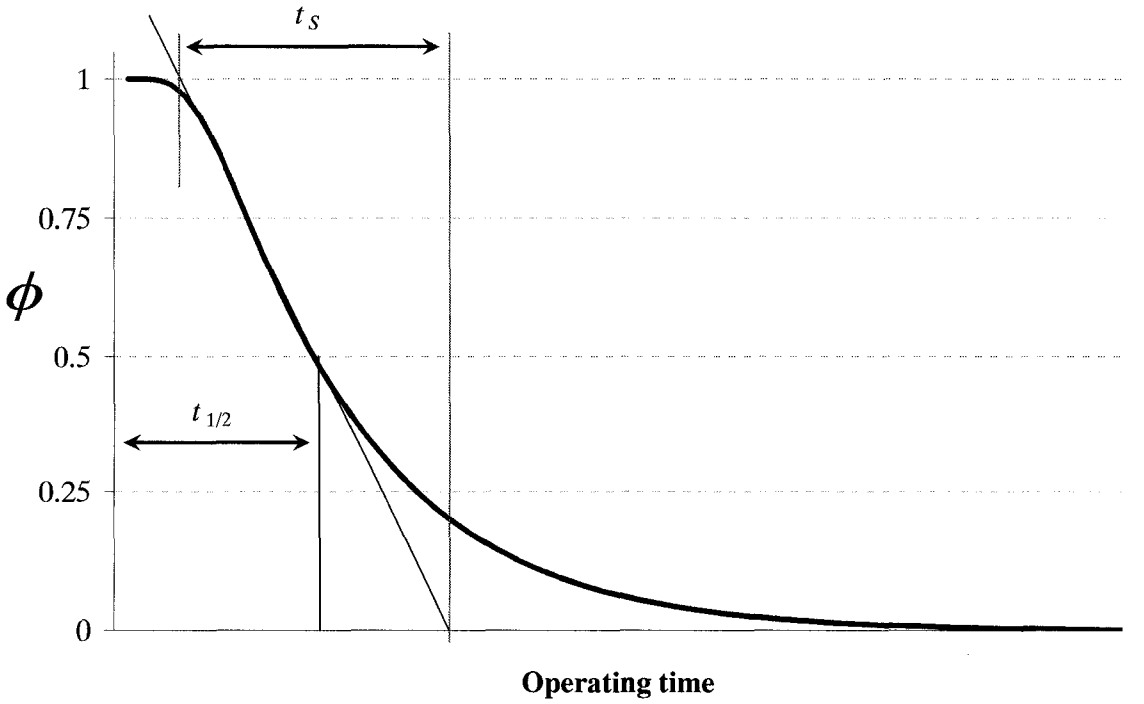

Figure 7.2. Plot of dimensionless flux versus dimensionless time for the purpose of evaluation of the diffusion coefficient.

The problem with this approach is that the ultimate steady-state is usually reached after a long time. Besides the error corresponding to the measurement of an extra variable increases the error associated with the diffusion coefficient.

7.2.4 Integration method

To minimize the influence of random errors on the evaluation of transport properties several methods can be introduced. A critical review of these methods is presented by Scheichl et al. [9]. The most common and simple approach to reduce the random errors of the measurement apparatus is the integration of the flux. By integrating the flux provided by Equation (7.12), the accumulated flux, M, can be expressed by:

$$M = \int_0^t J(L,t)\,dt = D\frac{(C_1 - C_L)}{L}t - 2\frac{L(C_1 - C_0)}{\pi^2}\sum_{n=1}^{\infty}\frac{(-1)^n}{n^2}\exp\left(-n^2\pi^2\frac{Dt}{L^2}\right) + 2\frac{L(C_1 - C_0)}{\pi^2}\sum_{n=1}^{\infty}\frac{(-1)^n}{n^2} \quad (7.27)$$

Since $\sum_{n=1}^{\infty}\frac{(-1)^n}{n^2}=-\frac{\pi^2}{12}$, therefore

$$M=\int_0^t J(L,t)\,dt=D\frac{(C_1-C_L)}{L}t-2\frac{L(C_1-C_0)}{\pi^2}\sum_{n=1}^{\infty}\frac{(-1)^n}{n^2}\exp\left(-n^2\pi^2\frac{Dt}{L^2}\right)-\frac{L(C_1-C_0)}{6} \qquad (7.28)$$

The asymptote of this curve can be evaluated by letting $t\to\infty$ in the above equation:

$$M_\infty=D\frac{(C_1-C_L)}{L}t-\frac{L(C_1-C_0)}{6} \qquad (7.29)$$

To find the time lag of the membrane based on this method, the intercept of the asymptote with time axis, $M_\infty=0$ must be determined:

$$\theta_{CP}=\frac{L^2}{6D}\frac{(C_1-C_0)}{(C_1-C_L)}=\frac{L^2}{6D}\frac{(p_1-p_0)}{(p_1-p_L)} \qquad (7.30)$$

Then diffusion coefficient can be calculated using experimental time lag:

$$D=\frac{L^2}{6\theta_{CP}}\frac{(p_1-p_0)}{(p_1-p_L)} \qquad (7.31)$$

where subscripts L, 1, 0 correspond to the permeate partial pressure, the feed partial pressure after and the feed partial pressure before a step change, respectively.

7.2.5 Applications of constant pressure systems for the determination of the diffusion coefficient

Zeigel's method [7] did not achieve the expected popularity. It has been used only by a few researchers and mostly for pervaporation [10-15,17]. The reason for the lack of popularity could be the required accuracy of the permeate flow measurement. Zeigel et al. [7] employed a hydrogen detector to accurately measure the permeate rate of hydrogen over its isotope deuterium through a poly(vinyl fluoride) membrane. The carrier gas was nitrogen. Pye et al. [10] employed a gas chromatography to study the permeabilities of CH_4/H_2 mixture passing through the polyimide membranes. The carries gas was helium. They showed that existence of water vapor retards the permeation rate in polyimide films. A quick look at their results for the effect of composition shows that generally the hydrogen permeability increases with increasing hydrogen concentration in the feed stream. For methane, the general trend shows a decrease in permeability at low concentrations of methane and an increase at high methane concentration in the feed

stream. There was one experimental point which did not follow the trend. Watson et al. [11-13] employed this method along with a mass spectrometer and a vacuum permeation cell to study the pervaporation behavior. The values for $t_{1/2}$ measured by Watson and Payne [11] were around one second, and their apparatus design was associated with drawbacks addressed by Yeom et al. [14], who designed a more precise equipment and measured the diffusion coefficient for pervaporation of water through a hydrophilic poly(vinyl alcohol) membrane and a hydrophobic poly(dimethylsiloxane) membrane. Yeom et al. reported the diffusion coefficients based on three evaluation approaches, $t_{1/2}$, the point of inflection, and flow integration. In their results, $t_{1/2}$ provides the highest values for the diffusion coefficient while the lowest value comes for evaluation of the point of inflection. The integration method provided diffusion coefficients between the values from the other two methods. Kim and Lee [15] used the apparatus of Yeom et al. [14] to study the gas transport properties of organic–inorganic hybrids of poly(amide-6-b-ethylene oxide) and silica prepared via in situ polymerization.

Ash et al. [16] adopted the approach introduced by Ziegel [7] and extended it to a concentration-dependent diffusion coefficient. They compared several concentration dependent diffusion coefficient models and showed that the diffusion coefficient could change between 0.3 to 5 times of the constant diffusion coefficient because of the dependence on concentration. Shah et al. [17] employed a numerical procedure to find the concentration dependent diffusion coefficient of acetone in polydimethylsiloxane (PDMS). They used nitrogen as carrier gas for both feed and sweep gas.

7.3 Experimental setups

Two testing systems were employed in this study. The first one was a constant pressure system equipped with low range MKS flowmeter having the permeate flow through the membrane. Figure 7.3 presents a schematic diagram of the first system. A three way valve is used to switch from a low pressure gas source to a pre-set high pressure gas source. This change can be done instantaneously. The feed pressure is monitored using a pressure transducer having the range of 14.7-1800 ± 2.8 kPa (0-250 ± 0.4 psig). The volume of the system between the permeate side of the membrane and the

flow meter and that between feed side of the membrane and three way valve is minimized to reduce potential effect of the dynamics up and downstream from the membrane.

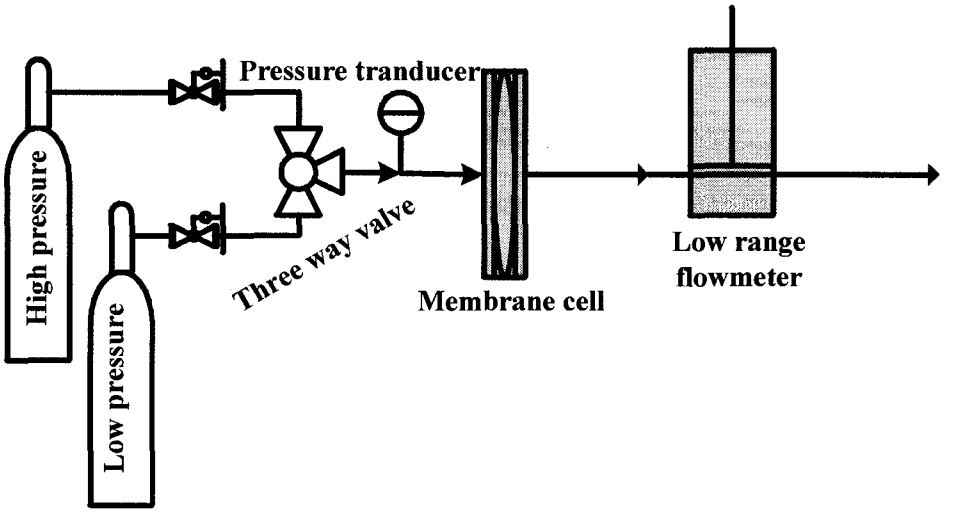

Figure 7.3. Schematic of a constant pressure system without sweep utilizing a low flow mass flow controller.

The system shown in Figure 7.3 was also utilized to examine the difference between methods for the evaluation of the diffusion coefficient in different testing systems. More specifically, the cell with the membrane used in the current study (93.6 μm thick polyphenylene oxide membrane) was used previously in a constant volume system [18]. The advantage of system in Figure 7.3 is that the permeation rate is evaluated from one flow measurement. Therefore, the accuracy of permeation rate is equal to the accuracy of the low flow controller. On the other hand, because of using a relatively thick membrane, which was dictated by the requirements of a constant volume system [18], the resulting permeation rate was low making this setup with such thick membrane ineffective for the tests using gas mixtures.

The second system in the current study was a constant pressure system with sweep gas. The critical aspect of the proposed method for the evaluation of the diffusion coefficient in the presence of back permeating gas a capability for a continuous and accurate monitoring of the permeation rate of gases. The schematic diagram of a single permeation cell, which is a part of an automatic four-cell sweep-gas-constant-pressure

system, is presented in Figure 7.4. The permeation cell houses a circular membrane of the diameter of 4.1 cm. The cell is made of a 316 stainless steel, and consists of two detachable parts. The lower part is a high-pressure chamber equipped with the inlet and outlet tubes for the flow of the feed (F) and the retentate (R) streams, respectively. The upper part is also equipped with the inlet and outlet tubes for the flow of the sweep (S) and sweep + permeate (SP) streams, respectively. The membrane is mounted on the stainless steel porous plate having the porosity of 100 μm, which is embedded in the upper part of the cell. The membrane is separated from the porous plate by a filter paper of similar porosity, which prevents damaging of the membrane by the porous plate when the membrane is under the pressure. Under the operating conditions, the porous plate and the filter paper should have no resistance to the gas flow.

The pressure of the feed stream, which should be similar as the pressure of the retentate stream is controlled by a two-stage pressure regulator and monitored by an pressure transducer (PT1) from MKS Instruments, having the reading range of 14.7 – 3500 kpa (0 - 500 psig). The flow rate of stream R is controlled by a needle valve (NV) and monitored by an MKS mass flow meter (MFM1) having the reading range of 0-10 $\pm$ 0.1 cm^3/min. The flow rate of stream S is controlled by an MKS mass flow controller (MFC) having the control range of 0-10 cm^3/min. The line carrying the SP stream is open to atmosphere so that the gas in the SP stream is at atmospheric pressure. The exact pressure at the permeate side is provided by an absolute pressure transducer (PT2) from MKS Instruments, having the reading range of 0-345 kPa (0-50 psia). The flow rate of stream SP is monitored by an MKS mass flow meter (MFM2) identical to MFM1.

Spin coated dense PPO films were used as membranes in this project. The details of membrane preparation procedure are given elsewhere [18]. The thicknesses of membranes, as determined by a micrometer, were 23 and 29 μm. These membranes were used for evaluation of the diffusion coefficient. A different membrane with a thickness of 5 μm was used for measurement of the permeation rate and hence evaluation of the permeability coefficient. The flow rates, pressures and temperatures of different streams were recorded with a frequency of up to one data set per 0.3 s. The data was recorded not only during, but also before the experiment to ensure that all MFMs, MFCs and pressure

gauges were stable. Composition of all streams was analyzed using a GOW-MAC 580 gas chromatograph equipped with a molecular sieve 5A column.

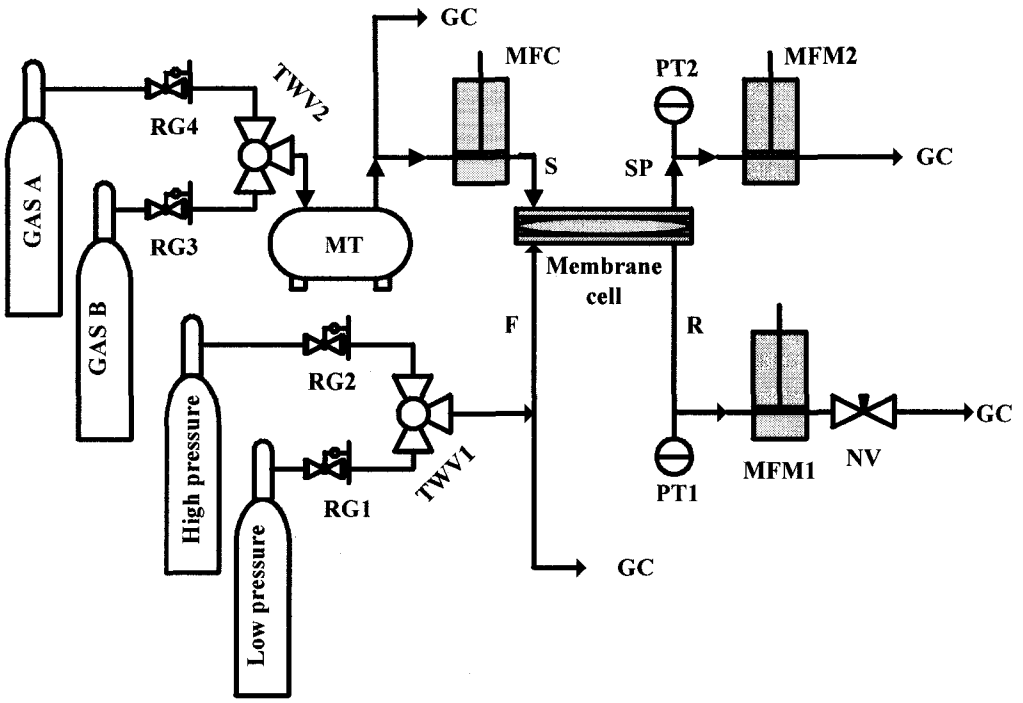

Figure 7.4. Schematic of a constant pressure system with sweep.

7.4 Experimental method

In our previous study, the effect of back diffusion and back permeation of air on the apparent membrane permeability was investigated and it was found that the combined effect of these phenomena was considerably greater than that predicted using a simple transport model [6]. More realistic models for the gas transport in the membrane could not be used because of a lack of the data on interactions of nitrogen and oxygen in the membrane. In fact, experimental data on interactions of gases inside the membrane is rare in the literature. Theoretical models developed for this purpose contain adjustable parameters, which are evaluated by fitting to experimental data. On the other hand, considering that the discrepancy between the predicted and observed effects of back diffusion and back permeation on the apparent membrane permeability arise from the

interactions of the permeating gases with the membrane matrix [6], this discrepancy can be used as a starting point for experimental evaluation of these interactions. In our previous work, the concentration of the gas in contact with the permeate side of the membrane was evaluated by solving the governing ordinary differential equations [6]. To remove this uncertainty, in the current study the concentration of the gas in contact with permeate side of the membrane can be controlled directly by adjusting the composition of the sweep gas in the system shown in Figure 7.4.

To determine the diffusion coefficient of gas A in the presence of gas B in the membrane matrix, pure A from a compressed gas cylinder was used as a feed, while the mixture of A and B of known composition for sweeping the permeate side of the membrane was prepared in 0.075 m^3 mixing tank (MT). The composition of the sweep gas was set using regulators RG3 and RG4; however, the actual composition was measured by sending the sweep gas directly to the gas chromatograph. The regulators RG1 and RG2 were set to 240 and 930 kPa (20 and 120 psig), respectively. Initially feed side (F) of the membrane was swept with pure A at 240 kPa (20 psig). The permeate side (S) was also swept using the gas mixture from the MT. The system was allowed to operate for at least 24 hours in order to reach steady state at the low feed pressure. During this time, both output compositions were monitored periodically. The stability of the composition data was considered as an indicator of the steady state conditions. The dynamic gas permeation experiment was initiated by a sudden change of the position of the three way valve thus changing the feed pressure of gas A from 240 to 930 kPa (20 to 120 psig). The set flow of gas A in the stream S was maintained constant regardless of the feed pressure by means of a mass flow controller (MFC). The permeation rate (Q) at a given time was determined from the difference between the readings of MFM2 and MFC. To minimize the error associated with the readings of the mass flow controllers, the change in permeation rate due to the step change in feed pressure was determined from the difference between the reading of the MFM2 and its initial reading before pressurization the step change in feed pressure. This way, if there were any error in calibration of MFM2, it would cancel out during the calculation of ϕ by Equation (7.15).

7.5 Results and discussion

The main objective of this study was to develop and implement a procedure for the measurement of gas transport properties when the tested gas is not the only gas present in the membrane matrix. This was achieved by sweeping the permeate side of the membrane with a gas mixture. The composition of the sweep gas was controlled and in the limiting case, the sweep gas was the same as the feed gas (system 2), or its flow rate was equal to zero (system 1). In both of these cases, there is only one gas present in the membrane matrix during the actual gas permeation test.

7.5.1 Diffusion coefficient of a single gas

The diffusion coefficient of a gas is typically determined from experiments in which the tested gas is the only gas present in the membrane matrix during the actual test. Using the data from a dynamic gas permeation test in a constant pressure system, the diffusion coefficient can be determined using several different approaches. In the following section, the diffusion coefficients determined from the same gas permeation data, however using different analytical approaches are compared.

Figure 7.5 presents the results of typical dynamic gas permeation test in a constant pressure system depicted in Figure 7.3 using oxygen as a feed; the dimensionless permeation rate (ϕ) is plotted versus time in Figure 7.5a and the accumulated flux versus time is plotted in Figure 7.5b. The time at which the feed pressure changes from 2 to 15 bar is considered as a time zero. For ϕ <0.45 and t < 250 s, the time-dependent dimensionless flux can be modelled by the following equation

$$\phi = 3.052\exp(-0.02331\,t) \tag{7.32}$$

The above equation is plotted along with the experimental data in Figure 7.5a, and it is evident that at relatively short times corresponding to ϕ > 0.6, Equation (7.32) deviates from the experimental data. The time lag (θ_{cp}), i.e., the time for which ϕ = 1 in Figure 7.5a, is $\theta_{cp} = 47.9$ s, and the corresponding diffusion coefficient determined from Equation (7.22) is D = 1.28×10^{-11} m²/s. The slope of asymptote in Figure 7.5a is $\sigma = -0.02331\,s^{-1}$ and substituting this slope into Equation (7.23) leads to D = 2.07×10^{-11} m²/s. Using the original Ziegel's method [7], the half time in Figure 7.5a is $t_{1/2}$ = 77 s and

the corresponding diffusion coefficient from Equation (7.24) becomes $D = 1.58\times10^{-11}$ m²/s. Alternatively, the point of inflection occurs at $t = 57$ s and the slope at this point is 0.0137 s^{-1}. Therefore, for $t_s = 73$ s the corresponding diffusion coefficient from Equation (7.26) is $D = 2.03\times10^{-11}$ m²/s. Considering the integral approach, using the asymptote to accumulated the flux in Figure 7.5b leads to $\theta_{cp} = 89.34$ s. Thus, the diffusion coefficient from Equation (7.31) becomes $D = 1.52\times10^{-11}$ m²/s.

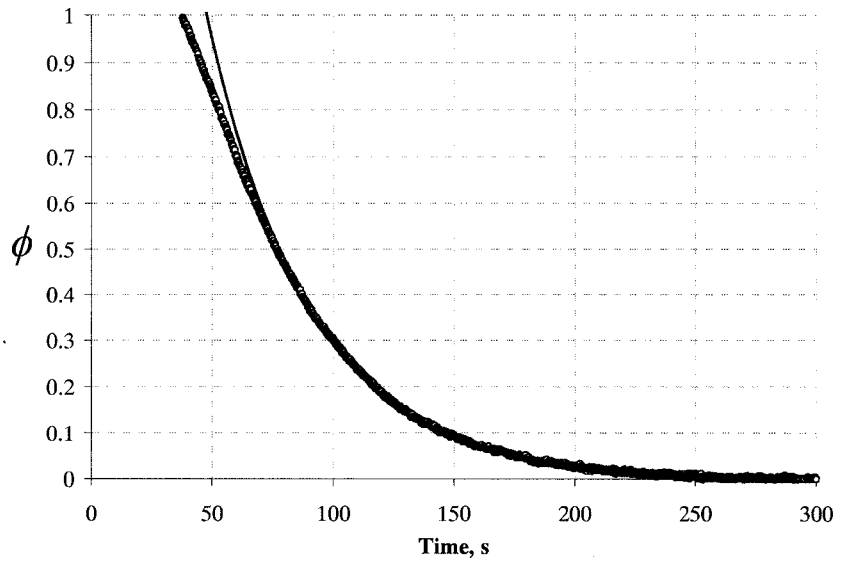

a)

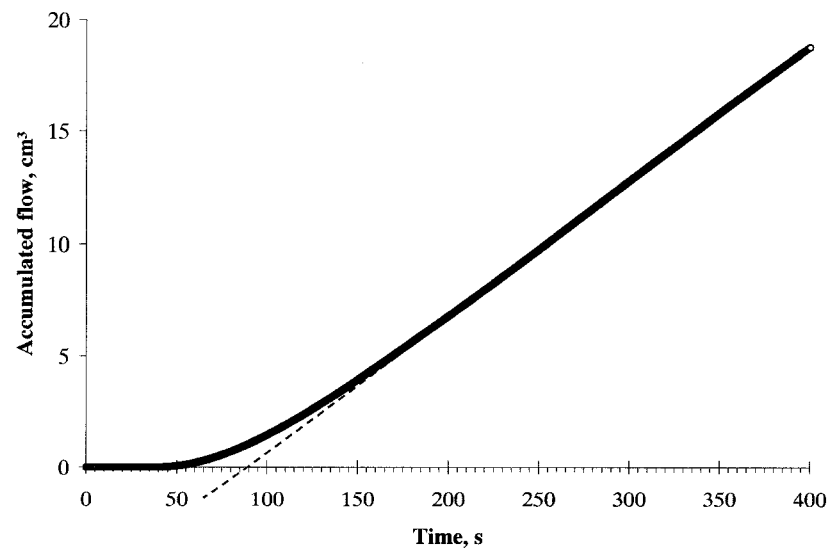

b)

Figure 7.5. Evaluation of the diffusion coefficient using a) exponential equation fitted to the experimental data, and b) asymptote to the accumulated flux.

It is therefore evident that five different values for the diffusion coefficient of oxygen ranging from 1.28×10^{-11} to 2.07×10^{-11} m^2/s are found using different approaches arising from the original Ziegel's method. It is important to emphasize that for a constant volume system the diffusion coefficient of oxygen in the PPO membrane ranges between 1.2×10^{-11} to 1.7×10^{-11} m^2/s, which is comparable to the variation in the diffusion coefficient from the CP system [18]. However, in case of a constant volume system, the variation was due to different feed pressures in the time lag experiments rather than from different approaches used to evaluate the diffusion coefficient.

One of the reasons for the variation in the diffusion coefficient from different approaches could be imperfect step change in the feed pressure. In reality, the actual pressurization step was accomplished in roughly 2.5 s; therefore, it was not truly an instantaneous pressurization. This imperfect step change in the feed pressure is a result of manual operation of the pressure regulator and a resistance to gas flow between the pressure regulator and the membrane surface. In addition, there was a slight overshoot in the feed pressure, which disappeared after 20 s. The overshoot resulted from the response of a pressure control mechanism of the regulator to a step change in pressure.

If the experimental data followed exactly the proposed model, the pre-exponential constant in Equation (7.32), i.e., the intercept, would be 2 rather than 3.052. This deviation is evident in Figure 7.5a. Because of this difference, the diffusion coefficient determined from the slope is 60% greater than the diffusion coefficient determined from the intercept. The difference between the two diffusion coefficients should not be surprising considering a non-instantaneous pressurization of the membrane. Because of this non-instantaneous pressurization, the corresponding θ_{cp} is overestimated, which leads to underestimation of the diffusion coefficient. At the same time, the diffusion coefficient from the slope is most likely overestimated, because apart from an imperfect step change in the feed pressure, overestimation of θ_{cp} could also arise from overestimation of the slope in Figure 7.5a. The values of the diffusion coefficient from the half time and from the integral method are close to each other and fall in between the two values from the slope and intercept in Figure 7.5a. As shown in Figure 7.2, at τ corresponding to $\phi = 0.5$ (the half time approach), ϕ is a strong function of τ. Consequently, uncertainties in the initial and final steady state permeation rates do not translate into a significant

uncertainty in the experimentally evaluated half time. On the other hand, the integral approach is independent of the final steady state permeation rate, which reduces the random error.

The integral approach was selected to evaluate the diffusion coefficient in dynamic gas permeation experiments in the presence of back permeation.

7.5.2 Effect of back permeation on the diffusion coefficient

The second system shown in Figure 7.4 was employed to measure the diffusion coefficient of individual gases in the presence of back permeation. Two gas mixtures for the sweep gas were considered, oxygen/nitrogen and methane/nitrogen. Consequently, the diffusion coefficient in four different combinations of the forward and back permeating gases were determined, two of them being nitrogen in the presence of two different back permeating gases – oxygen and methane, respectively. The compositions of the binary mixtures for the sweep gas were varied from 0% to 100% of the back permeating gas, with increment of 20%. Consequently, for a given feed gas, six different compositions of the sweep gas were used, one of them being 0% of the back permeating gas, which served as a reference.

Figure 7.6 presents the results for the experiments with a mixture of oxygen and nitrogen as a sweep gas. Figure 7.6a shows the effect of the composition of the sweep gas on the relative diffusion coefficient of nitrogen in PPO. Figure 7.6b is an equivalent of Figure 7.6a for oxygen being the forward permeating gas. The experiments summarized in Figure 7.6 were performed on two PPO membranes, having similar average thickness, simultaneously. Moreover, the experiments for some compositions of the sweep gas were repeated after completion of the entire series of experiments.

In general the presence of back permeating oxygen and back permeating nitrogen increases the respective relative diffusion coefficients of nitrogen and oxygen. There are however, no clear trends between the composition of the sweep gas and the relative diffusion coefficient. On the other hand, in both cases it appears to be a local minimum in the relative diffusion coefficient of the forward permeating gas. In case of the diffusion coefficient of nitrogen, this local minimum occurs at 40% of oxygen in the sweep gas (Figure 7.6a), and in case of the diffusion coefficient of oxygen, this local minimum

occurs at 80% of nitrogen in the sweep gas. The location of the minima is generally consistent for both tested membranes and is confirmed in the repeated tests.

The effect of the presence of the back permeating gas on the diffusion coefficient appears to be a little bit stronger in case of tests with nitrogen compared to the tests with oxygen as a feed gas. This could be due to the fact that oxygen is more permeable than nitrogen in PPO. Consequently, at the same partial pressures of the back permeating oxygen and nitrogen, the back permeation rate of oxygen should be greater than the back permeation rate of nitrogen. On the other, hand, if oxygen and nitrogen did not interact with each other and/or with the membrane, the diffusion coefficient of the forward permeating gas should not be affected by the presence of the back permeating gas.

Figure 7.7 presents the combined effect of the feed pressure and the composition of the sweep gas on the permeability of oxygen. It is important to emphasize that for the purpose of Figure 7.7 a thin (5 μm) PPO membrane was used rather than the two relatively thick PPO membranes used for the purpose of the measurement of the diffusion coefficient. There are several important observations that can be made considering Figure 7.7. First, the effect of feed pressure on the oxygen permeability is generally much stronger in the presence of back permeating nitrogen. Moreover, when sweep gas is pure oxygen, the permeability coefficient of oxygen decreases with increase in feed pressure. The effect of feed pressure on the permeability coefficient of oxygen is gradually inverted when the concentration of back permeating nitrogen in the sweep increases. For pure nitrogen as a sweep gas, the permeability coefficient of oxygen increases with the feed pressure. On the other hand, the effect of composition of the sweep is much stronger at low rather than high feed pressures. In fact at the low feed pressure of 240 kPa (20 psia), there is a clear permeability minimum at around 20% of nitrogen in the sweep gas stream. This minimum gradually disappears as the feed pressure increases, and at the highest feed pressure of 930 kPa (120 psia), it becomes a local maximum.

Figure 7.8 presents the results for the experiments with the mixtures of methane and nitrogen as a sweep gas. Figure 7.8a shows the effect of the composition of the sweep gas on the relative diffusion coefficient of nitrogen in PPO, while Figure 7.8b is an equivalent of Figure 7.8a for methane being the forward permeating gas. The experiments

summarized in Figure 7.8 were performed on the same PPO membranes used in Figure 7.6.

Focusing on Figure 7.8a, it can be seen that the relative diffusion coefficient of nitrogen increases with an increase in the concentration of methane; it reaches the maximum value of 1.6 at 40% of methane in the sweep gas. As the concentration of methane in the sweep gas further increases the relative diffusion coefficient of nitrogen sharply decreases reaching the minimum value of 0.6 at 80% of methane in the sweep gas. While at this time we cannot offer any rational explanation for the trend seen in Figure 7.8a, the magnitude of changes in the relative diffusion coefficient of nitrogen in the presence of methane is significantly larger than in case of back permeating oxygen in Figure 7.6a. It is important to note that oxygen is more permeable than methane; consequently, the argument used to explain a stronger influence of back permeating oxygen than back permeating nitrogen for the results in Figure 7.6, is not applicable. On the other hand, it is well known that methane has stronger interactions with PPO than oxygen, which could lead to a strong effect of the back permeating methane on the relative diffusion coefficient of nitrogen in Figure 7.8a.

Figure 7.8b presents the effect of back permeating nitrogen on the relative diffusion coefficient of methane in PPO. Unlike the previous figures, there is a clear trend between the composition of the sweep gas and the relative diffusion coefficient of methane. More specifically, as the concentration of nitrogen in the sweep gas increases, the relative diffusion coefficient of methane decreases. The magnitude of this decrease is different for the two PPO membranes shown in Figure 7.8b. For the sweep gas containing pure nitrogen the relative diffusion coefficients of methane in the two PPO membranes drops to 0.3 and 0.55, respectively.

The major advantage of using a gas mixture at the permeate side rather than at the feed side of the membrane, is the possibility of the determination of the diffusion coefficient of a single gas in the presence of another gas by monitoring the changes in the time-dependent permeation rate rather than with an aid of time-dependent composition of permeate stream. While the rigorous explanation of the results shown in Figures 7.6-7.8 is not possible at this point, these figures demonstration a successful application of the

new method for the measurement of the diffusion coefficient in the presence of back permeating gas for different combinations of forward and back permeating gases.

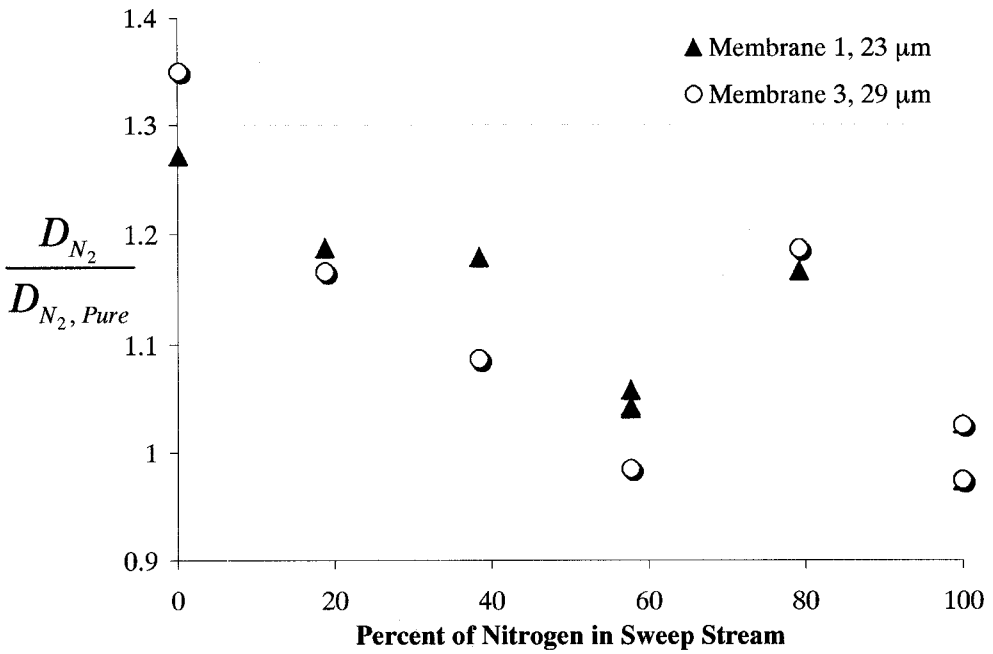

a)

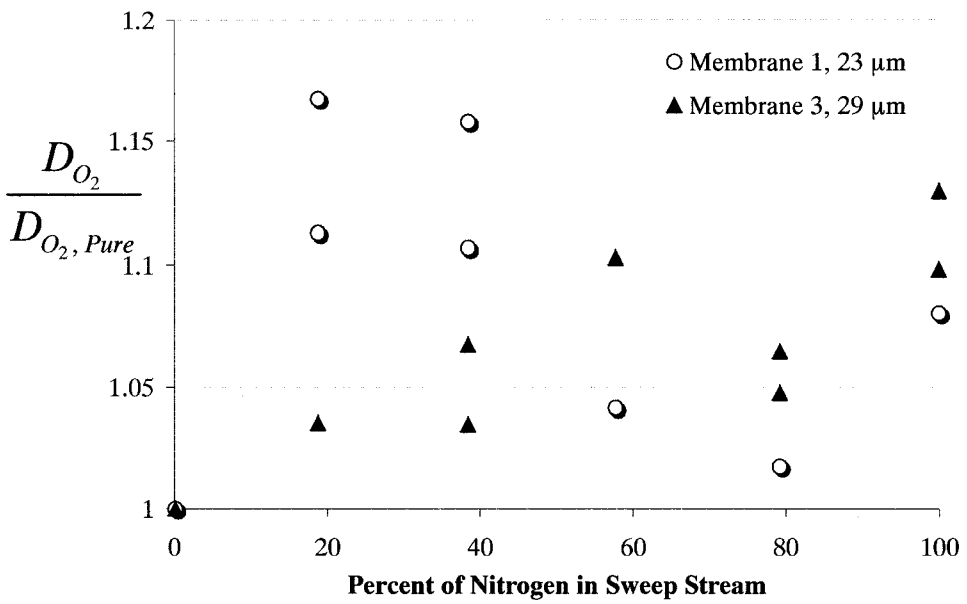

b)

Figure 7.6. Diffusion coefficient ratio evaluated for **a)** Nitrogen, and **b)** Oxygen, when sweep gas composition changes.

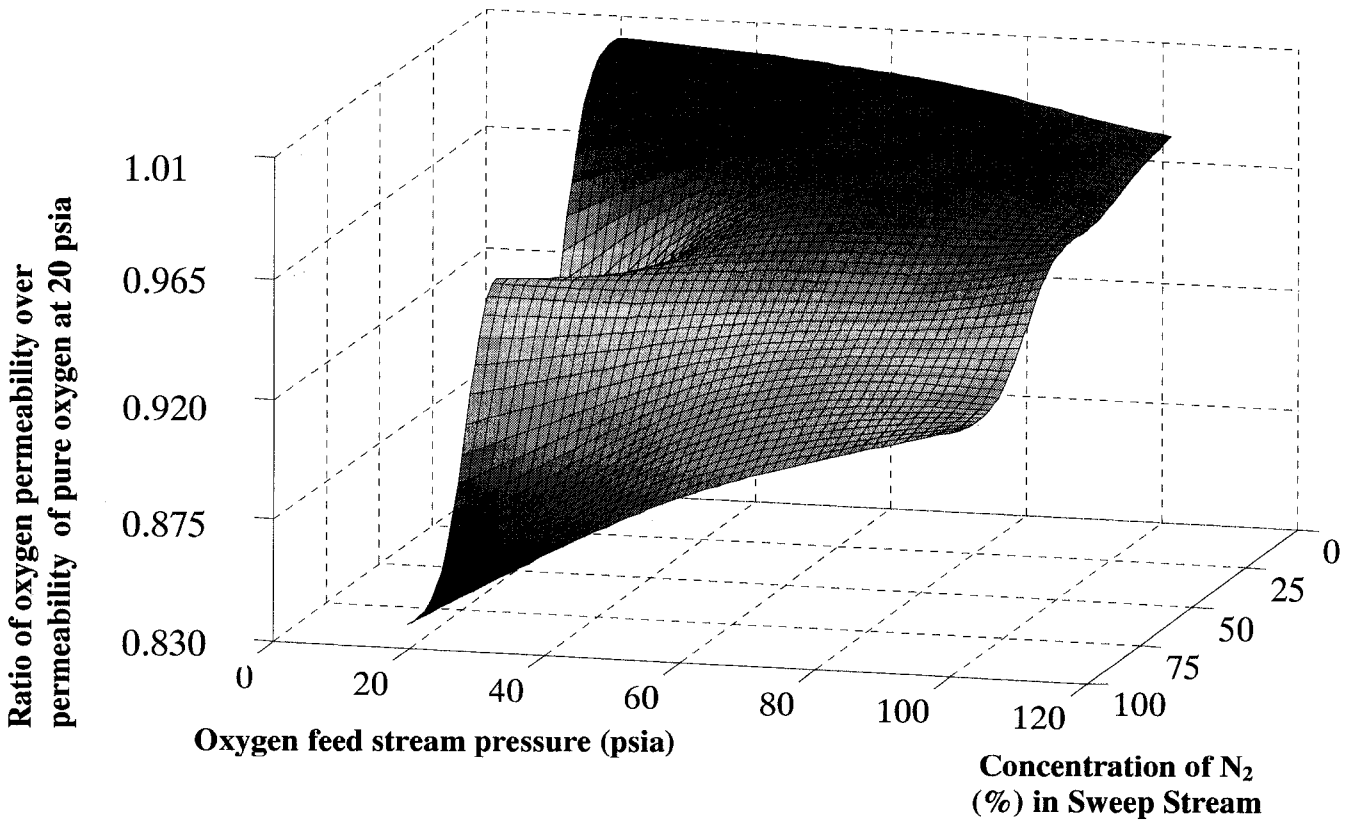

Figure 7.7. Effect of feed pressure and composition of the sweep gas on the permeability coefficient of oxygen in PPO.

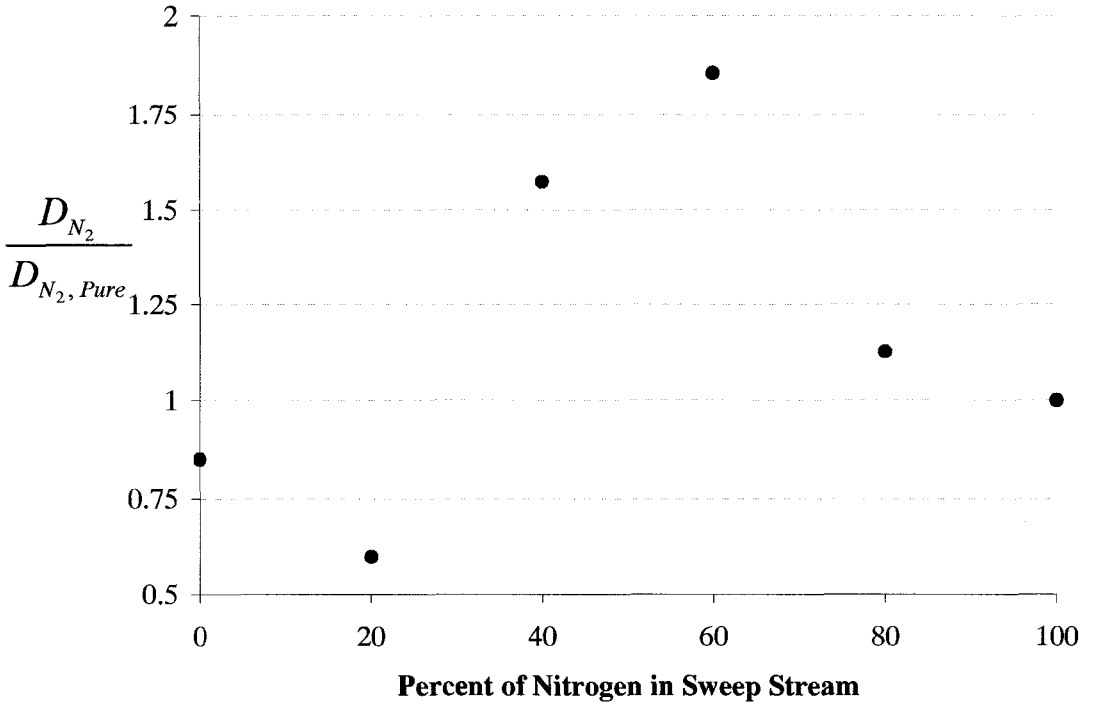

a)

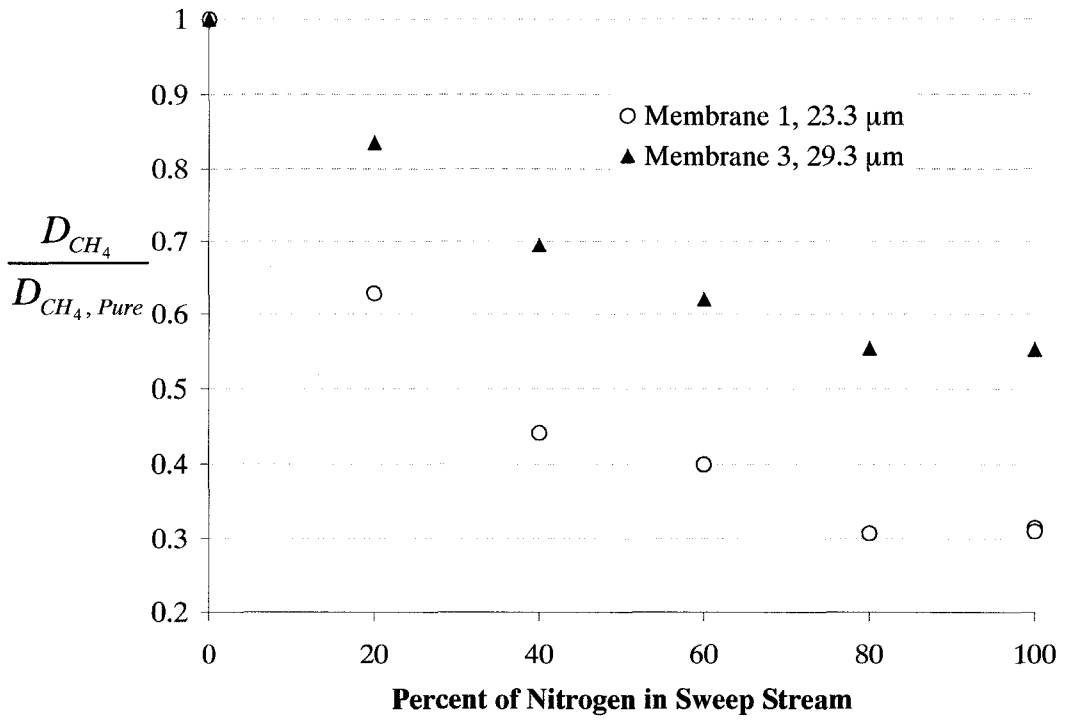

b)

Figure 7.8. Diffusion coefficient ratio evaluated for **a)** Nitrogen, and **b)** Methane, when sweep gas composition changes.

7.6. Conclusions

A novel method for the determination of the diffusion coefficient of a single gas in the presence of a back permeating gas was developed. The actual diffusion coefficient was determined from the transient gas permeation rate resulting from a step change in the feed pressure, while the permeate side of membrane was swept with a binary gas mixture containing different compositions of the forward and back permeating gases. The new method was used for the determination of the diffusion coefficient of nitrogen in PPO in the presence of back permeating oxygen and methane, respectively; also, the diffusion coefficient of oxygen in the presence of back permeating nitrogen and the diffusion coefficient of methane in the presence of back permeating nitrogen were measured. The results indicate that generally the diffusion coefficients of nitrogen and oxygen increase when another gas is present in the membrane matrix. The effect of back permeating oxygen on the diffusion coefficient of nitrogen is generally stronger than the effect of back permeating nitrogen on the diffusion coefficient of oxygen. In case experiments involving methane, the influence of back permeating gas on the diffusion coefficient of the forward permeating gas is much stronger than in experiments involving only nitrogen and oxygen. In particular, with forward permeating gas being methane, the diffusion coefficient of this gas in PPO decreases with increasing concentration of back permeating nitrogen.

While the rigorous explanation of the experimental results of this study is not possible at this point, these results demonstrate a successful application of the new method for the measurement of the diffusion coefficient in the presence of back permeating gas for different combinations of forward and back permeating gases.

Acknowledgement

The authors gratefully acknowledge the financial support for this project provided by the Natural Science and Engineering Research Council of Canada.

Nomenclature

C: Concentration of gas in membrane (mol/m^3)

C_0: Initial concentration of gas at the feed face of membrane (mol/m^3)

C_L: Concentration of gas at the permeate face of membrane (mol/m^3)

C_1: Concentration of gas at the feed face of membrane after step change in feed pressure (mol/m^3)

D: Diffusion coefficient in membrane (m^2/s)

J: Gas flux ($mol/m^2 s$)

J_0: Initial gas flux ($mol/m^2 s$)

J_∞: Steady state gas flux ($mol/m^2 s$)

L: Membrane thickness (m)

M: Accumulated flux ($m^3 m^{-2}$)

p_0: Feed pressure (Pa)

p_L: Permeate pressure (Pa)

P: Permeability coefficient in membrane (mol/m Pa s)

S: Solubility coefficient in membrane (mol/m^3 Pa)

t: Time (s)

w: Composition

x: Distance from the feed face of membrane (m)

Greek Symbols:

α: Separation factor

ϕ: Dimensionless gas permeation rate (flux)

θ_{cp}': Dimensionless time lag in constant pressure system (Equation 7.18)

θ_{cp}: Time lag in constant pressure systems (s)

σ': Dimensionless slope of the asymptote

σ: Slope of the asymptote (s^{-1})

τ: Dimensionless time

Subscripts:

A, B: Components

p: permeate

f: feed

S: slope

L: Permeate

0: Initial

1: Feed

References

1. L.M. Robeson, Correlation of separation factor versus permeability for polymeric membranes, J. Membr. Sci. 62 (1991) 165-185.
2. L.M. Robeson, The upper bond revised, J. Membr. Sci. 320 (2008) 390–400.
3. B.D. Freeman, I. Pinnau, Gas and liquid separations using membranes: An overview, ACS Symposium series 876: Advanced Materials for Membrane Separations, American Chemical Society, Washington, DC (2004) 1-23.
4. M.H. Klopffer, B. Flaconnèche, Transport properties of gases in polymers: Bibliographic review, Oil & Gas Science and Technology-Rev. IFP 56(3) (2001) 223-244.
5. B. Flaconnèche, J. Martin, M.H. Klopffer, Transport properties of gases in polymers: Experimental methods, Oil & Gas Science and Technology-Rev. IFP 56(3) (2001) 223-244.
6. S. Lashkari, A. Tran, B. Kruczek, Effect of Back Diffusion and Back Permeation of Air on Membrane Characterization in Constant Pressure System, J. Membr. Sci. 324 (2008) 162-172.
7. K.D. Ziegel, H.K. Frensdorff, D.E. Blair, Measurement of hydrogen transport in poly-(vinyl Fluoride) films by the permeation-rate method, Journal of polymer Science: Part A-2, 7 (1969) 809-819.
8. G E. Favre, N. Morlier, D. Roizard, Experimental evidence and implications of an imperfect upstream pressure step for the time lag technique, J. Membr. Sci. 207 (2002) 59-72.
9. R. Scheichl, M.H. Klopffer, Z. Benjelloun-Dabaghi, B. Flaconnèche, Permeation of gases in polymers: parameter identification and nonlinear regression analysis, J. Membr. Sci. 254 (2005) 275-293.
10. D.G. Pye, H.H. Hoehn, M. Panar, Measurement of gas permeability of polymers. II. Apparatus for determination of permeabilities of mixed gases and vapors, Journal of Applied Polymer Science 20 (1976) 287-301.
11. J.M. Watson, P.A. Payne, A study of organic compound pervaporation through silicon rubber, J. Membr, Sci. 49 (1990) 171-205.

12. J.M. Watson, G.S. Zhang, P.A. Payne, The diffusion mechanism in silicon rubber, J. Membr. Sci. 73 (1992) 55-71.
13. J.M. Watson, M.G. Baron, Precise static and dynamic permeation measurements using a continous-flow vacuum cell, J. Membr. Sci. 106 (1995) 259-268.
14. C.K. Yeom, B.S. Kim, J.M. Lee, Precise on-line measurements of permeation transients through dense polymeric membranes using a new permeation apparatus, J. Membr. Sci. 161 (1999) 55-66.
15. J.H. Kim, Y.M. Lee, Gas permeation properties of poly(amid-6-b-ethylene oxide)-silica hybrid membranes, J. Membr, Sci. 193 (2001) 209-225.
16. R. Ash, S.E. Espenhahn, T. Foley, Transport through a slab membrane governed by a concentration-dependent diffusion coefficient. Part V. Transient-state fluxes, J. Membr. Sci. 218 (2003) 39-54.
17. M.R. Shah, R.D. Noble, D.E. Clough, Measurement of sorption and diffusion in non porous membranes by transient permeation experiments, J. Membr, Sci. 287 (2007) 111–118.
18. S. Lashkari, Q. Wang, B. Kruczek, Effect of Resistance to Gas Accumulation in Multi-Tank Receivers on Membrane Characterization by the Time Lag Method. Part I: Reconciliation of the membrane properties, to be submitted to J. Membr. Sci.

Chapter 8

Conclusions, contributions and recommendations

In this chapter, a summary of the most significant conclusions derived from this thesis are be presented. Contribution of this study to the existing science and technology of membrane characterization and also recommendations for further research in this area are stated.

8.1 Conclusions

The focus of the current study was an accurate measurement of transport properties of gas separation membranes. Two common apparatus for these measurements are constant volume (CV) system and constant pressure (CP) system; both were studied in this thesis. Separate conclusions for each system are listed below.

Constant volume system:

The receiver's resistance of constant volume systems was previously studied theoretically and experimentally. In this thesis, the concept of resistance was extended to practical system configurations, and a numerical solution and an optimization method were utilized to reconcile the experimental results. The following conclusions were made for CV systems based on both experimental and theoretical findings:

- The time lag at any position in the receiver depends on the resistance of the portion of receiver downstream from that specific position towards the largest volume connected to the receiver. Existence of a large free resistance volume in the receiver magnifies the resistance of tubes positioned prior to that volume in the direction of flow.

- For a receiver with multiple accumulation tanks, the tanks should have the same volumes. If a specific total volume of the receiver is required, it is the best to split the required volume into as many accumulation tanks as possible.
- In general, receiver's resistances in series can not be added together. Only identical resistances in series are additive. The same rule is valid for membranes in series, which means that the electrical resistance analogy is not applicable for membranes in series. The analytical equations derived in this study confirm this concept. The exact electrical element analogy for membranes in series is provided by Siegel [1].
- The best position for the pressure sensor is where the receiver's time lag is zero. Receiver time lag can be determined using the provided analytical equations.
- Data reconciliation incorporating the resistance of the receiver in the membrane model would improve the reconciled membrane properties. The time lag differences between different positions in the receiver were reduced to a reasonable level by using the optimization procedure.

Constant Pressure System

A fully automated bubble flow meter was designed and utilized in systematic study of the effect of back diffusion and back permeation of air components in a traditional constant pressure system. The results lead to design of a novel technique for measurement of diffusion coefficient of a single gas under controllable back permeation conditions. The following conclusions were made for CP systems based on both experimental and theoretical findings:

- A fully-automated soap bubble flowmeter was designed and tested. Data reveals that this flowmeter can be used for a continuous measurement of very low gas flow rates that other types of flowmeters could not measure. The minimum flow rate measured by this experiment was 1×10^{-4} cm^3/s or 4×10^{-10} mol/s. This minimum can be improved by isolating the experimental surroundings.
- To minimize the effects of back diffusion and back permeation, it is recommended to perform experiments at conditions corresponding to Peclet number of at least 10 and preferably more. While the Peclet number can be

maximized by increasing the velocity of the forward permeating gas in the bubble flow meter and increasing the length of the tube, the latter is recommended.

- The effect of back diffusion and back permeation on the apparent permeability of the forward permeating gas is more significant than the theoretically predicted effect of these phenomena. On the other hand, the theoretical trends are consistent with the experimental ones. The deviation between the theoretical and experimental data can be qualitatively explained on the basis of dual mode sorption in glassy polymers. In addition, it is speculated the discrepancies between the theoretical and experimental date are also due to interactions of the permeating species with the membrane, which were not taken into consideration in the membrane transport model.

Constant Pressure System with Sweep

- A novel technique for the measurement of diffusion coefficient of single gases, in the presence of a controllable back permeation was developed and successfully applied in four different combinations of the forward and back permeating gases.
- The diffusion coefficients of nitrogen and oxygen increase when another gas is present in the membrane matrix. The effect of back permeating oxygen on the diffusion coefficient of nitrogen is generally stronger than the effect of back permeating nitrogen on the diffusion coefficient of oxygen.
- In case experiments involving methane, the influence of back permeating gas on the diffusion coefficient of the forward permeating gas is much stronger than in experiments involving only nitrogen and oxygen. In particular, with forward permeating gas being methane, the diffusion coefficient of this gas in PPO decreases with increasing concentration of back permeating nitrogen.

8.2 Contributions

The major contributions of the current study are summarized as follows:

- A clear description of the resistance of the receiver in constant volume systems was provided. Also, two approaches for solving the problem were presented. The first approach was to retrieve the transport properties of membranes by using an

optimization procedure. The second one was to correct the position of the pressure transducer in order to achieve the correct experimental results. This study helps to produce accurate measurement data in any laboratory. The problem with reproducibility of the results was greatly reduced. The experimental results which were corrected and verified based on the presented approach for constant volume systems, show good agreement with the data produced in constant pressure systems. It should be mentioned that inconsistencies of data for these two measurement systems are so common that they are almost accepted to be different without any specific reason. Therefore, the most important contribution in this area is the confidence that comes with the data provided using the proposed approaches.

- A fully automated bubble flowmeter was designed and assembled. The lowest flow rate measured by this apparatus was 1×10^{-4} cm^3/s or 4×10^{-10} mol/s, which is well below the range of any available commercial flowmeter. This flowmeter can be employed to measure even lower flow rates. The accuracy of bubble flowmeters, unlike most of the flowmeters, is based on the measured value not the full range of the instrument. Thus, the existence of such a flowmeter may prove to be of a great benefit for many researches and industries. Besides, since this flowmeter is fully automated, it can collect data without the presence of an operator and can be employed in the areas, where isolation is mandatory or beneficial.
- A novel method for the measurement of diffusion coefficient in the presence of controllable back permeation was presented. It can be employed to verify different transport mechanisms in glassy polymeric membranes. Many theories for the transport of gases in glassy polymers exist. However, lack of clear and accurate experimental results, which could verify different existing theories, has been the major obstacle for better understanding of the transport mechanisms in polymeric membranes. The novel technique to measure the diffusion coefficient in the presence of back permeation may help to remove this obstacle.
- One of the most important contributions of this study was to provide methods and suggestions for accurate measurements in three ways: (1) Pinpointing the

inherited problems of measurement systems (e.g. receiver resistance in constant volume systems and back permeation of air in constant pressure systems), (2) introducing new equipment for these measurements, or (3) developing a new measurement technique. This thesis contributes in all these three areas.

8.3 Recommendations

The following recommendations are proposed for further research and studies in this field:

Constant volume system:

- The effect of the pressure rise in the receiver on the slope of asymptote was studied experimentally and compared with numerical solution; however, more investigation is required to determine the magnitude of this effect.
- The simplex optimization method was used for the data reconciliation. Existence of multiple minima, which could not be handled by the simplex method made the optimization cumbersome. The optimization procedure should be repeated with different initial values to increase the confidence of getting to a global minimum. In addition, simplex method is very time consuming, and the time required to reach the final results is not practical for a common use of the program. Other optimization methods might provide faster and better results.

Constant pressure system:

- Back diffusion and back permeation of oxygen and nitrogen, as a binary gas system, were studied. It is suggested to extend the study to ternary systems. Some examples of what could be expected from the ternary system of CH_4/Air provided in Appendix C.
- Dynamic of back diffusion and back permeation tests were carried out partially in this thesis (Appendix C). More dynamic experiments are recommended. In particular, it would be desired to have a slower change in time dependent permeation rate. Interval of composition sampling might be an obstacle in dynamic experiments.

- Variation of room pressure and temperature introduced a random error to bubble flowmeter measurements. Therefore, a well-controlled experimental environment would increase the accuracy of bubble flowmeter measurements. Experiments in such environment are recommended.

Constant pressure system with sweep gas:

- Diffusion coefficient of oxygen and nitrogen were measured for six different compositions of these gases in the sweep stream. Since the pattern presents a minimum, more experimental points are required to produce a solid conclusion for this phenomenon. Therefore, additional data, especially close to the minimum composition is recommended.
- Measurement of diffusion coefficient for other binary gases in PPO membrane is recommended using the novel method of controllable back permeation; measurement of diffusion coefficient for other binary gases in other membranes is also recommended.
- Theoretical study of the influence of the second gas on diffusion coefficient of the first gas in membrane is suggested. The experimental data provided in this thesis can be employed to correlate the parameters of a model for the prediction of gas diffusion coefficient in the membrane, incorporating interaction parameters between the gases. Stephan-Maxwell model would be a good starting point.

Comparison of constant volume system and constant pressure system:

- Mauviel et al. [2] presented the difference between permeability of propane for constant pressure and constant volume systems as a function of pressure. However, they did not provide any solid explanation for their difference. Research on this difference, using the optimized CV and CP systems is recommended.

References

1. R.A. Siegel, Algebraic, Differential, and integral Relations for membranes in series and other multilaminar media: Permeabilities, solute consumption, lag times, and mean first passage times, J. Phys. Chem. 95 (1991) 2556-2565
2. Guillain Mauviel, Julien Berthiaud, C´ecile Vallieres, Denis Roizard, Eric Favre, Dense membrane permeation: From the limitations of the permeability concept back to the solution-diffusion model, J. Membr. Sci. 266 (2005) 62–67

Appendix A

Effect of a Resistance-Free Tank on the Resistance to Gas Transport in High Vacuum Tube

B. Kruczek[1]*, F. Shemshaki[1], S. Lashkari[1], H.L. Frisch[2]

Journal of Membrane Science, 280 (2006) 29-36

[1] Department of Chemical Engineering
University of Ottawa
161 Louis Pasteur Street
Ottawa, ON K1N 6N5, Canada
Fax: (613) 562-5172
Phone: (613) 562-5800 ext. 6302
E-mail: kruczek@eng.uottawa.ca

[2] Department of Chemistry
University at Albany
1400 Washington Avenue
Albany, NY 12222
USA

* **To whom correspondence should be addressed.**

Available online at www.sciencedirect.com
SCIENCE DIRECT®
Journal of Membrane Science 280 (2006) 29–36
journal of MEMBRANE SCIENCE
www.elsevier.com/locate/memsci

Effect of a resistance-free tank on the resistance to gas transport in high vacuum tube

B. Kruczek [a,*], F. Shemshaki [a], S. Lashkari [a], R. Chapanian [a], H.L. Frisch [b]

[a] *Department of Chemical Engineering, University of Ottawa, 161 Louis Pasteur Street, Ottawa, Ont. K1N 6N5, Canada*
[b] *Department of Chemistry, University at Albany, 1400 Washington Avenue, Albany, NY 12222, USA*

Received 8 August 2005; received in revised form 28 December 2005; accepted 3 January 2006
Available online 13 February 2006

Abstract

The expression for the time lag in a cylindrical tube, into which a gas at very low flow rate enters at one end while the other end is connected to a resistance-free accumulation tank, has been derived assuming that the gas transport in the tube is a diffusive process. Assuming a constant diffusion coefficient of the gas in the tube allowed obtaining an analytical expression for the time lag using the concept of linear asymptotes and Laplace transformation of the governing partial differential equation. The obtained expression indicates that if the pressure response is monitored in the tube, the presence of the tank at the end of the tube would lead to a negative time lag in the tube. The time lag becomes more negative as the distance from the tank increases and the volume of the tank increases while the cross-sectional area of the tube decreases.

The comparison of the model with the experimental data obtained in tests with nitrogen in which the pressure response to a step increase in feed pressure of membrane was monitored in the tube at two different distances from the membrane cell, indicates that the error due to resistance to gas transport in the tube on the experimental time lag of tested medium is even greater than that predicted by the model. This is because of the assumption of constant diffusion coefficient in the tube, which does not allow predicting the experimentally observed increase in the slope of the asymptote with the distance from the membrane cell.

Keywords: Time lag; Diffusion coefficient of gas in tube; Fick's second law of diffusion

1. Introduction

The time lag method, which originates from the analysis of Daynes [1] is nowadays a basis of generally accepted technique to assess the permeability and diffusion coefficients of gases in porous and nonporous media. The numerous refinements of the original time lag analysis have been made over the years, and are summarized by Rutherford and Do [2]. All these refinements are concerned with the boundary conditions and the properties of tested medium; hence they can be referred to as "internal" refinements.

In our recent paper [3] we considered the effect of resistance to accumulation of gases downstream from the membrane on the experimentally measured time lag. Assuming that the gas permeating through the membrane accumulates in a straight cylindrical tube and that accumulation is a diffusive process characterized by a constant diffusion coefficient (D), we derived the following expression for the experimental time lag:

$$\theta_{\text{exp}} = \theta_{\text{m}} + \frac{L^2}{6D} - \frac{(L-x)^2}{2D} \tag{1}$$

where θ_{m} is the actual time lag of membrane, L the length of the tube, and x is the distance from the membrane where the pressure response is monitored. It is important to emphasize that this correction is only of significance for the special case dealt with earlier [3]. In this unusual and undesirable case, the downstream receiver has a small diameter tube and the receiver pressure is very low so that Knudsen diffusion, rather than conventional viscous flow is responsible for transport away from the downstream membrane face. Eq. (1) can be considered as an "external" refinement of the original time lag analysis.

In this paper the effect of the resistance to gas transport in a cylindrical vacuum tube on the experimental time lag is investigated in the configuration, in which the tube is followed by a cylindrical accumulation tank, and the internal radius of the

* Corresponding author. Tel.: +1 613 562 5800x6302; fax: +1 613 562 5172.
E-mail address: kruczek@eng.uottawa.ca (B. Kruczek).

0376-7388/$ – see front matter © 2006 Elsevier B.V. All rights reserved.
doi:10.1016/j.memsci.2006.01.001

tank is much larger than the internal radius of the tube. The expression for the time lag is developed by using the concept of the asymptotic solution of the Laplace-transformed governing partial differential equation. The mathematical model is then verified experimentally in the configuration with and without the tank at the end of the tube. In both cases the pressure response is monitored simultaneously by two pressure transducers installed on the tube at different distances from the membrane cell. The diffusion coefficient of the gas downstream from the membrane is evaluated using the empirical model of Knudsen.

2. Diffusion coefficient in cylindrical tubes

The steady molar flux (J) of an ideal gas through a cylindrical tube can be described by the Knudsen empirical formula [4]:

$$J = \frac{\Delta p}{L}\frac{\tilde{D}}{RT} \tag{2}$$

where Δp is the pressure drop in the tube, L the length of the tube, R the universal gas constant, T the absolute temperature, and $\tilde{D}$ is an integral quantity defined as [4]:

$$\tilde{D} = \frac{\tilde{p}r^2}{8\eta} + \frac{2}{3}r\sqrt{\frac{8RT}{\pi M}}\left(\frac{1+C_1\tilde{p}}{1+C_2\tilde{p}}\right) \tag{3}$$

where $\tilde{p}$ is the mean pressure in the tube, r the radius of the tube, η the dynamic viscosity of the gas, M the molecular mass of the gas, and C_1 and C_2 are constants, which are determined by solving the following set of equations:

$$\frac{C_1}{C_2} = \frac{3\zeta\sqrt{\frac{\pi M}{RT}}\tilde{p}}{8\sqrt{2}\eta} \tag{4}$$

$$C_2 - C_1 = 0.6117\sqrt{\frac{M}{RT}}\frac{r}{\eta} \tag{5}$$

The coefficient of slip (ζ) is evaluated using the Maxwell's deduction from the kinetic theory of gases [5]:

$$\zeta = \frac{\eta}{\tilde{p}}\sqrt{\frac{\pi RT}{2M}}\left(\frac{2-f}{f}\right) \tag{6}$$

where f is a fraction of gas molecules, which lose the momentum as a result of adsorption and desorption at the walls of tube. While f depends on the nature of the gas and the tube surface, it is usually close to unity [6,7]. With $f=1$, solving simultaneously Eqs. (3) and (4) leads to the following expressions for the constants C_1 and C_2:

$$C_1 = 0.8768\sqrt{\frac{M}{RT}}\frac{r}{\eta} \tag{7}$$

$$C_2 = 1.4885\sqrt{\frac{M}{RT}}\frac{r}{\eta} \tag{8}$$

At very low pressures, regardless of the value of f, Eq. (3) approaches the expression for the diffusion coefficient in the Knudsen flow regime:

$$\tilde{D} \to D_K = \frac{2}{3}r\sqrt{\frac{8RT}{\pi M}} \tag{9}$$

Eq. (8) is valid when a gas molecule collides much more frequently with the walls of the tube rather than with other gas molecules. Such conditions exist when the mean free path of gas molecules (λ) is much greater than the internal radius of the tube, i.e., $r/\lambda < 0.1$.

At high pressures, the second term of Eq. (3) becomes much smaller than the first term, and Eq. (3) approaches the expression for the diffusion coefficient in the Poiseuille flow regime:

$$\tilde{D} \to \tilde{D}_P = \frac{\tilde{p}r^2}{8\eta} \tag{10}$$

Eq. (10) is valid when $r/\lambda \gg 1$.

The Knudsen empirical formula is a special case of Fick's first law. Considering a differential element of the tube of the length dx, Eq. (2) becomes:

$$J = -\frac{D}{RT}\frac{dp}{dx} \tag{11}$$

In which

$$D = \frac{pr^2}{8\eta} + \frac{2}{3}r\sqrt{\frac{8RT}{\pi M}}\left(\frac{1+C_1 p}{1+C_2 p}\right) \tag{12}$$

It is important to emphasize that Eq. (11) uses D rather than $\tilde{D}$, because the pressure in the differential element is uniform and thus $\tilde{p}$is replaced p. Consequently, D in Eq. (12) represents a local diffusion coefficient of the gas in the tube at x where the pressure is equal to p.

Assuming $f=1$, Fig. 1 presents the graphical illustration of the diffusion coefficient of N_2 at 23 °C in two cylindrical tubes of radii 0.193 and 5.0 cm determined using Eq. (12). The horizontal dashed lines in Fig. 1 represent the corresponding Knudsen diffusion coefficients. It should be noted that the tube radius not only affects the diffusion coefficient, but also the range of

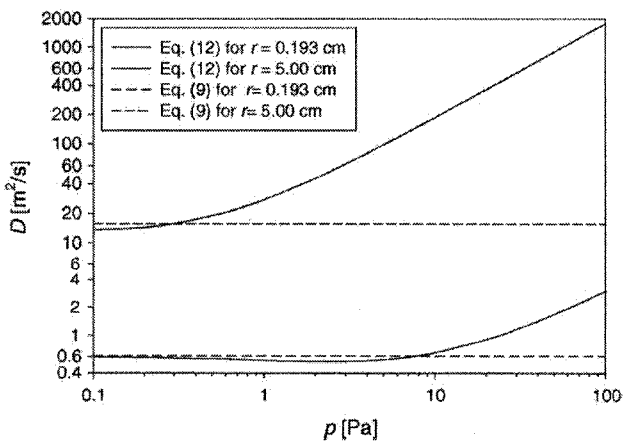

Fig. 1. Effect of pressure on the diffusion coefficient of N_2 at 23 °C in standard stainless steel tubes according to the empirical model of Knudsen [4] (solid lines). Dashed lines indicate the corresponding coefficients in pure Knudsen regime.

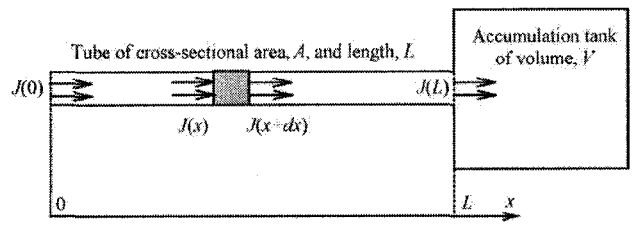

Fig. 2. Simplified configuration of a constant volume system for the modeling purposes.

pressures, in which the diffusion coefficient is relatively constant. The smaller the radius, the larger the pressure range with a relatively constant D. For example, for $r=0.193$ cm, the conditions for $r/\lambda<0.1$, i.e., for the Knudsen flow regime, exist at $p<0.49$ Pa. On the other hand, for the pressures up to 10 Pa the diffusion coefficient does not differ more than 10% from the corresponding Knudsen diffusion coefficient.

3. Mathematical formulation of the problem

Fig. 2 presents a simplified configuration of a constant volume system consisting of a cylindrical tube of length L and a cross-sectional area A, and a cylindrical tank of volume V. Initially, there is no flow of the gas, and the tube and the tank are at uniform pressure. At time $t>0$, the gas starts to flow into the tube at $x=0$, and is accumulated in the tank. The gas flow at $x=0$ may originate from any source, including membrane permeation. Assuming applicability of the ideal gas law, the mass balance in the differential element of the tube of length dx is given by Eq. (13):

$$J_x - J_{x+dx} = \frac{1}{RT}\frac{\partial p}{\partial t}dx \tag{13}$$

Dividing both sides by dx and letting $dx \to 0$, Eq. (13) becomes:

$$\frac{1}{RT}\frac{\partial p}{\partial t} = -\frac{\partial J}{\partial x} \tag{14}$$

Substituting Eq. (11) into Eq. (14) and assuming that D is constant, leads to

$$\frac{\partial p(x,t)}{\partial t} = D\frac{\partial^2 p(x,t)}{\partial x^2} \tag{15}$$

Eq. (15), which is simply Fick's second law, is valid only when D is constant. In case of a tube of internal radius of 0.193 cm shown in Fig. 1, this assumption may be justified up to 10 Pa. It is important to emphasize that $r=0.193$ cm represents the internal radius of a standard 1/4 in. stainless steel tube. The accumulation of the gas in the tank is also a diffusive process; however, if the internal radius of the tank is large, the corresponding diffusion coefficient will be large, and the resistance to accumulation of the gas in the tank will be negligible.

Assuming no resistance to accumulation of the gas in the tank, the pressure in the tank will, at any time, be uniform and equal to the pressure at the end of the tube, i.e., $p(\text{tank},t)=p(x=L,t)$. Consequently, the rates of pressure increase in the tank and at the end of tube will be the same. Assuming applicability of the ideal gas law, the rate of the pressure increase in the tank, and thus at the end of tube, may be expressed in terms of the gas flux leaving tube:

$$\frac{dp(\text{tank})}{dt} = A\frac{RT}{V}J(L,t) = \frac{dp(L,t)}{dt} \tag{16}$$

The gas flux leaving the tube is given by the Fick's first law of diffusion:

$$J(L,t) = -\frac{D}{RT}\left(\frac{\partial p(x,t)}{\partial x}\right)_L \tag{17}$$

Combining Eqs. (16) and (17) yields the following expression:

$$\frac{dp(L,t)}{dt} = -\frac{DA}{V}\left(\frac{\partial p(x,t)}{\partial x}\right)_L \tag{18}$$

Eq. (18) represents one of two boundary conditions required for the solution of Eq. (15). The other boundary condition is expressed in terms of the gas flux entering the tube:

$$\left(\frac{\partial p(x,t)}{\partial x}\right)_0 = -\frac{RT}{D}J(0,t) \tag{19}$$

Before initiation of the flow the tube and the tank are at uniform pressure, thus the initial condition is expressed by

$$p(x,0) = p_0 = \text{constant} \tag{20}$$

4. Expression for time lag of the tube

The expression for the time lag of the tube may be obtained using the concept of the asymptotic solution [8] following the same procedure as in Ref. [3]. This procedure requires transformation of the governing partial differential equation using the Laplace transforms and then the solution of the transformed equation.

Application of the Laplace transform to Eq. (15) along with the initial condition given by Eq. (20) leads to the following ordinary differential equation:

$$\frac{d^2\bar{p}}{dx^2} - q^2\bar{p} + \frac{p_0}{D} = 0 \tag{21}$$

where $\bar{p} = \bar{p}(x,s) = \int_0^\infty e^{-st}p(x,t)\,dt$ and $q^2 = s/D$. Eq. (21) has the following particular solution:

$$\bar{p}(x,s) = M\sinh(qx) + N\cosh(qx) + \frac{p_0}{s} \tag{22}$$

The constants M and N may be determined from the Laplace transforms of the boundary conditions, which are as follows:

$$\left(\frac{d\bar{p}(x)}{dx}\right)_L = -\frac{V}{AD}(s\bar{p}(L) - p_0) \tag{23}$$

$$\left(\frac{d\bar{p}(x)}{dx}\right)_0 = -\frac{RT}{D}\bar{J}(0) \tag{24}$$

where $\bar{J} = \bar{J}(x,s) = \int_0^\infty e^{-st}J(x,t)\,dt$. Application of Eqs. (23) and (24) leads to the following expressions for M and N:

$$M = -\frac{\bar{J}(0)RT}{Dq} \tag{25}$$

$$N = -M\frac{\frac{A}{Vq}\cosh(qL) + \sinh(qL)}{\cosh(qL) + \frac{A}{Vq}\sinh(qL)} \tag{26}$$

Therefore, the final form of the particular solution is given by

$$\bar{p}(x,s) - \frac{p_0}{s} = \left(\frac{\bar{J}(0)RT}{\sqrt{Ds}}\right) \times \frac{\frac{A}{V}\sqrt{\frac{D}{s}}\cosh\left(\sqrt{\frac{s}{D}}(L-x)\right) + \sinh\left(\sqrt{\frac{s}{D}}(L-x)\right)}{\cosh\left(\sqrt{\frac{s}{D}}L\right) + \frac{A}{V}\sqrt{\frac{D}{s}}\sinh\left(\sqrt{\frac{s}{D}}L\right)} \tag{27}$$

According to the asymptotic solution concept [8], when the Laplace transform of any quantity has the form:

$$\bar{y}(s) = \frac{f(s)}{s^2\Delta(s)} \tag{28}$$

and $f(s)/\Delta(s)$ is regular at $s=0$, the expression for the time lag is given by the following equation:

$$\theta = \frac{f(0)\frac{d\Delta}{ds}(0) - \Delta(0)\frac{df}{ds}(0)}{f(0)\Delta(0)} = \frac{\frac{d\Delta}{ds}(0)}{\Delta(0)} - \frac{\frac{df}{ds}(0)}{f(0)} \tag{29}$$

The determination of expressions for $f(s)$ and $\Delta(s)$ requires the expression for $\bar{J}(x=0)$.

4.1. Constant flux at tube entrance

If the flux at the tube entrance is constant, i.e., $J(0)=F$, then $\bar{J}(0) = F/s$. Consequently, by equating the right hand sides of Eqs. (27) and (28), it can be shown that the following expressions for $f(s)$ and $\Delta(s)$ are obtained:

$$f(s) = FRT\left(\frac{A}{V}\cosh\left(\sqrt{\frac{s}{D}}(L-x)\right) + \sqrt{\frac{s}{D}}\sinh\left(\sqrt{\frac{s}{D}}(L-x)\right)\right) \tag{30}$$

$$\Delta(s) = \cosh\left(\sqrt{\frac{s}{D}}L\right) + \frac{A}{V}\sqrt{\frac{D}{s}}\sinh\left(\sqrt{\frac{s}{D}}L\right) \tag{31}$$

Evaluation of Eqs. (30) and (31) and their first derivatives at $s=0$, and substitution of the resulting expressions into Eq. (29) leads to the following expression for the experimental time lag:

$$\theta_{\exp} = \frac{\frac{L^2}{D}\left(\frac{L}{6} + \frac{V}{2A}\right)}{L + \frac{V}{A}} - \frac{(L-x)^2}{2D} - \frac{V(L-x)}{AD} \tag{32}$$

4.2. Time dependent flux at tube entrance

If the tube entrance represents the outlet of a slab membrane, and the membrane is subjected to a step increase in feed pressure, the gas flux entering the tube will depend on time, i.e., $J(0)=f(t)$. The exact dependence of the gas flux on time at the tube entrance depends on the membrane properties, and the initial and boundary conditions for the membrane. In the simplest case, the permeability coefficient (P_m) and the diffusion coefficient (D_m) of the gas in membrane are independent of the gas concentration (c), and the following initial and boundary conditions are assumed [1]:

$$c(x',0) = 0 \tag{33}$$

$$c(0,t) = \frac{p_f P_m}{D_m} = \text{const.} \tag{34}$$

$$c(l_m,t) \approx 0 \tag{35}$$

where p_f is the feed pressure and l_m is the membrane thickness. Eq. (33) implies that the constant in Eq. (20) is zero. The positions, $x'=0$ and $x'=l_m$ correspond to the feed and permeate faces of the membrane, respectively. For such specified conditions, it can be shown that the Laplace transform from the gas flux entering the tube is given by the following expression [3]:

$$\bar{J}(0) = \frac{B}{\sqrt{s}\sinh\left(\sqrt{\frac{s}{D_m}}l\right)} \quad \text{with } B = \frac{p_f P_m A_m}{A\sqrt{D_m}} \tag{36}$$

where A_m is the membrane area.

Substituting Eq. (36) into Eq. (27) and then equating the right hand sides of Eqs. (27) and (28) leads, after rearrangements, to the following expressions for $f(s)$ and $\Delta(s)$:

$$f(s) = \frac{BRT}{\sqrt{D}}\left(\cosh\left(\sqrt{\frac{s}{D}}(L-x)\right) + \frac{V}{A}\sqrt{\frac{s}{D}}\sinh\left(\sqrt{\frac{s}{D}}(L-x)\right)\right) \tag{37}$$

$$\Delta(s) = \frac{V}{A\sqrt{D}}\frac{\cosh\left(\sqrt{\frac{s}{D}}L\right)\sinh\left(\sqrt{\frac{s}{D_m}}l_m\right)}{\sqrt{s}} + \frac{\sinh\left(\sqrt{\frac{s}{D}}L\right)\sinh\left(\sqrt{\frac{s}{D_m}}l_m\right)}{s} \tag{38}$$

Evaluation of Eqs. (37) and (38) and their first derivatives at $s=0$, and substitution of the resulting expressions into Eq. (28) leads to the following equation for the time lag:

$$\theta_{\exp} = \theta_m + \frac{\frac{L^2}{D}\left(\frac{L}{6} + \frac{V}{2A}\right)}{L + \frac{V}{A}} - \frac{(L-x)^2}{2D} - \frac{V(L-x)}{AD} \tag{39}$$

where

$$\theta_m = \frac{l_m^2}{6D_m} \tag{40}$$

It is important to note that Eq. (40) represents a well-know expression for the time lag of membrane, which is subject to the initial and boundary conditions specified by Eqs. (33)–(35), and for which Henry's law is applicable and the diffusion coefficient is independent of gas concentration [1]. Since the membrane and the tube are in series, regardless of the expression for $J(x=0)$, the above analysis should always lead to Eq. (39). Changing the

properties of membrane and the initial and boundary conditions would result in a different expression for θ_m [2].

It is important to note that in the limiting case of $V=0$, i.e., for the configuration without the tank, Eq. (39) simplifies to Eq. (1).

5. Experimental

Fig. 3 presents the schematic diagram of the gas permeation system used in this project. A membrane is sandwiched between the two cylindrical parts of a stainless steel cell. The effective area for gas permeation in the cell, $A_m = 9.08 \times 10^{-4}$ m^2. The inflow volume consists of a standard 1/4 in. stainless steel tubing and a buffer tank of volume 26.50×10^{-3} m^3, which can be pressurized up to 931 kPa using a gas from a compressed gas cylinder. The buffer tank is equipped with a relief valve (RV) and an absolute pressure gauge (P_f) having a 0–1207 kPa range and a 6.9 kPa reading accuracy. The reading of this pressure gauge during the gas permeation experiment is considered to be the pressure at the feed face of the membrane (p_f). This pressure is adjusted manually by a pressure regulator (PR) and the relief valve.

The outflow volume consists of a standard 1/4 in. stainless steel tube of length $L=2.365$ m and an accumulation tank of volume $V=2.250 \times 10^{-3}$ m^3. The internal radius of the tube $r=0.193$ cm, thus its cross-sectional area $A=1.17 \times 10^{-5}$ m^2. The configuration of the outflow volume in Fig. 3 is typical for a constant volume system, except the length of the tube and the volume of the tank are exaggerated for the illustration purposes. The outflow volume is equipped with two absolute pressure transducers, a rotary vacuum pump (Edwards model RV3), and several two-way manually operated valves (Swagelock model SS-DSVCR4) with VCR fittings. The pressure transducers P_1 and P_2 (MKS model 627B11TBC1B) have a linear range from 0 to 1333 Pa with a 0.0267 Pa reading accuracy and the maximum error corresponding to 0.12% of the read pressure; they are connected to a personal computer equipped with a LabView software. The pressure transducers are installed in the tube 0.495 and 2.28 m from the membrane cell. With V3 closed the outflow volume, as determined by a gas expansion technique, is 58.7×10^{-6} m^3. On the other hand, the active volume, i.e., $A \times L = 27.7 \times 10^{-6}$ m^3. The difference between the total volume and the active volume of 31.0×10^{-6} m^3 represents intermediate volumes associated with valves, fittings, pressure transducers, and the membrane cell.

A membrane, which is utilized as a medium to provide time lag in the pressure response, is a solution-cast high molecular polyphenylene oxide (PPO) film prepared by complete evaporation of solvent, of thickness $l_m = 39.5 \times 10^{-6}$ m.

Before each experiment the system was evacuated, during which all valves except V1 were in the open position. Once the desired vacuum was reached V4 was closed, and the pressure in the volume enclosed between V1 and V4, which includes the membrane cell, the tube and the accumulation tank was monitored for at least 30 min to ensure that there was no leak, after which V2 was closed. The experiments were performed at the same initial pressure of 0.13 Pa. With V1 closed, the pressure in the buffer tank was set at the desired level. The experiments were performed at four different feed pressures. The temperature during experiments was not controlled; however, it remained relatively constant at 23 ± 1 °C. The experiments were initiated by opening V1. After pressurization of the membrane the data was collected for at least 5 min with a frequency of one data set per 1 s.

6. Results and discussion

6.1. Experiments without tank

Fig. 4 presents the progress of the first 120 s of the gas permeation experiment in the configuration without the tank, i.e., with V3 closed. The pressure responses in Fig. 4 are monitored 0.495 m (p_1) and 2.280 m (p_2) from the membrane cell.

It can be noticed that 20 s after the initiation of the experiment, the pressures recorded by the two pressure transducers start to differ from each other. In the period between 42 and 63 s the difference between p_1 and p_2 reaches the maximum value exceeding 2 Pa. As the experiment progresses $\Delta p = p_1 - p_2$ decreases. For example, at 100, 200 and 300 s after initiation of the experiment the corresponding Δps are 1.38, 0.77, and

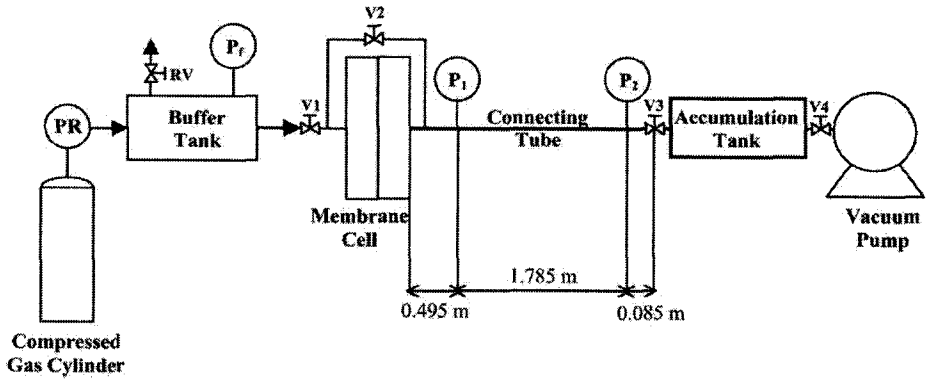

Fig. 3. Schematic diagram of the experimental constant volume system. P_1 and P_2 are the MKS pressure transducers (model 627B11TBC1B); P_f is the absolute pressure transducer; PR is the pressure regulator; RV is the relief valve.

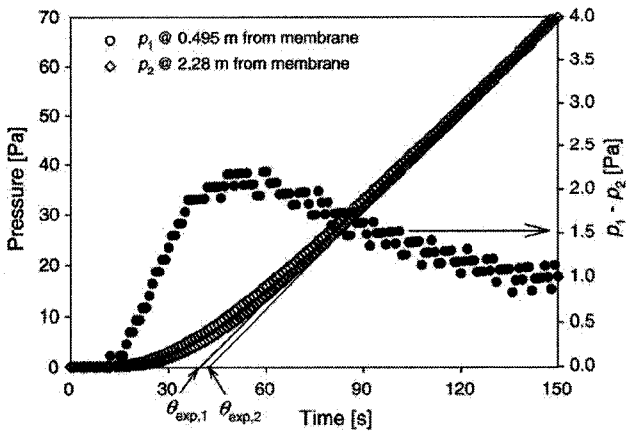

Fig. 4. Progress of N_2 permeation experiment through PPO membrane monitored at two different distances from the membrane cell in a standard 1/4 in. stainless steel tube of length $L = 2.365$ m. Initial pressure, $p_0 = 0.13$ Pa; feed pressure, $p_f = 206.8$ kPa; temperature, $T = 23\,^{\circ}C$.

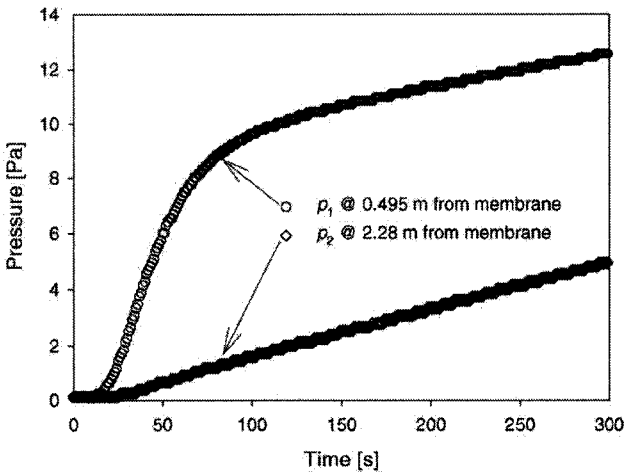

Fig. 5. Progress of N_2 permeation experiment through PPO membrane monitored at two different distances from the membrane cell in a standard 1/4 in. stainless steel tube of length $L = 2.415$ m in the configuration with a cylindrical tank of volume $V = 2.250 \times 10^{-3}$ m^3 attached at the end of the tube. Initial pressure, $p_0 = 0.13$ Pa; feed pressure, $p_f = 206.8$ kPa; temperature, $T = 23\,^{\circ}C$.

0.56 Pa, respectively. The difference between the pressure responses leads to a difference between the time lags. For the experiment depicted in Fig. 4, the experimental time lags based on p_1 and p_2, are $\theta_{exp,1} = 39.5$ s and $\theta_{exp,2} = 42.5$ s, respectively. Thus, there is a difference of 3.0 s between the experimental time lags at the two positions.

Different pressure responses at different distances from the membrane leading to different time lags are direct consequence of the resistance to accumulation of N_2 in the tube. The resistance to accumulation prevents uniform distribution of gas molecules downstream from the membrane leading to a higher concentration of the gas near the membrane.

For the experiment depicted in Fig. 4, $V = 0$, and Eq. (39) becomes Eq. (1). Knowing the diffusion coefficient of the gas in the tube (D calculated for N_2 at 23 °C in the tube having $r = 0.193$ cm using Eq. (8) is 0.61 m^2/s), Eq. (1) may be used for the prediction of the difference between the experimental time lags at different distances from the membrane. With $D = 0.61$ m^2/s and $L = 2.365$ m, it follows from Eq. (1) that the difference between the experimental time lags at 2.28 and 0.495 m from the membrane cell should be 2.9 s, which is in excellent agreement with the experimentally observed difference between the $\theta_{exp,2}$ and $\theta_{exp,1}$. Alternatively, D could be evaluated using Eq. (11); for the tube having $r = 0.193$ cm and N_2 at the initial pressure of 0.13 Pa and 23 °C and with $f = 1$, the diffusion coefficient is 0.60 m^2/s.

Knowing θ_{exp}, Eq. (1) may be used to determine the actual time lag of the membrane. For the experiment depicted in Fig. 4, for $x = 0.495$ m and $\theta_{exp} = 39.5$ s, $\theta_m = 40.9$ s. On the other hand, for $x = 2.28$ m and $\theta_{exp} = 42.5$ s, $\theta_m = 41.0$ s.

The error in the time lag of membrane due to the resistance to gas accumulation in the 1/4 in. tube is evident. On the other hand, its magnitude is rather small. Moreover, as already mentioned the length of the tube in the system used in this study was exaggerated for the illustration purposes. Such a length of tubing in the actual gas permeation system would represent an inept apparatus design. Therefore, in a properly designed system the error in the time lag of membrane due to the resistance to accumulation of gas in the tube should practically be negligible.

6.2. Experiments with tube and tank

Fig. 5 presents the progress of the first 300 s of the gas permeation experiment similar to the one depicted in Fig. 4. The only difference between the experiments shown in Figs. 4 and 5 is the configuration of the outflow volume, while the membrane, the initial pressure and the feed pressure are the same. The experiment presented in Fig. 5 was performed with open V3, thus, with the tank incorporated into the outflow volume. Opening V3 also increased the length of tubing by 5 cm, i.e., $L = 2.415$ m. Because of inclusion of the tank in the outflow volume, the rate of pressure rise in the experiment shown in Fig. 5 is much slower than that in Fig. 4, but most importantly the difference between the pressure responses at 0.495 and 2.28 m from the membrane cell, which at 150 s reaches 8.2 Pa, is significantly greater than that in Fig. 4. As the experiment progresses, the difference between p_1 and p_2 slightly decreases; at 300 s this difference drops to 7.7 Pa. It can be noticed that between 150 and 300 s the pressure responses in both positions are linear, but not parallel to each other. Using the slopes of the pressure response between 150 and 300 s at the two positions the following experimental time lags are obtained: at 0.495 m, $\theta_{exp,1} = -677$ s; at 2.28 m, $\theta_{exp,2} = 8.6$ s. It should be remembered that actual time lag of membrane estimated based on the pressure responses shown in Fig. 4 and Eq. (1), $\theta_m = 41$ s. Therefore, incorporation of the tank in the outflow volume results in a very large negative error in the experimental time lag, whose magnitude depends on the distance from the membrane cell.

The experimental results presented in Fig. 5 may be explained by considering the model given by Eq. (39). The large negative error is caused by the last term on the right hand side of Eq. (39), $-(V(L-x)/AD)$. Assuming $\theta_m = 41$ s, the substitution

Table 1
Summary of the analysis of the permeation experiments in the configuration with the tank in the outflow volume

p_f (kPa)	x (m)	Slope[a] (Pa s^{-1})	θ_{exp}[a] (s)	θ_m[b] (s)
207	0.495	0.0128	−677	−59.2
	2.280	0.0166	8.6	47.3
345	0.495	0.0186	−696	−78.2
	2.280	0.0265	0.8	39.5
620	0.495	0.0291	−667	−49.2
	2.280	0.0457	7.9	46.6
758	0.495	0.0349	−643	−25.2
	2.280	0.0560	8.1	46.8

Polymer: PPO; gas: N_2; initial pressure: $p_0 = 0.13$ Pa; temperature: $T = 23$ °C.
[a] Based on the pressure response between 150 and 300 s from the initiation of the experiment.
[b] Evaluated from Eq. (39) using θ_{exp} and the following parameters: $D = 0.60\ m^2\ s^{-1}$, $L = 2.415$ m, $V = 2.25 \times 10^{-3}\ m^3$, $A = 1.17 \times 10^{-5}\ m^2$.

of the numbers into Eq. (39) leads to the following predicted experimental time lags: at 0.495 m, $\theta_{exp,1} = -577$ s; at 2.28 m, $\theta_{exp,2} = 2.3$ s. The predicted experimental time lags deviate considerably from the observed experimental time lags, particularly at the position closer to the membrane cell. The experimental time lags may also be used to evaluate the time lag of membrane using Eq. (39).

Table 1 summarizes the analysis of the gas permeation experiments performed at different feed pressures in the configuration with the tank in the outflow volume. The table lists the slope of the asymptote, which is determined from the pressure response between 150 and 300 s, the experimental time lag determined from the asymptote, and the time lag of membrane determined from the experimental time lag using Eq. (39). It should be pointed out that in every test the experimentally observed time lag at $x = 0.495$ m is much less than the predicted value of −577 s, and consequently the predicted θ_m is much less than the 41 s, i.e., the actual time lag of the membrane. In fact, the predicted θ_m based on θ_{exp} at $x = 0.495$ m is a negative number in every experiment. On the other hand, θ_{exp} at $x = 2.28$ m is generally greater than 2.3 s and consequently θ_m, except for the experiment at 345 kPa, is slightly greater than 41 s. The discrepancy between the predicted θ_m and the actual time lag of membrane is a result of the assumption of constant D, which implies a constant slope of the asymptote. However, as shown in Table 1 the slope of the asymptote at $x = 2.28$ m is greater than the slope of the asymptote at $x = 0.495$ m, and the difference between the slopes at the two positions increases with the feed pressure. In addition, the presence of intermediate volumes associated with valves, fittings, pressure transducers, and the membrane cell, may have also contributed to the discrepancies between the predicted and observed θ_m.

Assuming that the diffusion coefficient in the tube is constant, the slope of the asymptote is given by the following expression:

$$\frac{dp}{dt} = \frac{A_m p_f P_m RT}{V_t l_m} \tag{41}$$

where V_t is the total outflow volume. Since D depends on p, dp/dt will be a function of x even after disappearance of a highly non-linear pressure response immediately after pressurization of the membrane.

The determination of dp/dt as a function of x would require a numerical solution of Eq. (15) in which D depends on p according to Eq. (12). On the other hand, the existence of a greater slope of the asymptote at $x = 2.28$ m than at $x = 0.495$ m can be explained qualitatively by considering the dependence of the diffusion coefficient on pressure shown in Fig. 1. For the 1/4 in. tube and the pressures greater than 2.4 Pa, the diffusion coefficient increases with pressure. As the gas accumulates in the outflow volume and the diffusion coefficient increases, the distribution of gas molecules must become more uniform leading to a decrease in the difference between p_1 and p_2. Thus, the slope of the asymptote will increase with the distance from the membrane cell, and at some distance it will be equal to the slope determined from Eq. (41).

The time lag is the intercept of the asymptote of the pressure response curve with the time axis. Therefore, if the slope of the asymptote is less than the slope determined from Eq. (41), the experimental time lag will decrease leading to underestimation of θ_m evaluated from Eq. (39). On the other hand, if the experimental slope of asymptote is greater than the slope determined from Eq. (41), the experimental time lag will increase leading to overestimation of θ_m evaluated from Eq. (39). The apparent closeness of θ_m evaluated from Eq. (39) at $x = 2.28$ m in 41 s indicates that the slope at $x = 2.28$ m is similar to that from Eq. (41). The dependence of the slope of the asymptote on the distance from the membrane cell magnifies the effects of resistance to gas transport in the tube predicted by Eq. (39).

As already mentioned, the length of tubing and the volume of the tank downstream from the membrane were exaggerated in this study, and in practical systems such a configuration of the outflow volume would represent an inept apparatus design. On the other hand, if the pressure transducer were installed on the tube, the effects of the resistance to gas transport in the tube would affect the experimental time lag even when the length of tube was minimized. For small L, the second and third terms on the right hand side of Eq. (39) are small. However, if $L - x > 0$, the fourth term might contribute significantly to the experimental time lag. The best solution, of course, would be to install the pressure transducer on the tank, which would eliminate the fourth term altogether. On the other hand, for a given volume of the tank, if 1/2 in. rather than 1/4 in. tubes were used, A and D would increase minimizing the fourth term. Another way to minimize the fourth term would be to decrease the volume of the tank.

It is important to emphasize that the configuration in which the accumulation tank is located at the end of tube, i.e., at $x = L$, simplifies the mathematical analysis. If a tank were located at $x < L$, or if there were multiple tanks at different distances from the membrane cell, the analytical solution of the mathematical problem would become very complicated. On the other hand, for any configuration of the outflow volume, the influence of the resistance to gas transport downstream from the tested medium could be evaluated by solving numerically the resulting set of partial differential equations.

7. Conclusions

The effect of the presence of a resistance-free accumulation tank at the end of a tube on the experimental time lag has been modeled by assuming that the gas transport in the tube is a diffusive process characterized by a constant diffusion coefficient. The latter assumption was necessary to obtain analytically the final expression for the experimental time lag by using the concept of the asymptotic solution. According to the proposed model, which is given by Eq. (39), if the pressure response is monitored in the tube, the resistance to gas transport in the tube would lead to underestimation of the time lag of tested medium. The magnitude of the error increases with the distance of the pressure transducer from the tank and the volume of the tank. The error also increases with decrease in the cross-sectional area of tube.

The comparison of the model with the experimental data obtained in the tests in which the pressure response to a step increase in feed pressure of membrane was monitored in the tube at two different distances from the membrane cell, indicates that the error due to resistance to gas transport in the tube on the experimental time lag of the tested medium is even greater than that predicted by the model. This is because of the assumption of constant diffusion coefficient in the tube, which does not allow predicting the experimentally observed increase in the slope of the asymptote with the distance from the membrane cell.

To minimize the error in the time lag of tested medium due to resistance to gas transport in the tube, the pressure response should be monitored in the tank. In this case, the resistance to gas transport in the tube would lead to an overestimation of the time lag of tested medium. However, in a well-designed system, in which the length of the tube is minimized while its cross-sectional area is maximized, the positive error should be negligible.

Acknowledgement

The authors gratefully acknowledge the financial support for this project provided by the Natural Science and Engineering Research Council of Canada.

Nomenclature

A	cross-sectional area of permeate collector tube (m^2)
A_m	membrane area (m^2)
c	concentration of gas in membrane ($mol\,m^{-3}$)
C_1	constant in Eq. (3) defined by Eq. (6) (Pa^{-1})
C_2	constant in Eq. (3) defined by Eq. (7) (Pa^{-1})
D	diffusion coefficient of gas in tube ($m^2\,s^{-1}$)
$\tilde{D}$	average diffusion coefficient of gas in tube ($m^2\,s^{-1}$)
D_K	Knudsen diffusion coefficient of gas in tube ($m^2\,s^{-1}$)
D_m	diffusion coefficient of gas in membrane ($m^2\,s^{-1}$)
$\tilde{D}_P$	average diffusion coefficient in the Poiseuille flow regime ($m^2\,s^{-1}$)
f	fraction of gas molecules that lose momentum as a result of adsorption and desorption at the walls of tube; assumed to be unity
J	gas flux within the tube ($mol\,m^{-2}\,s^{-1}$)
l_m	membrane thickness (m)
L	length of permeate collector tube (m)
M	molecular mass ($kg\,mol^{-1}$)
p	pressure (Pa)
$\tilde{p}$	average pressure (Pa)
p_f	feed pressure (Pa)
p_0	initial pressure (Pa)
p_1	pressure response monitored 0.495 m from the membrane cell (Pa)
p_2	pressure response monitored 2.280 m from the membrane cell (Pa)
P_m	permeability coefficient of gas in membrane ($mol\,m^{-1}\,Pa^{-1}\,s^{-1}$)
r	internal radius of tube (m)
R	universal gas constant ($J\,mol^{-1}\,K^{-1}$)
t	time (s)
T	absolute temperature (K)
x	position within the tube (m)
x'	position within the membrane (m)

Greek symbols

ζ	coefficient of slip (m)
η	dynamic viscosity of the gas ($kg\,m^{-1}\,s^{-1}$)
θ_{exp}	experimental time lag of membrane (s)
θ_m	actual time lag of membrane (s)
λ	mean free path of gas molecules (m)

References

[1] H.A. Daynes, The process of diffusion through a rubber membrane, R. Soc. Proc. A97 (1920) 286.
[2] S.W. Rutherford, D.D. Do, Review of time lag permeation technique as a method for characterization of porous media and membranes, Adsorption 3 (1997) 283.
[3] B. Kruczek, H.L. Frisch, R. Chapanian, Analytical solution for the effective time lag of a membrane in a permeate tube collector in which Knudsen flow regime exists, J. Membr. Sci. 256 (2005) 57.
[4] L.B. Loeb, The Kinetic Theory of Gases, Dover Publications, Inc., New York, 1961, pp. 278–300.
[5] W.D. Niven, The Scientific Papers of James Clerk Maxwell, Dover publications, New York, 1965.
[6] L.J. Stacy, A determination by the constant deflection method of the value of the coefficient of slip for rough and for smooth surfaces in air, Phys. Rev. 21 (1923) 239.
[7] K.S.V. Dyke, The coefficients of viscosity and slip of air and of carbon dioxide by the rotating cylinder method, Phys. Rev. 21 (1923) 250.
[8] H.S. Carslaw, J.C. Jaeger, Conduction of Heat in Solids, 2nd ed., Clarendon Press, Oxford, 1959, p. 402.

Appendix B

Mathematical Derivation of General Solution for a Receiver with Multiple Tanks

B.1 Introduction

The schematic diagram of a generalized multi-tank receiver is presented in Figure B.1. It consists of n tubes with constant cross sectional area A and different lengths making the stem of the equipment or the main line. The individual tubes are separated by a branch line which connects a tank V_i to the stem by means of a tube with a cross sectional area A_{Vi} and the length H_i.

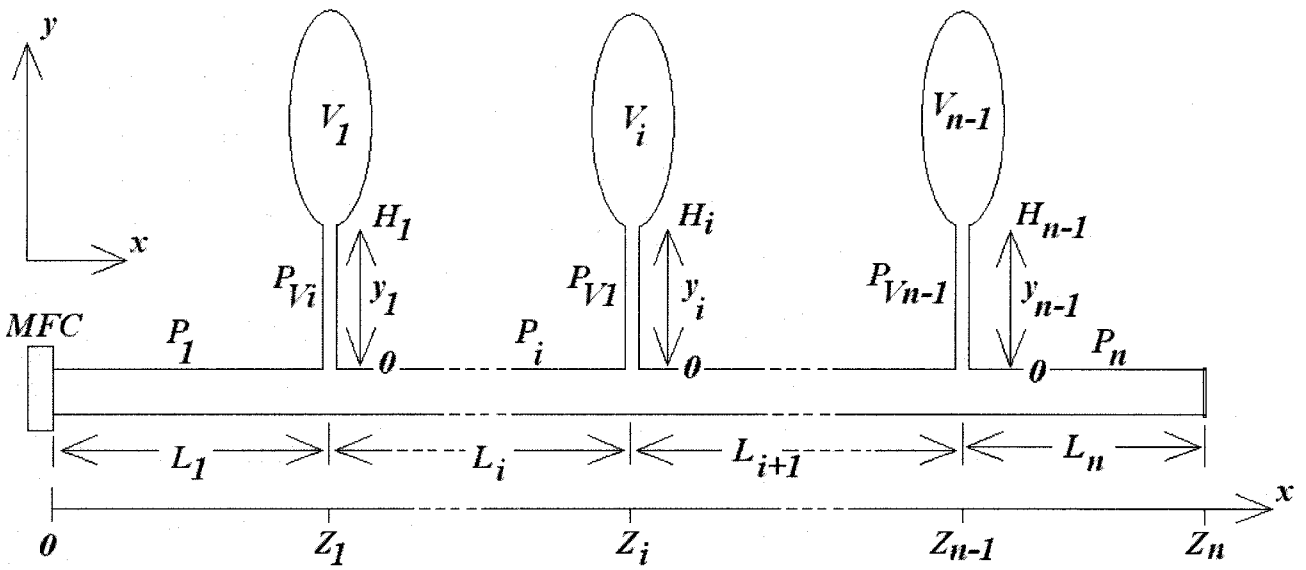

Figure B.1. Schematic representation of a multi-tank receiver of CV system for the modeling purposes.

Since the main objective here is to characterize the resistance to gas accumulation, input flow is assumed to be constant. This assumption makes it possible to determine time lag of the system using the concept of asymptotic solution. For a tube L_i the following diffusion equation, in which D is Knudsen diffusion coefficient, can be applied:

$$\frac{\partial p_i}{\partial t} = D\frac{\partial^2 p_i}{\partial x^2} \tag{B.1}$$

Using the Laplace transform Eq.(B1) becomes:

$$s\bar{p}_i - p_0 = D\frac{\partial^2 \bar{p}_i}{\partial x^2} \tag{B.2}$$

Therefore, for the tube L_i :

$$\bar{p}_i - \frac{p_0}{s} = M_i \sinh(qx) + N_i \cosh(qx) \tag{B.3}$$

Where q is:

$$q = \sqrt{\frac{s}{D}} \tag{B.4}$$

B.2 Boundary Conditions

In general, there are six boundary conditions, which will be applied to evaluate six unknowns $M_1, N_1, M_i, N_i, M_n, N_n$.

B.C.1. End of the stem (main line) is closed:

$$@ \quad x = Z_n \qquad \frac{\partial \bar{p}_n}{\partial x} = 0 \tag{B.5}$$

Differentiation of Eq. (B.3) leads to:

$$\frac{\partial \bar{p}_i}{\partial x} = M_i q \cosh(qx) + N_i q \sinh(qx) \tag{B.6}$$

Substituting Eq. (B.6) for $i = n$ into Eq. (B.5) gives:

$$N_n = -M_n \frac{\cosh(qZ_n)}{\sinh(qZ_n)} \tag{B.7}$$

Substituting Equation (B.7) in Equation (B.3):

$$\bar{p}_n - \frac{p_0}{s} = M_n \left(\sinh(qx) - \frac{\cosh(qZ_n)}{\sinh(qZ_n)} \cosh(qx) \right) \tag{B.8}$$

$$\bar{p}_n - \frac{p_0}{s} = M_n \left(\frac{M_n}{M_n} \sinh(qx) + \frac{N_n}{M_n} \cosh(qx) \right) \tag{B.9}$$

Where $\frac{M_n}{M_n} = 1$ and $\frac{N_n}{M_n} = -\frac{\cosh(qZ_n)}{\sinh(qZ_n)}$

B.C.2. At the entrance of the first tube

$@ x = 0 \qquad Q_1(0,t) = Q_1(0) H(t)$

where, $Q_1(0)$ is constant and $H(t) = \begin{cases} 0 & t < 0 \\ 1 & t \geq 0 \end{cases}$ is step function. Therefore,

$$\frac{\partial p_1(0,t)}{\partial x} = -\frac{RT}{D}\frac{Q_1(0,t)}{A} \tag{B.10}$$

Taking the Laplace transform from Equation (B.10) leads to:

$$\frac{\partial \overline{p}_1(0,s)}{\partial x} = -\frac{RT}{D}\frac{Q_1(0)}{sA} = -\frac{\alpha}{sD} = -\frac{\alpha q}{s^2} \tag{B.11}$$

where $\alpha = \dfrac{RTQ_1(0)}{A}$ is constant. It follows from comparison Eq. (B.11) with Eq. (B.6) that:

$$M_1 = -\frac{RTQ_1(0)}{sDA} = -\frac{qRTQ_1(0)}{s^2} = -\frac{\alpha q}{s^2} \tag{B.12}$$

B.C.3. At the entrance of a tank V_i

$$@\ y_i=H_i \qquad \left(\frac{\partial \overline{p}_{Vi}}{\partial y_i}\right)_{H_i} = -\frac{V_i s}{A_{Vi}D_{Vi}}\left(\overline{p}_{Vi}(H_i) - \frac{p_0}{s}\right) \tag{B.13}$$

Substituting Eqs. (B.3) and (B.6) into Eq. (B.13) leads to:

$$M_{Vi}\cosh(q_{Vi}H_i) + N_{Vi}\sinh(q_{Vi}H_i) = -\frac{V_i q_{Vi}}{A_{Vi}}\left(M_{Vi}\sinh(q_{Vi}H_i) + N_{Vi}\cosh(q_{Vi}H_i)\right) \tag{B.14}$$

or

$$N_{Vi} = -M_{Vi}\frac{\cosh(q_{Vi}H_i) + \dfrac{V_i q_{Vi}}{A_{Vi}}\sinh(q_{Vi}H_i)}{\sinh(q_{Vi}H_i) + \dfrac{V_i q_{Vi}}{A_{Vi}}\cosh(q_{Vi}H_i)} \tag{B.15}$$

$$M_{Vi} = -N_{Vi}\frac{\sinh(q_{Vi}H_i) + \dfrac{V_i q_{Vi}}{A_{Vi}}\cosh(q_{Vi}H_i)}{\cosh(q_{Vi}H_i) + \dfrac{V_i q_{Vi}}{A_{Vi}}\sinh(q_{Vi}H_i)} \tag{B.16}$$

$$\overline{p}_{Vi} - \frac{p_0}{s} = M_{Vi}\left(\sinh(q_{Vi}y_i) + \frac{N_{Vi}}{M_{Vi}}\cosh(q_{Vi}y_i)\right)$$

$$\overline{p}_{Vi} - \frac{p_0}{s} = M_{Vi}\left(\sinh(q_{Vi}y_i) - \frac{\cosh(q_{Vi}H_i) + \dfrac{V_i q_{Vi}}{A_{Vi}}\sinh(q_{Vi}H_i)}{\sinh(q_{Vi}H_i) + \dfrac{V_i q_{Vi}}{A_{Vi}}\cosh(q_{Vi}H_i)}\cosh(q_{Vi}y_i)\right)$$

$$\overline{p}_{Vi} - \frac{p_0}{s} = -M_{Vi}\left(\frac{\cosh\left(q_{Vi}\left(H_i - y_i\right)\right) + \frac{V_i q_{Vi}}{A_{Vi}}\sinh\left(q_{Vi}\left(H_i - y_i\right)\right)}{\sinh\left(q_{Vi}H_i\right) + \frac{V_i q_{Vi}}{A_{Vi}}\cosh\left(q_{Vi}H_i\right)}\right) \tag{B.17}$$

B.Cs 4-6 represent the conditions at the entrance of a branch line, i.e., at $x = Z_i$ and $y_i = 0$.

B.C.4.

$$@\ x = Z_i \qquad DA\left(\frac{\partial \overline{p}_i}{\partial x}\right)_{Z_i} = DA\left(\frac{\partial \overline{p}_{i+1}}{\partial x}\right)_{Z_i} + D_{Vi}A_{Vi}\left(\frac{\partial \overline{p}_{Vi}}{\partial y_i}\right)_0 \tag{B.18}$$

Substituting Eq. (B.6) into Eq. (B.18) gives:

$$DAq\left(M_i\cosh\left(qZ_i\right) + N_i\sinh\left(qZ_i\right)\right) = DAq\left(M_{i+1}\cosh\left(qZ_i\right) + N_{i+1}\sinh\left(qZ_i\right)\right) + D_{Vi}A_{Vi}q_{Vi}M_{Vi} \tag{B.19}$$

B.C.5.

$$@ \quad x = Z_i \qquad \left(\overline{p}_{i+1}\right)_{Z_i} = \left(\overline{p}_{Vi}\right)_0 \tag{B.20}$$

Substituting Eq. (B.3) into Eq. (B.20) gives:

$$N_{Vi} = M_{i+1}\sinh\left(qZ_i\right) + N_{i+1}\cosh\left(qZ_i\right) \tag{B.21}$$

Also, substituting Eq. (B.21) into Eq.16) leads to:

$$M_{Vi} = -\frac{\sinh\left(q_{Vi}H_i\right) + \frac{V_i q_{Vi}}{A_{Vi}}\cosh\left(q_{Vi}H_i\right)}{\cosh\left(q_{Vi}H_i\right) + \frac{V_i q_{Vi}}{A_{Vi}}\sinh\left(q_{Vi}H_i\right)}\left(M_{i+1}\sinh\left(qZ_i\right) + N_{i+1}\cosh\left(qZ_i\right)\right) \tag{B.22}$$

B.C.6.

$$@ \quad x = Z_i \qquad \left(\overline{p}_i\right)_{Z_i} = \left(\overline{p}_{i+1}\right)_{Z_i} \tag{B.23}$$

Substituting Eq. (B.3) into Eq. (B.23) gives:

$$M_i\sinh\left(qZ_i\right) + N_i\cosh\left(qZ_i\right) = M_{i+1}\sinh\left(qZ_i\right) + N_{i+1}\cosh\left(qZ_i\right) \tag{B.24}$$

B.3 General equations

Combining Eqs. (B.19) and (B.24) leads to:

$$\times(\cosh(qZ_i))\left\{M_i\cosh(qZ_i)+N_i\sinh(qZ_i)=(M_{i+1}\cosh(qZ_i)+N_{i+1}\sinh(qZ_i))+\frac{D_{Vi}A_{Vi}q_{Vi}}{DAq}M_{Vi}\right.$$
$$\times(-\sinh(qZ_i))\left.M_i\sinh(qZ_i)+N_i\cosh(qZ_i)=M_{i+1}\sinh(qZ_i)+N_{i+1}\cosh(qZ_i)\right.$$

$$M_i=(M_{i+1}\cosh(qZ_i)\cosh(qZ_i)+N_{i+1}\sinh(qZ_i)\cosh(qZ_i))+\frac{D_{Vi}A_{Vi}q_{Vi}}{DAq}M_{Vi}\cosh(qZ_i)$$
$$-M_{i+1}\sinh(qZ_i)\sinh(qZ_i)-N_{i+1}\cosh(qZ_i)\sinh(qZ_i)$$

or

$$M_i=M_{i+1}+\lambda_i M_{Vi}\cosh(qZ_i) \tag{B.25}$$

where

$$\lambda_i=\frac{D_{Vi}A_{Vi}q_{Vi}}{DAq}=\frac{A_{Vi}}{A}\sqrt{\frac{D_{Vi}}{D}} \tag{B.26}$$

In a similar way:

$$\times(-\sinh(qZ_i))\left\{M_i\cosh(qZ_i)+N_i\sinh(qZ_i)=(M_{i+1}\cosh(qZ_i)+N_{i+1}\sinh(qZ_i))+\frac{D_{Vi}A_{Vi}q_{Vi}}{DAq}M_{Vi}\right.$$
$$\times(\cosh(qZ_i))\left.M_i\sinh(qZ_i)+N_i\cosh(qZ_i)=M_{i+1}\sinh(qZ_i)+N_{i+1}\cosh(qZ_i)\right.$$

$$M_i=(-M_{i+1}\cosh(qZ_i)\sinh(qZ_i)-N_{i+1}\sinh(qZ_i)\sinh(qZ_i))-\frac{D_{Vi}A_{Vi}q_{Vi}}{DAq}M_{Vi}\sinh(qZ_i)$$
$$+M_{i+1}\sinh(qZ_i)\cosh(qZ_i)+N_{i+1}\cosh(qZ_i)\cosh(qZ_i)$$

or

$$N_i=N_{i+1}-\lambda_i M_{Vi}\sinh(qZ_i) \tag{B.25}$$

Therefore:

$$\begin{cases}M_i=M_{i+1}+\lambda_i M_{Vi}\cosh(qZ_i)\\ N_i=N_{i+1}-\lambda_i M_{Vi}\sinh(qZ_i)\end{cases} \tag{B.26}$$

Combining equations for lines downstream from the line *i* gives:

$$\begin{cases}M_i=M_n+\sum_{j=i}^{n-1}\lambda_j M_{Vj}\cosh(qZ_j)\\ N_i=N_n-\sum_{j=i}^{n-1}\lambda_j M_{Vj}\sinh(qZ_j)\end{cases} \tag{B.27}$$

Consequently:

$$M_1=M_n+\sum_{j=1}^{n-1}\lambda_j M_{Vj}\cosh(qZ_j)=-\frac{\alpha q}{s^2} \tag{B.28}$$

and

$$M_n = \frac{-\alpha q / s^2}{1 + \sum_{j=1}^{n-1} \lambda_j \frac{M_{Vj}}{M_n} \cosh(qZ_j)} \tag{B.29}$$

In order to determine M_i and N_i Eq. (B.22) must be applied.

$$M_{Vi} = -\frac{\sinh(q_{Vi}H_i) + \frac{V_i q_{Vi}}{A_{Vi}} \cosh(q_{Vi}H_i)}{\cosh(q_{Vi}H_i) + \frac{V_i q_{Vi}}{A_{Vi}} \sinh(q_{Vi}H_i)} \left(M_{i+1} \sinh(qZ_i) + N_{i+1} \cosh(qZ_i)\right) \tag{B.22}$$

By substituting Eq. (B.27) into Eq. (B.3), the last part of Eq. (B.22) can be evaluated:

$$\begin{aligned} M_{i+1}\sinh(qZ_i) + N_{i+1}\cosh(qZ_i) &= M_n \sinh(qZ_i) + N_n \cosh(qZ_i) + \\ &\sum_{j=i+1}^{n-1} \lambda_j M_{Vj} \cosh(qZ_j)\sinh(qZ_i) - \sum_{j=i+1}^{n-1} \lambda_j M_{Vj} \sinh(qZ_j)\cosh(qZ_i) \\ &= M_n \sinh(qZ_i) + N_n \cosh(qZ_i) + \\ &\sum_{j=i+1}^{n-1} \lambda_j M_{Vj} \left(\cosh(qZ_j)\sinh(qZ_i) - \sinh(qZ_j)\cosh(qZ_i)\right) \\ &= M_n \sinh(qZ_i) + N_n \cosh(qZ_i) - \sum_{j=i+1}^{n-1} \lambda_j M_{Vj} \sinh\left(q(Z_j - Z_i)\right) \end{aligned} \tag{B.30}$$

Substituting Eq. (B.30) into Eq. (B.22) gives:

$$\frac{M_{Vi}}{M_n} = -\frac{\sinh(q_{Vi}H_i) + \frac{V_i q_{Vi}}{A_{Vi}} \cosh(q_{Vi}H_i)}{\cosh(q_{Vi}H_i) + \frac{V_i q_{Vi}}{A_{Vi}} \sinh(q_{Vi}H_i)} \left(\sinh(qZ_i) + \frac{N_n}{M_n} \cosh(qZ_i) - \sum_{j=i+1}^{n-1} \lambda_j \frac{M_{Vj}}{M_n} \sinh\left(q(Z_j - Z_i)\right) \right)$$

or

$$\frac{M_{Vi}}{M_n} = -\delta_i \sinh(qZ_i) - \delta_i \frac{N_n}{M_n} \cosh(qZ_i) + \delta_i \sum_{j=i+1}^{n-1} \lambda_j \frac{M_{Vj}}{M_n} \sinh\left(q(Z_j - Z_i)\right) \tag{B.32}$$

where,

$$\delta_i = \frac{\sinh(q_{Vi}H_i) + \frac{V_i q_{Vi}}{A_{Vi}} \cosh(q_{Vi}H_i)}{\cosh(q_{Vi}H_i) + \frac{V_i q_{Vi}}{A_{Vi}} \sinh(q_{Vi}H_i)} \tag{B.34}$$

and

$$\frac{N_n}{M_n} = -\frac{\cosh(qZ_n)}{\sinh(qZ_n)} \tag{B.35}$$

Eq. (B.32) can be rearranged to:

$$\frac{M_{Vi}}{M_n} = \frac{\delta_i}{\sinh(qZ_n)}\left(\cosh\left(q(Z_n - Z_i)\right) + \sum_{j=i+1}^{n-1}\lambda_j\left(\frac{M_{Vj}}{M_n}\sinh(qZ_n)\right)\sinh\left(q(Z_j - Z_i)\right)\right) \tag{B.36}$$

or

$$\frac{M_{Vi}}{M_n}\sinh(qZ_n) = q\frac{\delta_i}{q}\left(\cosh\left(q(Z_n - Z_i)\right) + \sum_{j=i+1}^{n-1}\lambda_j\left(\frac{M_{Vj}}{M_n}\sinh(qZ_n)\right)\sinh\left(q(Z_j - Z_i)\right)\right) \tag{B.37}$$

B.4 Equation for the main line

To find a general equation for the main line (stem), Eq. (B.3) can be used:

$$\overline{p}_i - \frac{p_0}{s} = M_i\sinh(qx_i) + N_i\cosh(qx_i) \tag{B.3}$$

Substituting Eq. (B.27) into Eq. (B.3) gives:

$$\overline{p}_i - \frac{p_0}{s} = M_n\left(\sinh(qx_i) + \frac{N_n}{M_n}\cosh(qx_i)\right) + M_n\sum_{j=i}^{n-1}\lambda_j\frac{M_{Vj}}{M_n}\left(\cosh(qZ_j)\sinh(qx_i) - \sinh(qZ_j)\cosh(qx_i)\right) \tag{B.38}$$

Then, also substituting Eq. (B.35) gives:

$$\overline{p}_i - \frac{p_0}{s} = -\frac{M_n}{\sinh(qZ_n)}\left(\cosh\left(q(Z_n - x_i)\right) + \sum_{j=i}^{n-1}\lambda_j\frac{M_{Vj}}{M_n}\sinh\left(q(Z_j - x_i)\right)\sinh(qZ_n)\right) \tag{B.39}$$

Using Eq. (B.29) for M_n the general equation for tube L_i will be:

$$\overline{p}_i - \frac{p_0}{s} = \frac{\alpha q/s^2\left(\cosh\left(q(Z_n - x_i)\right) + \sum_{j=i}^{n-1}\lambda_j\frac{M_{Vj}}{M_n}\sinh(qZ_n)\sinh\left(q(Z_j - x_i)\right)\right)}{\sinh(qZ_n)\left(1 + \sum_{j=1}^{n-1}\lambda_j\frac{M_{Vj}}{M_n}\cosh(qZ_j)\right)} \tag{B.40}$$

Comparing to the general equation in Jaeger's approach, $\overline{p}_i - \frac{p_0}{s} = \frac{f_i(s)}{s^2\,\Delta(s)}$

$$f_i(s) = \alpha q\left[\cosh\left(q(Z_n - x)\right) + \sum_{j=i}^{n-1}\lambda_j\left(\frac{M_{Vj}}{M_n}\sinh(qZ_n)\right)\sinh\left(q(Z_j - x)\right)\right] \tag{B.41}$$

$$\Delta(s)=\sinh(qZ_n)+\sum_{j=1}^{n-1}\lambda_j\left(\frac{M_{Vj}}{M_n}\sinh(qZ_n)\right)\cosh(qZ_j) \tag{B.42}$$

B.5 Equation for a branch

Combining Eqs. (B.17), (B.29) and (B.36) will lead to a general solution for a branch:

$$\overline{p}_{Vi}-\frac{p_0}{s}=\frac{\alpha\delta_i q}{s^2}\left(\frac{\cosh(q(Z_n-Z_i))+\sum_{j=i+1}^{n-1}\lambda_j\left(\frac{M_{Vj}}{M_n}\sinh(qZ_n)\right)\sinh(q(Z_j-Z_i))}{\sinh(qZ_n)+\sum_{j=1}^{n-1}\lambda_j\left(\frac{M_{Vj}}{M_n}\sinh(qZ_n)\right)\cosh(qZ_j)}\right)\times \left(\frac{\cosh(q_{Vi}(H_i-y_i))+\frac{V_i q_{Vi}}{A_{Vi}}\sinh(q_{Vi}(H_i-y_i))}{\sinh(q_{Vi}H_i)+\frac{V_i q_{Vi}}{A_{Vi}}\cosh(q_{Vi}H_i)}\right) \tag{B.43}$$

Comparing to the general equation in Jaeger's approach, $\overline{p}_{Vi}-\frac{p_0}{s}=\frac{f_{Vi}(s)}{s^2\,\Delta_V(s)}$

$$f_{Vi}(s)=\alpha q\delta_i\left(\cosh(q(Z_n-Z_i))+\sum_{j=i+1}^{n-1}\lambda_j\left(\frac{M_{Vj}}{M_n}\sinh(qZ_n)\right)\sinh(q(Z_j-Z_i))\right)\times \left(\cosh(q_{Vi}(H_i-y_i))+\frac{V_i q_{Vi}}{A_{Vi}}\sinh(q_{Vi}(H_i-y_i))\right) \tag{B.44}$$

$$\Delta_V(s)=\left(\sinh(qZ_n)+\sum_{j=1}^{n-1}\lambda_j\left(\frac{M_{Vj}}{M_n}\sinh(qZ_n)\right)\cosh(qZ_j)\right)\left(\sinh(q_{Vi}H_i)+\frac{V_i q_{Vi}}{A_{Vi}}\cosh(q_{Vi}H_i)\right)$$

$$\Delta_V(s)=\Delta(s)\left(\sinh(q_{Vi}H_i)+\frac{V_i q_{Vi}}{A_{Vi}}\cosh(q_{Vi}H_i)\right) \tag{B.45}$$

B.6 Limits of some parameters

$$\delta_i=\frac{\sinh(q_{Vi}H_i)+\frac{V_i q_{Vi}}{A_{Vi}}\cosh(q_{Vi}H_i)}{\cosh(q_{Vi}H_i)+\frac{V_i q_{Vi}}{A_{Vi}}\sinh(q_{Vi}H_i)} \tag{B.34}$$

$$\lim_{s\to 0}\frac{\delta_j}{q_{Vj}}=\lim_{s\to 0}\frac{H_j\dfrac{\sinh\left(q_{Vj}H_j\right)}{q_{Vj}H_j}+\dfrac{V_j}{A_{Vj}}\cosh\left(q_{Vj}H_j\right)}{\cosh\left(q_{Vj}H_j\right)+\dfrac{V_jq_{Vj}}{A_{Vj}}\sinh\left(q_{Vj}H_j\right)}=\left(H_j+\frac{V_j}{A_{Vj}}\right) \tag{B.46}$$

$$\lim_{s\to 0}\frac{\delta_j}{q_{Vj}}=\lim_{s\to 0}\frac{H_j\dfrac{\sinh\left(q_{Vj}H_j\right)}{q_{Vj}H_j}+\dfrac{V_j}{A_{Vj}}\cosh\left(q_{Vj}H_j\right)}{\cosh\left(q_{Vj}H_j\right)+\dfrac{V_jq_{Vj}}{A_{Vj}}\sinh\left(q_{Vj}H_j\right)}=\left(H_j+\frac{V_j}{A_{Vj}}\right) \tag{B.47}$$

$$\lim_{s\to 0}\lambda_i\frac{\delta_i}{q}=\frac{A_{Vi}}{A}\left(H_i+\frac{V_i}{A_{Vi}}\right)=\frac{A_{Vi}H_i}{A}+\frac{V_i}{A} \tag{B.48}$$

Therefore, the differentiation of δ_j can be written in different forms as follow:

$$\frac{d\delta_i}{dq_{Vi}} = \frac{\left(H_i + \frac{V_i}{A_{Vi}}\right)}{\left(\cosh\left(q_{Vi}H_i\right) + \frac{V_i q_{Vi}}{A_{Vi}}\sinh\left(q_{Vi}H_i\right)\right)^2} - \frac{\frac{D}{D_{Vi}}q^2\left(\frac{V_i}{A_{Vi}}\right)^2 H_i}{\left(\cosh\left(q_{Vi}H_i\right) + \frac{V_i q_{Vi}}{A_{Vi}}\sinh\left(q_{Vi}H_i\right)\right)^2} \tag{B.49}$$

$$\lambda_j \lim_{s\to 0}\frac{d\delta_j}{dq} = \lambda_j\sqrt{\frac{D}{D_{Vj}}}\lim_{s\to 0}\frac{d\delta_j}{dq_{Vj}} = \left(\frac{A_{Vj}}{A}H_j + \frac{V_j}{A}\right) \tag{B.50}$$

$$\lim_{s\to 0}\frac{1}{q_{Vj}^2}\frac{d\delta_j}{dq_{Vj}} = \lim_{s\to 0}\frac{\left(H_j + \frac{V_j}{A_{Vj}}\right)\cosh\left(q_{Vj}H_j\right)}{q_{Vj}^2\left(\cosh\left(q_{Vj}H_j\right) + \frac{V_j q_{Vj}}{A_{Vj}}\sinh\left(q_{Vj}H_j\right)\right)} - \left(H_j + \frac{V_j}{A_{Vj}}\right)^2 H_j - \left(\frac{V_j}{A_{Vj}}\right)^2 H_j \tag{B.51}$$

$$\lambda_j\frac{d\delta_j}{dq} = \lambda_j\sqrt{\frac{D}{D_{Vj}}}\frac{d\delta_j}{dq_{Vj}} = \lambda_j\sqrt{\frac{D}{D_{Vj}}}\frac{\left(H_j + \frac{V_j}{A_{Vj}}\right) - \left(\frac{V_j q_{Vj}}{A_{Vj}}\right)^2 H_j}{\left(\cosh\left(q_{Vj}H_j\right) + \frac{V_j q_{Vj}}{A_{Vj}}\sinh\left(q_{Vj}H_j\right)\right)^2} \tag{B.52}$$

$$\lambda_j \lim_{s\to 0}\frac{1}{q^2}\frac{d\delta_j}{dq} = \lim_{s\to 0}\frac{1}{q^2}\lambda_j\frac{\delta_j}{q}\frac{\left(H_j + \frac{V_j}{A_{Vj}}\right)\cosh\left(q_{Vj}H_j\right) + \frac{V_j q_{Vj}}{A_{Vj}}H_j\sinh\left(q_{Vj}H_j\right)}{H_j\frac{\sinh\left(q_{Vj}H_j\right)}{q_{Vi}H_j} + \frac{V_j}{A_{Vj}}\cosh\left(q_{Vj}H_j\right)} - \frac{D}{D_{Vj}}\left(\frac{A_{Vi}H_i}{A} + \frac{V_i}{A}\right)\left(H_j^2 + 2\frac{V_j}{A_{Vj}}H_j\right) \tag{B.53}$$

$$\lambda_j \lim_{s\to 0}\frac{1}{q^2}\frac{d\delta_j}{dq} = \lim_{s\to 0}\frac{1}{q^2}\lambda_j \frac{\delta_j}{q}\frac{\left(H_j+\frac{V_j}{A_{Vj}}\right)\cosh\left(q_{Vj}H_j\right)}{H_j\frac{\sinh\left(q_{Vj}H_j\right)}{q_{Vi}H_j}+\frac{V_j}{A_{Vj}}\cosh\left(q_{Vj}H_j\right)}+\frac{D}{D_{Vj}}\frac{A_{Vi}}{A}\frac{V_j}{A_{Vj}}H_j^2-\frac{D}{D_{Vj}}\left(\frac{A_{Vi}H_i}{A}+\frac{V_i}{A}\right)\left(H_j^2+2\frac{V_j}{A_{Vj}}H_j\right) \quad \text{(B.54)}$$

$$\lambda_j \lim_{s\to 0}\frac{1}{q^2}\frac{d\delta_j}{dq} = \lim_{s\to 0}\frac{1}{q^2}\lambda_j \frac{\delta_j}{q}\frac{\left(H_j+\frac{V_j}{A_{Vj}}\right)\cosh\left(q_{Vj}H_j\right)}{H_j\frac{\sinh\left(q_{Vj}H_j\right)}{q_{Vi}H_j}+\frac{V_j}{A_{Vj}}\cosh\left(q_{Vj}H_j\right)}-\frac{D}{D_{Vj}}\frac{A_{Vi}}{A}\left\{\left(H_j+\frac{V_j}{A_{Vj}}\right)^2 H_j+\left(\frac{V_j}{A_{Vj}}\right)^2 H_j\right\} \quad \text{(B.55)}$$

Differentiations of the above relationships lead to:

$$\frac{d\delta_i}{dq_{Vi}} = \frac{\left\{\left(\left(H_i+\frac{V_i}{A_{Vi}}\right)\cosh\left(q_{Vi}H_i\right)+\frac{V_iq_{Vi}}{A_{Vi}}H_i\sinh\left(q_{Vi}H_i\right)\right)\left(\cosh\left(q_{Vi}H_i\right)+\frac{V_iq_{Vi}}{A_{Vi}}\sinh\left(q_{Vi}H_i\right)\right)-\right.}{\left.\left(\left(H_i+\frac{V_i}{A_{Vi}}\right)\sinh\left(q_{Vi}H_i\right)+\frac{V_iq_{Vi}}{A_{Vi}}H_i\cosh\left(q_{Vi}H_i\right)\right)\left(\sinh\left(q_{Vi}H_i\right)+\frac{V_iq_{Vi}}{A_{Vi}}\cosh\left(q_{Vi}H_i\right)\right)\right\}}{\left(\cosh\left(q_{Vi}H_i\right)+\frac{V_iq_{Vi}}{A_{Vi}}\sinh\left(q_{Vi}H_i\right)\right)^2}$$

$$\frac{d\delta_i}{dq_{Vi}} = \frac{\left\{\begin{array}{l}\left(\left(H_i+\frac{V_i}{A_{Vi}}\right)\cosh^2\left(q_{Vi}H_i\right)+\left(H_i+\frac{V_i}{A_{Vi}}\right)\frac{V_iq_{Vi}}{A_{Vi}}\cosh\left(q_{Vi}H_i\right)\sinh\left(q_{Vi}H_i\right)\right)+\left(\frac{V_iq_{Vi}}{A_{Vi}}H_i\cosh\left(q_{Vi}H_i\right)\sinh\left(q_{Vi}H_i\right)+\left(\frac{V_iq_{Vi}}{A_{Vi}}\right)^2H_i\sinh^2\left(q_{Vi}H_i\right)\right)\\ -\left(\left(H_i+\frac{V_i}{A_{Vi}}\right)\sinh^2\left(q_{Vi}H_i\right)+\left(H_i+\frac{V_i}{A_{Vi}}\right)\frac{V_iq_{Vi}}{A_{Vi}}\cosh\left(q_{Vi}H_i\right)\sinh\left(q_{Vi}H_i\right)\right)-\left(\frac{V_iq_{Vi}}{A_{Vi}}H_i\cosh\left(q_{Vi}H_i\right)\sinh\left(q_{Vi}H_i\right)+\left(\frac{V_iq_{Vi}}{A_{Vi}}\right)^2H_i\cosh^2\left(q_{Vi}H_i\right)\right)\end{array}\right\}}{\left(\cosh\left(q_{Vi}H_i\right)+\frac{V_iq_{Vi}}{A_{Vi}}\sinh\left(q_{Vi}H_i\right)\right)^2}$$

$$\frac{d\delta_i}{dq_{Vi}} = \frac{\left\{\left(H_i+\frac{V_i}{A_{Vi}}\right)-\left(\frac{V_iq_{Vi}}{A_{Vi}}\right)^2H_i\right\}\left(\cosh^2\left(q_{Vi}H_i\right)-\sinh^2\left(q_{Vi}H_i\right)\right)}{\left(\cosh\left(q_{Vi}H_i\right)+\frac{V_iq_{Vi}}{A_{Vi}}\sinh\left(q_{Vi}H_i\right)\right)^2}$$

$$\frac{d\delta_i}{dq_{Vi}} = \frac{\left(H_i+\frac{V_i}{A_{Vi}}\right)}{\left(\cosh\left(q_{Vi}H_i\right)+\frac{V_iq_{Vi}}{A_{Vi}}\sinh\left(q_{Vi}H_i\right)\right)^2}-\frac{\frac{D}{D_{Vi}}q^2\left(\frac{V_i}{A_{Vi}}\right)^2H_i}{\left(\cosh\left(q_{Vi}H_i\right)+\frac{V_iq_{Vi}}{A_{Vi}}\sinh\left(q_{Vi}H_i\right)\right)^2} \qquad (------)$$

$$\delta_j = \frac{\sinh\left(q_{Vj}H_j\right)+\frac{V_jq_{Vj}}{A_{Vj}}\cosh\left(q_{Vj}H_j\right)}{\cosh\left(q_{Vj}H_j\right)+\frac{V_jq_{Vj}}{A_{Vj}}\sinh\left(q_{Vj}H_j\right)}$$

$$\lim_{s\to0}\frac{\delta_j}{q_{Vj}} = \lim_{s\to0}\frac{H_j\frac{\sinh\left(q_{Vj}H_j\right)}{q_{Vj}H_j}+\frac{V_j}{A_{Vj}}\cosh\left(q_{Vj}H_j\right)}{\cosh\left(q_{Vj}H_j\right)+\frac{V_jq_{Vj}}{A_{Vj}}\sinh\left(q_{Vj}H_j\right)} = \left(H_j+\frac{V_j}{A_{Vj}}\right)$$

$$\frac{d\delta_j}{dq_{Vj}} = \frac{\left(H_j + \frac{V_j}{A_{Vj}}\right)\cosh\left(q_{Vj}H_j\right) + \frac{V_j q_{Vj}}{A_{Vj}} H_j \sinh\left(q_{Vj}H_j\right)}{\cosh\left(q_{Vj}H_j\right) + \frac{V_j q_{Vj}}{A_{Vj}}\sinh\left(q_{Vj}H_j\right)} - \delta_j \frac{\left(H_j + \frac{V_j}{A_{Vj}}\right)\sinh\left(q_{Vj}H_j\right) + \frac{V_j q_{Vj}}{A_{Vj}} H_j \cosh\left(q_{Vj}H_j\right)}{\cosh\left(q_{Vj}H_j\right) + \frac{V_j q_{Vj}}{A_{Vj}}\sinh\left(q_{Vj}H_j\right)}$$

$$\frac{d\delta_j}{dq_{Vj}} = \frac{\left(H_j + \frac{V_j}{A_{Vj}}\right)\cosh\left(q_{Vj}H_j\right)}{\cosh\left(q_{Vj}H_j\right) + \frac{V_j q_{Vj}}{A_{Vj}}\sinh\left(q_{Vj}H_j\right)} + q_{Vj}^2 \frac{\frac{V_j}{A_{Vj}} H_j^2 \frac{\sinh\left(q_{Vj}H_j\right)}{q_{Vj}H_j}}{\cosh\left(q_{Vj}H_j\right) + \frac{V_j q_{Vj}}{A_{Vj}}\sinh\left(q_{Vj}H_j\right)} - q_{Vj}^2 \frac{\delta_j}{q_{Vj}} \frac{\left(H_j^2 + \frac{V_j}{A_{Vj}} H_j\right)\frac{\sinh\left(q_{Vj}H_j\right)}{q_{Vj}H_j} + \frac{V_j}{A_{Vj}} H_j \cosh\left(q_{Vj}H_j\right)}{\cosh\left(q_{Vj}H_j\right) + \frac{V_j q_{Vj}}{A_{Vj}}\sinh\left(q_{Vj}H_j\right)}$$

$$\lim_{s\to 0} \frac{1}{q_{Vj}^2}\frac{d\delta_j}{dq_{Vj}} = \lim_{s\to 0} \frac{\left(H_j + \frac{V_j}{A_{Vj}}\right)\cosh\left(q_{Vj}H_j\right)}{q_{Vj}^2\left(\cosh\left(q_{Vj}H_j\right) + \frac{V_j q_{Vj}}{A_{Vj}}\sinh\left(q_{Vj}H_j\right)\right)} + \frac{V_j}{A_{Vj}} H_j^2 - \left(H_j + \frac{V_j}{A_{Vj}}\right)\left(H_j^2 + 2\frac{V_j}{A_{Vj}} H_j\right)$$

$$\frac{V_j}{A_{Vj}} H_j^2 - \left(H_j + \frac{V_j}{A_{Vj}}\right)\left(H_j^2 + 2\frac{V_j}{A_{Vj}} H_j\right) = \frac{V_j}{A_{Vj}} H_j^2 - H_j^3 - 2\frac{V_j}{A_{Vj}} H_j^2 - \frac{V_j}{A_{Vj}} H_j^2 - 2\left(\frac{V_j}{A_{Vj}}\right)^2 H_j = -H_j^3 - 2\frac{V_j}{A_{Vj}} H_j^2 - 2\left(\frac{V_j}{A_{Vj}}\right)^2 H_j = -\left(H_j + \frac{V_j}{A_{Vj}}\right)^2 H_j - \left(\frac{V_j}{A_{Vj}}\right)^2 H_j$$

$$\lim_{s\to 0} \frac{1}{q_{Vj}^2}\frac{d\delta_j}{dq_{Vj}} = \lim_{s\to 0} \frac{\left(H_j + \frac{V_j}{A_{Vj}}\right)\cosh\left(q_{Vj}H_j\right)}{q_{Vj}^2\left(\cosh\left(q_{Vj}H_j\right) + \frac{V_j q_{Vj}}{A_{Vj}}\sinh\left(q_{Vj}H_j\right)\right)} - \left(H_j + \frac{V_j}{A_{Vj}}\right)^2 H_j - \left(\frac{V_j}{A_{Vj}}\right)^2 H_j$$

$$\lim_{s\to 0}\frac{1}{q_{Vj}^2}\frac{d\delta_j}{dq_{Vj}}=\lim_{s\to 0}\frac{\left(H_j+\frac{V_j}{A_{Vj}}\right)\cosh\left(q_{Vj}H_j\right)}{q_{Vj}^2\left(\cosh\left(q_{Vj}H_j\right)+\frac{V_jq_{Vj}}{A_{Vj}}\sinh\left(q_{Vj}H_j\right)\right)}-\left(H_j+\frac{V_j}{A_{Vj}}\right)^2H_j-\left(\frac{V_j}{A_{Vj}}\right)^2H_j$$

$$q_i=\sqrt{\frac{s}{D_i}}\qquad\&\qquad\lambda_i=\frac{D_{Vi}A_{Vi}q_{Vi}}{DAq}=\frac{A_{Vi}}{A}\sqrt{\frac{D_{Vi}}{D}}\qquad\Rightarrow\qquad q_{Vi}=q\sqrt{\frac{D}{D_{Vi}}}\quad or\quad q=q_{Vi}\sqrt{\frac{D_{Vi}}{D}}\qquad\Rightarrow\qquad\frac{df}{dq}=\sqrt{\frac{D}{D_{Vi}}}\frac{df}{dq_{Vi}}$$

$$\delta_i=q_{Vi}\frac{H_i\frac{\sinh\left(q_{Vi}H_i\right)}{q_{Vi}H_i}+\frac{V_i}{A_{Vi}}\cosh\left(q_{Vi}H_i\right)}{\cosh\left(q_{Vi}H_i\right)+\frac{V_iq_{Vi}^2}{A_{Vi}}H_i\frac{\sinh\left(q_{Vi}H_i\right)}{q_{Vi}H_i}}=q\sqrt{\frac{D}{D_{Vi}}}\frac{H_i\frac{\sinh\left(q_{Vi}H_i\right)}{q_{Vi}H_i}+\frac{V_i}{A_{Vi}}\cosh\left(q_{Vi}H_i\right)}{\cosh\left(q_{Vi}H_i\right)+\frac{V_iq_{Vi}^2}{A_{Vi}}H_i\frac{\sinh\left(q_{Vi}H_i\right)}{q_{Vi}H_i}}$$

$$\lim_{s\to 0}\lambda_i\frac{\delta_i}{q}=\frac{A_{Vi}}{A}\left(H_i+\frac{V_i}{A_{Vi}}\right)=\frac{A_{Vi}H_i}{A}+\frac{V_i}{A}$$

$$\lambda_j\frac{d\delta_j}{dq}=\lambda_j\sqrt{\frac{D}{D_{Vj}}}\frac{d\delta_j}{dq_{Vj}}=\sqrt{\frac{D}{D_{Vj}}}\lambda_j\frac{\left(H_j+\frac{V_j}{A_{Vj}}\right)\cosh\left(q_{Vj}H_j\right)+\frac{V_jq_{Vj}}{A_{Vj}}H_j\sinh\left(q_{Vj}H_j\right)}{\cosh\left(q_{Vj}H_j\right)+\frac{V_jq_{Vj}}{A_{Vj}}\sinh\left(q_{Vj}H_j\right)}-\sqrt{\frac{D}{D_{Vj}}}\lambda_j\delta_j\frac{\left(H_j+\frac{V_j}{A_{Vj}}\right)\sinh\left(q_{Vj}H_j\right)+\frac{V_jq_{Vj}}{A_{Vj}}H_j\cosh\left(q_{Vj}H_j\right)}{\cosh\left(q_{Vj}H_j\right)+\frac{V_jq_{Vj}}{A_{Vj}}\sinh\left(q_{Vj}H_j\right)}$$

$$\lambda_j\frac{d\delta_j}{dq}=\lambda_j\sqrt{\frac{D}{D_{Vj}}}\frac{d\delta_j}{dq_{Vj}}=\sqrt{\frac{D}{D_{Vj}}}\lambda_j\frac{\left(H_j+\frac{V_j}{A_{Vj}}\right)\cosh\left(q_{Vj}H_j\right)+\frac{V_jq_{Vj}}{A_{Vj}}H_j\sinh\left(q_{Vj}H_j\right)}{\cosh\left(q_{Vj}H_j\right)+\frac{V_jq_{Vj}}{A_{Vj}}\sinh\left(q_{Vj}H_j\right)}-\sqrt{\frac{D}{D_{Vj}}}\lambda_j\delta_j\frac{\left(H_j+\frac{V_j}{A_{Vj}}\right)\sinh\left(q_{Vj}H_j\right)+\frac{V_jq_{Vj}}{A_{Vj}}H_j\cosh\left(q_{Vj}H_j\right)}{\cosh\left(q_{Vj}H_j\right)+\frac{V_jq_{Vj}}{A_{Vj}}\sinh\left(q_{Vj}H_j\right)}$$

$$\lambda_j \frac{d\delta_j}{dq} = \lambda_j \sqrt{\frac{D}{D_{Vj}}} \frac{d\delta_j}{dq_{Vj}} = \lambda_j \sqrt{\frac{D}{D_{Vj}}} \frac{\left(H_j + \frac{V_j}{A_{Vj}}\right) - \left(\frac{V_j q_{Vj}}{A_{Vj}}\right)^2 H_j}{\left(\cosh\left(q_{Vj} H_j\right) + \frac{V_j q_{Vj}}{A_{Vj}} \sinh\left(q_{Vj} H_j\right)\right)^2}$$

$$\lambda_j \lim_{s\to 0} \frac{d\delta_j}{dq} = \lambda_j \sqrt{\frac{D}{D_{Vj}}} \lim_{s\to 0} \frac{d\delta_j}{dq_{Vj}} = \left(\frac{A_{Vj}}{A} H_j + \frac{V_j}{A}\right)$$

$$\delta_i = \frac{\sinh\left(q_{Vi} H_i\right) + \frac{V_i q_{Vi}}{A_{Vi}} \cosh\left(q_{Vi} H_i\right)}{\cosh\left(q_{Vi} H_i\right) + \frac{V_i q_{Vi}}{A_{Vi}} \sinh\left(q_{Vi} H_i\right)}$$

$$\lambda_j \lim_{s\to 0} \frac{d\delta_j}{dq} = \lambda_j \sqrt{\frac{D}{D_{Vj}}} \lim_{s\to 0} \frac{d\delta_j}{dq_{Vj}} = \left(\frac{A_{Vj}}{A} H_j + \frac{V_j}{A}\right)$$

$$\lambda_j \lim_{s\to 0} \frac{1}{q^2} \frac{d\delta_j}{dq} = \lambda_j \sqrt{\frac{D}{D_{Vj}}} \lim_{s\to 0} \frac{1}{q^2} \frac{d\delta_j}{dq_{Vj}} = \lambda_j \sqrt{\frac{D}{D_{Vj}}} \lim_{s\to 0} \frac{\left(H_j + \frac{V_j}{A_{Vj}}\right) \cosh\left(q_{Vj} H_j\right) + \frac{V_j q_{Vj}}{A_{Vj}} H_j \sinh\left(q_{Vj} H_j\right)}{q^2 \left(\cosh\left(q_{Vj} H_j\right) + \frac{V_j q_{Vj}}{A_{Vj}} \sinh\left(q_{Vj} H_j\right)\right)} - \frac{D}{D_{Vj}} \lim_{s\to 0} \lambda_j \frac{\delta_j}{q} \frac{\left(H_j^2 + \frac{V_j}{A_{Vj}} H_j\right) \frac{\sinh\left(q_{Vj} H_j\right)}{q_{Vj} H_j} + \frac{V_j}{A_{Vj}} H_j \cosh\left(q_{Vj} H_j\right)}{\cosh\left(q_{Vj} H_j\right) + \frac{V_j q_{Vj}}{A_{Vj}} \sinh\left(q_{Vj} H_j\right)}$$

$$\lambda_j \lim_{s\to 0} \frac{1}{q^2} \frac{d\delta_j}{dq} = \lambda_j \sqrt{\frac{D}{D_{Vj}}} \lim_{s\to 0} \frac{1}{q^2} \frac{d\delta_j}{dq_{Vj}} = \lambda_j \sqrt{\frac{D}{D_{Vj}}} \lim_{s\to 0} \frac{\left(H_j + \frac{V_j}{A_{Vj}}\right) \cosh\left(q_{Vj} H_j\right) + \frac{V_j q_{Vj}}{A_{Vj}} H_j \sinh\left(q_{Vj} H_j\right)}{q^2 \left(\cosh\left(q_{Vj} H_j\right) + \frac{V_j q_{Vj}}{A_{Vj}} \sinh\left(q_{Vj} H_j\right)\right)} - \frac{D}{D_{Vj}} \left(\frac{A_{Vj}}{A} H_j + \frac{V_j}{A}\right) \left(H_j^2 + 2 \frac{V_j}{A_{Vj}} H_j\right)$$

$$\lambda_j \lim_{s\to 0}\frac{1}{q^2}\frac{d\delta_j}{dq} = \lambda_j\sqrt{\frac{D}{D_{Vj}}}\lim_{s\to 0}\frac{1}{q^2}\frac{d\delta_j}{dq_{Vj}} = \lambda_j\sqrt{\frac{D}{D_{Vj}}}\lim_{s\to 0}\frac{\left(H_j+\frac{V_j}{A_{Vj}}\right)}{q^2\left(\cosh\left(q_{Vj}H_j\right)+\frac{V_j q_{Vj}}{A_{Vj}}\sinh\left(q_{Vj}H_j\right)\right)^2} - \frac{A_{Vj}}{A}\frac{D}{D_{Vj}}\left(\frac{V_j}{A_{Vj}}\right)^2 H_j$$

$$\lambda_j \lim_{s\to 0}\frac{1}{q^2}\frac{d\delta_j}{dq} = \lambda_j\sqrt{\frac{D}{D_{Vj}}}\lim_{s\to 0}\frac{1}{q^2}\frac{d\delta_j}{dq_{Vj}} = \lambda_j\sqrt{\frac{D}{D_{Vj}}}\left(H_j+\frac{V_j}{A_{Vj}}\right)\lim_{s\to 0}\frac{\cosh\left(q_{Vj}H_j\right)}{q^2\left(\cosh\left(q_{Vj}H_j\right)+\frac{V_j q_{Vj}}{A_{Vj}}\sinh\left(q_{Vj}H_j\right)\right)} + \frac{D}{D_{Vj}}\frac{V_j}{A}H_j^2 - \frac{D}{D_{Vj}}\left(\frac{A_{Vj}}{A}H_j+\frac{V_j}{A}\right)\left\{\left(H_j^2+\frac{V_j}{A_{Vj}}H_j\right)+\frac{V_j}{A_{Vj}}H_j\right\}$$

$$\lambda_j \lim_{s\to 0}\frac{1}{q^2}\frac{d\delta_j}{dq} = \lambda_j\sqrt{\frac{D}{D_{Vj}}}\lim_{s\to 0}\frac{1}{q^2}\frac{d\delta_j}{dq_{Vj}} = \sqrt{\frac{D}{D_{Vj}}}\lim_{s\to 0}\lambda_j\delta_j\frac{\left(H_j+\frac{V_j}{A_{Vj}}\right)\cosh\left(q_{Vj}H_j\right)+\frac{V_j q_{Vj}}{A_{Vj}}H_j\sinh\left(q_{Vj}H_j\right)}{q^2\left(\sinh\left(q_{Vi}H_i\right)+\frac{V_i q_{Vi}}{A_{Vi}}\cosh\left(q_{Vi}H_i\right)\right)} - \frac{D}{D_{Vj}}\left(\frac{A_{Vi}H_i}{A}+\frac{V_i}{A}\right)\left(H_j^2+2\frac{V_j}{A_{Vj}}H_j\right)$$

$$\lambda_j \lim_{s\to 0}\frac{1}{q^2}\frac{d\delta_j}{dq} = \lim_{s\to 0}\frac{1}{q^2}\lambda_j\frac{\delta_j}{q}\frac{\left(H_j+\frac{V_j}{A_{Vj}}\right)\cosh\left(q_{Vj}H_j\right)+\frac{V_j q_{Vj}}{A_{Vj}}H_j\sinh\left(q_{Vj}H_j\right)}{H_j\frac{\sinh\left(q_{Vj}H_j\right)}{q_{Vi}H_j}+\frac{V_j}{A_{Vj}}\cosh\left(q_{Vj}H_j\right)} - \frac{D}{D_{Vj}}\left(\frac{A_{Vi}H_i}{A}+\frac{V_i}{A}\right)\left(H_j^2+2\frac{V_j}{A_{Vj}}H_j\right)$$

B.7 Time lag for the main line

Since $\theta_i = \dfrac{f_i(0)\Delta'(0)-f_i'(0)\Delta(0)}{f_i(0)\Delta(0)} = \dfrac{\Delta'(0)}{\Delta(0)} - \dfrac{f_i'(0)}{f_i(0)}$, we need to find the derivatives of the relevant terms.

$$\frac{M_{Vj}}{M_n}\sinh\left(qZ_n\right) = \delta_j\cosh\left(q\left(Z_n-Z_j\right)\right)+\delta_j\sum_{m=j+1}^{n-1}\lambda_m\sinh\left(q\left(Z_m-Z_j\right)\right)\left(\frac{M_{Vm}}{M_n}\sinh\left(qZ_n\right)\right)$$

$$\frac{M_{Vj}}{M_n}\sinh\left(qZ_n\right)=\delta_j\cosh\left(q\left(Z_n-Z_j\right)\right)+\delta_j\sum_{m=j+1}^{n-1}\lambda_m\delta_m\sinh\left(q\left(Z_m-Z_j\right)\right)\left[\begin{array}{l}\cosh\left(q\left(Z_n-Z_m\right)\right)\\+\sum_{k=m+1}^{n-1}\lambda_k\sinh\left(q\left(Z_k-Z_m\right)\right)\left(\frac{M_{Vk}}{M_n}\sinh\left(qZ_n\right)\right)\end{array}\right]$$

$$\frac{M_{Vj}}{M_n}\sinh\left(qZ_n\right)=\delta_j\cosh\left(q\left(Z_n-Z_j\right)\right)+\delta_j\sum_{m=j+1}^{n-1}\lambda_m\delta_m\sinh\left(q\left(Z_m-Z_j\right)\right)\cosh\left(q\left(Z_n-Z_m\right)\right)$$
$$+\delta_j\sum_{m=j+1}^{n-1}\lambda_m\delta_m\sinh\left(q\left(Z_m-Z_j\right)\right)\sum_{k=m+1}^{n-1}\lambda_k\delta_k\sinh\left(q\left(Z_k-Z_m\right)\right)\left[\begin{array}{l}\cosh\left(q\left(Z_n-Z_k\right)\right)\\+\sum_{l=k+1}^{n-1}\lambda_l\sinh\left(q\left(Z_l-Z_k\right)\right)\left(\frac{M_{Vl}}{M_n}\sinh\left(qZ_n\right)\right)\end{array}\right]$$

$$\begin{aligned}\frac{M_{Vj}}{M_n}\sinh\left(qZ_n\right)&=\delta_j\cosh\left(q\left(Z_n-Z_j\right)\right)+\delta_j\sum_{m=j+1}^{n-1}\lambda_m\delta_m\sinh\left(q\left(Z_m-Z_j\right)\right)\cosh\left(q\left(Z_n-Z_m\right)\right)\\&+\delta_j\sum_{m=j+1}^{n-1}\lambda_m\delta_m\sinh\left(q\left(Z_m-Z_j\right)\right)\sum_{k=m+1}^{n-1}\lambda_k\delta_k\sinh\left(q\left(Z_k-Z_m\right)\right)\cosh\left(q\left(Z_n-Z_k\right)\right)\\&+\delta_j\sum_{m=j+1}^{n-1}\lambda_m\delta_m\sinh\left(q\left(Z_m-Z_j\right)\right)\sum_{k=m+1}^{n-1}\lambda_k\delta_k\sinh\left(q\left(Z_k-Z_m\right)\right)\sum_{l=k+1}^{n-1}\lambda_l\sinh\left(q\left(Z_l-Z_k\right)\right)\left(\frac{M_{Vl}}{M_n}\sinh\left(qZ_n\right)\right)\end{aligned}\qquad\text{(B.56)}$$

Therefore Eq.(B.42) can be rewritten as:

$$\Delta(s)=\sinh(qZ_n)+\sum_{j=1}^{n-1}\lambda_j\cosh(qZ_j)\left[\begin{array}{l}\delta_j\cosh\left(q\left(Z_n-Z_j\right)\right)+\delta_j\sum_{m=j+1}^{n-1}\lambda_m\delta_m\sinh\left(q\left(Z_m-Z_j\right)\right)\cosh\left(q\left(Z_n-Z_m\right)\right)\\ +\delta_j\sum_{m=j+1}^{n-1}\lambda_m\delta_m\sinh\left(q\left(Z_m-Z_j\right)\right)\sum_{k=m+1}^{n-1}\lambda_k\delta_k\sinh\left(q\left(Z_k-Z_m\right)\right)\cosh\left(q\left(Z_n-Z_k\right)\right)\\ +\delta_j\sum_{m=j+1}^{n-1}\lambda_m\delta_m\sinh\left(q\left(Z_m-Z_j\right)\right)\sum_{k=m+1}^{n-1}\lambda_k\delta_k\sinh\left(q\left(Z_k-Z_m\right)\right)\sum_{l=k+1}^{n-1}\lambda_l\sinh\left(q\left(Z_l-Z_k\right)\right)\left(\frac{M_{Vl}}{M_n}\sinh(qZ_n)\right)\end{array}\right]$$

$$\begin{aligned}\Delta(s)=&\sinh(qZ_n)+\sum_{j=1}^{n-1}\lambda_j\delta_j\cosh(qZ_j)\cosh\left(q\left(Z_n-Z_j\right)\right)\\ &+\sum_{j=1}^{n-1}\lambda_j\delta_j\cosh(qZ_j)\sum_{m=j+1}^{n-1}\lambda_m\delta_m\sinh\left(q\left(Z_m-Z_j\right)\right)\cosh\left(q\left(Z_n-Z_m\right)\right)\\ &+\sum_{j=1}^{n-1}\lambda_j\delta_j\cosh(qZ_j)\sum_{m=j+1}^{n-1}\lambda_m\delta_m\sinh\left(q\left(Z_m-Z_j\right)\right)\sum_{k=m+1}^{n-1}\lambda_k\delta_k\sinh\left(q\left(Z_k-Z_m\right)\right)\cosh\left(q\left(Z_n-Z_k\right)\right)\\ &+\sum_{j=1}^{n-1}\lambda_j\delta_j\cosh(qZ_j)\sum_{m=j+1}^{n-1}\lambda_m\delta_m\sinh\left(q\left(Z_m-Z_j\right)\right)\sum_{k=m+1}^{n-1}\lambda_k\delta_k\sinh\left(q\left(Z_k-Z_m\right)\right)\sum_{l=k+1}^{n-1}\lambda_l\sinh\left(q\left(Z_l-Z_k\right)\right)\left(\frac{M_{Vl}}{M_n}\sinh(qZ_n)\right)\end{aligned}$$

$$\lim_{s\to0}\frac{\Delta(s)}{q}=Z_n+\lim_{s\to0}\sum_{j=1}^{n-1}\lambda_j\frac{\delta_j}{q}\cosh(qZ_j)\cosh\left(q\left(Z_n-Z_j\right)\right)$$

Using Equation (B.48):

$$\lim_{s\to0}\frac{\Delta(s)}{q}=Z_n+\lim_{s\to0}\sum_{j=1}^{n-1}\left(\frac{A_{Vj}H_j}{A}+\frac{V_j}{A}\right)=\frac{V_{total}}{A}\qquad\text{(B.57)}$$

$$
\begin{aligned}
2Dq\Delta'(s) = {} & Z_n \cosh(qZ_n) + \sum_{j=1}^{n-1} \lambda_j \frac{d\delta_j}{dq} \cosh(qZ_j) \cosh\left(q(Z_n - Z_j)\right) \\
& + \sum_{j=1}^{n-1} \lambda_j \delta_j Z_j \sinh(qZ_j) \cosh\left(q(Z_n - Z_j)\right) + \sum_{j=1}^{n-1} \lambda_j \delta_j (Z_n - Z_j) \cosh(qZ_j) \sinh\left(q(Z_n - Z_j)\right) \\
& + \sum_{j=1}^{n-1} \lambda_j \frac{d\delta_j}{dq} \cosh(qZ_j) \sum_{m=j+1}^{n-1} \lambda_m \delta_m \sinh\left(q(Z_m - Z_j)\right) \cosh\left(q(Z_n - Z_m)\right) \\
& + \sum_{j=1}^{n-1} \lambda_j \delta_j Z_j \sinh(qZ_j) \sum_{m=j+1}^{n-1} \lambda_m \delta_m \sinh\left(q(Z_m - Z_j)\right) \cosh\left(q(Z_n - Z_m)\right) \\
& + \sum_{j=1}^{n-1} \lambda_j \delta_j \cosh(qZ_j) \left[\begin{array}{l} \displaystyle\sum_{m=j+1}^{n-1} \lambda_m \frac{d\delta_m}{dq} \sinh\left(q(Z_m - Z_j)\right) \cosh\left(q(Z_n - Z_m)\right) \\ \displaystyle + \sum_{m=j+1}^{n-1} \lambda_m \delta_m (Z_m - Z_j) \cosh\left(q(Z_m - Z_j)\right) \cosh\left(q(Z_n - Z_m)\right) \\ \displaystyle + \sum_{m=j+1}^{n-1} \lambda_m \delta_m (Z_n - Z_m) \sinh\left(q(Z_m - Z_j)\right) \sinh\left(q(Z_n - Z_m)\right) \end{array} \right] \\
& + q^4(\cdots)
\end{aligned}
$$

$$2D\lim_{s\to 0}\frac{\Delta'(s)}{q}=\lim_{s\to 0}\frac{1}{q^2}\left[Z_n\cosh(qZ_n)+\sum_{j=1}^{n-1}\lambda_j\frac{d\delta_j}{dq}\cosh(qZ_j)\cosh\left(q(Z_n-Z_j)\right)\right]$$
$$+\lim_{s\to 0}\sum_{j=1}^{n-1}\lambda_j\frac{\delta_j}{q}Z_j^2\frac{\sinh(qZ_j)}{qZ_j}\cosh\left(q(Z_n-Z_j)\right)+\lim_{s\to 0}\sum_{j=1}^{n-1}\lambda_j\frac{\delta_j}{q}(Z_n-Z_j)^2\cosh(qZ_j)\frac{\sinh\left(q(Z_n-Z_j)\right)}{q(Z_n-Z_j)}$$
$$+\lim_{s\to 0}\sum_{j=1}^{n-1}\lambda_j\frac{d\delta_j}{dq}\cosh(qZ_j)\sum_{m=j+1}^{n-1}\lambda_m\frac{\delta_m}{q}(Z_m-Z_j)\frac{\sinh\left(q(Z_m-Z_j)\right)}{q(Z_m-Z_j)}\cosh\left(q(Z_n-Z_m)\right)$$
$$+\lim_{s\to 0}\sum_{j=1}^{n-1}\lambda_j\frac{\delta_j}{q}\cosh(qZ_j)\left[\sum_{m=j+1}^{n-1}\lambda_m\frac{d\delta_m}{dq}(Z_m-Z_j)\frac{\sinh\left(q(Z_m-Z_j)\right)}{q(Z_m-Z_j)}\cosh\left(q(Z_n-Z_m)\right)+\sum_{m=j+1}^{n-1}\lambda_m\frac{\delta_m}{q}(Z_m-Z_j)\cosh\left(q(Z_m-Z_j)\right)\cosh\left(q(Z_n-Z_m)\right)\right]$$

Using Eqs. (B.48), (B.50) and (B.53):

$$2D\lim_{s\to 0}\frac{\Delta'(s)}{q}=\lim_{s\to 0}\frac{1}{q^2}\left[Z_n\cosh(qZ_n)+\sum_{j=1}^{n-1}\lambda_j\frac{\delta_j}{q}\frac{\left(H_j+\frac{V_j}{A_{Vj}}\right)\cosh(q_{Vj}H_j)+\frac{V_jq_{Vj}}{A_{Vj}}H_j\sinh(q_{Vj}H_j)}{H_j\frac{\sinh(q_{Vj}H_j)}{q_{Vi}H_j}+\frac{V_j}{A_{Vj}}\cosh(q_{Vj}H_j)}\cosh(qZ_j)\cosh\left(q(Z_n-Z_j)\right)\right]$$
$$-\sum_{j=1}^{n-1}\frac{D}{D_{Vj}}\left(\frac{A_{Vj}H_j}{A}+\frac{V_j}{A}\right)\left(H_j^2+2\frac{V_j}{A_{Vj}}H_j\right)+\sum_{j=1}^{n-1}\left(\frac{A_{Vj}H_j}{A}+\frac{V_j}{A}\right)\left[Z_j^2+(Z_n-Z_j)^2\right]$$
$$+\sum_{j=1}^{n-1}\left(\frac{A_{Vj}H_j}{A}+\frac{V_j}{A}\right)\sum_{m=j+1}^{n-1}\left(\frac{A_{Vm}H_m}{A}+\frac{V_m}{A}\right)(Z_m-Z_j)$$
$$+\sum_{j=1}^{n-1}\left(\frac{A_{Vj}H_j}{A}+\frac{V_j}{A}\right)\left[\sum_{m=j+1}^{n-1}\left(\frac{A_{Vm}H_m}{A}+\frac{V_m}{A}\right)(Z_m-Z_j)+\sum_{m=j+1}^{n-1}\left(\frac{A_{Vm}H_m}{A}+\frac{V_m}{A}\right)(Z_m-Z_j)\right]$$

$$2D\lim_{s\to 0}\frac{\Delta'(s)}{q}=\lim_{s\to 0}\frac{1}{q^2}\left[Z_n\cosh(qZ_n)+\sum_{j=1}^{n-1}\lambda_j\frac{\delta_j}{q}\frac{\left(H_j+\frac{V_j}{A_{Vj}}\right)\cosh(q_{Vj}H_j)+\frac{V_jq_{Vj}}{A_{Vj}}H_j\sinh(q_{Vj}H_j)}{H_j\frac{\sinh(q_{Vj}H_j)}{q_{Vi}H_j}+\frac{V_j}{A_{Vj}}\cosh(q_{Vj}H_j)}\cosh(qZ_j)\cosh\left(q(Z_n-Z_j)\right)\right]$$
$$+\sum_{j=1}^{n-1}\left(\frac{A_{Vj}H_j}{A}+\frac{V_j}{A}\right)\left(-\frac{D}{D_{Vj}}H_j^2-2\frac{D}{D_{Vj}}\frac{V_j}{A_{Vj}}H_j+Z_j^2+(Z_n-Z_j)^2\right)$$
$$+3\sum_{j=1}^{n-1}\left(\frac{A_{Vj}H_j}{A}+\frac{V_j}{A}\right)\sum_{m=j+1}^{n-1}\left(\frac{A_{Vm}H_m}{A}+\frac{V_m}{A}\right)(Z_m-Z_j)$$

Therefore:

$$\lim_{s\to 0}\frac{\Delta'(s)}{\Delta(s)}=\lim_{s\to 0}\frac{1}{2Dq^2\frac{\Delta(s)}{q}}\left[Z_n\cosh(qZ_n)+\sum_{j=1}^{n-1}\lambda_j\frac{\delta_j}{q}\frac{\left(H_j+\frac{V_j}{A_{Vj}}\right)\cosh(q_{Vj}H_j)+\frac{V_jq_{Vj}}{A_{Vj}}H_j\sinh(q_{Vj}H_j)}{H_j\frac{\sinh(q_{Vj}H_j)}{q_{Vi}H_j}+\frac{V_j}{A_{Vj}}\cosh(q_{Vj}H_j)}\cosh(qZ_j)\cosh\left(q(Z_n-Z_j)\right)\right]$$
$$-\frac{A}{V_{total}}\sum_{j=1}^{n-1}\left(\frac{A_{Vj}H_j}{A}+\frac{V_j}{A}\right)\left(\frac{1}{2D_{Vj}}H_j^2+\frac{1}{D_{Vj}}\frac{V_j}{A_{Vj}}H_j-\frac{Z_j^2+(Z_n-Z_j)^2}{2D}\right)$$
$$+\frac{3}{2D}\frac{A}{V_{total}}\sum_{j=1}^{n-1}\left(\frac{A_{Vj}H_j}{A}+\frac{V_j}{A}\right)\sum_{m=j+1}^{n-1}\left(\frac{A_{Vm}H_m}{A}+\frac{V_m}{A}\right)(Z_m-Z_j)\qquad\text{(B.58)}$$

Starting from Eq. (B.41):

$$f_i(s) = \alpha q\left[\cosh\left(q\left(Z_n - x\right)\right) + \sum_{j=i}^{n-1}\lambda_j\left(\frac{M_{Vj}}{M_n}\sinh\left(qZ_n\right)\right)\sinh\left(q\left(Z_j - x\right)\right)\right] \tag{B.41}$$

$$\lim_{s\to 0}\frac{f_i(s)}{q} = \lim_{q\to 0}\alpha\left\{\cosh\left(q\left(Z_n - x\right)\right) + \sum_{j=i}^{n-1}\lambda_j\left(\frac{M_{Vj}}{M_n}\sinh\left(qZ_n\right)\right)\sinh\left(q\left(Z_j - x\right)\right)\right\} = \alpha \tag{B.59}$$

$$f_i(s) = \alpha q\cosh\left(q\left(Z_n - x\right)\right) +$$
$$\alpha q\sum_{j=i}^{n-1}\lambda_j\delta_j\sinh\left(q\left(Z_j - x\right)\right)\left[\begin{array}{l}\cosh\left(q\left(Z_n - Z_j\right)\right) + \\ \sum_{m=j+1}^{n-1}\lambda_m\delta_m\sinh\left(q\left(Z_m - Z_j\right)\right)\cosh\left(q\left(Z_n - Z_m\right)\right) + \\ \sum_{m=j+1}^{n-1}\lambda_m\delta_m\sinh\left(q\left(Z_m - Z_j\right)\right)\sum_{k=m+1}^{n-1}\lambda_k\delta_k\sinh\left(q\left(Z_k - Z_m\right)\right)\cosh\left(q\left(Z_n - Z_k\right)\right) + \\ \sum_{m=j+1}^{n-1}\lambda_m\delta_m\sinh\left(q\left(Z_m - Z_j\right)\right)\sum_{k=m+1}^{n-1}\left(\begin{array}{l}\lambda_k\delta_k\sinh\left(q\left(Z_k - Z_m\right)\right)\times \\ \sum_{l=k+1}^{n-1}\lambda_l\sinh\left(q\left(Z_l - Z_k\right)\right)\left(\frac{M_{Vl}}{M_n}\sinh\left(qZ_n\right)\right)\end{array}\right)\end{array}\right]$$

$$2Dq\,f_i'(s)=\frac{f_i(s)}{q}+\alpha q(Z_n-x)\sinh\big(q(Z_n-x)\big)+\alpha q\sum_{j=i}^{n-1}\lambda_j\frac{d\delta_j}{dq}\sinh\big(q(Z_j-x)\big)\cosh\big(q(Z_n-Z_j)\big)+$$
$$\alpha q\sum_{j=i}^{n-1}\lambda_j\delta_j(Z_j-x)\cosh\big(q(Z_j-x)\big)\cosh\big(q(Z_n-Z_j)\big)+\alpha q\sum_{j=i}^{n-1}\lambda_j\delta_j(Z_n-Z_j)\sinh\big(q(Z_j-x)\big)\sinh\big(q(Z_n-Z_j)\big)+$$
$$\alpha q\sum_{j=i}^{n-1}\lambda_j\frac{d\delta_j}{dq}\sinh\big(q(Z_j-x)\big)\sum_{m=j+1}^{n-1}\lambda_m\delta_m\sinh\big(q(Z_m-Z_j)\big)\cosh\big(q(Z_n-Z_m)\big)+$$
$$\alpha q\sum_{j=i}^{n-1}\lambda_j\delta_j(Z_j-x)\cosh\big(q(Z_j-x)\big)\sum_{m=j+1}^{n-1}\lambda_m\delta_m\sinh\big(q(Z_m-Z_j)\big)\cosh\big(q(Z_n-Z_m)\big)+$$
$$\alpha q\sum_{j=i}^{n-1}\lambda_j\delta_j\sinh\big(q(Z_j-x)\big)\sum_{m=j+1}^{n-1}\lambda_m\frac{d\delta_m}{dq}\sinh\big(q(Z_m-Z_j)\big)\cosh\big(q(Z_n-Z_m)\big)+$$
$$\alpha q\sum_{j=i}^{n-1}\lambda_j\delta_j\sinh\big(q(Z_j-x)\big)\sum_{m=j+1}^{n-1}\lambda_m\delta_m(Z_m-Z_j)\cosh\big(q(Z_m-Z_j)\big)\cosh\big(q(Z_n-Z_m)\big)+$$
$$\alpha q\sum_{j=i}^{n-1}\lambda_j\delta_j\sinh\big(q(Z_j-x)\big)\sum_{m=j+1}^{n-1}\lambda_m\delta_m(Z_n-Z_m)\sinh\big(q(Z_m-Z_j)\big)\sinh\big(q(Z_n-Z_m)\big)+$$
$$\alpha q^5(\cdots)$$

$$\lim_{s\to 0}\frac{f_i'(s)}{f_i(s)}=\frac{1}{2Dq^2}+\frac{1}{2D\dfrac{f_i(s)}{\alpha q}}(Z_n-x)\sinh\left(q(Z_n-x)\right)+\frac{1}{2Dq\dfrac{f_i(s)}{\alpha q}}\sum_{j=i}^{n-1}\lambda_j\frac{d\delta_j}{dq}\sinh\left(q(Z_j-x)\right)\cosh\left(q(Z_n-Z_j)\right)+$$

$$+\frac{1}{2Dq\dfrac{f_i(s)}{\alpha q}}\sum_{j=i}^{n-1}\lambda_j\delta_j(Z_j-x)\cosh\left(q(Z_j-x)\right)\cosh\left(q(Z_n-Z_j)\right)+\frac{1}{2Dq\dfrac{f_i(s)}{\alpha q}}\sum_{j=i}^{n-1}\lambda_j\delta_j(Z_n-Z_j)\sinh\left(q(Z_j-x)\right)\sinh\left(q(Z_n-Z_j)\right)+$$

$$\frac{1}{2Dq\dfrac{f_i(s)}{\alpha q}}\sum_{j=i}^{n-1}\lambda_j\frac{d\delta_j}{dq}\sinh\left(q(Z_j-x)\right)\sum_{m=j+1}^{n-1}\lambda_m\delta_m\sinh\left(q(Z_m-Z_j)\right)\cosh\left(q(Z_n-Z_m)\right)+$$

$$\frac{1}{2Dq\dfrac{f_i(s)}{\alpha q}}\sum_{j=i}^{n-1}\lambda_j\delta_j(Z_j-x)\cosh\left(q(Z_j-x)\right)\sum_{m=j+1}^{n-1}\lambda_m\delta_m\sinh\left(q(Z_m-Z_j)\right)\cosh\left(q(Z_n-Z_m)\right)+$$

$$\frac{1}{2Dq\dfrac{f_i(s)}{\alpha q}}\sum_{j=i}^{n-1}\lambda_j\delta_j\sinh\left(q(Z_j-x)\right)\sum_{m=j+1}^{n-1}\lambda_m\frac{d\delta_m}{dq}\sinh\left(q(Z_m-Z_j)\right)\cosh\left(q(Z_n-Z_m)\right)+$$

$$\frac{1}{2Dq\dfrac{f_i(s)}{\alpha q}}\sum_{j=i}^{n-1}\lambda_j\delta_j\sinh\left(q(Z_j-x)\right)\sum_{m=j+1}^{n-1}\lambda_m\delta_m(Z_m-Z_j)\cosh\left(q(Z_m-Z_j)\right)\cosh\left(q(Z_n-Z_m)\right)+$$

$$\frac{1}{2Dq\dfrac{f_i(s)}{\alpha q}}\sum_{j=i}^{n-1}\lambda_j\delta_j\sinh\left(q(Z_j-x)\right)\sum_{m=j+1}^{n-1}\lambda_m\delta_m(Z_n-Z_m)\sinh\left(q(Z_m-Z_j)\right)\sinh\left(q(Z_n-Z_m)\right)+$$

$$q^4(\cdots)$$

$$\lim_{s\to 0}\frac{f_i'(s)}{f_i(s)}=\lim_{s\to 0}\frac{1}{2Dq^2}+\frac{1}{2D}(Z_n-x)^2+\frac{1}{2D}\sum_{j=i}^{n-1}\left(\frac{A_{Vj}}{A}H_j+\frac{V_j}{A}\right)(Z_j-x)+\frac{1}{2D}\sum_{j=i}^{n-1}\left(\frac{A_{Vj}}{A}H_j+\frac{V_j}{A}\right)(Z_j-x)$$

$$\lim_{s\to 0}\frac{f_i'(s)}{f_i(s)}=\lim_{s\to 0}\frac{1}{2Dq^2}+\frac{(Z_n-x)^2}{2D}+\frac{1}{AD}\sum_{j=i}^{n-1}\left(A_{Vj}H_j+V_j\right)\left(Z_j-x\right) \tag{B.60}$$

Using Eqs. (B.58) and (B.60):

$$\theta_i=\frac{f_i(0)\Delta'(0)-f_i'(0)\Delta(0)}{f_i(0)\Delta(0)}=\frac{\Delta'(0)}{\Delta(0)}-\frac{f_i'(0)}{f_i(0)}$$

$$\begin{aligned}\theta_i=\lim_{s\to 0}\beta&-\frac{A}{V_{total}}\sum_{j=1}^{n-1}\left(\frac{A_{Vj}H_j}{A}+\frac{V_j}{A}\right)\left(\frac{1}{2D_{Vj}}H_j^2+\frac{1}{D_{Vj}}\frac{V_j}{A_{Vj}}H_j-\frac{Z_j^2+\left(Z_n-Z_j\right)^2}{2D}\right)\\&+\frac{3}{2D}\frac{A}{V_{total}}\sum_{j=1}^{n-1}\left(\frac{A_{Vj}H_j}{A}+\frac{V_j}{A}\right)\sum_{m=j+1}^{n-1}\left(\frac{A_{Vm}H_m}{A}+\frac{V_m}{A}\right)\left(Z_m-Z_j\right)-\frac{(Z_n-x)^2}{2D}-\frac{1}{AD}\sum_{j=i}^{n-1}\left(A_{Vj}H_j+V_j\right)\left(Z_j-x\right)\end{aligned} \tag{B.61}$$

In which β is:

$$\beta=\frac{1}{2Dq^2\dfrac{\Delta(s)}{q}}\left[Z_n\cosh\left(qZ_n\right)+\sum_{j=1}^{n-1}\lambda_j\frac{\delta_j}{q}\frac{\left(H_j+\dfrac{V_j}{A_{Vj}}\right)\cosh\left(q_{Vj}H_j\right)+\dfrac{V_jq_{Vj}}{A_{Vj}}H_j\sinh\left(q_{Vj}H_j\right)}{H_j\dfrac{\sinh\left(q_{Vj}H_j\right)}{q_{Vi}H_j}+\dfrac{V_j}{A_{Vj}}\cosh\left(q_{Vj}H_j\right)}\cosh\left(qZ_j\right)\cosh\left(q\left(Z_n-Z_j\right)\right)\right]-\frac{1}{2Dq^2} \tag{B.62}$$

Eq. (31) can be rewritten as:

$$\beta=\frac{1}{2Dq^2\dfrac{\Delta(s)}{q}}\left[Z_n\cosh\left(qZ_n\right)+\sum_{j=1}^{n-1}\gamma_j\right]-\frac{1}{2Dq^2}$$

$$\beta = \frac{1}{2Dq^2 \dfrac{\Delta(s)}{q}}\left[Z_n \cosh(qZ_n) + \sum_{j=1}^{n-1} \gamma_j - \frac{\Delta(s)}{q} \right] \tag{B.63}$$

where γ_j is:

$$\gamma_j = \lambda_j \frac{\delta_j}{q} \frac{\left(H_j + \dfrac{V_j}{A_{Vj}} \right) \cosh(q_{Vj} H_j) + \dfrac{V_j q_{Vj}}{A_{Vj}} H_j \sinh(q_{Vj} H_j)}{H_j \dfrac{\sinh(q_{Vj} H_j)}{q_{Vi} H_j} + \dfrac{V_j}{A_{Vj}} \cosh(q_{Vj} H_j)} \cosh(qZ_j) \cosh\left(q(Z_n - Z_j)\right) \tag{B.64}$$

Since $\dfrac{\Delta(s)}{q}$ is:

$$\frac{\Delta(s)}{q} = Z_n \frac{\sinh(qZ_n)}{qZ_n} + \sum_{j=1}^{n-1} \lambda_j \frac{\delta_j}{q} \cosh(qZ_j) \left[\begin{array}{l} \cosh\left(q(Z_n - Z_j)\right) \\ +q^2 \displaystyle\sum_{m=j+1}^{n-1} \lambda_m \frac{\delta_m}{q} (Z_m - Z_j) \frac{\sinh\left(q(Z_m - Z_j)\right)}{q(Z_m - Z_j)} \cosh\left(q(Z_n - Z_m)\right) \\ +q^4(\cdots) \end{array} \right]$$

The following terms can be simplified:

$$\sigma = \frac{\left(H_j + \dfrac{V_j}{A_{Vj}} \right) \cosh(q_{Vj} H_j) + \dfrac{V_j q_{Vj}}{A_{Vj}} H_j \sinh(q_{Vj} H_j)}{H_j \dfrac{\sinh(q_{Vj} H_j)}{q_{Vi} H_j} + \dfrac{V_j}{A_{Vj}} \cosh(q_{Vj} H_j)} - 1 = \frac{\left(H_j + \dfrac{V_j}{A_{Vj}} \right) \cosh(q_{Vj} H_j) + \dfrac{V_j q_{Vj}}{A_{Vj}} H_j \sinh(q_{Vj} H_j) - \dfrac{\sinh(q_{Vj} H_j)}{q_{Vi} H_j} - \dfrac{V_j}{A_{Vj}} \cosh(q_{Vj} H_j)}{H_j \dfrac{\sinh(q_{Vj} H_j)}{q_{Vi} H_j} + \dfrac{V_j}{A_{Vj}} \cosh(q_{Vj} H_j)}$$

$$\sigma = \frac{H_j \cosh\left(q_{Vj}H_j\right) + \frac{V_j q_{Vj}}{A_{Vj}} H_j \sinh\left(q_{Vj}H_j\right) - H_j \frac{\sinh\left(q_{Vj}H_j\right)}{q_{Vi}H_j}}{H_j \frac{\sinh\left(q_{Vj}H_j\right)}{q_{Vi}H_j} + \frac{V_j}{A_{Vj}} \cosh\left(q_{Vj}H_j\right)} = \frac{H_j\left[\cosh\left(q_{Vj}H_j\right) - \frac{\sinh\left(q_{Vj}H_j\right)}{q_{Vi}H_j}\right] + q^2 \frac{D}{D_{Vj}} \frac{V_j}{A_{Vj}} H_j^2 \frac{\sinh\left(q_{Vj}H_j\right)}{q_{Vj}H_j}}{H_j \frac{\sinh\left(q_{Vj}H_j\right)}{q_{Vi}H_j} + \frac{V_j}{A_{Vj}} \cosh\left(q_{Vj}H_j\right)}$$

Using Taylor's expansion:

$$\cosh\left(q_{Vj}H_j\right) - \frac{\sinh\left(q_{Vj}H_j\right)}{q_{Vi}H_j} = \left(1 + \frac{q_{Vj}^2 H_j^2}{2} + \cdots\right) - \left(1 + \frac{q_{Vj}^2 H_j^2}{6} + \cdots\right) = \frac{q_{Vj}^2 H_j^2}{3} + q_{Vj}^4(\cdots)$$

Thus:

$$\sigma = \frac{H_j \cosh\left(q_{Vj}H_j\right) + \frac{V_j q_{Vj}}{A_{Vj}} H_j \sinh\left(q_{Vj}H_j\right) - H_j \frac{\sinh\left(q_{Vj}H_j\right)}{q_{Vi}H_j}}{H_j \frac{\sinh\left(q_{Vj}H_j\right)}{q_{Vi}H_j} + \frac{V_j}{A_{Vj}} \cosh\left(q_{Vj}H_j\right)} = q^2 \frac{D}{D_{Vj}} \frac{H_j\left[\frac{H_j^2}{3} + q_{Vj}^2(\cdots)\right] + \frac{V_j}{A_{Vj}} H_j^2 \frac{\sinh\left(q_{Vj}H_j\right)}{q_{Vj}H_j}}{H_j \frac{\sinh\left(q_{Vj}H_j\right)}{q_{Vi}H_j} + \frac{V_j}{A_{Vj}} \cosh\left(q_{Vj}H_j\right)}$$

Substituting into Eq. (B.63):

$$\beta = \frac{1}{2Dq^2 \frac{\Delta(s)}{q}} \left[\begin{array}{l} Z_n\left(\cosh\left(qZ_n\right) - \frac{\sinh\left(qZ_n\right)}{qZ_n}\right) + \sum_{j=1}^{n-1}\left(\gamma_j - \lambda_j \frac{\delta_j}{q} \cosh\left(qZ_j\right)\cosh\left(q\left(Z_n - Z_j\right)\right)\right) \\ -q^2 \sum_{j=1}^{n-1} \lambda_j \frac{\delta_j}{q} \cosh\left(qZ_j\right) \sum_{m=j+1}^{n-1} \lambda_m \frac{\delta_m}{q}\left(Z_m - Z_j\right) \frac{\sinh\left(q\left(Z_m - Z_j\right)\right)}{q\left(Z_m - Z_j\right)} \cosh\left(q\left(Z_n - Z_m\right)\right) \end{array} \right]$$

$$\beta = \frac{1}{2D\dfrac{\Delta(s)}{q}}\left[\begin{array}{l}\dfrac{Z_n}{q^2}\left(\cosh(qZ_n)-\dfrac{\sinh(qZ_n)}{qZ_n}\right)+\displaystyle\sum_{j=1}^{n-1}\lambda_j\frac{\delta_j}{q}\frac{\sigma}{q^2}\cosh(qZ_j)\cosh\left(q\left(Z_n-Z_j\right)\right)\\ -\displaystyle\sum_{j=1}^{n-1}\lambda_j\frac{\delta_j}{q}\cosh(qZ_j)\sum_{m=j+1}^{n-1}\lambda_m\frac{\delta_m}{q}\left(Z_m-Z_j\right)\frac{\sinh\left(q\left(Z_m-Z_j\right)\right)}{q\left(Z_m-Z_j\right)}\cosh\left(q\left(Z_n-Z_m\right)\right)\end{array}\right]$$

$$\lim_{s\to 0}\beta = \frac{1}{2D\dfrac{V_{total}}{A}}\left[\frac{Z_n^3}{3}+\sum_{j=1}^{n-1}\left(\frac{A_{Vj}H_j}{A}+\frac{V_j}{A}\right)\frac{D}{D_{Vj}}\frac{H_j^2\left(\dfrac{H_j}{3}+\dfrac{V_j}{A_{Vj}}\right)}{H_j+\dfrac{V_j}{A_{Vj}}}-\sum_{j=1}^{n-1}\left(\frac{A_{Vj}H_j}{A}+\frac{V_j}{A}\right)\sum_{m=j+1}^{n-1}\left(\frac{A_{Vm}H_m}{A}+\frac{V_m}{A}\right)\left(Z_m-Z_j\right)\right]$$

$$\lim_{s\to 0}\beta = \frac{AZ_n^3}{6DV_{total}}+\frac{A}{2DV_{total}}\sum_{j=1}^{n-1}\frac{A_{Vj}}{A}\frac{D}{D_{Vj}}H_j^2\left(\frac{H_j}{3}+\frac{V_j}{A_{Vj}}\right)-\frac{A}{2DV_{total}}\sum_{j=1}^{n-1}\left(\frac{A_{Vj}H_j}{A}+\frac{V_j}{A}\right)\sum_{m=j+1}^{n-1}\left(\frac{A_{Vm}H_m}{A}+\frac{V_m}{A}\right)\left(Z_m-Z_j\right) \qquad \text{(B.65)}$$

Substituting Eq. (B.65) into Eq. (B.61):

$$\begin{aligned}\theta_i = {} & \frac{AZ_n^3}{6DV_{total}}+\frac{A}{2DV_{total}}\sum_{j=1}^{n-1}\frac{D}{D_{Vj}}\frac{A_{Vj}}{A}H_j^2\left(\frac{H_j}{3}+\frac{V_j}{A_{Vj}}\right)-\frac{A}{2DV_{total}}\sum_{j=1}^{n-1}\left(\frac{A_{Vj}H_j}{A}+\frac{V_j}{A}\right)\sum_{m=j+1}^{n-1}\left(\frac{A_{Vm}H_m}{A}+\frac{V_m}{A}\right)\left(Z_m-Z_j\right)\\ & -\frac{A}{V_{total}}\sum_{j=1}^{n-1}\left(\frac{A_{Vj}H_j}{A}+\frac{V_j}{A}\right)\left(\frac{1}{2D_{Vj}}H_j^2+\frac{1}{D_{Vj}}\frac{V_j}{A_{Vj}}H_j-\frac{Z_j^2+\left(Z_n-Z_j\right)^2}{2D}\right)\\ & +\frac{3}{2D}\frac{A}{V_{total}}\sum_{j=1}^{n-1}\left(\frac{A_{Vj}H_j}{A}+\frac{V_j}{A}\right)\sum_{m=j+1}^{n-1}\left(\frac{A_{Vm}H_m}{A}+\frac{V_m}{A}\right)\left(Z_m-Z_j\right)-\frac{\left(Z_n-x\right)^2}{2D}-\frac{1}{AD}\sum_{j=i}^{n-1}\left(A_{Vj}H_j+V_j\right)\left(Z_j-x\right)\end{aligned}$$

$$\theta_i = \frac{AZ_n^3}{6DV_{total}} + \sum_{j=1}^{n-1}\left(\frac{A_{Vj}H_j^3}{6D_{Vj}V_{total}} + \frac{V_j}{2D_{Vj}V_{total}}H_j^2\right) - \sum_{j=1}^{n-1}\left(\frac{A_{Vj}H_j}{V_{total}} + \frac{V_j}{V_{total}}\right)\left(\frac{1}{2D_{Vj}}H_j^2 + \frac{1}{D_{Vj}}\frac{V_j}{A_{Vj}}H_j - \frac{Z_j^2 + (Z_n - Z_j)^2}{2D}\right)$$
$$- \frac{1}{2D}\sum_{j=1}^{n-1}\left(\frac{A_{Vj}H_j}{V_{total}} + \frac{V_j}{V_{total}}\right)\sum_{m=j+1}^{n-1}\left(\frac{A_{Vm}H_m}{A} + \frac{V_m}{A}\right)(Z_m - Z_j) + \frac{3}{2D}\sum_{j=1}^{n-1}\left(\frac{A_{Vj}H_j}{V_{total}} + \frac{V_j}{V_{total}}\right)\sum_{m=j+1}^{n-1}\left(\frac{A_{Vm}H_m}{A} + \frac{V_m}{A}\right)(Z_m - Z_j)$$
$$- \frac{(Z_n - x)^2}{2D} - \frac{1}{AD}\sum_{j=i}^{n-1}(A_{Vj}H_j + V_j)(Z_j - x)$$

$$\theta_i = \frac{AZ_n^3}{6DV_{total}} + \sum_{j=1}^{n-1}\left(\frac{A_{Vj}H_j^3}{6D_{Vj}V_{total}} + \frac{V_jH_j^2}{2D_{Vj}V_{total}}\right)$$
$$- \sum_{j=1}^{n-1}\left(\frac{A_{Vj}H_j^3}{2D_{Vj}V_{total}} + \frac{3V_jH_j^2}{2D_{Vj}V_{total}} + \frac{V_j^2H_j}{D_{Vj}A_{Vj}V_{total}}\right) + \sum_{j=1}^{n-1}\left(\frac{A_{Vj}H_j}{V_{total}} + \frac{V_j}{V_{total}}\right)\left(\frac{Z_j^2 + (Z_n - Z_j)^2}{2D}\right)$$
$$+ \frac{1}{D}\sum_{j=1}^{n-1}\left(\frac{A_{Vj}H_j}{V_{total}} + \frac{V_j}{V_{total}}\right)\sum_{m=j+1}^{n-1}\left(\frac{A_{Vm}H_m}{A} + \frac{V_m}{A}\right)(Z_m - Z_j) - \frac{(Z_n - x)^2}{2D} - \frac{1}{AD}\sum_{j=i}^{n-1}(A_{Vj}H_j + V_j)(Z_j - x)$$

$$\theta_i = \frac{AZ_n^3}{6DV_{total}} - \sum_{j=1}^{n-1}\frac{A_{Vj}H_j}{D_{Vj}V_{total}}\left(\frac{H_j^2}{3} + \frac{V_jH_j}{A_{Vj}} + \left(\frac{V_j}{A_{Vj}}\right)^2\right) + \sum_{j=1}^{n-1}\left(\frac{A_{Vj}H_j}{V_{total}} + \frac{V_j}{V_{total}}\right)\left(\frac{Z_j^2 + (Z_n - Z_j)^2}{2D}\right)$$
$$+ \frac{1}{D}\sum_{j=1}^{n-1}\left(\frac{A_{Vj}H_j}{V_{total}} + \frac{V_j}{V_{total}}\right)\sum_{m=j+1}^{n-1}\left(\frac{A_{Vm}H_m}{A} + \frac{V_m}{A}\right)(Z_m - Z_j) - \frac{(Z_n - x)^2}{2D} - \frac{1}{AD}\sum_{j=i}^{n-1}(A_{Vj}H_j + V_j)(Z_j - x) \qquad \text{(B.66)}$$

Eq. (B.66) predicts the position dependent time lag in the main line (stem) of the CV system described in Fig. B.1.

Equation (B.66) can be separated in three parts as:

$$\frac{\theta_i}{\theta_0} = \frac{\Upsilon}{\theta_0} + \frac{\Psi}{\theta_0} - 3\left(\frac{Z_n - x}{Z_n}\right)^2 - 6\sum_{j=i}^{n-1}\left(\frac{A_{Vj}H_j + V_j}{AZ_n}\right)\left(\frac{Z_j - x}{Z_n}\right) \tag{4.30}$$

where:

$$\theta_0 = \frac{Z_n^2}{6D} \tag{4.32}$$

$$\frac{\Upsilon}{\theta_0} = \frac{AZ_n}{V_{total}} - 6\sum_{j=1}^{n-1}\frac{DA_{Vj}H_j}{D_{Vj}V_{total}}\left(\frac{1}{3}\left(\frac{H_j}{Z_n}\right)^2 + \frac{V_jH_j}{A_{Vj}Z_n^2} + \left(\frac{V_j}{A_{Vj}Z_n}\right)^2\right) + 3\sum_{j=1}^{n-1}\left(\frac{A_{Vj}H_j}{V_{total}} + \frac{V_j}{V_{total}}\right)\left(\frac{Z_j^2 + \left(Z_n - Z_j\right)^2}{Z_n^2}\right) \tag{4.34}$$

$$\frac{\Psi}{\theta_0} = 6\frac{V_{total}}{AZ_n}\sum_{j=1}^{n-1}\left(\frac{A_{Vj}H_j + V_j}{V_{total}}\right)\sum_{k=j+1}^{n-1}\left(\frac{A_{Vk}H_k + V_k}{V_{total}}\right)\left(\frac{Z_k - Z_j}{Z_n}\right) \tag{4.35}$$

The following equation can also be useful:

$$\lim_{s\to 0}\left(\frac{\Delta'(s)}{\Delta(s)} - \frac{1}{2Dq^2}\right) = \Upsilon + \Psi \tag{B.67}$$

B.8 Time lag for a branch

To determine the position dependent time lag in any branch Eqs. (B.44) and (B.45) can be used:

$$f_{Vi}(s) = \alpha q\delta_i\left(\cosh\left(q\left(Z_n - Z_i\right)\right) + \sum_{j=i+1}^{n-1}\lambda_j\left(\frac{M_{Vj}}{M_n}\sinh\left(qZ_n\right)\right)\sinh\left(q\left(Z_j - Z_i\right)\right)\right)\left(\cosh\left(q_{Vi}\left(H_i - y_i\right)\right) + \frac{V_iq_{Vi}}{A_{Vi}}\sinh\left(q_{Vi}\left(H_i - y_i\right)\right)\right) \tag{B.44}$$

$$\Delta_V(s) = \Delta(s)\left(\sinh(q_{Vi}H_i) + \frac{V_i q_{Vi}}{A_{Vi}}\cosh(q_{Vi}H_i)\right) \tag{B.45}$$

$$\Delta_V'(s) = \Delta'(s)\left(\sinh(q_{Vi}H_i) + \frac{V_i q_{Vi}}{A_{Vi}}\cosh(q_{Vi}H_i)\right) + \frac{\Delta(s)}{2D_{Vi}q_{vi}^2}\left(\left(H_i + \frac{V_i}{A_{Vi}}\right)\cosh(q_{Vi}H_i) + \frac{V_i q_{Vi}}{A_{Vi}}H_i\sinh(q_{Vi}H_i)\right)$$

$$\frac{\Delta_V'(s)}{\Delta_V(s)} = \frac{\Delta'(s)}{\Delta(s)} + \frac{\left(H_i + \frac{V_i}{A_{Vi}}\right)\cosh(q_{Vi}H_i) + \frac{V_i q_{Vi}}{A_{Vi}}H_i\sinh(q_{Vi}H_i)}{2D_{Vi}q_{vi}^2\left(\sinh(q_{Vi}H_i) + \frac{V_i q_{Vi}}{A_{Vi}}\cosh(q_{Vi}H_i)\right)}$$

$$\frac{\Delta_V'(0)}{\Delta_V(0)} = \frac{\Delta'(0)}{\Delta(0)} + \lim_{s\to 0}\frac{\left(H_i + \frac{V_i}{A_{Vi}}\right)\cosh(q_{Vi}H_i)}{2Dq^2\left(H_i\frac{\sinh(q_{Vi}H_i)}{q_{Vi}H_i} + \frac{V_i}{A_{Vi}}\cosh(q_{Vi}H_i)\right)} + \frac{\frac{V_i}{A_{Vi}}H_i^2}{2D_{Vi}\left(H_i + \frac{V_i}{A_{Vi}}\right)} \tag{B.68}$$

$$f_{Vi}(s) = \alpha q\delta_i\left(\cosh(q(Z_n - Z_i)) + \sum_{j=i+1}^{n-1}\lambda_j\left(\frac{M_{Vj}}{M_n}\sinh(qZ_n)\right)\sinh(q(Z_j - Z_i))\right)\times$$
$$\left(\cosh(q_{Vi}(H_i - y_i)) + \frac{V_i q_{Vi}}{A_{Vi}}\sinh(q_{Vi}(H_i - y_i))\right)$$

$$f_{Vi}(s) = \delta_i f_i(s, x = Z_i)\left(\cosh(q_{Vi}(H_i - y_i)) + \frac{V_i q_{Vi}}{A_{Vi}}\sinh(q_{Vi}(H_i - y_i))\right)$$

$$\frac{f'_{Vi}(s)}{f_{Vi}(s)}=\frac{f_i'(s,x=Z_i)}{f_i(s,x=Z_i)}+\frac{\frac{d\delta_i}{dq}}{2Dq\delta_i}+\frac{\sqrt{\frac{D}{D_{Vi}}}\frac{d}{dq_{Vi}}\left(\cosh\left(q_{Vi}(H_i-y_i)\right)+\frac{V_iq_{Vi}}{A_{Vi}}\sinh\left(q_{Vi}(H_i-y_i)\right)\right)}{2Dq\left(\cosh\left(q_{Vi}(H_i-y_i)\right)+\frac{V_iq_{Vi}}{A_{Vi}}\sinh\left(q_{Vi}(H_i-y_i)\right)\right)} \tag{B.69}$$

$$\theta_{Vi}=\frac{\Delta'_V(s)}{\Delta_V(s)}-\frac{f'_{Vi}(s)}{f_{Vi}(s)}=\left(\frac{\Delta'(0)}{\Delta(0)}-\frac{f_i'(0,x=Z_i)}{f_i(0,x=Z_i)}\right)+\lim_{s\to0}\frac{\left(H_i+\frac{V_i}{A_{Vi}}\right)\cosh\left(q_{Vi}H_i\right)}{2Dq^2\left(H_i\frac{\sinh\left(q_{Vi}H_i\right)}{q_{Vi}H_i}+\frac{V_i}{A_{Vi}}\cosh\left(q_{Vi}H_i\right)\right)}+\frac{\frac{V_i}{A_{Vi}}H_i^2}{2D_{Vi}\left(H_i+\frac{V_i}{A_{Vi}}\right)}-\lim_{s\to0}\frac{\frac{d\delta_i}{dq}}{2Dq\delta_i}-$$

$$\lim_{s\to0}\frac{\sqrt{\frac{D}{D_{Vi}}}\frac{d}{dq_{Vi}}\left(\cosh\left(q_{Vi}(H_i-y_i)\right)+\frac{V_iq_{Vi}}{A_{Vi}}\sinh\left(q_{Vi}(H_i-y_i)\right)\right)}{2Dq\left(\cosh\left(q_{Vi}(H_i-y_i)\right)+\frac{V_iq_{Vi}}{A_{Vi}}\sinh\left(q_{Vi}(H_i-y_i)\right)\right)}$$

$$\frac{\frac{d}{dq_{Vi}}\left(\cosh\left(q_{Vi}(H_i-y_i)\right)+\frac{V_iq_{Vi}}{A_{Vi}}\sinh\left(q_{Vi}(H_i-y_i)\right)\right)}{q_{Vi}\left(\cosh\left(q_{Vi}(H_i-y_i)\right)+\frac{V_iq_{Vi}}{A_{Vi}}\sinh\left(q_{Vi}(H_i-y_i)\right)\right)}=\frac{q_{Vi}\left(\left((H_i-y_i)^2+\frac{V_i}{A_{Vi}}(H_i-y_i)\right)\frac{\sinh\left(q_{Vi}(H_i-y_i)\right)}{q_{Vi}(H_i-y_i)}+\frac{V_i}{A_{Vi}}(H_i-y_i)\cosh\left(q_{Vi}(H_i-y_i)\right)\right)}{q_{Vi}\left(\cosh\left(q_{Vi}(H_i-y_i)\right)+\frac{V_iq_{Vi}}{A_{Vi}}\sinh\left(q_{Vi}(H_i-y_i)\right)\right)}$$

$$\lim_{s\to0}\frac{\sqrt{\frac{D}{D_{Vi}}}\frac{d}{dq_{Vi}}\left(\cosh\left(q_{Vi}(H_i-y_i)\right)+\frac{V_iq_{Vi}}{A_{Vi}}\sinh\left(q_{Vi}(H_i-y_i)\right)\right)}{2D\left(q_{Vi}\sqrt{\frac{D_{Vi}}{D}}\right)\left(\cosh\left(q_{Vi}(H_i-y_i)\right)+\frac{V_iq_{Vi}}{A_{Vi}}\sinh\left(q_{Vi}(H_i-y_i)\right)\right)}=\frac{1}{2D_{Vi}}\left((H_i-y_i)^2+2\frac{V_i}{A_{Vi}}(H_i-y_i)\right)$$

$$\theta_{Vi} = \theta_i\left(x = Z_i\right) + \lim_{s\to 0}\frac{1}{2Dq^2}\left(\frac{\left(H_i + \frac{V_i}{A_{Vi}}\right)\cosh\left(q_{Vi}H_i\right)}{\left(H_i\frac{\sinh\left(q_{Vi}H_i\right)}{q_{Vi}H_i} + \frac{V_i}{A_{Vi}}\cosh\left(q_{Vi}H_i\right)\right)} - \frac{\frac{d\delta_i}{dq_{vi}}}{\frac{\delta_i}{q_{Vi}}}\right) + \frac{\frac{V_i}{A_{Vi}}H_i^2}{2D_{Vi}\left(H_i + \frac{V_i}{A_{Vi}}\right)} - \frac{1}{2D_{Vi}}\left(\left(H_i - y_i\right)^2 + 2\frac{V_i}{A_{Vi}}\left(H_i - y_i\right)\right)$$

$$\phi_i = \left(\frac{\left(H_i + \frac{V_i}{A_{Vi}}\right)\cosh\left(q_{Vi}H_i\right)}{\left(H_i\frac{\sinh\left(q_{Vi}H_i\right)}{q_{Vi}H_i} + \frac{V_i}{A_{Vi}}\cosh\left(q_{Vi}H_i\right)\right)} - \frac{\frac{d\delta_i}{dq_{vi}}}{\frac{\delta_i}{q_{Vi}}}\right) = \left(\begin{array}{l}\dfrac{\left(H_i + \frac{V_i}{A_{Vi}}\right)\cosh\left(q_{Vi}H_i\right)}{\left(H_i\frac{\sinh\left(q_{Vi}H_i\right)}{q_{Vi}H_i} + \frac{V_i}{A_{Vi}}\cosh\left(q_{Vi}H_i\right)\right)} \\ -\dfrac{\dfrac{\left(H_i + \frac{V_i}{A_{Vi}}\right)}{\left(\cosh\left(q_{Vi}H_i\right) + \frac{V_i q_{Vi}}{A_{Vi}}\sinh\left(q_{Vi}H_i\right)\right)^2} - \dfrac{\frac{D}{D_{Vi}}q^2\left(\frac{V_i}{A_{Vi}}\right)^2 H_i}{\left(\cosh\left(q_{Vi}H_i\right) + \frac{V_i q_{Vi}}{A_{Vi}}\sinh\left(q_{Vi}H_i\right)\right)^2}}{\dfrac{H_j\frac{\sinh\left(q_{Vj}H_j\right)}{q_{Vj}H_j} + \frac{V_j}{A_{Vj}}\cosh\left(q_{Vj}H_j\right)}{\cosh\left(q_{Vj}H_j\right) + \frac{V_j q_{Vj}}{A_{Vj}}\sinh\left(q_{Vj}H_j\right)}}\end{array}\right)$$

$$\phi_i = \frac{1}{\left(H_i\frac{\sinh\left(q_{Vi}H_i\right)}{q_{Vi}H_i} + \frac{V_i}{A_{Vi}}\cosh\left(q_{Vi}H_i\right)\right)\left(\cosh\left(q_{Vi}H_i\right) + \frac{V_i q_{Vi}}{A_{Vi}}\sinh\left(q_{Vi}H_i\right)\right)}\left(\begin{array}{l}\left(H_i + \frac{V_i}{A_{Vi}}\right)\cosh\left(q_{Vi}H_i\right)\left(\cosh\left(q_{Vi}H_i\right) + \frac{V_i q_{Vi}}{A_{Vi}}\sinh\left(q_{Vi}H_i\right)\right) \\ -\left(H_i + \frac{V_i}{A_{Vi}}\right) + \frac{D}{D_{Vi}}q^2\left(\frac{V_i}{A_{Vi}}\right)^2 H_i\end{array}\right)$$

$$\phi_i = \frac{1}{\left(H_i \frac{\sinh\left(q_{Vi}H_i\right)}{q_{Vi}H_i} + \frac{V_i}{A_{Vi}}\cosh\left(q_{Vi}H_i\right)\right)\left(\cosh\left(q_{Vi}H_i\right) + \frac{V_i q_{Vi}}{A_{Vi}}\sinh\left(q_{Vi}H_i\right)\right)} \left(\begin{array}{l} \left(H_i + \frac{V_i}{A_{Vi}}\right)\left(\cosh^2\left(q_{Vi}H_i\right) - 1\right) + \\ \frac{D}{D_{Vi}}q^2\left(H_i + \frac{V_i}{A_{Vi}}\right)\frac{V_i}{A_{Vi}}H_i\cosh\left(q_{Vi}H_i\right)\frac{\sinh\left(q_{Vi}H_i\right)}{q_{Vi}H_i} + \\ \frac{D}{D_{Vi}}q^2\left(\frac{V_i}{A_{Vi}}\right)^2 H_i \end{array} \right)$$

$$\lim_{s\to 0}\frac{1}{2Dq^2}\phi_i = \frac{1}{2D_{Vi}\left(H_i + \frac{V_i}{A_{Vi}}\right)}\left(\left(H_i + \frac{V_i}{A_{Vi}}\right)H_i^2 + \left(H_i + \frac{V_i}{A_{Vi}}\right)\frac{V_i}{A_{Vi}}H_i + \left(\frac{V_i}{A_{Vi}}\right)^2 H_i\right)$$

$$\lim_{s\to 0}\frac{1}{2Dq^2}\phi_i = \frac{H_i\left(H_i + \frac{V_i}{A_{Vi}}\right)}{2D_{Vi}} + \frac{\left(\frac{V_i}{A_{Vi}}\right)^2 H_i}{2D_{Vi}\left(H_i + \frac{V_i}{A_{Vi}}\right)}$$

$$\theta_{Vi} = \theta_i\left(x = Z_i\right) + \frac{H_i\left(H_i + \frac{V_i}{A_{Vi}}\right)}{2D_{Vi}} + \frac{\left(\frac{V_i}{A_{Vi}}\right)^2 H_i}{2D_{Vi}\left(H_i + \frac{V_i}{A_{Vi}}\right)} + \frac{\frac{V_i}{A_{Vi}}H_i^2}{2D_{Vi}\left(H_i + \frac{V_i}{A_{Vi}}\right)} - \frac{1}{2D_{Vi}}\left(\left(H_i - y_i\right)^2 + 2\frac{V_i}{A_{Vi}}\left(H_i - y_i\right)\right)$$

$$\theta_{Vi} = \theta_i(x = Z_i) + \frac{H_i\left(H_i + 2\frac{V_i}{A_{Vi}}\right)}{2D_{Vi}} - \frac{1}{2D_{Vi}}\left((H_i - y_i)^2 + 2\frac{V_i}{A_{Vi}}(H_i - y_i)\right) \quad \text{(B.70)}$$

Alternatively, starting from the original equation, Eq. (B.66), or its equivalent Eq. (4.30):

$$\theta_{i+1} = \Upsilon + \Psi - \frac{(Z_n - (Z_i + y))^2}{2D} - \frac{1}{AD}\sum_{j=i}^{n-1}(A_{Vj}H_j + V_j)(Z_j - (Z_i + y))$$

$$\theta_i(x = Z_i) = \Upsilon + \Psi - \frac{(Z_n - Z_i)^2}{2D} - \frac{1}{AD}\sum_{j=i}^{n-1}(A_{Vj}H_j + V_j)(Z_j - Z_i)$$

Let $n=i+2$, $Z_n=Z_{i+1}$, $H_i=Z_{i+1}-Z_i=Z_n-Z_i=Z_{i+2}-Z_i$, $H_{i+1}=0$.

$$\theta_{i+1} = \Upsilon + \Psi - \frac{(H_i - y)^2}{2D} - \frac{V_{i+1}}{AD}(H_i - y)$$

$$\theta_i(x = Z_i) = \Upsilon + \Psi - \frac{H_i^2}{2D} - \frac{H_i}{AD}(V_{i+1})$$

$$\theta_{i+1} = \theta_i(x = Z_i) + \frac{H_i^2}{2D} + \frac{H_i}{AD}(V_{i+1}) - \frac{(H_i - y)^2}{2D} - \frac{V_{i+1}}{AD}(H_i - y)$$

This equation is valid with the assumption of a constant cross sectional area and a constant diffusion coefficient.

B.9 Limitation to the previous equations

B.9.1. Special cases when all of the volumes are directly connected to the main line (H_j=0)

$$\theta_i = \Upsilon + \Psi - \frac{(Z_n - x)^2}{2D} - \frac{1}{AD}\sum_{j=i}^{n-1}V_j(Z_j - x)$$

$$\Upsilon = \frac{AZ_n^3}{6DV_{total}} + \sum_{j=1}^{n-1}\frac{V_i}{V_{total}}\left(\frac{Z_j^2 + (Z_n - Z_j)^2}{2D}\right)$$

$$\Psi = \frac{1}{D}\sum_{j=1}^{n-1}\frac{V_j}{V_{total}}\sum_{k=j+1}^{n-1}\frac{V_k}{A}(Z_k - Z_j)$$

If all volumes are zero, then:

$$\theta_i = \Upsilon + \Psi - \frac{(Z_n - x)^2}{2D}$$

$$\Upsilon = \frac{AZ_n^3}{6DV_{total}}$$

$$\Psi = 0$$

or

$$\theta_i = \frac{AZ_n^3}{6DV_{total}} - \frac{(Z_n - x)^2}{2D}$$

Since in this case $Z_n = \frac{V_{total}}{A}$ and $Z_n = l$; therefore, Eq. (4.3) applicable for a single tube is obtained

$$\theta(x) = \frac{l^2}{6D} - \frac{(l-x)^2}{2D} \tag{4.3}$$

If n=2 L_2=0 L_1=l H_1 =0 V_1=V. Therefore Z_n=l

$$\theta_i = \Upsilon + \Psi - \frac{(l-x)^2}{2D} - \frac{1}{AD}V(l-x)$$

$$\Upsilon = \frac{Al^3}{6DV_{total}} + \frac{V}{V_{total}}\left(\frac{l^2 + (l-l)^2}{2D}\right)$$

$$\Psi = 0$$

$$\theta_i = \frac{Al^3}{6DV_{total}} + \frac{Vl^2}{2DV_{total}} - \frac{(l-x)^2}{2D} - \frac{V(l-x)}{AD}$$

Substituting $\frac{V_{total}}{A} = l + \frac{V}{A}$ in this equation gives:

$$\theta(x) = \frac{\frac{l^2}{D}\left(\frac{l}{6} + \frac{V}{2A}\right)}{l + \frac{V}{A}} - \frac{(l-x)^2}{2D} - \frac{V(l-x)}{AD} \tag{4.5}$$

B.9.2. Special case for single tank as in Figure B.2, when $A_1 = A_2$. This requires, n=2 L_1= l_1 L_2= l_2 H_1=l_3 V_1=V. Therefore, Z_n=l_1+l_2

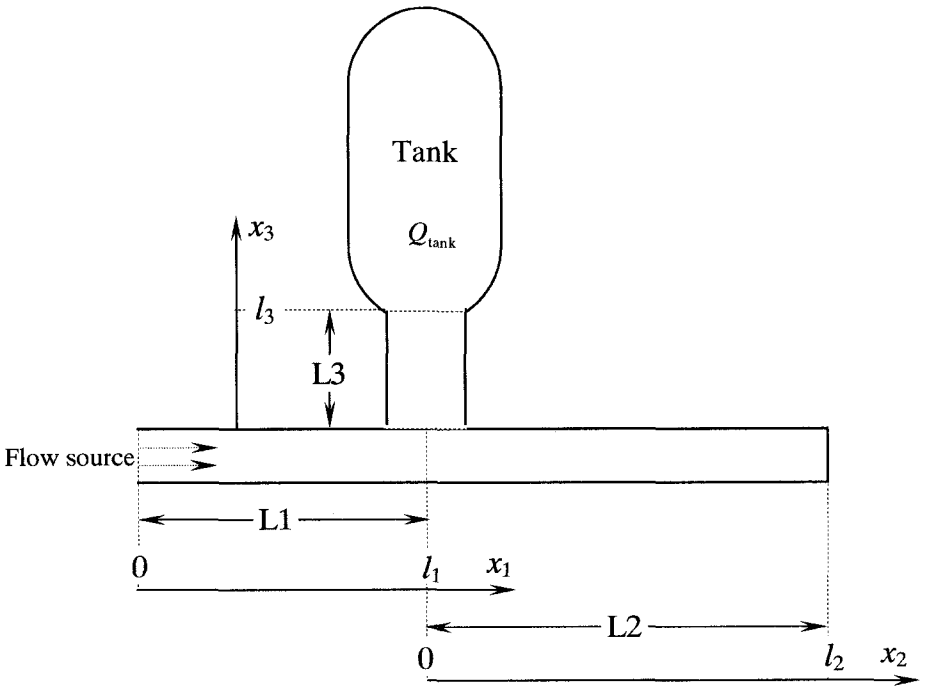

Figure B.2. Schematic representation of a single-tank receiver of CV system. Simplified configuration of an outflow receiver for the modeling purposes.

$$\frac{\theta_1}{\theta_0} = \frac{\Upsilon}{\theta_0} + \frac{\Psi}{\theta_0} - 3\left(\frac{l_1 + l_2 - x}{l_1 + l_2}\right)^2 - 6\left(\frac{A_3 l_3 + V}{A(l_1 + l_2)}\right)\left(\frac{l_1 - x}{l_1 + l_2}\right)$$

$$\frac{\theta_2}{\theta_0} = \frac{\Upsilon}{\theta_0} + \frac{\Psi}{\theta_0} - 3\left(\frac{l_1 + l_2 - x}{l_1 + l_2}\right)^2$$

where:

$$\theta_0 = \frac{(l_1 + l_2)^2}{6D} \qquad \frac{\Psi}{\theta_0} = 0$$

$$\frac{\Upsilon}{\theta_0} = \frac{AZ_n}{V_{total}} - 6\sum_{j=1}^{n-1} \frac{DA_{Vj}H_j}{D_{Vj}V_{total}}\left(\frac{1}{3}\left(\frac{H_j}{Z_n}\right)^2 + \frac{V_j H_j}{A_{Vj}Z_n^2} + \left(\frac{V_j}{A_{Vj}Z_n}\right)^2\right) + 3\sum_{j=1}^{n-1}\left(\frac{A_{Vj}H_j}{V_{total}} + \frac{V_j}{V_{total}}\right)\left(\frac{Z_j^2 + (Z_n - Z_j)^2}{Z_n^2}\right)$$

$$\frac{\Upsilon}{\theta_0} = \frac{A(l_1 + l_2)}{V_{total}} - 6\frac{DA_3 l_3}{D_3 V_{total}}\left(\frac{1}{3}\left(\frac{l_3}{l_1 + l_2}\right)^2 + \frac{Vl_3}{A_3(l_1 + l_2)^2} + \left(\frac{V}{A_3(l_1 + l_2)}\right)^2\right) + 3\left(\frac{A_3 l_3}{V_{total}} + \frac{V}{V_{total}}\right)\left(\frac{l_1^2 + (l_1 + l_2 - l_1)^2}{(l_1 + l_2)^2}\right)$$

$$\frac{\Upsilon}{\theta_0} = \frac{A(l_1 + l_2)}{V_{total}} - 6\frac{DA_3 l_3}{D_3 V_{total}(l_1 + l_2)^2}\left(\frac{l_3^2}{3} + \frac{Vl_3}{A_3} + \left(\frac{V}{A_3}\right)^2\right) + 3\left(1 - \frac{A(l_1 + l_2)}{V_{total}}\right)\left(\frac{(l_1 + l_2)^2 - 2l_1 l_2}{(l_1 + l_2)^2}\right)$$

$$\Upsilon = \frac{A(l_1+l_2)^3}{6DV_{total}} - \frac{A_3 l_3}{D_3 V_{total}}\left(\frac{l_3^2}{3}+\frac{Vl_3}{A_3}+\left(\frac{V}{A_3}\right)^2\right)+\left(1-\frac{A(l_1+l_2)}{V_{total}}\right)\left(\frac{(l_1+l_2)^2-2l_1l_2}{2D}\right)$$

It can be proved that:

$$-\frac{A_3 l_3}{D_3 V_{total}}\left(\frac{l_3^2}{3}+\frac{Vl_3}{A_3}+\left(\frac{V}{A_3}\right)^2\right) = 2\frac{V}{A_3 l_3}\left(1-\frac{A_3 l_3+V}{V_{total}}\right)\frac{l_3^2}{2D_3}+\frac{l_3^2}{2D_3}\left(1-\frac{2}{3}\frac{A_3 l_3}{V_{total}}\right)-\left(1+2\frac{V}{A_3 l_3}\right)\frac{l_3^2}{2D_3}$$

Therefore:

$$\Upsilon = -A\frac{l_1^3+l_2^3+3l_1l_2(l_1+l_2)}{3DV_{total}}+2\frac{V}{A_3 l_3}\left(1-\frac{A_3 l_3+V}{V_{total}}\right)\frac{l_3^2}{2D_3}+\frac{l_3^2}{2D_3}\left(1-\frac{2}{3}\frac{A_3 l_3}{V_{total}}\right)$$
$$-\left(1+2\frac{V}{A_3 l_3}\right)\frac{l_3^2}{2D_3}+\frac{l_1^2+l_2^2}{2D}+\frac{Al_1l_2(l_1+l_2)}{DV_{total}}$$

$$\Upsilon = \Phi-\left(1+2\frac{V}{A_3 l_3}\right)\frac{l_3^2}{2D_3}$$

$$\theta_1 = \Phi-\left(1+2\frac{V}{A_3 l_3}\right)\frac{l_3^2}{2D_3}-\left[3\left(\frac{l_1+l_2-x}{l_1+l_2}\right)^2-6\left(\frac{A_3 l_3+V}{A(l_1+l_2)}\right)\left(\frac{l_1-x}{l_1+l_2}\right)\right]\frac{(l_1+l_2)^2}{6D}$$

$$\theta_1 = \Phi-\left(1+2\frac{V}{A_3 l_3}\right)\frac{l_3^2}{2D_3}-\frac{l_2^2}{2D}-2\frac{Al_2(l_1-x)^2}{A2D(l_1-x)}-\left(1+2\frac{A_3 l_3+V}{A(l_1-x)}\right)\frac{(l_1-x)^2}{2D}$$

For L1, $x = x_1$

$$\theta_1 = \Phi-\left(1+2\frac{V}{A_3 l_3}\right)\frac{l_3^2}{2D_3}-\frac{l_2^2}{2D}-\left(1+2\frac{Al_2+A_3 l_3+V}{A(l_1-x_1)}\right)\frac{(l_1-x_1)^2}{2D}$$

for L2, $x = l_1+x_2$

$$\theta_2 = \Upsilon+\Psi-3\left(\frac{l_2-x_2}{l_1+l_2}\right)^2\frac{(l_1+l_2)^2}{6D}$$

$$\theta_2 = \Phi-\left(1+2\frac{V}{A_3 l_3}\right)\frac{l_3^2}{2D_3}-\frac{(l_2-x_2)^2}{2D}$$

For θ_3 Equation (4.31) should be used:

$$\frac{\theta_{Vi}}{\theta_0} = \frac{\theta_i(x=Z_i)}{\theta_0}+3\frac{D}{D_{Vi}}\frac{H_i\left(H_i+2\frac{V_i}{A_{Vi}}\right)}{Z_n^2}-3\frac{D}{D_{Vi}}\left(\left(\frac{H_i-y_i}{Z_n}\right)^2+2\frac{V_i}{A_{Vi}Z_n}\frac{(H_i-y_i)}{Z_n}\right) \quad (4.31)$$

$$\frac{\theta_3}{\theta_0}=\frac{\theta_1(x_1=l_1)}{\theta_0}+3\frac{D}{D_3}\frac{l_3\left(l_3+2\frac{V}{A_3}\right)}{(l_1+l_2)^2}-3\frac{D}{D_3}\left(\left(\frac{l_3-x_3}{l_1+l_2}\right)^2+2\frac{V}{A_3(l_1+l_2)}\frac{(l_3-x_3)}{(l_1+l_2)}\right)$$

$$\theta_1(x_1=l_1)=\Phi-\left(1+2\frac{V}{A_3l_3}\right)\frac{l_3^2}{2D_3}-\frac{l_2^2}{2D}-\left(1+2\frac{Al_2+A_3l_3+V}{A(l_1-x_1)}\right)\frac{(l_1-l_1)^2}{2D}=\Phi-\left(1+2\frac{V}{A_3l_3}\right)\frac{l_3^2}{2D_3}-\frac{l_2^2}{2D}$$

$$\theta_3=\Phi-\left(1+2\frac{V}{A_3l_3}\right)\frac{l_3^2}{2D_3}-\frac{l_2^2}{2D}+\frac{l_3(A_3l_3+2V)}{2D_3}-\frac{(l_3-x_3)^2}{2D_3}\left(1+2\frac{V}{A_3(l_3-x_3)}\right)$$

$$\theta_3=\Phi-\frac{l_2^2}{2D}-\frac{(l_3-x_3)^2}{2D_3}\left(1+2\frac{V}{A_3(l_3-x_3)}\right)$$

B.9.3. Single tank equation

It can be shown that in the limiting case, in which there is only one accumulation tank attached to the main line, Eq. (4.30) becomes Eq. (4.7) for the tube upstream from the junction point. Similarly, in this limiting case Eq. (4.31) becomes Eq. (4.9) for the connecting tube and Eq. (4.8) for the tube downstream from the connection point. This proves consistency between the model for a multiple-tank receiver developed in this study and the previously developed model for the receiver with a single tank. The following configuration will provide the result:

$$\begin{array}{lllll} n=3 & L_1=l_1 & L_2=L_3=0 & H_1=l_2 & H_2=l_3 \\ A=A_1 & A_{V1}=A_2 & A_{V2}=A_3 & V_1=0 & V_2=V \\ D=D_1 & D_{V1}=D_2 & D_{V2}=D_3 & Z_n=l_1 & \end{array} \qquad (4.36)$$

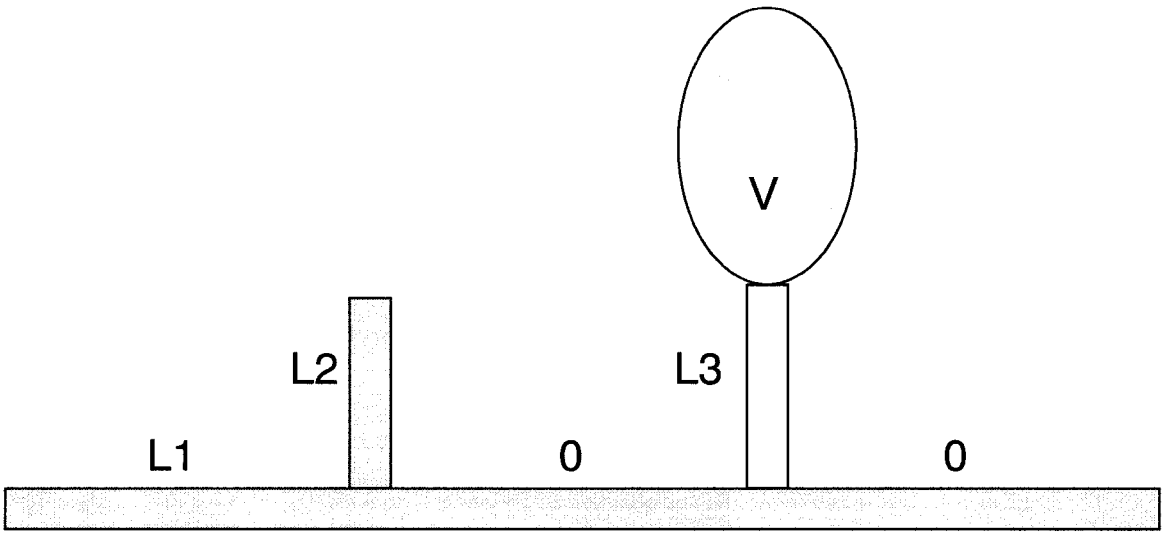

Eq. (4.32)
$$\theta_0 = \frac{l_1^2}{6D_1} \tag{B.71}$$

Eq. (4.35)
$$\frac{\Psi}{\theta_0} = 0 \tag{B.72}$$

Eq. (4.34)

$$\frac{\Upsilon}{\theta_0} = \frac{AZ_n}{V_{total}} - 6\sum_{j=1}^{n-1} \frac{DA_{Vj}H_j}{D_{Vj}V_{total}} \left(\frac{1}{3}\left(\frac{H_j}{Z_n}\right)^2 + \frac{V_j H_j}{A_{Vj}Z_n^2} + \left(\frac{V_j}{A_{Vj}Z_n}\right)^2 \right) + 3\sum_{j=1}^{n-1} \left(\frac{A_{Vi}H_i}{V_{total}} + \frac{V_i}{V_{total}} \right) \left(\frac{Z_j^2 + (Z_n - Z_j)^2}{Z_n^2} \right)$$

$$\frac{\Upsilon}{\theta_0} = \frac{A_1 l_1}{V_{total}} - 6\frac{D_1 A_2 l_2}{D_2 V_{total}} \frac{1}{3}\left(\frac{l_2}{l_1}\right)^2 - 6\frac{D_1 A_3 l_3}{D_3 V_{total}} \left(\frac{1}{3}\left(\frac{l_3}{l_1}\right)^2 + \frac{V l_3}{A_3 l_1^2} + \left(\frac{V}{A_3 l_1}\right)^2 \right) + 3\frac{A_2 l_2}{V_{total}} + 3\left(\frac{A_3 l_3}{V_{total}} + \frac{V}{V_{total}} \right)$$

$$\Upsilon = \frac{l_1^2}{6D_1}\frac{A_1 l_1}{V_{total}} - \frac{A_2 l_2^3}{3D_2 V_{total}} - \frac{A_3 l_3^3}{D_3 V_{total}} \left(\frac{1}{3} + \frac{V}{A_3 l_3} + \left(\frac{V}{A_3 l_3}\right)^2 \right) + \frac{l_1^2}{2D_1}\frac{A_2 l_2}{V_{total}} + \frac{l_1^2}{2D_1}\frac{A_3 l_3 + V}{V_{total}} \tag{B.73}$$

Eq. (4.30)

$$\frac{\theta_i}{\theta_0} = \frac{\Upsilon}{\theta_0} + \frac{\Psi}{\theta_0} - 3\left(\frac{Z_n - x}{Z_n}\right)^2 - 6\sum_{j=i}^{n-1} \left(\frac{A_{Vj}H_j + V_j}{AZ_n} \right) \left(\frac{Z_j - x}{Z_n} \right)$$

$$\frac{\theta_1}{\theta_0} = \frac{\Upsilon}{\theta_0} + \frac{\Psi}{\theta_0} - 3\left(\frac{l_1 - x_1}{l_1}\right)^2 - 6\left(\frac{A_2 l_2}{A_1 l_1}\right)\left(\frac{l_1 - x_1}{l_1}\right) - 6\left(\frac{A_3 l_3 + V}{A_1 l_1}\right)\left(\frac{l_1 - x_1}{l_1}\right) \tag{B.74}$$

Substituting from Eq. (B.71) into Eq. (B.74):

$$\theta_1 = \Upsilon - \frac{(l_1 - x_1)^2}{2D_1} - \frac{A_2 l_2}{D_1 A_1}(l_1 - x_1) - \frac{A_3 l_3 + V}{D_1 A_1}(l_1 - x_1) \tag{B.75}$$

By adding and subtracting $\frac{l_2^2}{2D_2}+\left(1+2\frac{V}{A_3l_3}\right)\frac{l_3^2}{2D_3}$ terms to Eq. (B.75)

$$\theta_1=\left[\Upsilon+\frac{l_2^2}{2D_2}+\left(1+2\frac{V}{A_3l_3}\right)\frac{l_3^2}{2D_3}\right]-\left(1+2\frac{V_{total}-A_1l_1}{A_1(l_1-x_1)}\right)\frac{(l_1-x_1)^2}{2D_1}-\frac{l_2^2}{2D_2}-\left(1+2\frac{V}{A_3l_3}\right)\frac{l_3^2}{2D_3} \quad \text{(B.76)}$$

which is equal to Equation (4.7) where Φ is equal to $\left[\Upsilon+\frac{l_2^2}{2D_2}+\left(1+2\frac{V}{A_3l_3}\right)\frac{l_3^2}{2D_3}\right]$. The next task is to show that Φ in Equation (4.11) is equal to its corresponding term in Eq. (B.76). By substituting Eq. (B.73) for its corresponding term in the bracket:

$$\left[\Upsilon+\frac{l_2^2}{2D_2}+\left(1+2\frac{V}{A_3l_3}\right)\frac{l_3^2}{2D_3}\right]=\frac{l_1^2}{6D_1}\frac{A_1l_1}{V_{total}}-\frac{A_2l_2^3}{3D_2V_{total}}-\frac{A_3l_3^3}{D_3V_{total}}\left(\frac{1}{3}+\frac{V}{A_3l_3}+\left(\frac{V}{A_3l_3}\right)^2\right)$$
$$+\frac{l_1^2}{2D_1}\frac{A_2l_2}{V_{total}}+\frac{l_1^2}{2D_1}\frac{A_3l_3+V}{V_{total}}+\frac{l_2^2}{2D_2}+\left(1+2\frac{V}{A_3l_3}\right)\frac{l_3^2}{2D_3}$$

$$\left[\Upsilon+\frac{l_2^2}{2D_2}+\left(1+2\frac{V}{A_3l_3}\right)\frac{l_3^2}{2D_3}\right]=\left(1+2\frac{V}{A_3l_3}\right)\frac{l_3^2}{2D_3}-\frac{l_3^2}{2D_3}\frac{A_3l_3}{V_{total}}\left(\frac{2}{3}+\frac{2V}{A_3l_3}+2\left(\frac{V}{A_3l_3}\right)^2\right)$$
$$+\frac{l_2^2}{2D_2}-\frac{A_2l_2^3}{3D_2V_{total}}+\frac{l_1^2}{6D_1}\frac{A_1l_1}{V_{total}}+\frac{l_1^2}{2D_1}\frac{A_3l_3+V}{V_{total}}+\frac{l_1^2}{2D_1}\frac{A_2l_2}{V_{total}}$$

$$\left[\Upsilon+\frac{l_2^2}{2D_2}+\left(1+2\frac{V}{A_3l_3}\right)\frac{l_3^2}{2D_3}\right]=2\frac{V}{A_3l_3}\left(1-\frac{A_3l_3+V}{V_{total}}\right)\frac{l_3^2}{2D_3}+\left[\frac{l_3^2}{2D_3}-\frac{2}{3}\frac{l_3^2}{2D_3}\frac{A_3l_3}{V_{total}}\right]$$
$$+\left[\frac{l_2^2}{2D_2}-\frac{l_2^2}{2D_2}\frac{2A_2l_2}{3V_{total}}\right]+\frac{l_1^2}{2D_1}\left(\frac{A_1l_1}{3V_{total}}+\frac{A_3l_3+V+A_2l_2}{V_{total}}\right)$$

Since $\frac{A_3l_3+V+A_2l_2}{V_{total}}=\frac{V_{total}-A_1l_1}{V_{total}}=1-\frac{A_1l_1}{V_{total}}$

$$\left[\Upsilon+\frac{l_2^2}{2D_2}+\left(1+2\frac{V}{A_3l_3}\right)\frac{l_3^2}{2D_3}\right]=2\frac{V}{A_3l_3}\left(1-\frac{A_3l_3+V}{V_{total}}\right)\frac{l_3^2}{2D_3}+\sum_{i=1}^{3}\frac{l_i^2}{2D_i}\left(1-\frac{2}{3}\frac{A_il_i}{V_{total}}\right)$$

which is the same as Eq. (4.10)

Using Eq. (4.31) for L2 and L3:

$$\frac{\theta_2}{\theta_0}=\frac{\theta_1(x_1=l_1)}{\theta_0}+3\frac{D_1}{D_2}\frac{l_2\left(l_2+2\frac{0}{A_2}\right)}{l_1^2}-3\frac{D_1}{D_2}\left(\left(\frac{l_2-x_2}{l_1}\right)^2+2\frac{0}{A_2l_1}\frac{(l_2-x_2)}{l_1}\right)$$

$$\frac{\theta_3}{\theta_0}=\frac{\theta_1(x_1=l_1)}{\theta_0}+3\frac{D_1}{D_3}\frac{l_3\left(l_3+2\frac{V}{A_3}\right)}{l_1^2}-3\frac{D_1}{D_3}\left(\left(\frac{l_3-x_3}{l_1}\right)^2+2\frac{V}{A_3l_1}\frac{(l_3-x_3)}{l_1}\right)$$

where from Eq. (4.33):

$$\frac{\theta_1(x_1=l_1)}{\theta_0}=\frac{\Upsilon}{\theta_0}+\frac{\Psi}{\theta_0}-3\left(\frac{l_1-l_1}{l_1}\right)^2-6\sum_{j=2}^{2}\left(\frac{A_{Vj}H_j+V_j}{A_1l_1}\right)\left(\frac{l_j-l_1}{l_1}\right)=\frac{\Upsilon}{\theta_0}$$

Therefore:

$$\frac{\theta_2}{\theta_0}=\frac{\Upsilon}{\theta_0}+3\frac{D_1}{D_2}\frac{l_2^2}{l_1^2}-3\frac{D_1}{D_2}\left(\frac{l_2-x_2}{l_1}\right)^2$$

$$\theta_2=\Upsilon+\frac{l_1^2}{6D_1}3\frac{D_1}{D_2}\frac{l_2^2}{l_1^2}-\frac{l_1^2}{6D_1}3\frac{D_1}{D_2}\left(\frac{l_2-x_2}{l_1}\right)^2$$

$$\theta_2=\left[\Upsilon+\frac{l_2^2}{2D_2}+\left(1+2\frac{V}{A_3l_3}\right)\frac{l_3^2}{2D_3}\right]+\frac{l_2^2}{2D_2}-\frac{(l_2-x_2)^2}{2D_2}-\frac{l_2^2}{2D_2}-\left(1+2\frac{V}{A_3l_3}\right)\frac{l_3^2}{2D_3}$$

Above expression corresponds to Eq. (4.8).

For L3:

$$\frac{\theta_3}{\theta_0}=\frac{\theta_1(x_1=l_1)}{\theta_0}+3\frac{D_1}{D_3}\frac{l_3\left(l_3+2\frac{V}{A_3}\right)}{l_1^2}-3\frac{D_1}{D_3}\left(\left(\frac{l_3-x_3}{l_1}\right)^2+2\frac{V}{A_3l_1}\frac{(l_3-x_3)}{l_1}\right)$$

$$\theta_3=\Upsilon+\frac{l_1^2}{6D_1}3\frac{D_1}{D_3}\frac{l_3\left(l_3+2\frac{V}{A_3}\right)}{l_1^2}-\frac{l_1^2}{6D_1}3\frac{D_1}{D_3}\left(\left(\frac{l_3-x_3}{l_1}\right)^2+2\frac{V}{A_3l_1}\frac{(l_3-x_3)}{l_1}\right)$$

$$\theta_3=\left[\Upsilon+\frac{l_2^2}{2D_2}+\left(1+2\frac{V}{A_3l_3}\right)\frac{l_3^2}{2D_3}\right]+\frac{l_3^2}{2D_3}\left(1+2\frac{V}{A_3l_3}\right)$$
$$-\frac{(l_3-x_3)^2}{2D_3}\left(1+2\frac{V}{A_3(l_3-x_3)}\right)-\frac{l_2^2}{2D_2}-\left(1+2\frac{V}{A_3l_3}\right)\frac{l_3^2}{2D_3}$$

Above expression the same as Eq. (4.9).

B.10 Case studies and applications

If $V \to \infty$ then $\theta(x) \to -\infty$

$$\theta(x) = \frac{\frac{l^2}{D}\left(\frac{l}{6} + \frac{V}{2A}\right)}{l + \frac{V}{A}} - \frac{(l-x)^2}{2D} - \frac{V(l-x)}{AD} \tag{4.5}$$

If $A \to \infty$, D increases and $\frac{l}{D} << 1$ therefore $|\theta(x)| << 1$

$$\theta(x) = \frac{l^2}{6D} - \frac{(l-x)^2}{2D} \tag{4.3}$$

B.10.1. The optimum volumes

An optimum configuration with n-1 accumulation tanks and n tubes, where $\sum_{j=1}^{n-1} V_j = V_{total}$ is constant, exists. The objective is to find the optimum volumes to create the lowest absolute time lag at the end of tubes ($x = Z_n$, $i = n$)

Since $\sum_{j=1}^{n-1} V_j = V_{total} \quad \Rightarrow \quad V_{n-1} = V_{total} - \sum_{j=1}^{n-2} V_j$

Therefore, using Eq. (4.30):

$$\left(\frac{\partial\left(\frac{\theta_i}{\theta_0}\right)}{\partial V_m}\right)_{Vi} = \left(\frac{\partial\left(\frac{\Upsilon}{\theta_0}\right)}{\partial V_m}\right)_{Vi} + \left(\frac{\partial\left(\frac{\Psi}{\theta_0}\right)}{\partial V_m}\right)_{Vi} + \Gamma \qquad \Gamma = \begin{cases} 6\frac{Z_{n-1} - Z_m}{AZ_n^2} & i \le m \\ 6\frac{Z_{n-1} - x}{AZ_n^2} & m < i < n \\ 0 & i = n \end{cases} \tag{B.77}$$

From Eq. (4.34):

$$\frac{\Upsilon}{\theta_0} = \frac{AZ_n}{V_{total}} - 6\sum_{j=1}^{n-1} \frac{DA_{Vj}H_j}{D_{Vj}V_{total}}\left(\frac{1}{3}\left(\frac{H_j}{Z_n}\right)^2 + \frac{V_j H_j}{A_{Vj}Z_n^2} + \left(\frac{V_j}{A_{Vj}Z_n}\right)^2\right) + 3\sum_{j=1}^{n-1}\left(\frac{A_{Vj}H_j}{V_{total}} + \frac{V_j}{V_{total}}\right)\left(\frac{Z_j^2 + (Z_n - Z_j)^2}{Z_n^2}\right) \tag{4.34}$$

$$\left(\frac{\partial\left(\frac{\Upsilon}{\theta_0}\right)}{\partial V_m}\right)_{Vi} = -6\frac{DA_{Vm}H_m}{D_{Vm}V_{total}}\left(\frac{H_m}{A_{Vm}Z_n^2} - 2V_m\left(\frac{1}{A_{Vm}Z_n}\right)^2\right) - 6\frac{DA_{Vn-1}H_{n-1}}{D_{Vn-1}V_{total}}\left(-\frac{H_{n-1}}{A_{Vn-1}Z_n^2} - 2V_{n-1}\left(\frac{1}{A_{Vn-1}Z_n}\right)^2\right)$$

$$+3\left(\frac{1}{V_{total}}\right)\left(\frac{Z_m^2+(Z_n-Z_m)^2}{Z_n^2} - \frac{Z_{n-1}^2+(Z_n-Z_{n-1})^2}{Z_n^2}\right)$$

or

$$\left(\frac{\partial\left(\frac{\Upsilon}{\theta_0}\right)}{\partial V_m}\right)_{Vi} = -6\frac{DA_{Vm}H_m}{D_{Vm}V_{total}}\left(\frac{H_m}{A_{Vm}Z_n^2} - 2V_m\left(\frac{1}{A_{Vm}Z_n}\right)^2\right) - 6\frac{DA_{Vn-1}H_{n-1}}{D_{Vn-1}V_{total}}\left(-\frac{H_{n-1}}{A_{Vn-1}Z_n^2} - 2V_{n-1}\left(\frac{1}{A_{Vn-1}Z_n}\right)^2\right)$$

$$+6\left(\frac{1}{V_{total}}\right)\left(\frac{Z_{n-1}-Z_m}{Z_n}\right)\left(1-\frac{Z_{n-1}+Z_m}{Z_n}\right)$$

From Eq. (4.35):

$$\left(\frac{\partial\left(\frac{\Psi}{\theta_0}\right)}{\partial V_m}\right)_{Vi} = 6\frac{Z_{n-1}-Z_m}{AZ_n^2V_{total}}\left(A_{Vn-1}H_{n-1}+V_{n-1}-A_{Vm}H_m-V_m\right)$$

Substituting into Eq. (B.77) gives:

$$\left(\frac{\partial\left(\frac{\theta_i}{\theta_0}\right)}{\partial V_m}\right)_{Vi} = -6\frac{1}{Z_n^2V_{total}}\left(\frac{D}{D_{Vm}}H_m^2 - 2\frac{D}{D_{Vm}}\frac{V_m}{A_{Vm}}H_m - \frac{D}{D_{Vn-1}}H_{n-1}^2 + 2\frac{D}{D_{Vn-1}}\frac{V_{n-1}}{A_{Vn-1}}H_{n-1}\right)$$

$$+6\left(\frac{1}{V_{total}}\right)\left(\frac{Z_{n-1}-Z_m}{Z_n}\right)\left(1-\frac{Z_{n-1}+Z_m}{Z_n}\right) + 6\frac{Z_{n-1}-Z_m}{AZ_n^2V_{total}}\left(A_{Vn-1}H_{n-1}+V_{n-1}-A_{Vm}H_m-V_m\right)+\Gamma$$

for $\left(\frac{\partial\left(\frac{\theta_i}{\theta_0}\right)}{\partial V_m}\right)_{Vi} = 0$ the optimum value for V_m can be determined

$$6\frac{1}{Z_n^2V_{total}}\left(-2\frac{D}{D_{Vm}}\frac{H_m}{A_{Vm}} + \frac{Z_{n-1}-Z_m}{A}\right)V_m = -6\frac{1}{Z_n^2V_{total}}\left(\frac{D}{D_{Vm}}H_m^2 - \frac{D}{D_{Vn-1}}H_{n-1}^2 + 2\frac{D}{D_{Vn-1}}\frac{V_{n-1}}{A_{Vn-1}}H_{n-1}\right)$$

$$+6\left(\frac{1}{V_{total}}\right)\left(\frac{Z_{n-1}-Z_m}{Z_n}\right)\left(1-\frac{Z_{n-1}+Z_m}{Z_n}\right) + 6\frac{Z_{n-1}-Z_m}{AZ_n^2V_{total}}\left(A_{Vn-1}H_{n-1}+V_{n-1}-A_{Vm}H_m\right)+\Gamma$$

or

$$V_m = \frac{\left[\left(\frac{D}{D_{Vn-1}}H_{n-1}^2 - \frac{D}{D_{Vm}}H_m^2 - 2\frac{D}{D_{Vn-1}}\frac{H_{n-1}}{A_{Vn-1}}V_{n-1}\right) + \left(\frac{1}{V_{total}}\right)\left(\frac{Z_{n-1}-Z_m}{Z_n}\right)\left(1-\frac{Z_{n-1}+Z_m}{Z_n}\right)\right.}{\left. + \frac{Z_{n-1}-Z_m}{A}\left(V_{n-1} + A_{Vn-1}H_{n-1} - A_{Vm}H_m\right) + \Gamma\frac{Z_n^2 V_{total}}{6}\right]} \qquad \text{(B.78)}$$

$$-2\frac{D}{D_{Vm}}\frac{H_m}{A_{Vm}} + \frac{Z_{n-1}-Z_m}{A}$$

for the end of the tube $i=n$, $\Gamma = 0$, therefore:

$$V_m = \frac{\frac{D}{D_{Vn-1}}H_{n-1}^2 - \frac{D}{D_{Vm}}H_m^2 - 2\frac{D}{D_{Vn-1}}\frac{H_{n-1}}{A_{Vn-1}}V_{n-1} + \frac{Z_{n-1}-Z_m}{A}\left(A_{Vn-1}H_{n-1} - A_{Vm}H_m + V_{n-1}\right)}{\left(-2\frac{D}{D_{Vm}}\frac{H_m}{A_{Vm}} + \frac{Z_{n-1}-Z_m}{A}\right)}$$

Then if H, A and D are the same for all the branches,

$$V_m = \frac{\left(-2\frac{H}{A_V}V_{n-1}\right) + \frac{Z_{n-1}-Z_m}{A}\left(V_{n-1}\right)}{\left(-2\frac{H}{A_V} + \frac{Z_{n-1}-Z_m}{A}\right)}$$

or $V_m = V_{n-1}$ for any m

Therefore, if all branches are the same configuration then all volumes should be equal. In general Equation (B.78) is useful for calculation of the optimum volume of the tanks. By specifying total volume and one of the volumes all other volumes can be optimized.

B.10.2. The optimum number of volumes

A configuration with n-1 volume and n tubes where

$V_i = \frac{V}{n-1}$, $H_i = H$, $A_{Vi} = A_V$ $i=1...n-1$ and $L_i = L$ $i=1...n$ exists. What would be the optimum n to create the lowest absolute time lag at the end of the main line?

From Eq. (4.32) $\theta_0 = \frac{Z_n^2}{6D} = \frac{L^2 n^2}{6D}$ and using Eq. (4.30)

$$n^2\frac{\theta_i}{\theta_0} = n^2\frac{\Upsilon}{\theta_0} + n^2\frac{\Psi}{\theta_0} - 3n^2\left(\frac{Ln-x}{Ln}\right)^2 - 6\sum_{j=i}^{n-1} n^2\left(\frac{A_V H + \frac{V}{n-1}}{ALn}\right)\left(\frac{Lj-x}{Ln}\right)$$

$$i = n \qquad x = Ln$$

$$n^2\frac{\theta_n}{\theta_0}=n^2\frac{\Upsilon}{\theta_0}+n^2\frac{\Psi}{\theta_0} \tag{B.79}$$

From Eq. (4.34)

$$\frac{\Upsilon}{\theta_0}=\frac{AZ_n}{V_{total}}-6\sum_{j=1}^{n-1}\frac{DA_{Vj}H_j}{D_{Vj}V_{total}}\left(\frac{1}{3}\left(\frac{H_j}{Z_n}\right)^2+\frac{V_jH_j}{A_{Vj}Z_n^2}+\left(\frac{V_j}{A_{Vj}Z_n}\right)^2\right)+3\sum_{j=1}^{n-1}\left(\frac{A_{Vj}H_j}{V_{total}}+\frac{V_j}{V_{total}}\right)\left(\frac{Z_j^2+\left(Z_n-Z_j\right)^2}{Z_n^2}\right) \tag{4.34}$$

$$n^2\frac{\Upsilon}{\theta_0}=n^2\frac{ALn}{V}-6n^2\sum_{j=1}^{n-1}\frac{DA_VH}{D_VV}\left(\frac{1}{3}\left(\frac{H}{Ln}\right)^2+\frac{\frac{V}{n-1}H}{A_VL^2n^2}+\left(\frac{\frac{V}{n-1}}{A_VLn}\right)^2\right)+3n^2\sum_{j=1}^{n-1}\left(\frac{A_VH}{V}+\frac{\frac{V}{n-1}}{V}\right)\left(\frac{j^2+\left(n-j\right)^2}{n^2}\right)$$

$$n^2\frac{\Upsilon}{\theta_0}=\frac{AL}{V}n^3-\frac{D}{D_V}\frac{A_VH}{V}\left(2\left(\frac{H}{L}\right)^2+\frac{6}{n-1}\left(\frac{V}{A_VH}\left(\frac{H}{L}\right)^2+\frac{1}{n-1}\left(\frac{V}{A_VH}\right)^2\left(\frac{H}{L}\right)^2\right)\right)\sum_{j=1}^{n-1}1$$
$$+3\left(\frac{A_VH}{V}+\frac{1}{n-1}\right)\left(2\sum_{j=1}^{n-1}j^2-2n\sum_{j=1}^{n-1}j+n^2\sum_{j=1}^{n-1}1\right)$$

$$n^2\frac{\Upsilon}{\theta_0}=\frac{AL}{V}n^3-\frac{D}{D_V}\frac{A_VH}{V}\left(\frac{H}{L}\right)^2\left(2\left(n-1\right)+6\frac{V}{A_VH}+\frac{6}{n-1}\left(\frac{V}{A_VH}\right)^2\right)$$
$$+3\left(\frac{A_VH}{V}+\frac{1}{n-1}\right)\left(2\sum_{j=1}^{n-1}j^2-2n\sum_{j=1}^{n-1}j+n^2\left(n-1\right)\right)$$

$$\sum_{j=1}^{n-1}j^2-n\sum_{j=1}^{n-1}j=\frac{n\left(n-1\right)\left(2n-1\right)}{6}-n\frac{n\left(n-1\right)}{2}=\frac{n\left(n-1\right)}{6}\left(2n-1-3n\right)=-\frac{\left(n+1\right)n\left(n-1\right)}{6}$$

Therefore,

$$n^2\frac{\Upsilon}{\theta_0}=\frac{AL}{V}n^3-2\frac{D}{D_V}\left(\frac{H}{L}\right)^2-\frac{4}{n-1}\frac{D}{D_V}\frac{V}{A_VH}\left(\frac{H}{L}\right)^2-2\left(n-1\right)\frac{D}{D_V}\frac{V}{A_VH}\left(\frac{H}{L}\right)^2\left(\frac{A_VH}{V}+\frac{1}{\left(n-1\right)}\right)^2$$
$$+n\left(n-1\right)\left(2n-1\right)\left(\frac{A_VH}{V}+\frac{1}{n-1}\right)$$

From Eq. (4.35):

$$n^2\frac{\Psi}{\theta_0}=6n^2\frac{V}{ALn}\sum_{j=1}^{n-1}\left(\frac{A_VH+\frac{V}{n-1}}{V}\right)\sum_{k=j+1}^{n-1}\left(\frac{A_VH+\frac{V}{n-1}}{V}\right)\left(\frac{k-j}{n}\right)$$

$$n^2\frac{\Psi}{\theta_0}=6\frac{V}{AL}\left(\frac{A_V H}{V}+\frac{1}{(n-1)}\right)^2\sum_{j=1}^{n-1}\sum_{k=j+1}^{n-1}(k-j)$$

$$\sum_{j=1}^{n-1}\sum_{k=j+1}^{n-1}(k-j)=\sum_{j=1}^{n-1}\left(\sum_{k=1}^{n-1}k-\sum_{k=1}^{j}k-j\sum_{k=j+1}^{n-1}1\right)=\sum_{j=1}^{n-1}\left(\frac{n(n-1)}{2}-\frac{j(j+1)}{2}-j(n-j-1)\right)$$

$$=\frac{n(n-1)}{2}\sum_{j=1}^{n-1}1-\left(n-\frac{1}{2}\right)\sum_{j=1}^{n-1}j+\frac{1}{2}\sum_{j=1}^{n-1}j^2=\frac{n(n-1)^2}{2}-\left(\frac{2n-1}{2}\right)\frac{n(n-1)}{2}+\frac{n(n-1)(2n-1)}{12}$$

$$=\frac{n(n-1)(n-2)}{6}$$

Substituting into Eq. (B.79) leads to:

$$n^2\frac{\theta_n}{\theta_0}=\frac{AL}{V}n^3-2\frac{D}{D_V}\left(\frac{H}{L}\right)^2-\frac{4}{n-1}\frac{D}{D_V}\frac{V}{A_V H}\left(\frac{H}{L}\right)^2-2(n-1)\frac{D}{D_V}\frac{V}{A_V H}\left(\frac{H}{L}\right)^2\left(\frac{A_V H}{V}+\frac{1}{(n-1)}\right)^2$$

$$+n(n-1)(2n-1)\left(\frac{A_V H}{V}+\frac{1}{n-1}\right)+6\frac{V}{AL}\left(\frac{A_V H}{V}+\frac{1}{(n-1)}\right)^2\frac{n(n-1)(n-2)}{6}$$

or

$$n^2\frac{\theta_n}{\theta_0}=\frac{AL}{V}n^3-2\frac{D}{D_V}\left(\frac{H}{L}\right)^2-\frac{4}{n-1}\frac{D}{D_V}\frac{V}{A_V H}\left(\frac{H}{L}\right)^2+n(n-1)(2n-1)\left(\frac{A_V H}{V}+\frac{1}{n-1}\right)$$

$$+(n-1)\left(\frac{V}{AL}n(n-2)-2\frac{D}{D_V}\frac{V}{A_V H}\left(\frac{H}{L}\right)^2\right)\left(\frac{A_V H}{V}+\frac{1}{(n-1)}\right)^2$$

(B.80)

There are three dimensionless parameters in the above equation

$$a=\frac{AL}{V}<<1\qquad b=\frac{A_V H}{V}<<1\qquad c=\frac{D}{D_V}\left(\frac{H}{L}\right)^2\approx\left(\frac{b}{a}\right)^2$$

Substituting in Equation (B.80):

$$n^2\frac{\theta_n}{\theta_0}=an^3-2c-\frac{4}{n-1}\frac{c}{b}+n(n-1)(2n-1)\left(b+\frac{1}{(n-1)}\right)+(n-1)\left(\frac{n(n-2)}{a}-2\frac{c}{b}\right)\left(b+\frac{1}{(n-1)}\right)^2$$

(B.81)

Eq. (B.81) shows an increase in the time lag by increasing n. It is possible to adjust a, b, and c to have zero time lag for any number of volumes at the end of the tube. Employing the same procedure a relationship can be found for the time lag to be zero at any other position.

Appendix C

Supplementary Material for "Effect of Back Diffusion and Back Permeation of Air on Membrane Characterization in Constant Pressure System"

In the current appendix some results from analytical and numerical calculations for a case with three tubes, including a bubble flowmeter tube, are presented. In all the following results, the gas transport mechanism in membrane is assumed to be governed by Equation (6.4), given in Chapter 6. In addition some experimental data and the corresponding calculated results, which were discarded from Chapter 6 for sake of brevity, are provided in this appendix.

C.1 System parameters

Figure C.1 is a schematic diagram for the case when CH_4 is transported from the membrane, passes through three tubes and eventually vanishes in free stream of air. At the same time air diffuses in the opposite direction according to its composition gradient. The flow rate of the feed gas is assumed to be high enough that concentration of air at the feed side of the membrane is negligible. Additional geometrical information of this system is presented in Table C.1.

The pressure inside tubes is constant and equal to the atmospheric pressure while the membrane feed pressure can be adjusted using a regulator connected to the gas cylinder. The temperature is constant and equal to ambient temperature (T=20°C). Component permeabilities through the poly-phenylene oxide membrane obtained from Chowdhury et al. [1] and are summarized in Table C.2. The data was substituted into equations developed in Section 6.2.2 (Chapter 6) and some selected results are presented in Figures C.2 to C.7.

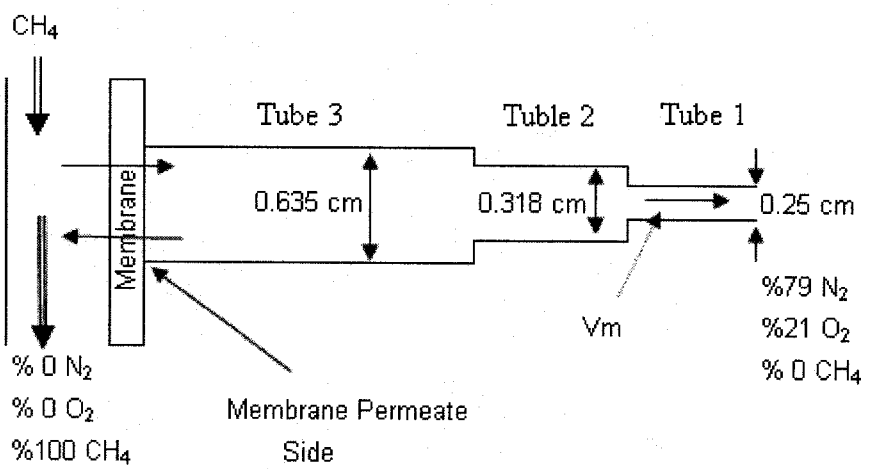

Figure C.1. Schematic diagram of system for a selected case (CH_4-Air)

Table C.1. Parameters of the system plotted in Figure C.1.

	Cross Section Area (cm^2)	Length (cm)
Tube 1	0.049	15
Tube 2	0.079	15
Tube 3	0.317	130
Membrane	10	Variable Thickness

Table C.2. Permeability of components through PPO membrane.

	Air	CH_4	CO_2	H_2	N_2	O_2
P_i(Barrer)	3.5	1.5	45	50	1.7	10

C.2 Binary systems at steady state conditions

Modeling for this part can be found in Chapter 6. Chapter 6 was restricted to O_2/N_2 system. Methane/Air can also be treated as binary system when air assumed to be a single component. Selected results for CH_4/Air are presented in this section. Analysis for ternary system of CH_4/Air(N_2,O_2) will be presented later in this appendix.

When methane is the forward permeating gas, air can back diffuse through the tubes and back permeate through the membrane. Figure C.2 presents the predictions for the concentration of methane at the permeate side of membrane. Note that without back diffusion, x_{CH4} = 1. The net velocity and flow rate versus methane feed pressure and membrane thickness are presented in Figures C.3 and C.4. Figure C.5 shows the error associated with the measurement of the permeability of methane due to back diffusion of air.

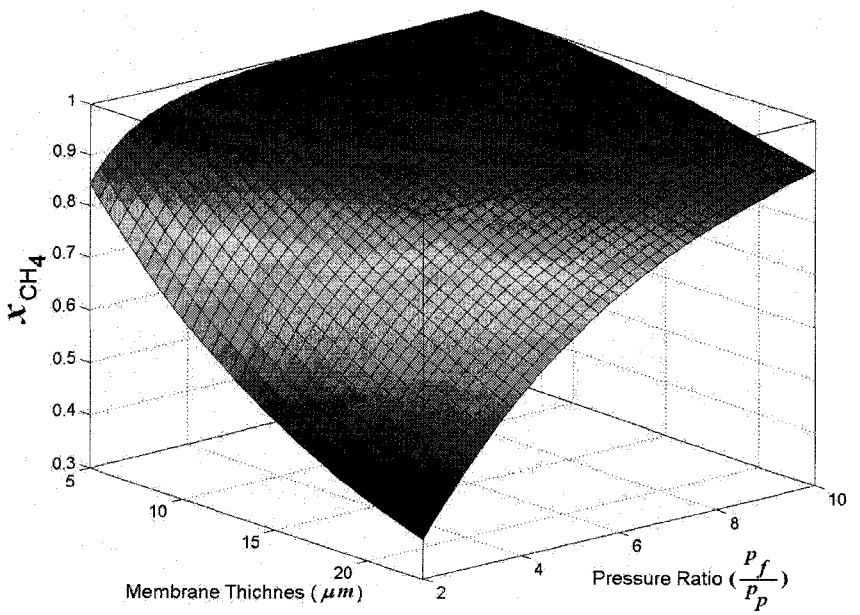

Figure C.2. Change of composition for methane in membrane permeate side.

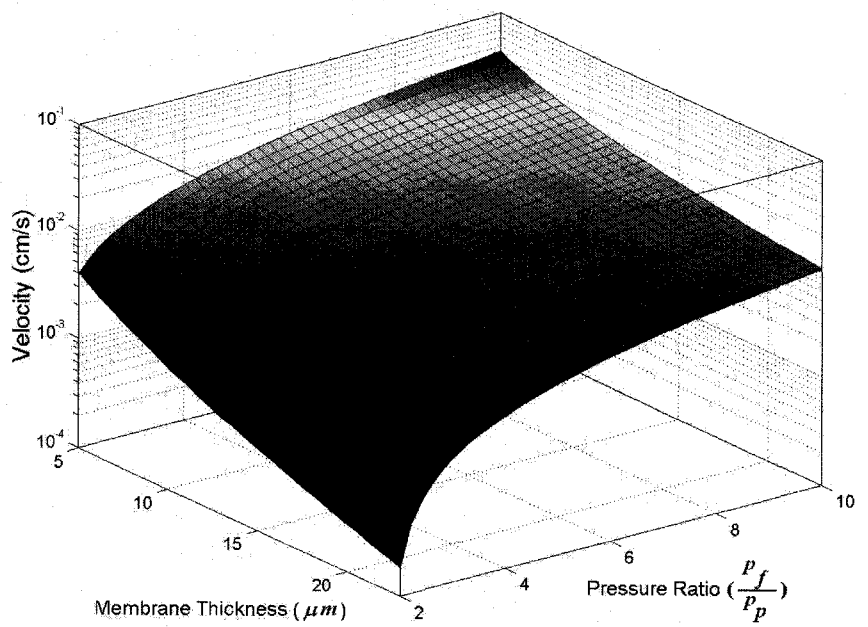

Figure C.3. Velocity measured in bubble flowmeter.

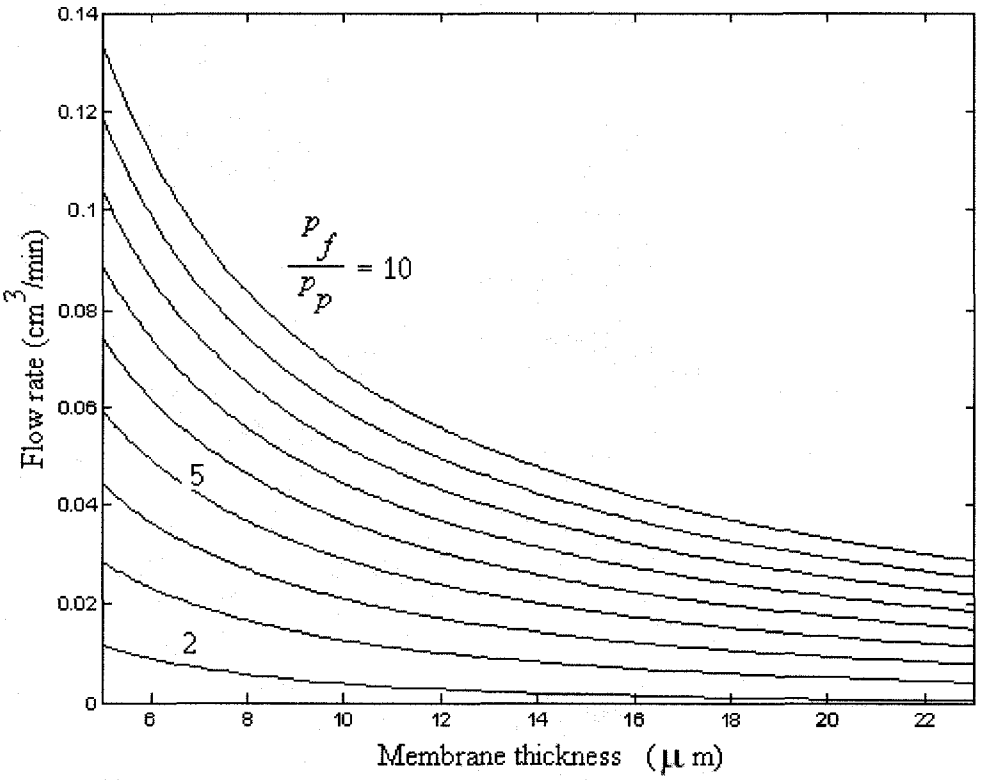

Figure C.4. Flow rate versus membrane thickness and pressure change in feed side.

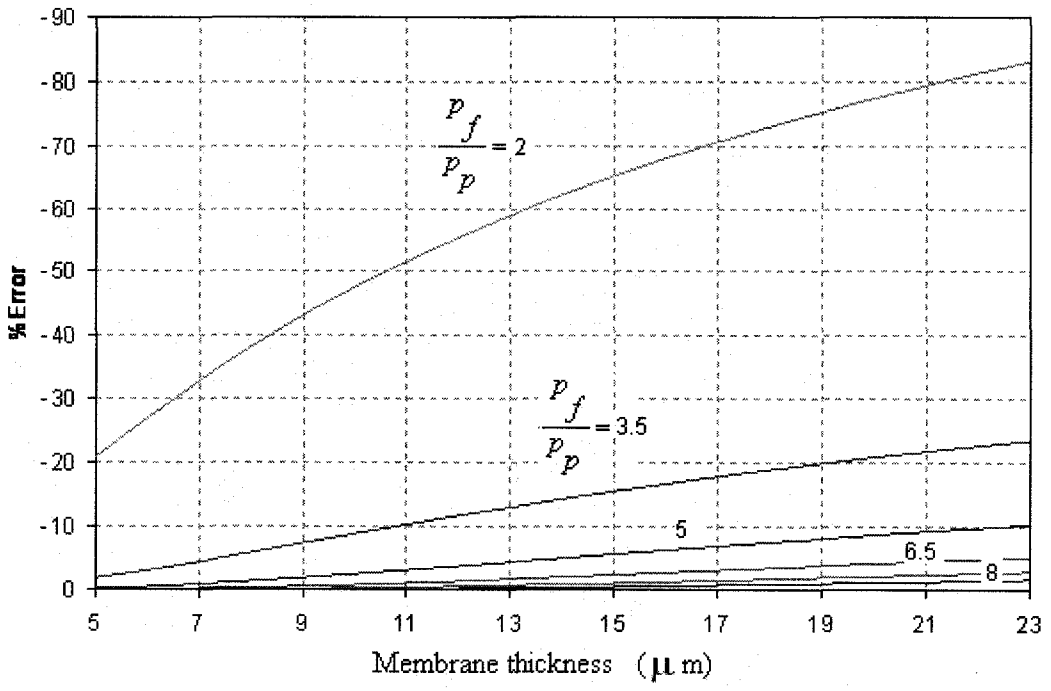

Figure C.5. Error percent in measured permeability of CH_4 due to back diffusion of air.

C.3 Ternary CH_4-Air (O_2, N_2) system at steady state condition

The solution for a multicomponent system is very similar to a binary system except that instead of Fick's first law for diffusion, the Stephan-Maxwell equation [2] is used which converts one simple equation for a binary system to a set of first order ordinary differential equations. The system of equations that must be solved simultaneously is as follows:

$$\frac{dx_i}{dz} = \sum_{j=1}^{n} \frac{\left(x_i N_j - x_j N_i\right)}{CD_{ij}} \qquad i = 1,2,...,n-1 \qquad \text{(C.1)}$$

Assuming applicability of the ideal gas law, the binary coefficients (D_{ij}) of Stephan-Maxwell equation are equal to the binary diffusion coefficients used in Fick's first law.

Because of a steady state assumption:

$$(N_i)_1 A_1 = (N_i)_2 A_2 = (N_i)_3 A_3 = (N_i)_m A_m \qquad \text{(C.2)}$$

In total there are 2n unknowns, x_i, N_i where $i = 1,2,...,n$. Therefore 2n independent equations are required to determine these 2n unknowns. Equation (6.4) presented in chapter 6 provides n equations. Equation (C.2) provides another (n-1) equations. In addition $\sum_i x_i = 1.0$ will supply another independent equation. Consequently, the resulting set of 2n equations can be solved for the corresponding 2n unknowns using numerical methods, for instance Rung-Kutta method.

The boundary conditions are the same as binary system boundary conditions.

The boundary conditions for CH_4-Air (O_2, N_2) system are:

$$@\ z = 0 \qquad x_{CH_4} = 0.00 \qquad x_{O_2} = 0.21 \qquad x_{N_2} = 0.79$$

The membrane feed composition is:

$$\left(x_{CH_4}\right)_f = 1.00 \qquad \left(x_{O_2}\right)_f = 0.00 \qquad \left(x_{N_2}\right)_f = 0.00$$

Other parameters used in this simulation are:

$$D_{CH_4-O_2} = 0.2123\ cm^2/s \qquad D_{CH_4-N_2} = 0.2088\ cm^2/s \qquad D_{N_2-O_2} = 0.1998\ cm^2/s$$

$$P_{CH_4} = 1.5\ Barrer \qquad P_{O_2} = 10\ Barrer \qquad P_{N_2} = 1.7\ Barrer$$

Solution for the CH_4-Air (O_2, N_2) system is presented graphically in Figures C.6 to C.8.

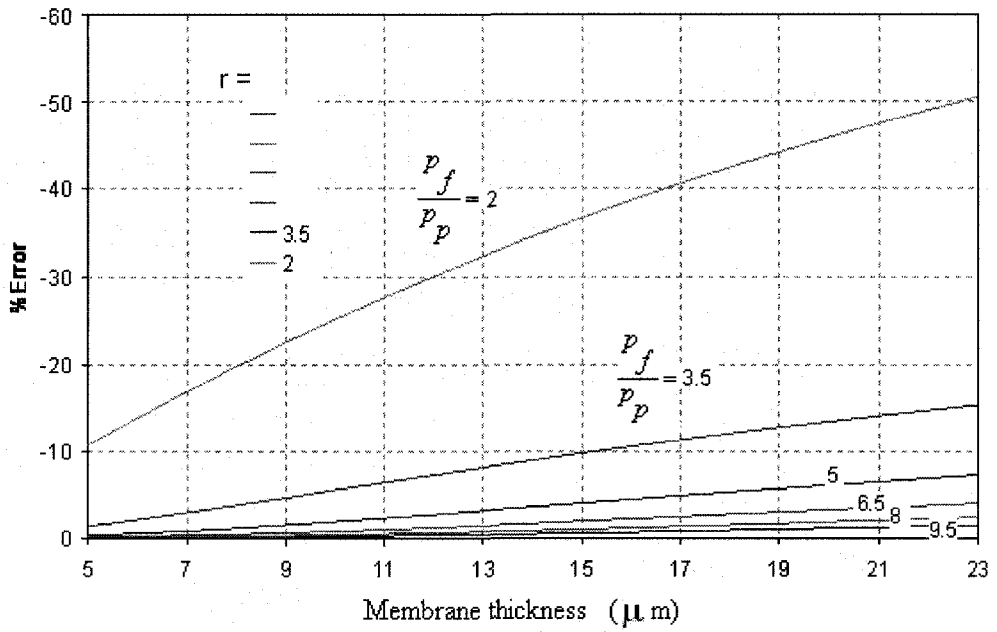

Figure C.6. Error percent in measured permeability of CH_4 due to the back diffusion of air through the tubes.

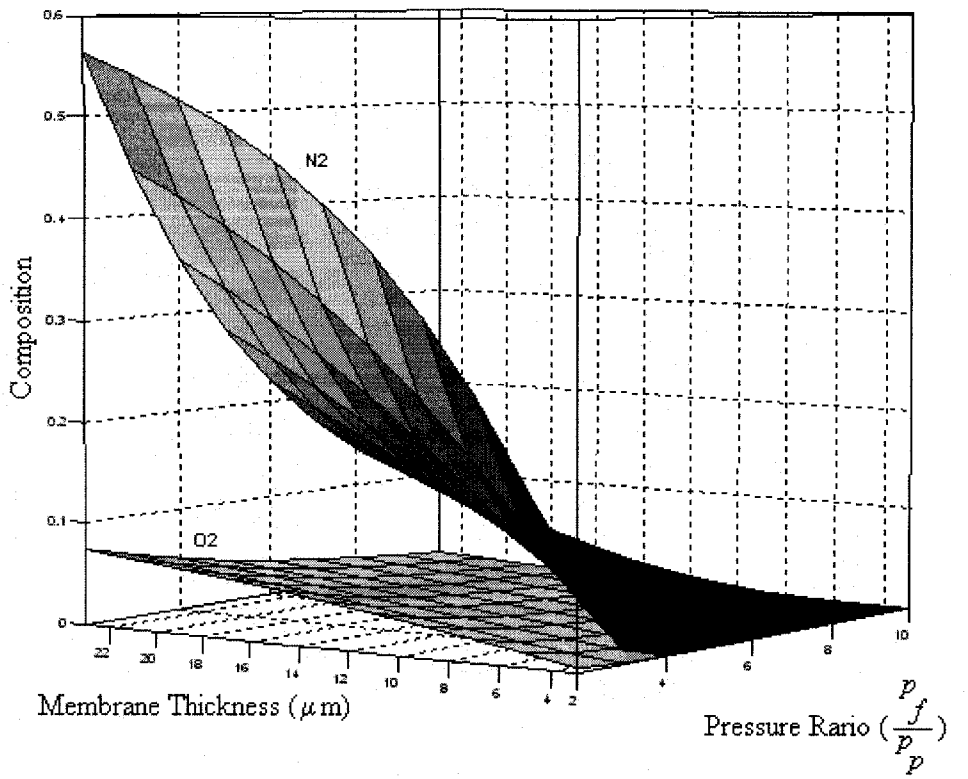

Figure C.7. Composition of N_2 and O_2 in membrane permeate side for ternary system.

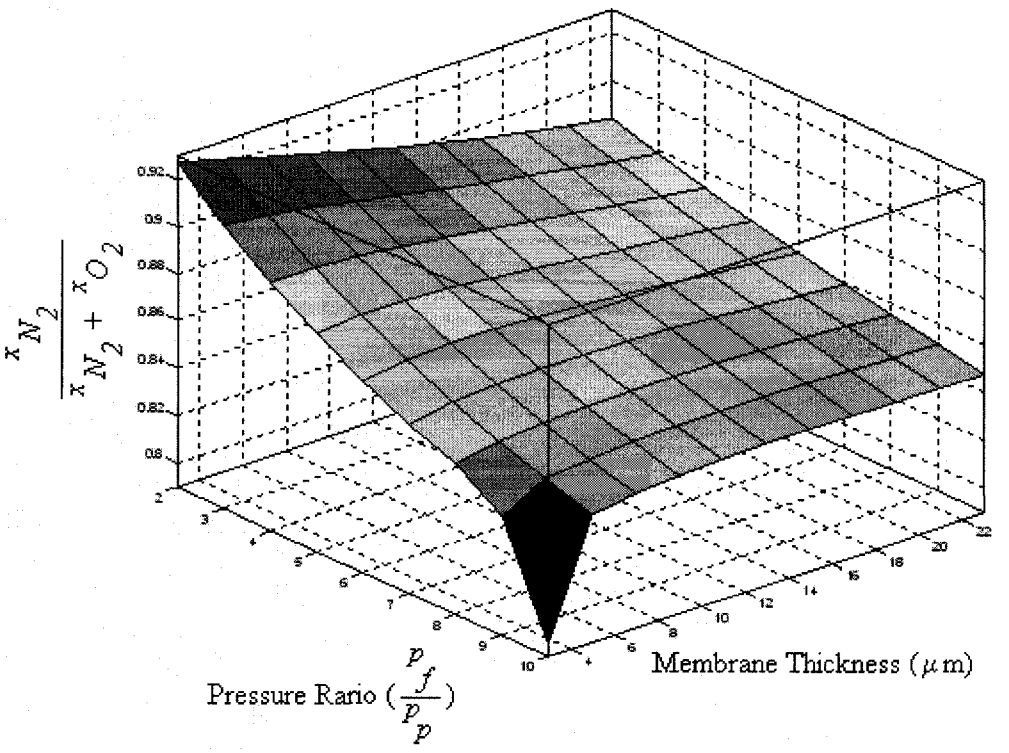

Figure C.8. Mole ratio of nitrogen in membrane permeate side for ternary system.

C.4 Binary CH_4-Air system at transient condition

The continuity equations at unsteady state conditions are:

$$C\frac{\partial x_A}{\partial t}+\frac{\partial N_A}{\partial z}=0$$
$$C\frac{\partial x_B}{\partial t}+\frac{\partial N_B}{\partial z}=0 \qquad \text{(C.3)}$$

where t denotes time.

Case 1:

For the first case, the simplest initial condition is applied:

@ $t = 0$ all $x = 0$

Feed pressure is 5 atm. Membrane thickness is 15 μm. The results are plotted in Figures C.9 and C.10.

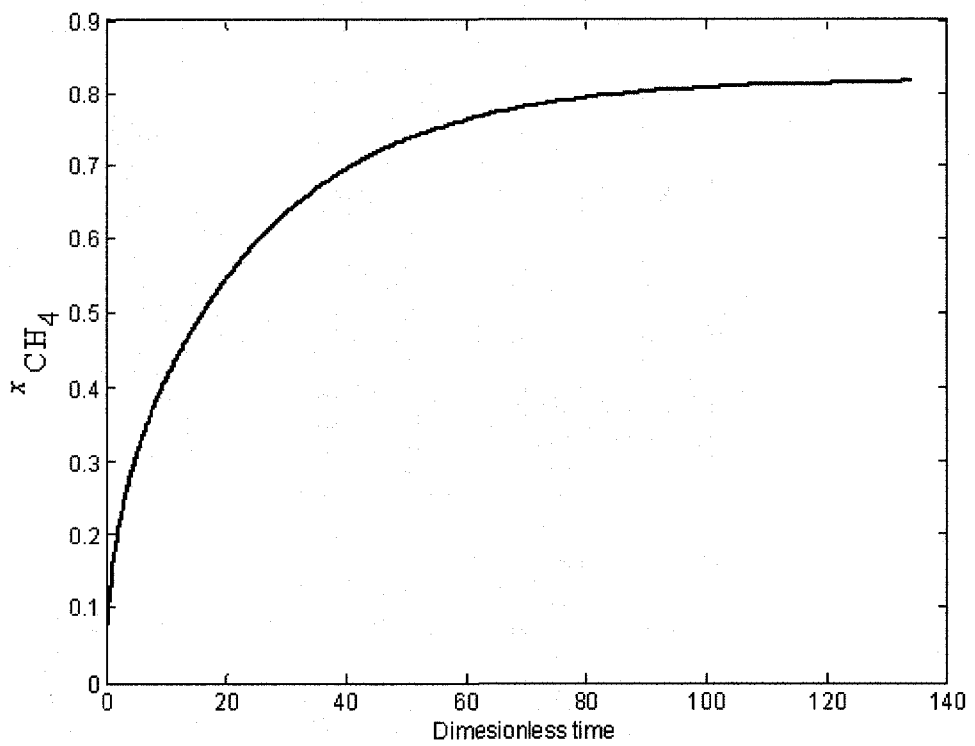

Figure C.9. Concentration of methane at the permeate side of membrane.

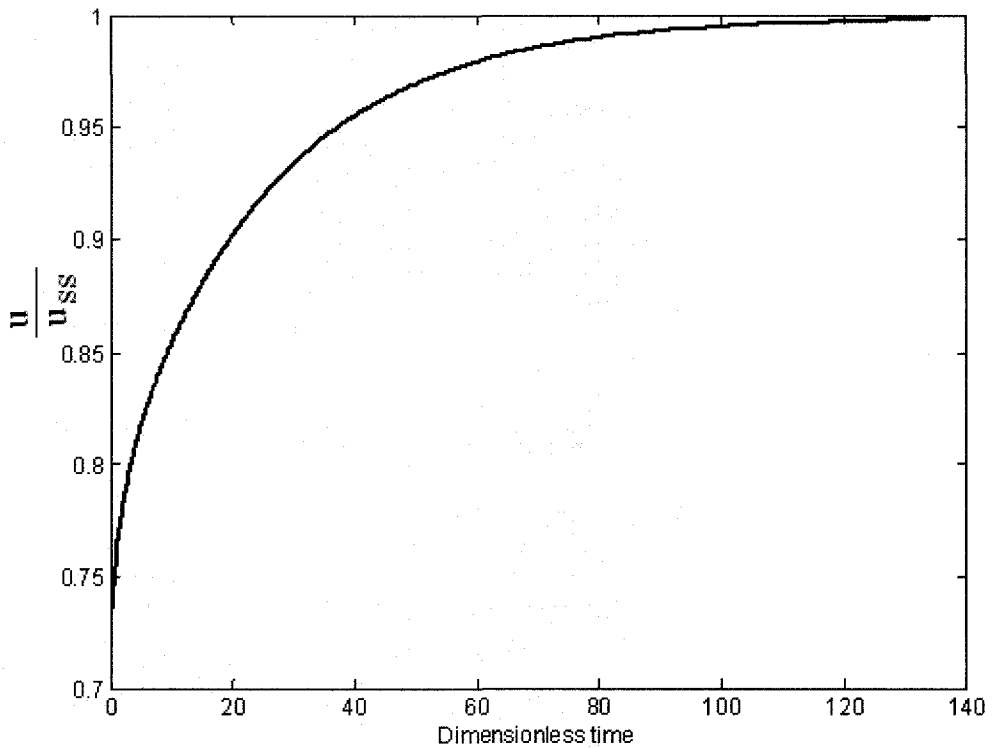

Figure C.10. Velocity change from transition to steady state condition.

Case 2:

In this case we assume that after getting to a steady state condition, the bubble flowmeter is connected to tube 3. Therefore, the initial condition is presented in Figure C.11. Furthermore, it is assumed that the geometric conditions do not change with changing the tubes. Feed pressure is 5 atm and membrane thickness is 15 μm.

Figure C.12 shows the change in the composition of methane at the permeate side of membrane versus time. Figure C.13 presents the nitrogen profile change as air back diffuses through the tubes.

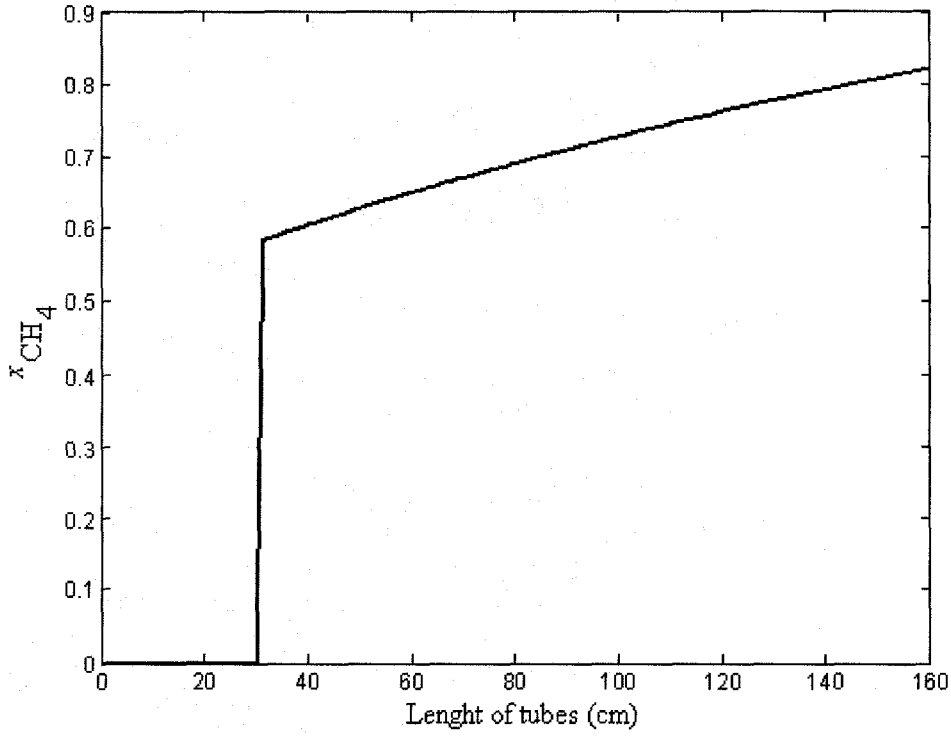

Figure C.11. Initial condition of Case 2.

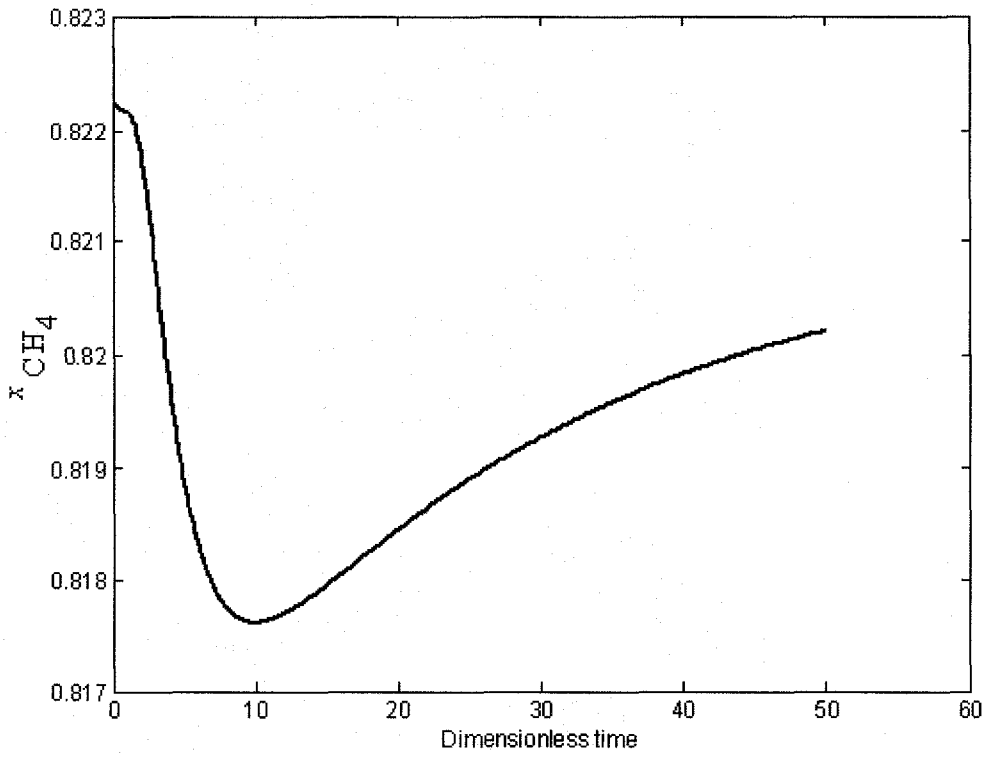

Figure C.12. Concentration of methane at the permeate side of membrane during a transition.

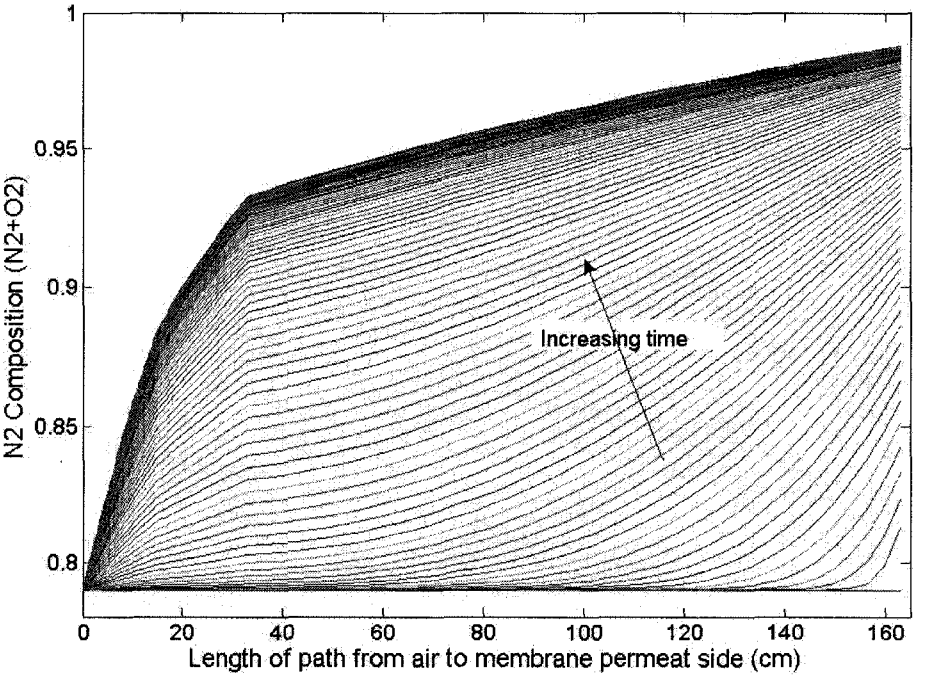

Figure C.13. Simulation represents the change of nitrogen composition through tubes in transition.

C.5 Experimental results for transition

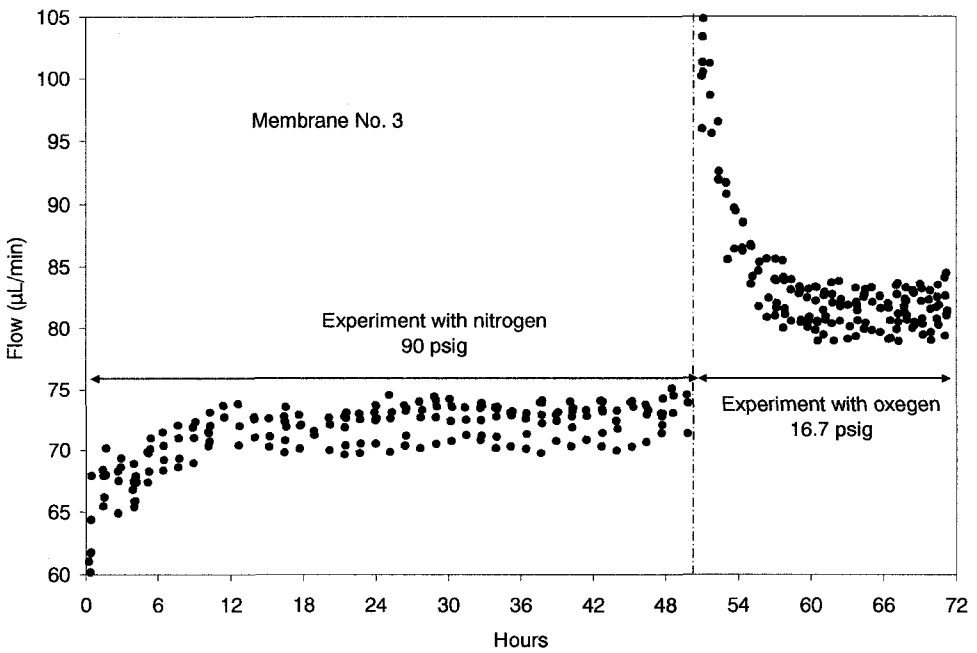

Figure C.14. Response of CP system for change in feed composition of a PPO membrane.

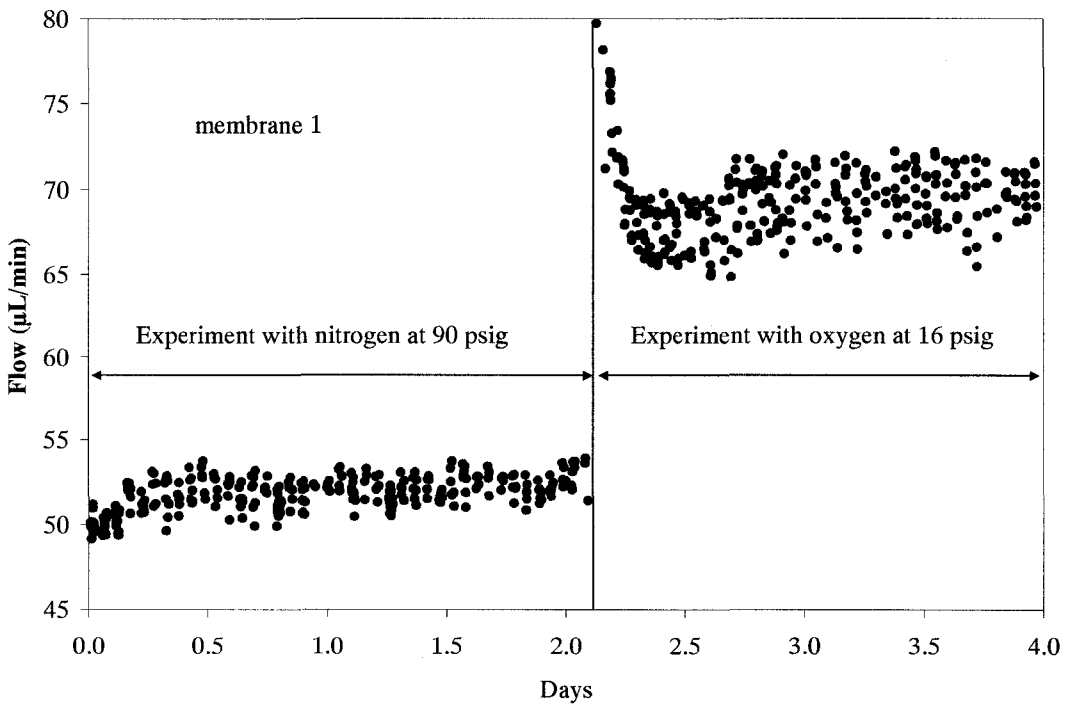

Figure C.15. Response of CP system for change in feed composition of a PPO membrane.

C.6 Experimental results

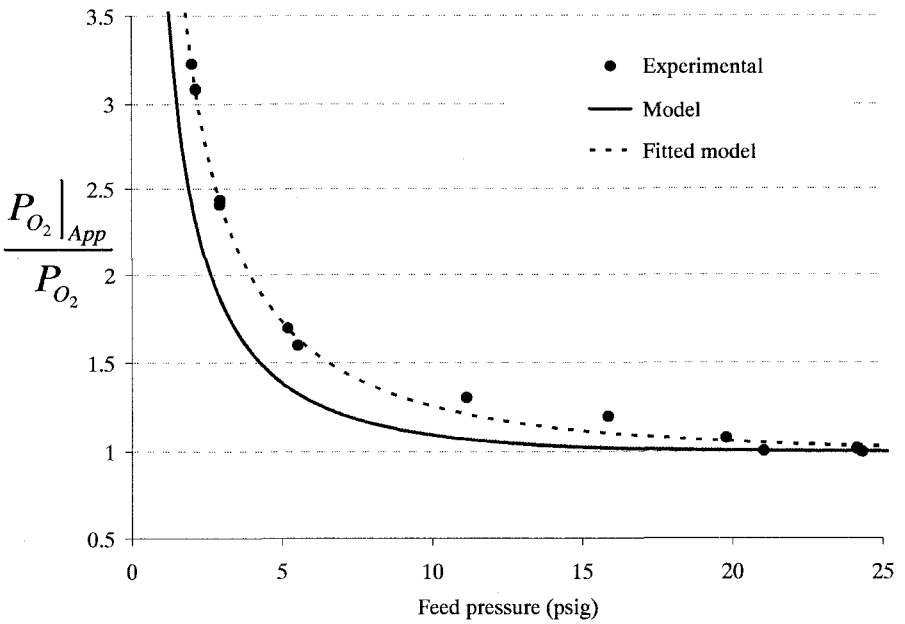

Figure C.16. Effect of back diffusion on apparent permeability when feed is pure oxygen for membrane 1. Model represents L_e = 37.4 cm and Fitted Model.

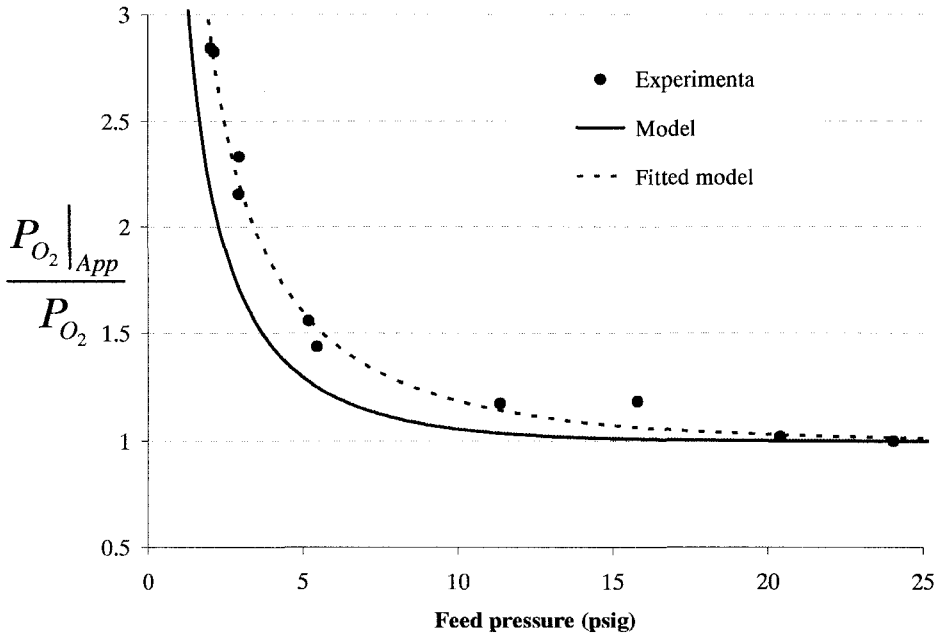

Figure C.17. Effect of back diffusion on apparent permeability when feed is pure oxygen for membrane 2. Model represents L_e = 38.8 cm and Fitted Model.

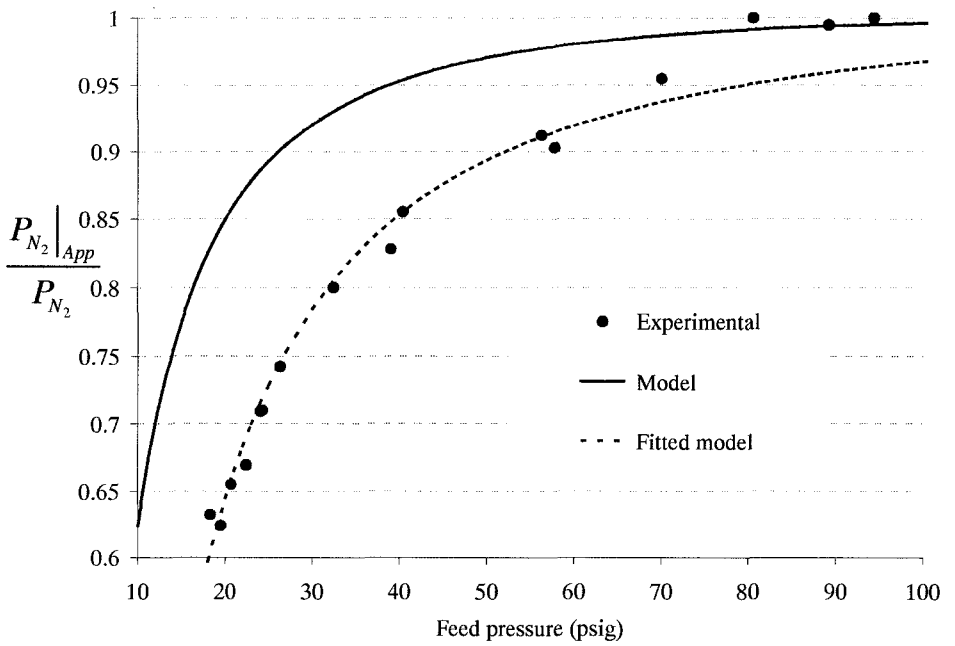

Figure C.18. Effect of back diffusion on apparent permeability when feed is pure nitrogen for membrane 1. Model represents L_e = 37.4 cm and Fitted Model.

Table C.3. Measured flow rate and pressure when oxygen is fed to membrane 1.

Flow (μL/min)	Pressure (psig)	Flow Deviation (μL/min)	Pressure Deviation (psi)	No. of points
91.539	24.307	2.071	0.139	329
92.387	24.127	2.126	0.191	422
79.605	21.045	1.970	0.166	612
80.209	19.789	1.969	0.192	573
69.719	15.937	1.657	0.192	300
71.297	15.851	1.645	0.221	827
54.668	11.139	1.177	0.103	24
33.249	5.522	0.793	0.222	895
33.099	5.183	0.645	0.016	905
27.015	2.946	0.293	0.008	251
26.590	2.933	0.493	0.013	621
24.690	2.128	0.335	0.008	248
24.401	2.009	0.299	0.010	363

Table C.4. Measured flow rate and pressure when oxygen is fed to membrane 2.

Flow (μL/min)	Pressure (psig)	Flow Deviation (μL/min)	Pressure Deviation (psi)	No. of points
117.312	24.044	3.028	0.150	513
101.743	20.403	2.991	0.691	1752
91.184	15.793	1.995	0.227	672
65.055	11.352	2.290	0.393	71
38.195	5.444	0.999	0.220	444
39.285	5.170	1.041	0.027	1218
33.548	2.947	0.723	0.014	350
30.835	2.933	0.847	0.008	350
29.326	2.126	0.471	0.008	232
27.987	2.015	0.527	0.011	1073

Table C.5. Measured flow rate and pressure when nitrogen is fed to membrane 1.

Flow (μL/min)	Pressure (psig)	Flow Deviation (μL/min)	Pressure Deviation (psi)	No. of points
6.359	18.270	0.265	0.010	15
6.684	19.450	0.327	0.030	17
7.471	20.725	0.313	0.016	48
8.285	22.488	0.464	0.048	51
9.417	24.127	0.229	0.032	100
9.498	24.302	0.302	0.022	37
10.762	26.333	0.286	0.036	94
14.292	32.453	0.335	0.021	79
17.789	39.047	0.235	0.018	209
19.017	40.409	0.185	0.019	102
28.254	56.290	0.452	0.057	149
28.716	57.811	0.318	0.022	260
36.864	70.152	0.558	0.084	388
44.402	80.691	0.594	0.080	335
48.890	89.305	0.572	0.127	228
52.000	94.489	0.778	0.149	183

References

1. G. Chowdhury, B. Kruczek, T. Matsuura, Polyphenylene oxide and modified Polyphenylene oxide membranes, Klluwer academic publishers, Boston, 2001
2. Ross Taylor, and R. Krishna; "Multicomponent Mass Transfer"; John Wiley & Sons, NY, 1993